

Copyright

by

William Rigoberto Delgado-Thompson

2017

**The Thesis Committee for William Rigoberto Delgado-Thompson
Certifies that this is the approved version of the following thesis**

**Incorporating Renewable Energy in a Desalination Plant – Case Study in El
Paso, Texas**

**APPROVED BY
SUPERVISING COMMITTEE:**

Timothy Beach, Supervisor

Sheryl Luzzadder-Beach, Co-supervisor

David Eaton

**Incorporating Renewable Energy in a Desalination Plant – Case Study in El
Paso, Texas**

by

William Rigoberto Delgado-Thompson

Thesis

Presented to the Faculty of the Graduate School of

The University of Texas at Austin

in Partial Fulfillment

of the Requirements

for the Degree of

Master of Arts

The University of Texas at Austin

August 2017

Dedication

I would like to dedicate this thesis to my great-grandmother, Irene P. Miller. Her appreciation for education is truly an inspiration to me and the rest of my family. At age 78, she earned her master's degree and was in the process of earning her doctoral degree when she lost her battle with cancer. Without the example of her work ethic and dedication to education, this thesis would not be possible. I am greatly honored to have the chance to continue her legacy and I would like to thank her for her guidance throughout the process of earning my master's degree. I also dedicate this thesis to my grandfathers, Dr. Rigoberto P. Delgado for setting the example to always make the most of the educational opportunities you have been given, and William Pickering Thompson for his work on water desalination plants in Kuwait and other parts of the Middle East, which inspired my interest in water desalination and expanding freshwater resources in arid climates.

Acknowledgements

First and foremost, I would like to acknowledge my parents and sister for your love and support throughout not just my graduate education but all of my life. I would also like to acknowledge my advisors, Dr. Tim Beach and Dr. Sheryl Luzzadder-Beach for their loving guidance and support throughout my master's career, and committee member, Dr. David Eaton for serving on my committee and incorporating his extensive knowledge to help make my thesis state of the art. I would like to thank Dr. Bill Hargrove, director of the Center for Environmental Resource Management at the University of Texas at El Paso (UTEP) for warmly welcoming me to UTEP and for introducing me to the administrators of the Kay Bailey Hutchison Desalination Plant and to researchers at UTEP's Center for Inland Desalination Systems. I would like to thank Art Ruiz, the plant's superintendent for the tour and insightful information on the plant's operation and future role in El Paso's water supplies. I would also like to acknowledge Manuel Perez, the plant's energy coordinator, for sharing the plant's energy consumption data with me and for always being available when I had questions and clarifications. I would like to thank Mr. Ed Archuleta, former CEO of El Paso Water (EPW), for sharing his insight regarding renewable energy in desalination. I would also like to thank all of the other officials whom I interviewed at EPW for their time and insight as well as EPW for its willingness to help with my thesis. I would like to thank Larry and Javier Perea of Solar Smart Living for sharing their knowledge on the solar energy industry in El Paso. Lastly, I would like to thank Diego Cruz of UTEP for sharing his knowledge of the HOMER model with me and Aleph Baumbach of HOMER Energy for helping me configure the model.

Abstract

Incorporating Renewable Energy in a Desalination Plant – Case Study in El Paso, Texas

William Rigoberto Delgado-Thompson, MA

The University of Texas at Austin, 2017

Supervisor: Timothy P. Beach

Co-supervisor: Sheryl L. Beach

El Paso is located in the westernmost part of Texas along the Rio Grande across from Ciudad Juarez, Mexico. Water supplies are a paramount concern for El Paso given its location in an arid climate. Although the Rio Grande runs past the city, prior appropriations for farming coupled with obligations to provide water to Mexico for agriculture limit the city's use of the river in dry years. As a result, groundwater from the Hueco Bolson and Mesilla aquifers plays a pivotal role in El Paso's water supplies. Both aquifers flow into Mexico and also primarily supply Ciudad Juarez's water needs. The Hueco Bolson's proximity to the Tularosa Basin, an enclosed prehistoric oceanic valley, causes the aquifer to have sizable supplies of freshwater and even larger amounts of brackish water. El Paso and Ciudad Juarez's rapid population growth has led to accelerated drawdowns of the Hueco Bolson's freshwater supplies, leaving both cities with increasingly brackish groundwater. In response to this problem, El Paso Water, El Paso's water utility, constructed the Kay Bailey Hutchison Desalination Plant in a joint project with Fort Bliss. The plant uses reverse osmosis to desalinate brackish water and serves as a buffer against brackish water intrusion from the Tularosa Basin. Reverse osmosis is an expensive, energy-intensive desalination process. El Paso's sunny climate provides a perfect opportunity to reduce the plant's long-term energy expenses through a solar-powered microgrid interconnected with the grid. Based on calculations from the HOMER model using the plant's energy consumption

data, a solar-powered microgrid could be a viable energy source that partially supplies the plant. The primary obstacles involve costs to build the microgrid and concerns from the grid administrator about potential damage to the grid. Therefore, it is important to look to the brisk decline in solar technology costs as well as to work with the grid administrator to increase the viability of such an endeavor. Given that desalination will play a greater role in El Paso's water supplies and those of the world, scholars and policymakers from El Paso and Ciudad Juarez have an excellent opportunity to make this binational region a world leader in desalination with renewable energy.

Table of Contents

Chapter 1 Introduction	1
Explanation of Project.....	1
Context of Project	3
Interviews.....	5
Why Solar Energy for Water Desalination?	8
Chapter 2.....	11
2.1 Current Water Supply Situation in El Paso County, Texas	11
History of Water Allocation in El Paso County.....	11
Farming and Population Trends.....	12
Current Water Supplies in El Paso.....	15
EPW Conservation Measures and Programs	19
Future Supply Issues	26
Summary	30
2.2 The Effects of Climate Change on El Paso’s Water Supplies	31
Introduction.....	31
Methodology.....	37
PRISM Model Results	45
Discussion.....	55
Summary.....	58
2.3 The History of the KBH Desalination Plant & The RO Desalination Process	60
The Reasons for the Construction of the KBH Plant.....	60
How the KBH Plant Works – the RO Process.....	62
2.4 Environmental Concerns of Desalination	68
KBH Plant Brine Disposal Policies	68
KBH Plant Energy Efficiency Policies.....	73
Summary	76
2.5 Literature Review.....	78
Benefits of a Grid-PV Hybrid Desalination Plant in Texas.....	78

Utilizing HOMER to Power Off-Grid Desalination Plants	80
Increasing Renewable Energy Use in Jordan Via Desalination.....	81
Challenges and Opportunities for Renewable Energy in Desalination	83
Chapter 3	86
3.1 HOMER Model Setup.....	86
Initial Project Design Window.....	86
Hourly Solar Radiation Data.....	88
Temperature Data.....	91
KBH Plant Electric Load Profile	92
Configuring Model Components: PV Module, Inverter, Battery, and Grid.....	108
The Project Tab.....	156
The Results Page.....	170
Summary	200
Chapter 4.....	201
4.1 Results of the HOMER Model.....	201
Initial Capital Cost	202
Energy Produced.....	206
Renewable Fraction & Energy Sold	211
Operating Cost & Cost of Energy.....	216
Net Present Cost & Discounted Payback Point	222
Summary	229
Chapter 5	231
5.1 HOMER Strengths and Weaknesses.....	231
HOMER Strengths	231
HOMER Weaknesses.....	232
Other Renewable Energy Modeling Programs	233
Summary	234
5.2 Limitations to Solar Energy via Microgrids in El Paso	236
David Torres Interview	236

Manuel Perez Interview	237
Larry Perea Interview	239
Ed Archuleta Interview – Unsuccessful Solar Project at KBH Plant	239
Summary	240
5.3 Future Role of Desalination and Renewable Energy in El Paso.....	241
Future Role of Desalination in El Paso’s Water Supplies	241
Future Role of Solar Energy in El Paso’s Desalination Operations ..	243
Summary	244
Chapter 6 Conclusions and Further Research.....	246
HOMER Model Results.....	246
KBH Plant’s Future Electricity Load Profile.....	246
Solar Power for the EWM Plant	247
International Technological Collaboration on Desalination	247
Appendix.....	249
References.....	250

Chapter 1 Introduction

Explanation of Project

This thesis assesses the economic feasibility of equipping the Kay Bailey Hutchison (KBH) desalination plant in El Paso, Texas with a solar-powered microgrid in tandem with the grid to reduce the energy costs of water desalination using a cost/benefit forecast. Currently, the KBH plant receives its electric power solely from the grid (A. Ruiz, personal communication, August 9, 2016). The points of comparison are the energy costs adjusted for inflation the plant will have 25 years¹ from now on its grid-only energy supply system versus the energy costs adjusted for interest payments and inflation if it invests in a solar-powered microgrid to supply its energy needs in tandem with the grid. The microgrid will use photovoltaic (PV) solar modules. This project also examines the obstacles of installing a microgrid such as the KBH plant's location on federal land, and the fluctuating nature of solar energy. It also addresses El Paso Electric Company's (EPE) concerns as the grid electricity provider regarding microgrids and other distributed generation systems' effects on the grid.

To evaluate the costs and benefits of gearing the KBH plant with a PV-grid hybrid energy system as opposed to supplying the plant's energy solely from the grid, this project uses the Hybrid Optimization for Multiple Energy Resources (HOMER) model developed by the National Renewable Energy Laboratory (NREL) (HOMER Energy, 2014). The HOMER model is a prominent tool that renewable energy researchers around the world use to assess the

¹ I selected 25 years as the comparison timeline based on the fact that the typical useful life so photovoltaic solar modules is 25 years (Pingel, Zemen, Frank, Geipel, & Berghold, 2009; Rodriguez & Amaratunga, 2008).

economic benefits of renewable energy. Scientists used HOMER to reduce electricity costs in Jos, Nigeria and to develop a system that supplies continuous power at a research station in Antarctica (Adaramola, Paul, & Oyewola, 2014; Henryson & Svensson, 2004). Furthermore, water desalination engineers at the Brackish Groundwater National Desalination Research Facility in Alamogordo, New Mexico used HOMER to determine the utility of using solar energy to desalinate water through the reverse osmosis and electro dialysis reversal processes (Karimi, Abkar, Aghajani, & Ghassemi, 2015).

The HOMER model uses an algorithm to calculate the least expensive electricity supply combination for an electricity load (Lilienthal & Lambert, 2004). To do this, HOMER assesses the available supplies of renewable energy sources at different times of year and hours of the day as well as the costs of installing renewable energy generators and compares them to grid energy prices. Based on these data, HOMER determines which combination and capacity of energy sources is the most economical to supply the KBH plant's load (Lilienthal & Lambert, 2004). Load data² and grid energy costs for the model are based on the KBH plant's energy consumption figures from 2011 through 2016 courtesy of El Paso Water (EPW), the plant's owner³.

This project uses twelve iterations of the HOMER model to conduct its economic assessment on the feasibility of installing a solar-powered microgrid to partially meet the KBH plant's electricity demands. The twelve iterations incorporate key distinguishing parameters that influence the economic viability of a solar-powered microgrid. These iterations are split into two

² This project only incorporates the power used to send water through the desalination process because power for the extraction process from the aquifers and to send brine to storage wells is tracked separately and was unavailable.

³ For further information on the setup and inputs of the HOMER model, see section 3.1.

groups of six. The first group of iterations does not incorporate net metering when calculating the KBH plant's energy costs while the second group does.

Each group has two subgroups of three iterations. One subgroup adopts the price per kilowatt of power production capacity to build and maintain a solar-powered microgrid that can produce 500 kilowatts of power. The other subgroup adopts the price per kilowatt of power production capacity to build and maintain a solar-powered microgrid that can generate 100 megawatts of power. These price scales illustrate that the cost to install a solar-powered microgrid per kilowatt of power production capacity falls as the microgrid's expected power production capacity rises due to economies of scale (Fu et al., 2016). Additionally, each iteration within each subgroup either contains PV modules that have no axis trackers, ones with single axis trackers, or ones with dual axis trackers.

Lastly, every iteration, regardless of group or subgroup, tests a microgrid whose PV modules contain an 85% derating factor or a 90% derating factor. The derating factor pertains to the efficiency of PV modules as a result of outside operating conditions (Ma, Yang, Lu, & Peng, 2015). These differentiating factors illustrate how seemingly small details make a monumental difference in the microgrid's setup costs and expected energy production and therefore the level of reduction in energy costs it will yield to the KBH plant as opposed to a grid-only energy delivery system.

Context of Project

El Paso is a growing city with approximately 800,000 residents located in the westernmost part of Texas across the Rio Grande from Ciudad Juarez, Mexico (EPW, 2014; TWDB, 2012). El Paso's location in an arid, transboundary region across from a city with twice

the number of inhabitants (see Figure 4) presents a particular challenge to secure water for more than three million people in a place with limited water resources (EPW, 2014; Fullerton, 2006; Jordan & Kurtz, 2012). In a year with normal precipitation, El Paso can count on Rio Grande surface water for about half of its water supplies (see Figure 11) (EPW, 2015). But, in drier years, El Paso must utilize groundwater resources to a greater degree (EPW, 2015). A spate of dry years combined with demand increases associated with rapid population growth has required both El Paso and Ciudad Juarez to withdraw greater amounts of water from the Hueco Bolson Aquifer, which has pulled brackish water from the nearby Tularosa Basin into the aquifer (Bredehoeft, Ford, Mace, & Rumbaugh, 2004; EPW, 2016; Heywood & Yeager, 2003; Hutchison, 2006; Sheng, 2013).

El Paso's water situation has required EPW to take monumental measures to ensure the integrity of El Paso's water supply that range from constructing the KBH desalination plant to intense water conservation measures (EPW, 2014, 2015, 2016). Furthermore, El Paso's location in a water-scarce, international locality serves as an excellent case study for future international collaborative initiatives to incorporate renewable energy in water desalination.

Chapter 2 describes El Paso's current water policies and how precipitation and temperature patterns associated with climate change will influence the city's future water policies and increase the role of desalination. This chapter also explains the reasons EPW built the KBH plant, how the RO process works, and EPW's current practices to minimize the plant's environmental footprint. Lastly, this chapter outlines precedent case studies of desalination plants powered with solar and other renewable energy sources in climates similar to El Paso's to illustrate the logistics and obstacles of powering the KBH plant with a solar-powered microgrid.

Chapter 3 explains the parameters and inputs to the HOMER model that generate the results on which this thesis bases its conclusions. This chapter also provides further explanation of the aforementioned variable factors that pertain to each iteration.

Chapter 4 describes the results of the HOMER model's cost/benefit forecast and demonstrates how these variable factors influence the economic feasibility of a solar-powered microgrid and the degree to which a solar-powered microgrid could reduce the KBH plant's energy costs.

Chapter 5 describes the strengths and weaknesses of HOMER and examines the obstacles related to constructing distributed generation systems in El Paso. This chapter also explores the future role of water desalination in El Paso and the potential for solar energy to play an increasing part in El Paso's future desalination operations as well as the city's electricity supplies as a whole.

Chapter 6 provides ideas for future studies that incorporate renewable energy in desalination, which include international initiatives to expand the use of renewable energy in desalination.

Interviews

In order to learn more about the KBH desalination plant and water desalination in El Paso and the policies regarding distributed generation in the context of El Paso, I conducted interviews with professors who study water desalination at the University of Texas at El Paso (UTEP), personnel at EPW, and the president of a local solar installation company. Their insight provided indispensable academic and professional perspectives that go beyond the literature and

played a pivotal role in enhancing the quality of this thesis. The interview methodology involved structured, non-recorded professional interviews in which I asked each person a set of questions regarding desalination and renewable energy in El Paso that pertained to their area of expertise (Ardani et al., 2017; Blakeslee, 1997; Turner, 2010). I took handwritten notes in order to archive their responses (Turner, 2010). Because the questions for these interviews did not involve personal information or experiences, Meghan Hammock, the IRB's program coordinator, determined that this thesis project did not require IRB oversight (personal communication, June 2, 2016).

My first interview was with Ed Archuleta, the water initiatives director at UTEP's Center for Inland Desalination Systems (CIDS). Mr. Archuleta also served as EPW's President and CEO from 1989 through 2013. The interview with Mr. Archuleta shed light on an unsuccessful initiative to equip the KBH plant with solar panels around 2010. He also described some of EPE's policies that reduce the economic viability of microgrids. My next interview was with Dr. Shane Walker. Dr. Walker is a professor at CIDS whose research focuses on improving the sustainability and efficiency of desalination. He provided me with important information regarding environmental concerns of water desalination related to the disposal of brine, the highly saline waste product that emerges from the desalination process. My interview with Scott Reinert, a hydrogeologist and water resources manager at EPW, yielded further details on the KBH plant's current and future brine disposal plans.

I also met with the KBH plant's superintendent, Art Ruiz. In addition to a tour of the plant, Mr. Ruiz provided extensive information on the plant's current operations as well as the future role of desalination in El Paso's water supply. EPW's energy management coordinator,

Manuel Perez, described the plant's current energy consumption patterns and plans to improve energy efficiency. One of these energy efficiency initiatives involves tracking the amount of energy used in each part of the desalination process (M. Perez, personal communication, August 4, 2016). In order to learn more about this initiative, I met with Manny Padilla, of Eaton, a power management company, to discuss the system Eaton will install to track the plant's energy usage at different steps of the desalination process. Furthermore, Mr. Perez supplied me with the plant's energy consumption data and elaborated on the logistical difficulties of incorporating solar energy from a microgrid into the plant's electricity supply.

David Torres, an economist at the plant, explained the current economic infeasibilities of installing a solar-powered microgrid. To procure a perspective from the solar industry on these difficulties as well as learn more about the changing role of solar energy in the El Paso area, I interviewed Larry Perea, the president of Smart Solar Living, a company based in Sunland Park, New Mexico, a town adjacent to El Paso. Lastly, I met with Diego Cruz, a doctoral student in electrical engineering at UTEP with experience using HOMER. Mr. Cruz gave a firsthand perspective on the strengths and weaknesses of HOMER.

Why Solar Energy for Water Desalination?

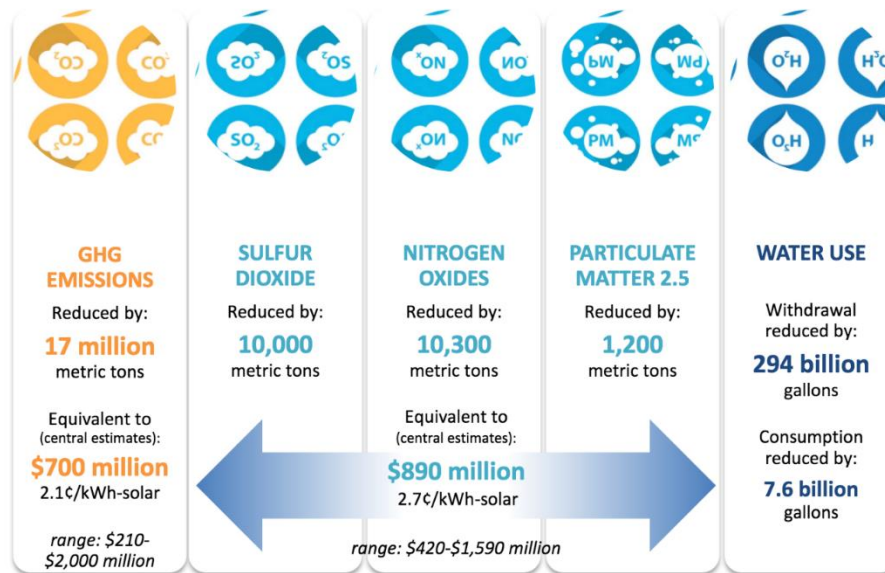
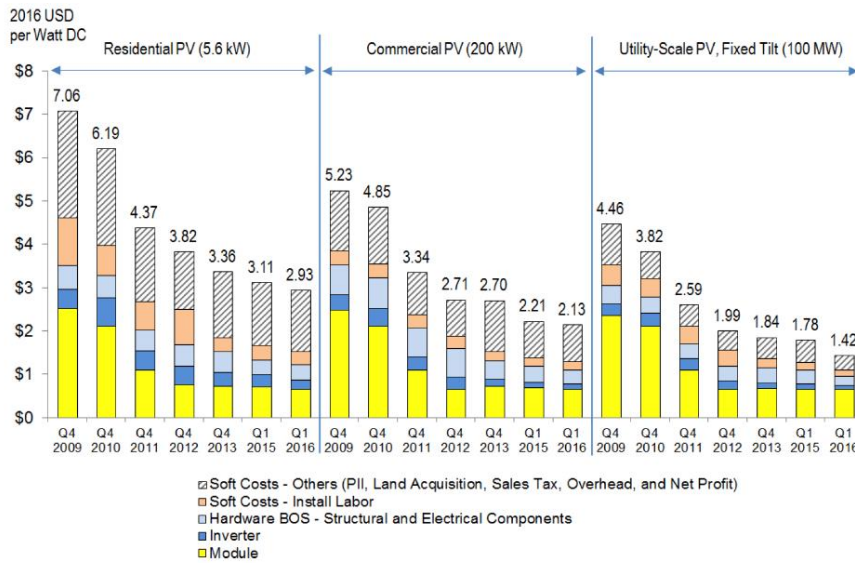


Figure ES-2. Annual environmental and health benefits of the 20 GW of solar power installed by the end of 2014

Figure 1 – Chart that illustrates the environmental benefits of the solar energy capacity installed by the end of the year 2014 compared to if fossil fuels had generated the equivalent amount of electricity (Wiser et al., 2016).

Although desalination’s energy efficiency has improved substantially in recent years, desalination still requires copious amounts of energy (Elimelech & Phillip, 2011; Fiorenza, Sharma, & Braccio, 2003; Shahzad, Burhan, Ang, & Ng, 2017). Fossil fuel-based energy serves as the predominant energy source for most of the world’s desalination plants; carbon dioxide emissions due to desalination currently stand at 76 million tons annually and are expected to rise to 218 million tons per year by 2040 (Shahzad et al., 2017; Shatat, Worall, & Riffat, 2013). These figures illustrate the fact that desalination is going to become an increasingly important water source due to a growing worldwide population that will require a greater amount of water (Fiorenza et al., 2003; Shahzad et al., 2017). In order to reduce desalination’s environmental footprint as well as its contributions to climate change, it is essential to develop cleaner, more

environmentally friendly energy resources to power desalination processes (El-Sayed, 2007; Shahzad et al., 2017). As Figure 1 shows, powering desalination plants with solar energy significantly reduces damage to the environment and helps mitigate climate change.



1. Values are inflation adjusted using the Consumer Price Index. Thus, historical values from our models are adjusted and presented as real USD instead of nominal USD.
2. Cost categories are aggregated for comparison purposes. For instance, "Soft Costs – Others" represents Pll, land acquisition, sales tax, and EPC/developer overhead and net profit.

Figure 2 – Chart that illustrates the declining costs of solar systems per watt in 2016 dollars between 2009 and 2016 (Fu et al., 2016)

Electricity costs account for 30 to 50% of total operational expenses for a reverse osmosis (RO) desalination plant such as the KBH plant (EPW, 2016; Gold & Webber, 2015).

Consequently, the main impediment to expanding solar energy in desalination is solar energy's historically high cost relative to that of fossil fuels (El-Sayed, 2007; Fiorenza et al., 2003). As of 2008, it cost between \$0.27/m³ and \$1.38/m³ to desalinate brackish water with conventional sources of energy such as fossil fuels while it cost between \$5.85/m³ and \$13.42/m³ to desalination brackish water with PV solar systems (Karagiannis & Soldatos, 2008; Shatat et al., 2013). But, according to Larry Perea, costs for PV solar systems have fallen by 70% in the last decade (personal communication, September 2, 2016). Figure 2 confirms this assessment. Thus,

the increasing cost of fossil fuels combined with the rapidly declining cost of solar energy systems has rendered solar energy an increasingly viable source to power desalination plants (Al-Karaghoul, Renne, & Kazmerski, 2009; El-Sayed, 2007; Fiorenza et al., 2003; Shahzad et al., 2017; Shatat et al., 2013). Increased concern and awareness of the environmental harm fossil fuels create has further advanced interest in augmenting the use of solar energy in desalination (Al-Karaghoul et al., 2009; Karimi et al., 2015; Shatat et al., 2013). For example, the world's largest desalination plant powered by PV modules in Al-Khafji, Saudi Arabia will be completed in 2017 (Shahzad et al., 2017). Given that El Paso receives 83.8% of possible sunshine in a normal year, equipping the KBH plant with a solar-powered microgrid is a perfect opportunity to harness this abundant energy source and for El Paso to lead the way in sustainable desalination (US Department of Commerce, NOAA, n.d.).

Chapter 2

2.1 CURRENT WATER SUPPLY SITUATION IN EL PASO COUNTY, TEXAS

History of Water Allocation in El Paso County

The United States Bureau of Reclamation allocates El Paso County's surface water for agriculture from Caballo Dam and Elephant Butte Dam on the Rio Grande upstream in south central New Mexico (Fullerton, 2006). The El Paso County Water Improvement District 1 allocates surface water to individual farmers in El Paso County (Fullerton, 2006). El Paso County has approximately 69,000 acres of irrigated land with water rights (Fullerton, 2006). The county receives a total of approximately 377,000 acre-feet of water for irrigation from the New Mexico reservoirs in a normal year (Fullerton, 2006). The 1906 Convention for the Equitable Division of the Waters of the Rio Grande diverts 74 million cubic meters (approximately 60,000 acre-feet) of water to Mexico each year, with provisions allowing for lower amounts of diversions in times of drought (Eaton & Hurlbut, 1992; Fullerton 2006). One acre-foot of water can supply a family of four with enough water for about two years (TRNCC, 2002; Fullerton, 2006).

At the beginning of the twentieth century, only 25,000 people lived in El Paso County, which meant that surface water was sufficient for agricultural use while ground water was sufficient for municipal use (Fullerton, 2006). As the City of El Paso grew, groundwater was not sufficient for municipal use and policymakers through the 1920 the Act for the Sale of Project Water for Miscellaneous Purposes had to transfer some agricultural surface water to municipal use (Michelsen & Wood, 2003; Cortez, 2003; Fullerton, 2006). The City of El Paso enacted this

law in order to reduce dependency on the rapidly depleting Mesilla and Hueco Bolson Aquifers below the city (Cortez, 2003; Tanski & Bath 1995; Fullerton, 2006).

The 1920 water transfer as just one of many transfers that occurred throughout the twentieth century. A 1941 contract provided water rights from 2000 acres of irrigated land to the City of El Paso (Cortez, 2001; Fullerton, 2006). A 1962 contract allowed farmers in El Paso County to lease their water rights to the City of El Paso for a minimum of 25 years (Cortez, 2001; Fullerton, 2006). The most significant change to water transfer contracts started in 1998 when the National Environmental Policy Act required the price per acre-foot of water transferred from agricultural to municipal purposes to be market driven (Cortez, 2001; Fullerton, 2006). This was to ensure that any water transferred was used in the most efficient way possible (Michelsen, 1994; Fullerton, 2006). At the turn of the millennium, a new contract pending approval from the Bureau of Reclamation allows El Paso County farmers to sell up to 85% of their water rights to the City of El Paso (Meritz, 2004; Fullerton, 2006).

Farming and Population Trends

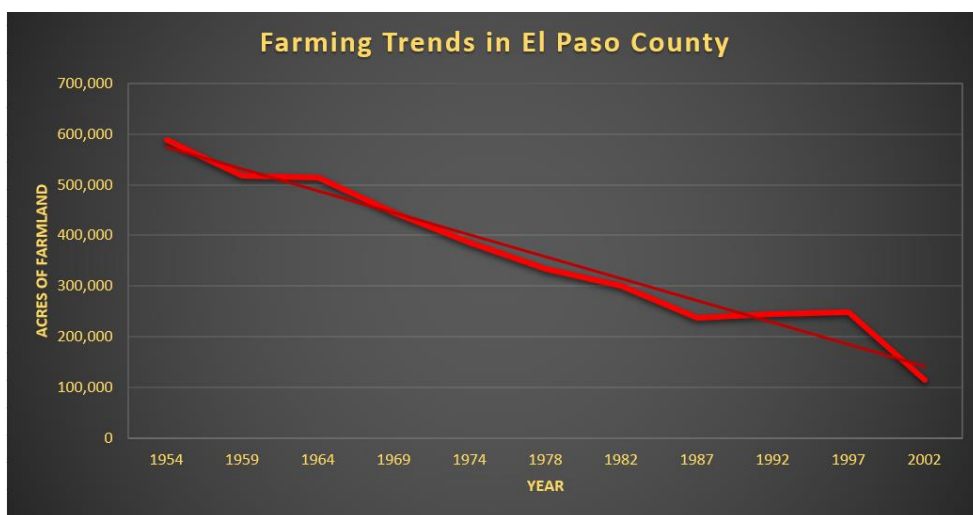


Figure 3 – Farming Trends in El Paso County from Table 2 in Fullerton (2006)

As Figure 3 shows, farming is on the decline in El Paso County. In the 48 years between 1954 and 2002, the amount of irrigated acreage has decreased from about 600,000 acres to 100,000 acres. Most of this is likely due to the urban growth in El Paso County, which has increased the value of land and made it more economically savvy for farmers to sell their land and water rights. There is also the possibility that farmers who want to continue farming have concerns about competing with the City of El Paso for water supplies. This is highly likely as Figure 4 indicates that the El Paso-Ciudad Juarez-Las Cruces metropolitan area is likely to reach approximately 3,000,000 inhabitants by 2020 with no signs of abating. In an arid region with limited groundwater supplies and only eight inches of rainfall a year on average, a rapidly growing population is likely to put a strong strain on water supplies that would make farming more difficult (EPW, 2014; Kelly, 2002).

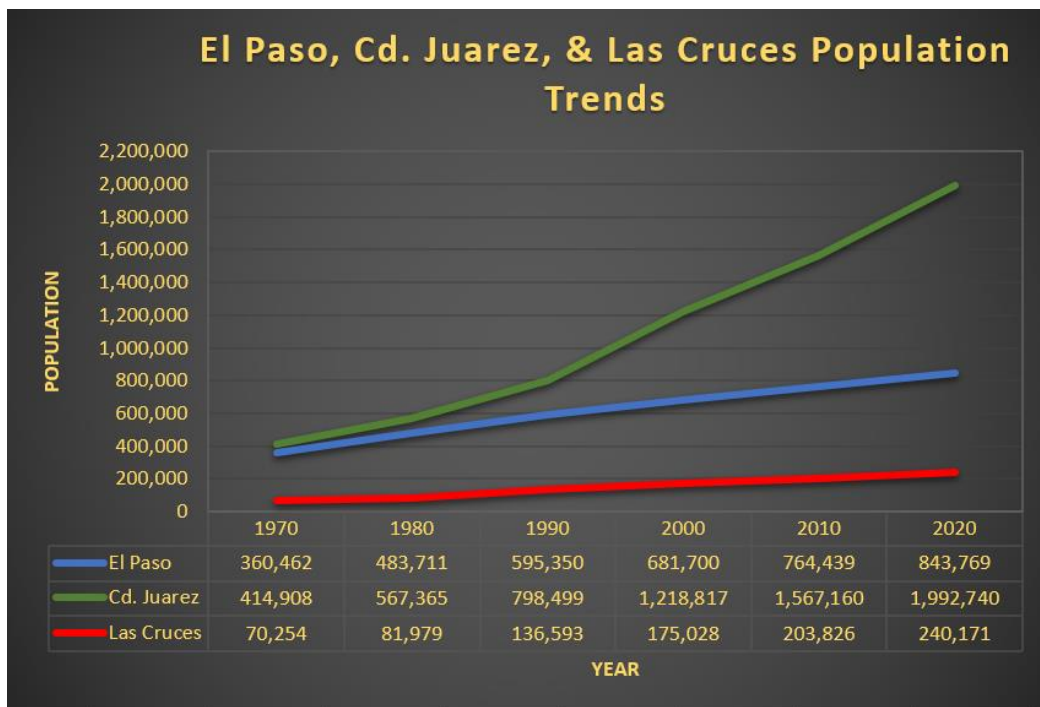


Figure 4 – Population Trends in El Paso, Texas, Cd. Juarez, Mexico, and Las Cruces, New Mexico from Table 3 in Fullerton (2006)

The population growth trends in Ciudad Juarez (hereafter Juarez), El Paso's sister city across the Rio Grande, are of particular importance. Between 1970 and 2000 the population of Juarez increased three fold while the populations of Las Cruces and El Paso only doubled (see Figure 4). Additionally, the difference in the size of the populations of El Paso and Juarez in 1970 was only about 55,000. In 2000, the Juarez population was almost twice that of El Paso and by 2010 it was more than twice that of El Paso. The difference between the populations of El Paso and Juarez is projected to be even larger by 2020 compared to 2010. Thus far there have been no indications that the rapid population growth on either side of the border is likely to abate any time soon (Borderplex Alliance, 2012).

The population growth trends in Juarez are especially important because Juarez relies on the same aquifers as El Paso in addition to the Rio Grande. Rapid population growth in Juarez will put large strains on the water supplies the two cities must share. As a newly industrialized country with a rapidly growing economy, Mexican consumers are likely to develop water consumption needs similar to those in the United States (Jenkins, 1991). Furthermore, Juarez's location on the US border makes it an attractive location for establishing large factories that export large quantities of materials to the United States with cheap labor (Abbott, 1997). This rapid growth in industry has brought many migrants from other parts of Mexico into Juarez (Pick, Viswanathan, & Hettrick, 2001). Rapid population combined with industrial growth will put an exceptionally large amount of stress on water resources. Therefore, the city of El Paso must collaborate with Juarez to establish an updated allocation system that will accommodate the water needs of a larger regional population.

Current Water Supplies in El Paso

The map in Figure 5, courtesy of El Paso Water 's (EPW) website, illustrates the location of the two primary aquifers that supply groundwater to El Paso and Juarez. The Franklin Mountains that split El Paso into an east side and a west side also split the Hueco Bolson and Mesilla Aquifers. The center of Juarez is located on the Mexican side of the border where the two aquifers almost touch. The Hueco Bolson Aquifer extends down the Rio Grande southeast of El Paso while the Mesilla Aquifer extends from Las Cruces down the Rio Grande and deep into Mexico. The extent of the aquifers on the map indicates that they supply farming communities in the region outside of El Paso County. If farming outside El Paso County continues, EPW will have to engage in expensive negotiations with farmers outside El Paso County for their water rights.

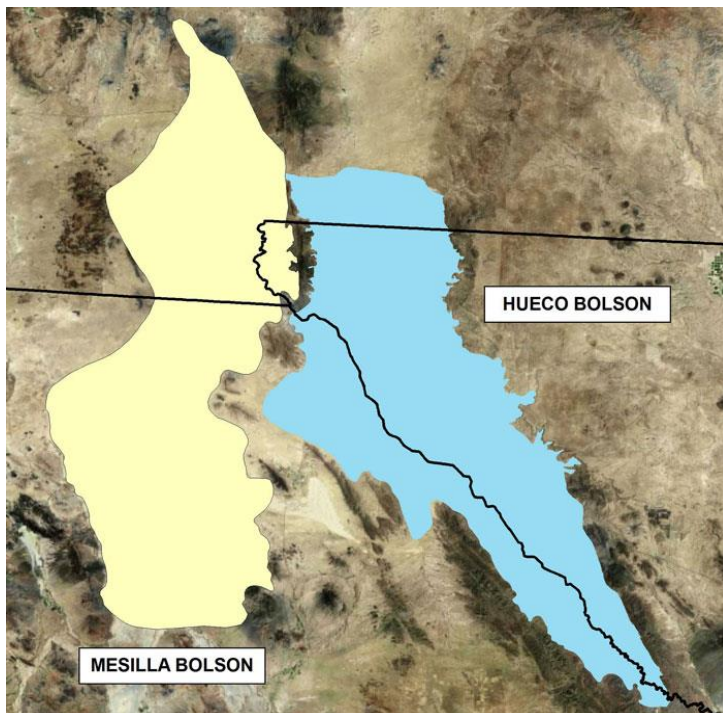


Figure 5 – Map of Hueco Bolson and Mesilla Aquifers (EPW, 2015)

EPW supplies about 90% of municipal water supplies in El Paso County (EPW, 2015). EPW purchases water through rights to irrigated land from El Paso County Water Improvement District No. 1, the local irrigation district (EPW, 2015). EPW also leases water rights from current farmers in El Paso County (EPW, 2015). EPW in recent years has expressed concern about overreliance on the Hueco Bolson Aquifer for its water supplies (EPW, 2015). EPW’s pumping from the Hueco Bolson Aquifer peaked in 1989 at 80,000 acre-feet per year (EPW, 2015). To address dependence on the Hueco Bolson Aquifer, EPW established four measures to manage water withdrawal from the aquifer: 1) increase rates for customers who use high amounts of water, 2) establish incentive programs that promote water conservation, 3) withdraw more surface water from the Rio Grande, and 4) reuse larger amounts of reclaimed water (EPW, 2015). Figure 6 demonstrates the amount of water EPW has pumped from the Hueco Bolson Aquifer from 1967 through 2015.

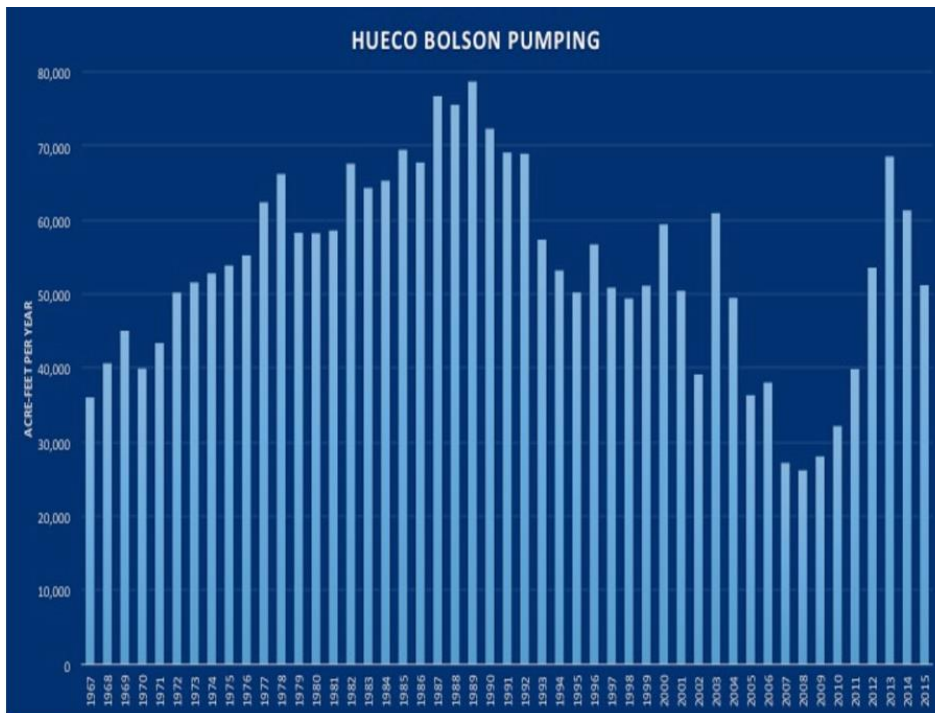


Figure 6 – Hueco Bolson Aquifer Pumping Data 1967-2015 (EPW, 2017)

The data do show an overall steady decline in pumping from the Hueco Bolson Aquifer through the 1990s. However, pumping did defy this trend in 2000, 2003, and through the mid 2010s. As EPW corroborates, this is indicative of drought upstream, which has in turn required the Bureau of Reclamation to release a lower amount of water from Elephant Butte and Caballo Dams (EPW, 2015). This strategy may be sustainable in the short term. However, in a drought situation that lasts decades, EPW will have to revert to more pumping from the Hueco Bolson Aquifer (EPW, 2015). Additionally, Figure 6 does not account for the amount of water Juarez is using from the two aquifers. With a growing population, Juarez will be forced to withdraw from the aquifers at a faster rate.

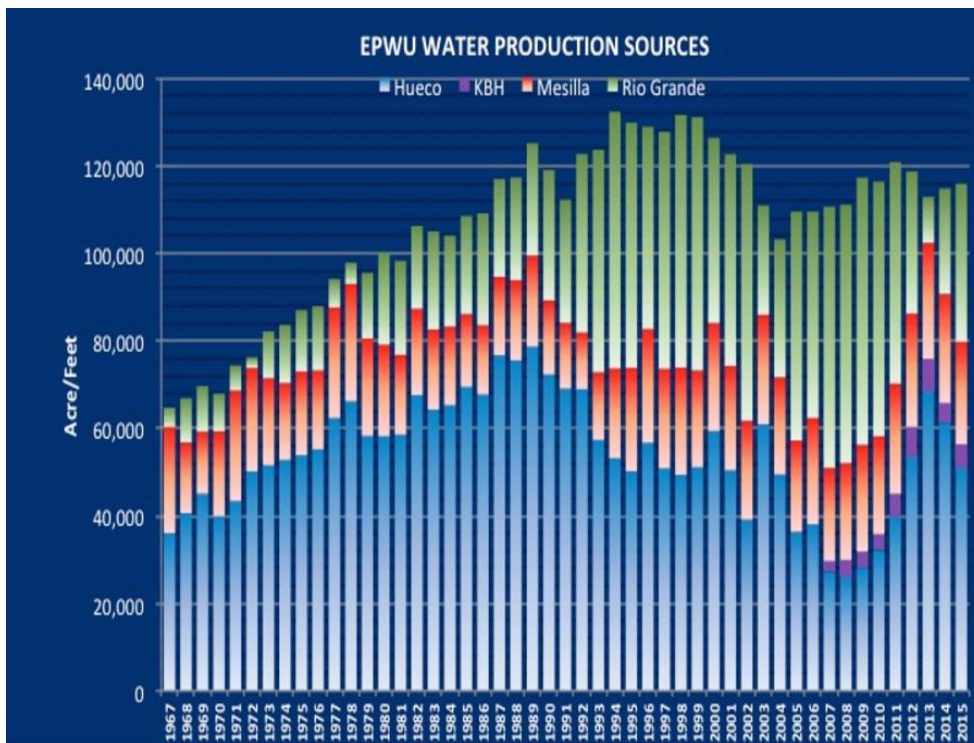


Figure 7 – EPW Water Production 1967-2015 (EPW, 2017)

Figure 7 illustrates the sources from which EPW obtains water. This figure illustrates that Rio Grande surface water comprised an increasing percentage EPW’s water starting in 1990.

By the 2010s, water from the newly inaugurated Kay Bailey Hutchison desalination plant played a more noticeable role in El Paso's water supply. The brackish water that feeds the plant comes from deep within in the Hueco Bolson Aquifer below its freshwater reserves (Ashworth, Herrera, & Albright, 2016; EPW, 2016). As EPW drills deeper into the Hueco Bolson Aquifer, the desalination plant's role in El Paso's water supply will rise exponentially (Ashworth, Herrera, & Albright, 2016; EPW, 2016). But, Figure 7 does not show consistent sizeable decreases in pumping from the Mesilla Aquifer at any point from 1995 through 2015 relative to the pumping levels from that aquifer in the 1980s and early 1990s. In fact, pumping from the Mesilla Aquifer was lowest in the late 1980s. Additionally, pumping from the both the Hueco Bolson and Mesilla Aquifers has increased noticeably from 2011 through 2015 relative to mid 2000s levels. This is likely due to the below average precipitation for the years 2010 through 2012 (EPW, 2015; US Department of Commerce, NOAA, n.d.). Although surface water increased in 2014 and 2015 relative to the low point for the 2010s in 2013, Mesilla pumping remained at about 2006 levels. Additionally, Hueco Bolson pumping did not gravitate back toward the lowest levels from the mid 2000s despite average and above average precipitation levels for the years 2014 and 2015 respectively (US Department of Commerce, NOAA, n.d.). This is a cause for concern as Las Cruces and the farming communities between El Paso and Las Cruces rely more heavily on the Mesilla Aquifer for their water (Ashworth et al., 2016). If Las Cruces continues to grow rapidly and a drought situation persists in the region, EPW will have to pay higher prices for water and deal with a possible water shortage (Fullerton, 2006).

EPW's current water supply is 131,000 acre-feet per year while its current total demand is about 118,000 acre-feet per year (EPW, 2015). During a normal year, El Paso receives about

60,000 acre-feet of water from the Rio Grande, 40,000 acre-feet from the Hueco Bolson Aquifer, 25,000 acre-feet from the Mesilla Aquifer, and 6,000 acre-feet from reclaimed water (EPW, 2015). EPW's water conservation measures have proven successful given that Figure 7 shows an average total water production per year in the 2000s that is about 15,000 acre-feet lower than in the 1990s despite the growing population. As a further testament to the success of water conservation measures, EPW claims that per capita water demand has decreased from 225 gallons per person per day in the 1970s to 132 gallons per person per day in 2013 (EPW, 2015).

However, population growth appears to catch up with water demand at the beginning of the 2010s as total water demand slowly rises compared to the mid and early 2000s even though it is lower than in the 1990s. Additionally, prolonged drought will require more pumping from the Mesilla and Hueco Bolson Aquifers whose supplies will be more constrained as Juarez and Las Cruces grow (Ashworth et al., 2016; EPW, 2015). Given that water production in the 2010s rose relative to that of the 2000s (see Figure 7), even with extreme conservation measures, the current supply may not suffice for a future larger population.

EPW Conservation Measures and Programs

Ordinances

EPW has a series of strict ordinances that apply year round for all EPW customers. Residents are not allowed to water on Mondays year-round (EPW, n.d.). However, residential customers may water their yards three days per week based on the number of their house address. Even numbered addresses may water on Tuesdays, Thursdays, or Saturdays (EPW, n.d.). Odd numbered addresses may water on Wednesdays, Fridays, or Sundays (EPW, n.d.). Schools, parks, golf courses, cemeteries, and industrial sites may water on Mondays,

Wednesdays, or Fridays (EPW, n.d.). Additionally, from April 1 through September 30, landscape watering for any site is only allowed before 10 am and after 6 pm on the site's designated watering days (EPW, n.d.).

Customers who would like a change in their irrigation days and hours must apply for a variance permit for which they have to demonstrate hardship (EPW, n.d.). Hardship includes relying on somebody else to do yard work because of age and/or health (EPW, n.d.). Hardship exceptions also apply for customers who have older irrigation systems that cannot irrigate within a certain time (EPW, n.d.). In times of extreme drought or other water emergencies, variance permits are discontinued immediately (EPW, n.d.).

EPW also has strict criteria for what constitutes wasting water. These include: 1) landscape watering on the wrong day and/or time without an exception permit, 2) letting water flow from one's yard into the street or storm drain system, 3) failure to repair leaks in hoses within five days after the discovery of the leak, and 4) washing impervious surfaces such as the driveway unless done to remove hazardous materials or other dangerous items (EPW, n.d.). Residents who wash their own cars may only do so with a bucket and a hose with an automatic shutoff valve (EPW, n.d.). During droughts and other water emergencies, car washing may only occur at commercial businesses with EPW-approved water recycling and treatment systems (EPW, n.d.). Violators of these measures are fined \$50 to \$500 per citation (EPW, n.d.). Figure 8 displays the number of citations and warnings EPW has issued between 2008 and 2014.

Year	Direct Calls to Customers	D-hangers	Verbal, Phone and Written Warnings	Citations
FY 2008-09	599	365	401	40
FY 2009-10	642	477	1,053	34
FY 2010-11	592	429	920	20
FY 2011-12	726	380	1,023	14
FY 2012-13	880	568	1,065	25
FY 2013-14	772	569	820	34

Figure 8 – Enforcement Figures of Water Conservation Ordinances from Table 11 in EPW (2014) Note: D-hangers are door hangers

These ordinances have proven successful as the number of citations issued peaked at 40 in fiscal year (FY) 2008-09 and has stayed between 20 and 34 for FY 2009-10 through FY 2013-14 with the exception of FY 2011-12 when citations were at a record low of 14 (EPW, 2014). FY 2010-11 and 2011-12 were drought years according to Figure 7 due to the fact that EPW received less surface water from the Rio Grande and withdrew more from the Hueco Bolson Aquifer compared to the most recent previous years despite EPW’s efforts to reduce reliance on it (EPW, 2015).

The fact that citations for FY 2010-11 were down to 20 and those for FY 2011-12 were at a record low of 14 suggests that EPW’s customers diligently conserved water during the drought. Furthermore, the graph displays an upward trend for all types of warnings issued to customers. Yet, the number of citations has not trended upward. This fact, combined with the steady decline in per capita water consumption for EPW customers (see Figure 10), also suggests that customers are heeding warnings and conserving water appropriately.

Outreach and Education Programs

In addition to its harsh water conservation ordinances, EPW has a large public awareness campaign through school presentations as well as workshops and training sessions (EPW, 2014). One important venue for these presentations is the Tech2O Water Resources Learning Center

that opened in 2008 (EPW, 2014). This center serves school groups, local policymakers, and the general public with interactive child and adult friendly resources that promote awareness of water use and conservation (EPW, 2014). In addition to the center, EPW sends representatives to schools, local non-profit organizations, and other community organizations to promote water conservation awareness (EPW, 2014). The following table displays the number of presentations EPW has conducted from fiscal years (FY) 2008-2009 through 2012-2013.

	Presentations at Tech₂O Center	Tech₂O Attendees	Outreach Presentations	Outreach Attendees
FY 2008-09	195	6,531	305	12,540
FY 2009-10	213	8,391	405	14,641
FY 2010-11	184	8,141	127	10,854
FY 2011-12	197	6,344	120	7,302
FY 2012-13	230	12,170	171	28,117

Figure 9 – EPW-sponsored water conservation public awareness events from Table 3 in EPW (2014)

EPW’s outreach programs have proven successful given that the number of attendees at both its outreach events and its events at the Tech₂O center has trended upward since the center opened. Furthermore, the number of attendees at the center between FY 2011-12 and FY 2012-13 almost doubled despite that fact that the number of events only rose by 33 from 197 to 230. The outreach events have proven even more successful because their numbers of attendees have risen steadily from 12,540 to 28,117 despite an overall drop in the number of outreach events. Some of the fall in attendance between FY 2009-10 and FY 2010-11 for all events could be attributed to the substantial drop in the number of events between the two fiscal years. However, FY 2012-13 posted the highest attendee record for outreach presentations ever despite only having 171 events as opposed to the peak of 405 in FY 2009-10.

These attendance figures at EPW programs (see Figure 9) indicate that EPW customers are interested and engaged in conserving water. The sharp rise in attendees at events at both the

center and away from the center implies that attendees are successfully encouraging more interest in water conservation. This fact, combined with the robust drop in per capita water usage between the 1970s and 2013, demonstrates that EPW customers are enthusiastic and willing to do their part toward water conservation (EPW, 2015). Given these successes, EPW should continue and expand their outreach programs. Because El Paso County is growing rapidly, more events such as these will be necessary to promote water conservation in order to accommodate a larger population.

Rebate and Incentive Programs

EPW's current rebate and incentive programs include one that distributes free low-flow showerheads that started in 2008, free faucet aerators for bathrooms and kitchens since 1991, and bleed off clamps to prevent water loss from evaporative air conditioners (EPW, 2014). EPW also had several other programs that ran between 1991 and 2007. These programs included rebates for turf, water-efficient washers, and low-flow toilets (EPW, 2014). EPW also distributed free waterless urinals for three years to commercial and government customers (EPW, 2014). One unsuccessful program involved distributing tank less water heaters that heat water right before it emerges from the showerhead. This program was discontinued after two years due to low participation (EPW, 2014). Figure 10 displays EPW's per capita water consumption from 1974 to 2013.

**WATER AND WASTEWATER UTILITY FUND
PER CAPITA WATER CONSUMPTION - CALENDAR YEAR**

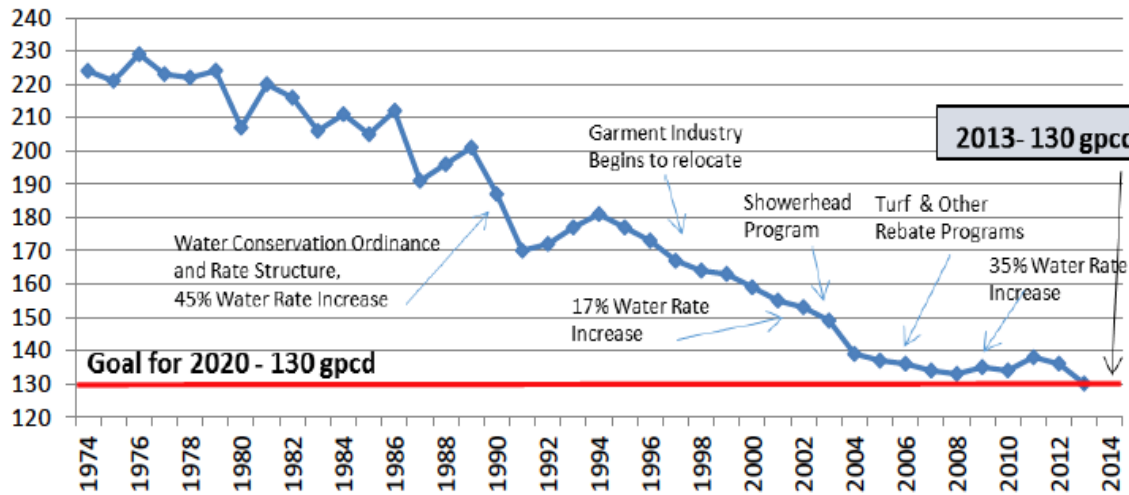


Figure 10 – EPW Customer Per Capita Water Consumption 1974-2013 (EPW, 2014)

Conclusions on EPW Conservation Measures

EPW’s per capita water consumption has steadily declined. Even though there is a correlation between the implementation of rebate and incentive programs and further decline in per capita water use, there is not enough evidence to conclude that these programs are a significant cause behind the decline in per capita water use. EPW did not provide figures for the number of people who participated in the programs to ascertain how successful they were. Nonetheless, if large numbers of people participated, then it is likely that the programs had non-negligible impacts on EPW’s per capita water use.

Other initiatives also could have also played an important role in the decline in per capita water use for EPW customers. These include the harsh ordinances and the sharp water rate increases in 1989 and 2009 respectively (see Figure 10). EPW only vaguely described outreach programs it had prior to FY 2008 (EPW, 2014, p. 5). These consisted of collaboration with local

non-profits to promote water conservation. Nevertheless, these programs, depending on their reach and effectiveness, may have contributed to the decline in per capita water use as well.

Another important event that may have contributed to the decline in per capita water use is the start of the garment industry's relocation to other places in 1997 (EPW, 2014). It is not clear if EPW implies that the garment industry relocated to Juarez or out of the region entirely. Regardless, the relocation of the garment industry outside EPW's service area most likely also had a noticeable effect on the decline in per capita water use given the large amount of water garment manufacturing requires (Maia, Alves, & Leão, 2011). However, it is important to note that per capita water use was already on a steady decline starting four years before the garment industry started to relocate (EPW, 2014).

EPW's conservation measures show a serious, concerted effort to reduce water usage in El Paso County. The education and outreach programs are clearly reaching growing numbers of people. EPW would be wise to restart rebate programs for turf, toilets, and washers to incorporate the latest water conservation technology and prepare for further population growth and potential long-term droughts in the future. Furthermore, EPW should publish figures on participation in its rebate programs in order to acquire a better idea of their effectiveness.

The strict laws for watering yards are great measures to control large amounts of water use. Similar measures worked well in Las Vegas to reduce residential outdoor water use (Morris, Devitt, Crites, Borden, & Allen, 1997; St. Hilaire et al., 2008). However, the fines need to be high enough to effectively discourage excessive water use and should be tailored to property size, average water consumption for the property, and the number of past citations. This is true because rich people are more likely to own large homes that consume a lot of water

(Corral-Verdugo, Bechtel, & Fraijo-Sing, 2003; Harlan, Yabiku, Larsen, & Brazel, 2009). They are also less likely to mind low fines relative to their income and will pay more attention to a larger ones based on measures such as the ones aforementioned (Corral-Verdugo, Bechtel, & Fraijo-Sing, 2003; Harlan, Yabiku, Larsen, & Brazel, 2009). Changing fine structures for violating water ordinances will help EPW greatly in reining in prodigal water users who may not mind paying fines that are too low for them.

Future Supply Issues

Prolonged future droughts are a key concern for EPW, especially given El Paso County's rapidly growing population (EPW, 2015). Per column 6 in Figure 11, surface water supplies from the Rio Grande during the most extreme drought conditions will drop to 10,000 AF/year (EPW, 2015). This would in turn require the Hueco Bolson and Mesilla Aquifers to supply 80,000 AF/year and 35,000 AF/year respectively to meet the demand of 131,000 AF/year assuming reclaimed water constitutes 6,000 AF/year (EPW, 2015). The first column in Figure 11 indicates a normal scenario while the successive columns indicate more extreme drought scenarios with the sixth column indicating a 'drought-of-record' scenario (EPW, 2015).

El Paso Water Utilities Conjunctive Use Components

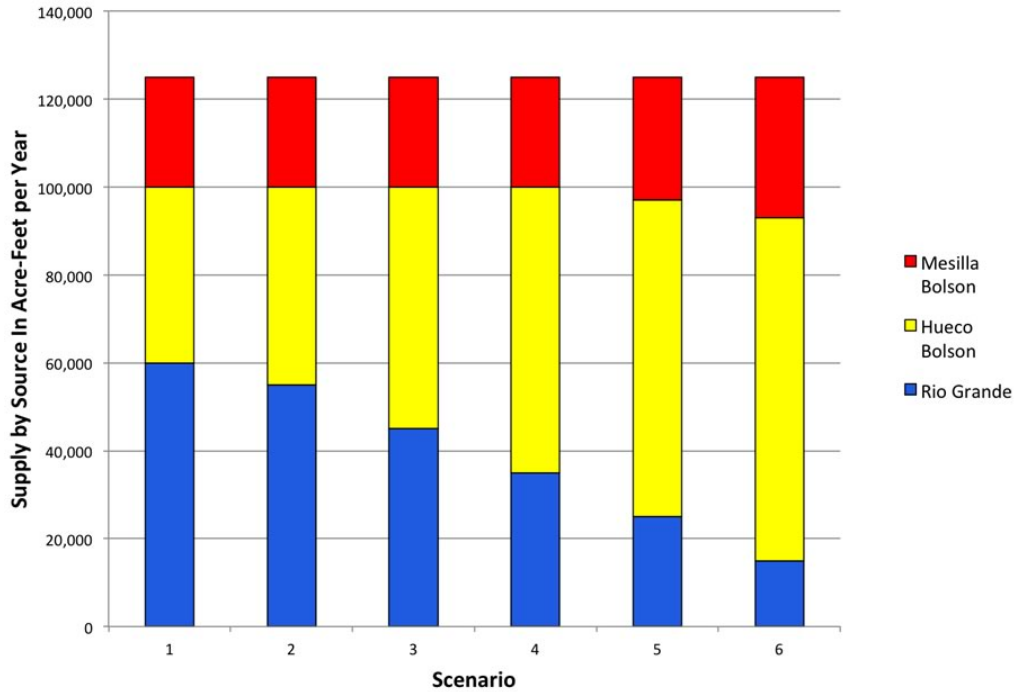


Figure 11 – EPW water supply sources based on drought magnitude (EPW, 2015)

EPW has proposed plans to alleviate pressure on the aquifers that include desalination of leftover irrigation water, increases in the use of reclaimed water, and the importation of water from areas outside of El Paso County as Figure 12 demonstrates (EPW, 2015). EPW’s plans to import groundwater from Capitan Reef and Dell City in addition to desalination (see Figure 12) attest to the high growth and high water needs in El Paso County. Furthermore, Figure 7’s desalination production figures for 2011 through 2015 show that desalination will likely play an increasing role in El Paso’s water supply, especially in years with below average precipitation such as 2011 and 2012 (EPW, 2015, 2016; US Department of Commerce, NOAA, n.d.).

Water Management Strategies for El Paso Water Utilities (2011 Plan)

	2010	2020	2030	2040	2050	2060
Supplies Currently Available to El Paso Water Utilities						
Conjunctive Use of Groundwater and Surface Water	125,000	125,000	125,000	125,000	125,000	125,000
Reclaimed Water Supply	6,000	6,000	6,000	6,000	6,000	6,000
Current Supply Available to EPWU	131,000	131,000	131,000	131,000	131,000	131,000
Proposed Management Strategies for El Paso Water Utilities						
Additional Conservation		3,000	7,000	11,000	16,000	22,000
Additional Reclaimed Water Supply		2,000	4,000	6,000	6,000	6,000
Recharge of Groundwater with Treated Surface Water		5,000	5,000	5,000	5,000	5,000
Desalination of Agricultural Drain Water		2,700	2,700	2,700	2,700	2,700
Additional Conjunctive Use		5,000	15,000	20,000	20,000	20,000
Groundwater from Capitan Reef				10,000	10,000	10,000
Groundwater From Dell City Area					10,000	20,000
Total Proposed Supply for El Paso Water Utilities	131,000	148,700	164,700	185,700	200,700	216,700
Demand for El Paso Water Utilities	118,167	145,445	162,190	176,770	191,728	207,702
Surplus Supplies	12,833	3,255	2,510	8,930	8,972	8,998

Figure 12 – EPW Future Water Supply Plans (EPW, 2014)

One weakness with EPW’s plans is their lack of explanation on how the cost to construct and maintain pipelines as well as import and desalinate water will affect ratepayers’ water bills (Ashworth et al., 2016; EPW, 2015). These costs will inevitably have to be passed on to EPW customers, which in turn could make water less affordable but no less necessary for lower income customers. For example, per capita income in 1980 was \$11491 in 1996 dollars and water was \$1.35 per gallon on average in 1996 dollars as well (Fullerton, 2006). This meant that

the average El Paso County resident could buy 8512 gallons of water in 1980. In 2000, per capita income was \$17212 in 1996 dollars and water was \$2.16 per gallon on average in 1996 dollars. This meant that the average El Paso County resident could buy only 7968 gallons of water in 2000, 500 gallons fewer than in 1980 (Fullerton, 2006).

The price of water is already rising more quickly than real income in El Paso County (Fullerton, 2006). These measures to expand water supplies in El Paso County would only make the price of water rise even more quickly relative to real income. Therefore, EPW's future plans must adequately address the affordability of water for customers while ensuring reliable supplies. Such programs could include a non-profit water fund that pays part of the water bill for low-income customers similar to the one the City of Austin administers for its utilities (Austin Energy, 2015).

Furthermore, EPW's supply plans may underestimate demand due to informal settlements and undercounting in the US Census of El Paso County residents (Ashworth et al., 2016; Gonzalez, 2013, p. 4; MALC, 2011). An approximately 9000-AF surplus as Figure 12 projects for the years 2040 through 2060 may not be sufficient to account for the needs of either this population or population growth that exceeds projections. Therefore, EPW's supply plans must account for these factors more explicitly. EPW's supply plans also need to factor in Juarez's growth and corresponding supply needs. This will require extensive and sincere collaboration with the Juarez water utility. Such collaboration must ensure that Juarez's utility is accurately measuring the amount of water supplied to its residents, including those in informal settlements. EPW must also consider contingency plans that involve negotiating with New Mexico for water rights despite past difficulties (Fullerton, 2006). Lastly, EPW must work with

the Bureau of Reclamation to reduce the large amount of bureaucracy for water transfers in the event of an extreme drought (Fullerton, 2006).

Summary

EPW faces pressing challenges to ensure that it can provide affordable, accessible water to its customers. As the next section explains, climate change will further exacerbate these issues. EPW's unique service area on an international border next to a large industrial city whose population is more than twice as large as that of the City of El Paso adds even more difficulty to the situation. EPW has proven its commitment to address the challenges of a growing population with a limited supply of water through its conservation laws, outreach initiatives, and rebate programs. The sharp drop in per capita water consumption is a further testament to the discipline and determination EPW and its customers have toward water conservation. Partnerships with Juarez are an absolute necessity for EPW that it must include in its future plans. EPW, the Bureau of Reclamation, State of New Mexico, and the Mexican Government must work in good faith to ensure that residents in El Paso County, New Mexico, and Mexico receive a fair supply of water. But, if everyone works together and commits to conserving water, El Paso County will continue to be a place future generations can proudly call home.

2.2 THE EFFECTS OF CLIMATE CHANGE ON EL PASO’S WATER SUPPLIES

Introduction

Temperature and precipitation changes in El Paso associated with climate change will increase the volatility of the city’s water supplies, which will in turn increase the importance of other water sources such as desalination (EPW 2015, 2016; Nielsen-Gammon, 2011; Sheng, 2013). This section explains precipitation and temperature changes in the El Paso area using the results from the PRISM model and others to suggest potential changes El Paso can make in order to adapt to a future water supply situation that includes a warmer climate with potentially more erratic precipitation. This section also uses the results of a case study in Phoenix by Gober & Kirkwood (2010) that used the WaterSim model as a point of comparison in order to provide further ideas for El Paso’s water future in a warmer, possibly more arid climate.

Overview of El Paso’s Precipitation and Temperature Regime

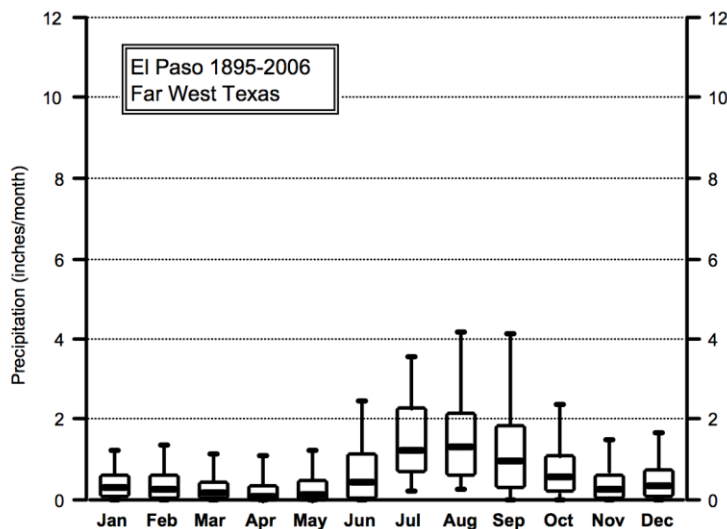


Figure 13 – Box and whisker plot for monthly precipitation in El Paso, Far West Texas. Bottom and top of box indicate 25th and 75th percentiles of precipitation. Bottom and top of whiskers represent 5th and 95th percentiles (Nielsen-Gammon, 2011).

El Paso is located in the driest part of Texas and has an average annual precipitation of just 8.71 inches (EPW, 2014; TWDB, 2012; US Department of Commerce, NOAA, n.d.). In comparison, the central and eastern parts of Texas, which contain Houston, Dallas/Fort Worth, San Antonio, and Austin, have an average annual precipitation between 30 and 55 inches (TWDB, 2012). As Figure 13 indicates, the months of November through June yield no precipitation at least a quarter of the time (Nielsen-Gammon, 2011). These unpredictable and volatile precipitation patterns attest to the importance El Paso has to place on groundwater to meet its water needs (EPW, 2015). In addition to low precipitation, the far west Texas region (see Figure 2.4 in Nielsen-Gammon, 2011) has contended with rising temperatures (see Figures 2.14-2.16 in Nielsen-Gammon, 2011) during the late twentieth century relative to the region's mean temperature from 1901 to 2000 (Nielsen-Gammon, 2011). As Figure 14 shows, this is especially apparent during the May through September period, the warmest period of the year (Nielsen-Gammon, 2011).

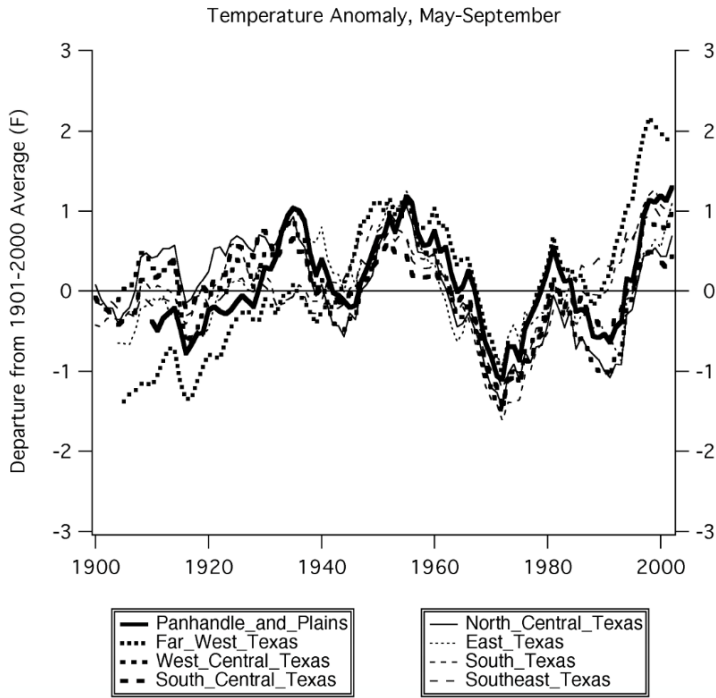


Figure 14 – Nine-year running mean of average values of May-September mean USHCN V2 temperature departures from long-term mean, in each of eight Texas climate regions from Figure 2.16 in Nielsen-Gammon (2011).

Geographical Location of El Paso

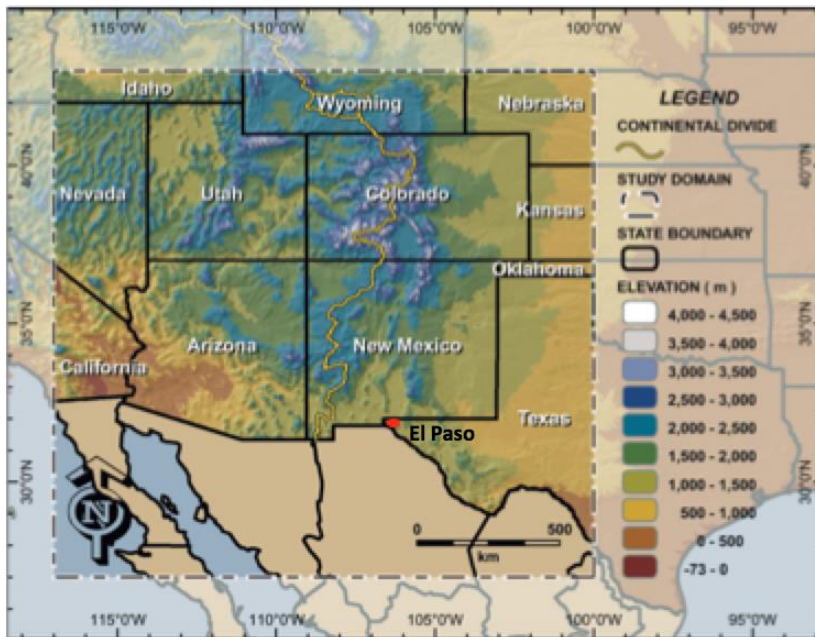


Figure 15 – Map of the American Southwest, which is the area in the study domain (Weiss, Castro, & Overpeck, 2009)

El Paso lies in the American Southwest (see Figure 15), a region that includes the western half of Texas, New Mexico, Arizona, Colorado, Utah, southeast California, the eastern half of Nevada, and parts of other adjacent states (Weiss et al., 2009). Temperatures across the American Southwest (hereafter Southwest) rose by 0.37°C per decade over the past 30 years as opposed to 0.31°C for the contiguous United States as a whole during the same time period (Sheng, 2013). Temperatures in far west Texas mirrored the temperature trends of the rest of the Southwest because they increased at a faster rate than those in other regions of the state during the twentieth century (see Figure 14 and Figures 2.14 & 2.15 in Nielsen-Gammon, 2011). The first evidence is that the temperature deviations in far west Texas from the early 1900s to the early 1940s were lower than those in other Texas regions. After this period, temperature deviations from the long-term mean in far west Texas topped those of other regions through the year 2000. Secondly, temperature deviations in far west Texas trended rapidly above the long-term mean from the late 1980s through the year 2000. They also increased at one of the fastest rates across the state during this timeframe. Furthermore, from the early to mid 1990s, temperature deviations were above the long-term mean in far west Texas while those of most other regions of the state were below it.

Precipitation Patterns of the Southwest

Precipitation across the Southwest is seasonal. Most of the region's precipitation either falls during the winter from frontal systems coming from the Pacific or during the North American summer monsoon (hereafter monsoon) (Dettinger, 2011; Weiss et al., 2009). The monsoon typically starts in July and runs through September, though it does occasionally begin as early as June (Ellis, Saffell, & Hawkins, 2004). The monsoon happens due to a change in

wind patterns from dry westerly to moist southerly (Ellis et al., 2004). The cause of these wind changes is a weak high pressure ridge over the Four Corners region, a low pressure gradient over the Colorado River Valley, and the Bermuda High off the southeastern US coast (Ellis et al., 2004). These three systems create a vacuum effect, which pulls winds into the Southwest that convey moisture from the Pacific Ocean, Gulf of California, and Gulf of Mexico (Ellis et al., 2004; Hales, 1974). Surface heating combined with orographic uplift sends the moist air skyward, which in turn produces frequent torrential rain events across the Southwest (Ellis et al., 2004). As Figure 13 illustrates, the monsoon supplies the vast majority of El Paso's precipitation (Nielsen-Gammon, 2011). The monsoon also disburses the majority of the whole southeastern corner of the Southwest's precipitation while Pacific frontal systems provide most of the northwestern corner of the Southwest's precipitation (Weiss et al., 2009).

The Southwest's unpredictable rainfall patterns make the region prone to drought (Sheng, 2013; Weiss et al., 2009). Tree ring records show that a major drought struck the Southwest in the 1100s, which scientists consider the worst drought in recent paleoclimate records (Cook, Woodhouse, Eakin, Meko, & Stahle, 2004; Meko, Stockton, & Boggess, 1995; Weiss et al., 2009). Tree ring records also document the sixteenth century drought, the most severe drought in the last 500 years, which is believed to have provoked intense fighting between European settlers and Native Americans (Meko et al., 1995; Stahle et al., 2000; Weiss et al., 2009). More recent important drought events include the drought of the late 1890s and early 1900s, the 1950s drought, and the early 2000s drought (Fye, Stahle, & Cook, 2003; Quiring & Goodrich, 2008; R Seager, 2007; Swetnam & Betancourt, 1998; Weiss et al., 2009).

Causes of Precipitation in the Southwest

The Pacific Decadal Oscillation (PDO), the Atlantic Multidecadal Oscillation (AMO), and the El Niño Southern Oscillation (ENSO) are important oceanic and atmospheric cycles that influence spatiotemporal variability of sea surface temperatures (SST), which drive precipitation sequences in the Southwest (Weiss et al., 2009). Figure 1 in Weiss and others (2009) compares ENSO, PDO, and AMO phases with precipitation and temperature patterns from 1945 to 2007. Both the 1950s and early 2000s droughts occurred when ENSO was predominantly in a La Niña phase, the PDO was primarily in a cool phase, and the AMO was mainly in a warm phase (Weiss et al., 2009). Weiss and others (2009) confirm that these phases of ENSO, PDO, and AMO play an important role in causing drought in the Southwest by suppressing jet stream and SST configurations that are favorable to precipitation. However, it is unclear if anthropogenic climate contributed to the droughts of the 1950s and early 2000s (Weiss et al., 2009). Therefore, more research is needed to ascertain how anthropogenic climate change influences the precipitation-causing phases of the ENSO, PDO, and AMO cycles and other factors that influence precipitation patterns in the Southwest (Anthes et al., 2006; Cane, 2005; St. Jacques, Sauchyn, & Zhao, 2010; Weiss et al., 2009).

Temperature Patterns of the Southwest

Temperatures across Texas and the Southwest will continue to rise significantly in the upcoming decades (Karl, Melillo, & Peterson, 2009; Nielsen-Gammon, 2011; Sheng, 2013). Global warming could alter the strength, frequency, and duration of the drought-causing phases of ENSO, PDO, and AMO (Anthes et al., 2006; Cane, 2005; Sheng, 2013; St. Jacques et al., 2010; Weiss et al., 2009). If this occurs, rainfall patterns across the Southwest could become

more unpredictable (Sheng, 2013). The broader Southwest rainfall patterns affect El Paso's water situation because its surface water supply depends on precipitation levels along the Rio Grande upstream of the city (EPW, 2015). Thus, the combination of erratic precipitation patterns and rising temperatures puts further stress on El Paso's water supplies (Nielsen-Gammon, 2011; Revelle & Waggoner, 1983).

Methodology

PRISM Model

I used the Parameter-elevations Regressions on Independent Slopes (PRISM) model, which researchers at Oregon State University's climate analysis program developed in 1991, to illustrate precipitation and temperature trends across El Paso County from 1979 to 2015 (Daly, Taylor, & Gibson, n.d.). The PRISM model includes point data, a digital elevation model (DEM), and various spatial datasets to map precipitation and temperature patterns across the United States, Canada, and other nations (Daly, Neilson, & Phillips, 1994; Daly et al., n.d.). The model maps precipitation and temperature using regularly spaced grid cells spread across study areas (Daly et al., 1994). Each grid cell within the PRISM model has a resolution such as 4km, which represents an area of 4km x 4km and has its own average precipitation and temperature data across the cell that corresponds to the findings from the nearest measuring stations (Daly et al., 2008, 1994). PRISM collects precipitation data from approximately 13,000 stations and temperature data from approximately 10,000 stations across the United States and Canada (Daly et al., 2008). A variety of agencies administer PRISM stations. These agencies, summarized in Table 3 of Daly and others (2008), include the National Weather Service Cooperative Observer

Program, the Weather Bureau Army Navy, and Remote Automatic Weather Stations supported by the United States Forest Service and the Bureau of Land Management.

The PRISM model analyzes is the effect of elevation on precipitation and temperature (Daly et al., 2008, 1994). PRISM estimates the orographic effect of precipitation on elevation at each precipitation station using a DEM with grid cells spaced at five-minute latitude and longitude intervals (Daly et al., 1994). PRISM allocates a topographic facet to each grid cell by assessing slope orientation (Daly et al., 1994). PRISM then estimates precipitation at each DEM cell with a windowing technique that creates a precipitation-DEM elevation regression function for the cell's facet from nearby precipitation stations (Daly et al., 1994). To account for uncertainty in precipitation estimates, PRISM creates a prediction interval whenever possible (Daly et al., 1994). To address temperature inversions as well as general temperature fluctuations with altitude, PRISM obtains temperature data for higher elevations from the Global Upper-Air Climatic Atlas, which uses model grid point data from the European Center for Medium Range Weather Forecasting (Daly et al., 2008).

In order to provide a thorough measurement of precipitation and temperature levels in each grid cell, PRISM constantly adjusts its frame of reference to account for small changes in elevation regimes across cells (Daly et al., 2008, 1994). To do this, PRISM uses multiple nearby stations whose data are weighted for each grid cell, which means that data from some stations play a larger role in forming the temperature and precipitation profile for a given grid cell than others (Daly et al., 2008). The variables that the weighting function incorporates include clustering, which limits the influence of stations placed close to many other stations, topographic facets, which integrate elevation's effects, and topographic indices, which measure a station's

propensity to absorb pools of cold air during inversion periods (Daly et al., 2008). Figure 2, Table 1, and Figure 4, along with their corresponding descriptions in Daly et al (1994), as well as Section 4 in Daly et al (2008) provide further details on the structure, variables, and equations PRISM uses to devise the functions that create precipitation and temperature datasets for grid cells.

PRISM incorporates various quality control measures in order to ensure the integrity and accuracy of the datasets it creates. Each station that provides PRISM with temperature and precipitation data does so for each hour in 24-hour intervals (Daly et al., 2008). At least 85% of all data points must be complete in order for a dataset to be considered valid (Daly et al., 2008). PRISM researchers calculated monthly precipitation averages at each station from 1971 to 2000 for each station with complete data during that period (Daly et al., 2008). Stations without complete data during that period had their averages calculated from data derived from their period of record and were adjusted to include a 30-year mean (Daly et al., 2008). Appendix A in Daly et al (2008) contains details on how these stations' data were adjusted. These averages were checked against historical records from locations close to the stations stored in ASSAY_QC, a database within PRISM (Daly et al., 2008; Gibson et al., 2002). Pages 182-183 in Gibson et al (2002) provide details on the methodology behind the ASSAY_QC test. Stations whose results ASSAY_QC listed as outliers had their data listed as missing (Gibson et al., 2002).

Another quality control measure checks temperature and precipitation stations for negative or anomalous values (Daly et al., 2008). The threshold for extreme temperature observations was 3°C above the record maximum temperature or 3°C below the record minimum temperature recorded in the state in which the station was located (Daly et al., 2008).

Temperature data from SNOTEL datasets had a propensity to display values within 0.1°C for ten or more consecutive days (Daly et al., 2005, 2008). Records that showed this behavior were set to missing (Daly et al., 2005, 2008). Section 2 in Daly et al (2005) details the adjustment process for affected SNOTEL temperature data. The threshold for extreme precipitation readings was any finding above 115% of the state record for precipitation during a 24-hour period (Daly et al., 2008). The criteria for anomalous readings were set above and below respective record values in order to incorporate potential new records into the data (Daly et al., 2008). Observations that exceeded these thresholds or showed negative precipitation were designated as missing data and discounted (Daly et al., 2008). Researchers also checked station elevations against corresponding points on a DEM to ensure elevation accuracy (Daly et al., 2008). Discrepancies in elevation between the DEM and station readings of greater than 200 meters were investigated and adjusted as necessary (Daly et al., 2008).

Weaknesses of the PRISM model include the fact that temperature and precipitation data for a given grid cell are the average values across that cell (Daly et al., 1994). If a grid cell is topographically diverse, precipitation and temperature data can deviate significantly from the cell's average. This means that average cell values may not represent those at some points in the cell (Daly et al., 1994). To minimize this effect, PRISM must rely on smaller resolutions, which require greater computing power (Daly et al., 1994). Another weakness is the limited number of measuring stations, which can lead to uncertainty and unrepresentative readings (Daly et al., 2008, 1994). Lastly, correctional measures to account for these uncertainties may yield adjusted readings that further diverge from actual figures (Daly et al., 2008).

Despite its weaknesses, PRISM maps are at the forefront of climate and precipitation datasets. PRISM has supplied official, peer-reviewed precipitation maps for all 50 states and the maps of a new official climate Atlas of the United States (Daly et al., 2008). PRISM also created climate maps for the contiguous United States that include 112 years of precipitation and temperature data (Daly et al., 2008). These accomplishments demonstrate the important role the PRISM model plays in precipitation and temperature mapping in the climatological and meteorological communities.

Englehart & Douglas (2003)

Englehart and Douglas (2003) utilized monthly temperature data from the United States Historical Climatological Network (USHCN) and the Mexico's National Meteorological Service (SMN) to measure temperature changes across southern New Mexico, south Texas, far west Texas, and northern Mexico. The study quantifies temperature trends in °C/decade using Spearman's rho test and the ordinary least squares regression test with a significance level of $P < 0.05$ (Englehart & Douglas, 2003). Data points came from readings from eleven USHCN stations in the United States and ten SMN stations in Mexico (Englehart & Douglas, 2003). Figure 1 in Englehart and Douglas (2003) displays the stations' location, including one in El Paso. The American stations had complete datasets while datasets from the Mexican stations had anywhere from 1% to 10% of monthly records missing (Englehart & Douglas, 2003). Furthermore, American stations had thorough documentation of station moves and instrument adjustments while their Mexican counterparts did not (Englehart & Douglas, 2003).

The combination of incomplete monthly temperature records and sparse reporting of station moves and instrument adjustments among Mexican stations limits the conclusions one

can make from their findings (Easterling, Peterson, & Karl, 1996; Englehart & Douglas, 2003). The stations were classified into three types based on population figures close to the station: 1) rural, 2) small urban, and 3) large urban (Englehart & Douglas, 2003). Stations whose nearby population, based on figures from the 2000 American and Mexican censuses, was below 2,500 were rural, those whose adjacent population was between 2,500 and 25,000 were small urban, and those whose surrounding population was greater than 25,000 were large urban (Englehart & Douglas, 2003). Stations located in urban areas on the US-Mexico Border were classified based on population figures on the American and Mexican sides of the border (Englehart & Douglas, 2003).

To ensure the integrity of datasets from each station, the researchers created time series plots between temperature and monthly values at each station to identify outliers (Englehart & Douglas, 2003). Using scatterplots, the researchers then compared stations with outliers to the records of stations within 50 km that partially overlapped with those of the original station (Englehart & Douglas, 2003). The stations used for comparison were not used in the researchers' study (Englehart & Douglas, 2003). If the scatterplots and the time series plots agreed that a data point was an outlier, said data point was removed and its values were listed as null (Englehart & Douglas, 2003). To estimate the value of data points listed as null, the researchers used the 'single best estimator' approach (Eischeid, Pasteris, Diaz, Plantico, & Lott, 2000; Englehart & Douglas, 2003). This technique replaces the null data point with the corresponding value from a nearby station whose results have the highest correlation with the rest of the data values from the null data point's station (Eischeid et al., 2000). Importantly, the

selected proxy station had to have a similar climatological pattern to that of the original station (Englehart & Douglas, 2003).

Englehart and Douglas's (2003) study contains some key weaknesses. The incomplete datasets and instrument adjustment problems at Mexican stations undermine the strength of the findings from these stations. Furthermore, the researchers failed to state whether the 'single best estimator' approach or other techniques could correct for these issues at the Mexican stations (Englehart & Douglas, 2003). Englehart and Douglas (2003) also omitted to explain the criteria they used to determine if proxy stations used for the 'single best estimator' approach had similar enough climatological regimes to those of stations with null data points. Lastly, the researchers failed to address how they accounted for the potential imperfections from readings as a result of instrument adjustment biases and the 'single best estimator' approach (Easterling et al., 1996; Englehart & Douglas, 2003).

WaterSim Model

Gober and Kirkwood (2010) use the WaterSim model to forecast the consequences of global warming on Phoenix's long-term water supply and suggest policy measures to sustainably manage Phoenix's growth while maintaining consistent water supplies for its growing population. WaterSim predicts Phoenix's future water consumption and availability patterns based on various scenarios of growth, urbanization, climatic uncertainty, and policy decisions from 2010 through 2030 (Gober & Kirkwood, 2010; Gober, Wentz, Lant, Tschudi, & Kirkwood, 2011). Gober and Kirkwood used various climate situations from the 2007 Intergovernmental Panel on Climate Change report to determine the values for WaterSim's input variables (Gober & Kirkwood, 2010; Solomon et al., 2007).

WaterSim uses the XLRM framework, which Lempert and others (2003) developed. ‘X’ stands for exogenous uncertainties, which are issues outside policymakers’ control but nevertheless important in policy formation (Lempert, Popper, & Bankes, 2003). An example for Phoenix is the minable groundwater supply (Gober et al., 2011). ‘L’ stands for policy levers, short-term actions that policymakers can take to immediately address the primary pressing issues (Lempert et al., 2003). Policy levers for Phoenix’s water supply include the retirement of nearby agricultural land and water-shortage plan adjustments (Gober et al., 2011). ‘R’ signifies relationships, which illustrates the way policy measures shift future outcomes (Lempert et al., 2003). In the case of Phoenix, the ‘R’ points to the equations within the WaterSim model that will provide the results that influence policy decisions (Gober et al., 2011). Section 3.1 in Gober et al (2011) describes the water supply and demand equations. ‘M’ refers to measures, or performance standards, that decision makers use to assess the desirability of different scenarios (Lempert et al., 2003). Water availability in gallons per capita daily is an example of ‘M’ as applied to Phoenix’s water situation (Gober et al., 2011). Table 1 in Gober and others (2011) displays more examples of components that comprise the XLRM framework.

WaterSim uses a stock-and-flow diagram to synthesize XLRM and create an idea on future water supply and demand scenarios for Phoenix (Gober et al., 2011). The main supply sources are the Salt/Verde and Colorado Rivers while the main demand predictor is population growth and land use patterns (Gober et al., 2011). The Colorado River water supply component of the model accounts for the rules of the Colorado River Compact (Gober et al., 2011). Figure 3 in Gober et al (2011) depicts WaterSim’s stock-and-flow diagram components that comprise Phoenix’s water supply and demand profile while Figure 5 in the same article shows WaterSim’s

input variables and corresponding output results. WaterSim's key weaknesses include the lack of water pricing and other water use reduction incentives as an influential variable on water demand, the exclusion of hypothetical water reuse infrastructure, and failure to explicitly include precipitation patterns as part of its calculations (Gober et al., 2011).

PRISM Model Results

PRISM Model Setup

The general understanding of precipitation pattern changes in light of global warming involves more humid areas becoming wetter while drier areas will become drier (Liu et al., 2012; Richard Seager, Naik, & Vecchi, 2010; Solomon et al., 2007). The PRISM model results for El Paso County point to a slight increase in mean annual temperatures across the county from 1979 to 2015 while precipitation patterns for the same time period in general also show a slight increase. The first step to configuring the PRISM model involved downloading the annual precipitation and average annual temperature data for all pertinent grid cells. Pertinent grid cells are those that are located partially or entirely within the blue outline of El Paso County in the right image of Figure 16.

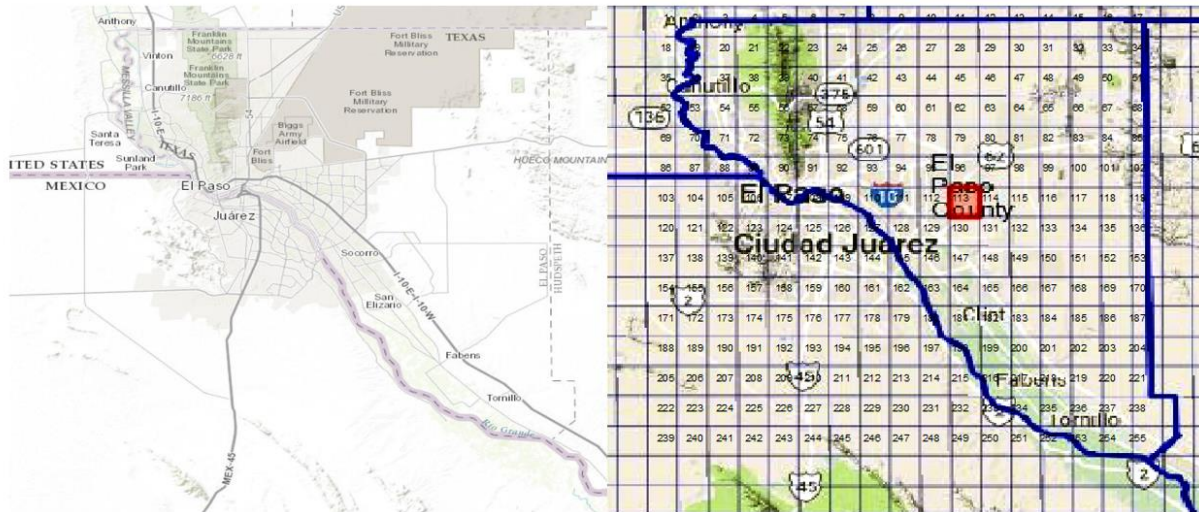


Figure 16 – PRISM grid cells (right image) used to map precipitation and temperature trends in El Paso County from 1979 to 2015 along with a topographic map of El Paso County (left image) from ArcMap.

My next step involved configuring ArcMap to illustrate annual precipitation and mean annual temperature patterns from PRISM data in El Paso County from 1979 to 2015 (see Figures 35 and 36) and to create an elevation profile of El Paso County (see Figure 18) to ascertain if elevation played a role in annual precipitation and mean annual temperature patterns. To begin, I composed a fishnet in ArcMap (see Figure 16), which consists of a set of grid cells that mimic those from the PRISM model. The grid cells in the fishnet were used to create a spatial reference with which I connected the data from the PRISM grid cells to the correct point in El Paso County in ArcMap. I did this by aligning the fishnet cells with the PRISM cells and then giving both sets of cells a common number that I used to pair datasets with cells. I then created tables that compiled the average year-over-year (YOY) changes in annual precipitation and average YOY mean annual temperature changes for each grid cell for the years 1979 through 2015. I utilized this measure to assess precipitation and temperature trends across El Paso County.

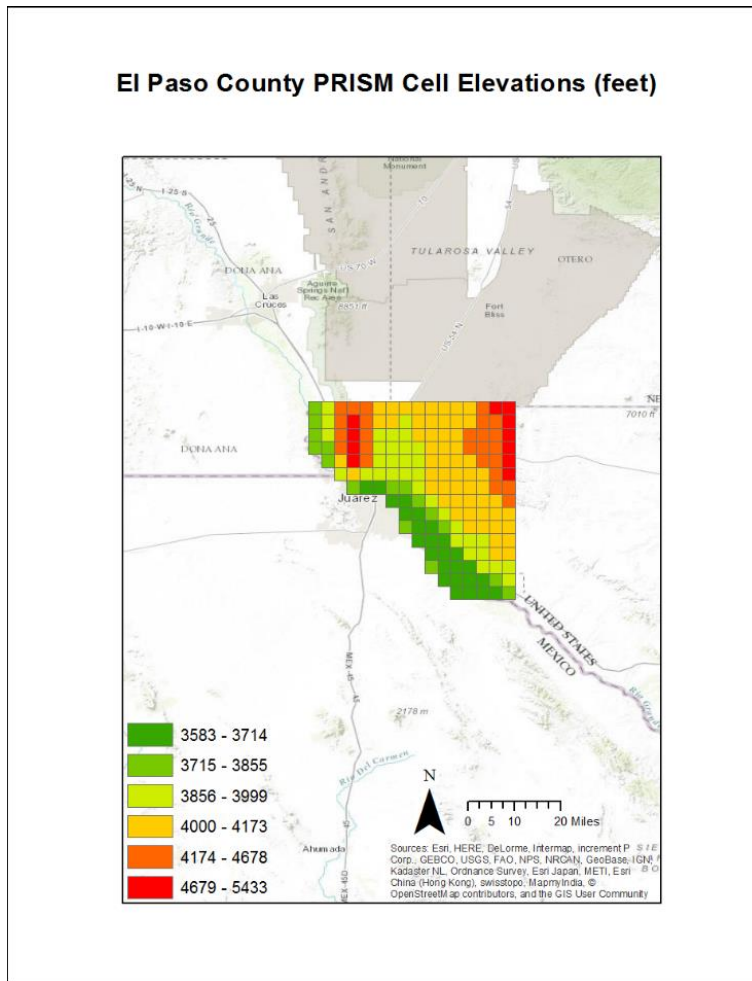


Figure 17 – Elevation of El Paso County PRISM grid cells

El Paso County Precipitation Trends

Figure 18 shows average YOY annual precipitation changes while Figure 19 shows average YOY changes in mean annual temperature. The first (top left) and last (bottom right) grid cells in both figures are colored gray because they serve as anchor points for the entire group of cells that covers El Paso County. Miguel Pavón, an ArcMap expert from the Texas Water Development Board, stated that these anchor points are necessary to prime ArcMap’s time slider function, which associates the average YOY annual precipitation or average YOY mean annual temperature change variables with the years 1979 to 2015 as the time variable (personal

communication, May 5, 2017). These anchor points are primed with minimum and maximum values for the entire group of cells because initial color-ramp symbology can't be drafted with null values; some initial min and max values are needed for 1979 and 2015, the first and last years, respectively (M. Pavon, personal communication, May 5, 2017). In order for the time slider function to process the entire group of cells, I had to select the first and last cells in the group (M. Pavón, personal communication, May 4, 2017). Because these minimum and maximum anchor values created anomalous readings for those cells, I excluded them from the dataset and instead labeled them as anchors in the legend.

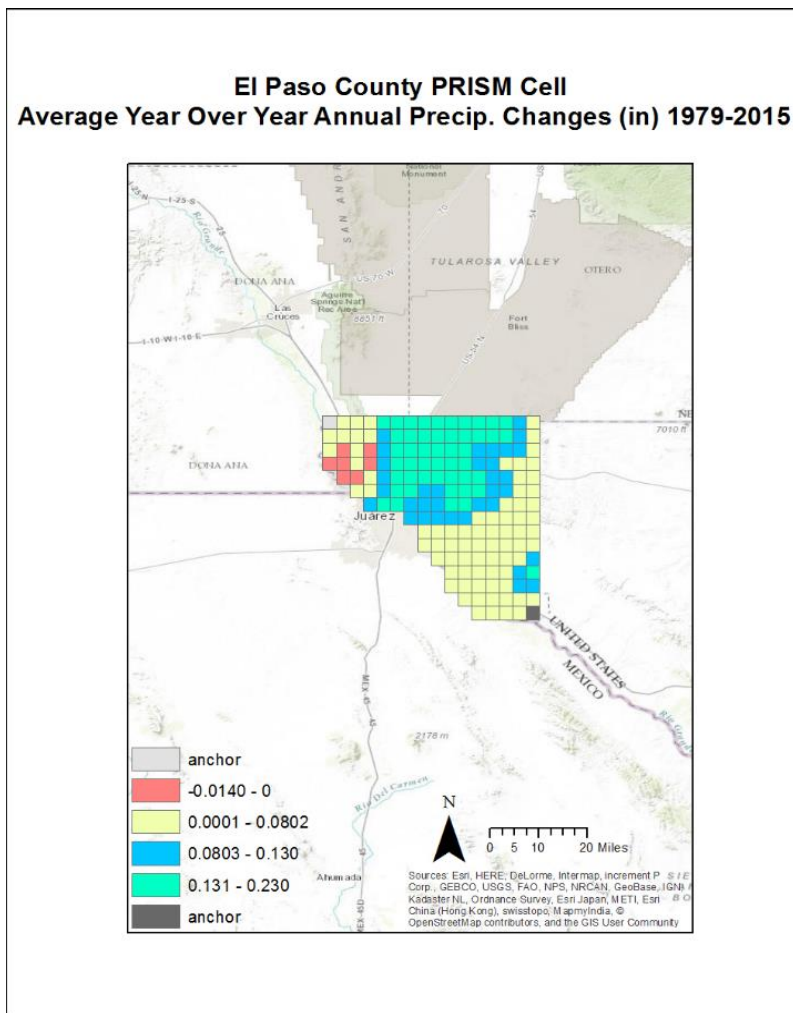


Figure 18 – Average YOY annual precipitation changes in El Paso County from 1979-2015

El Paso County's average YOY annual precipitation changes are relatively minimal in the southeast, far east, and northwest parts of the county. The north central part of the county, which encompasses the southeastern portions of the City of El Paso and Fort Bliss Military Reservation (see Figure 16) has the highest increases in average YOY annual precipitation change. But, the most their average YOY annual precipitation change increases is 0.23 inches. As Figure 17 confirms, these areas are mostly located in the county's middle elevation brackets, which does not suggest that high elevation plays a role. A tiny cluster of cells around the central and inner east and west sides of the City of El Paso shows a nominal decrease in average YOY precipitation changes. The PRISM model's findings of mostly negligible average YOY annual precipitation changes indicate that climate change's influence on precipitation patterns is unclear and uncertain, and therefore more investigation is necessary to ascertain how climate change will affect the key drivers of precipitation patterns in El Paso and the Southwest as a whole (Anthes et al., 2006; Cane, 2005; Liu et al., 2012; St. Jacques et al., 2010; Weiss et al., 2009). But, uncertain precipitation patterns could force El Paso to rely more on increasingly brackish groundwater resources, which in turn would require more water desalination (EPW, 2015, 2016).

Figures 2.19-2.21 in Nielsen-Gammon (2011) show the nine-year running mean of far west Texas' average annual precipitation values for 1980 through 2000 fluctuating between 1.25 times above and 1.25 times below the long-term mean precipitation values for far west Texas between 1901 and 2000. These graphs suggest that El Paso and the rest of far west Texas' precipitation patterns have drifted back and forth between large deficits relative to the long-term mean and large surpluses relative to the long-term mean during this period (Nielsen-Gammon,

2011). The exceptionally low average YOY annual precipitation changes depicted in Figure 18 combined with the presence of some negative average YOY annual precipitation changes in some cells could be evidence that confirms Nielsen-Gammon's (2011) findings of fluctuating precipitation patterns in far west Texas. The reason for this is due to the fact that low average YOY annual precipitation changes could be indicative of a large number of years with strong positive YOY annual precipitation changes combined with an equally large number of years with strong negative YOY annual precipitation changes, which leads to average YOY annual precipitation change values close to zero.

Phoenix and El Paso Precipitation Trend Comparison

Shepherd (2006) uses a combination of the Spatial Climate Analysis Service model, the PRISM model, and the Tropical Rainfall Measuring Mission model to measure changes in Phoenix's precipitation patterns from its pre-urban period (1895-1949) to its post-urban period (1950-2003). The models showed a statistically significant increase of 12-14% in mean precipitation rates in Phoenix between these time periods (Shepherd, 2006). Shepherd (2006) eliminates solely topographic factors as a cause and hypothesizes the reasons for this change to be interactions between urbanized surfaces and topography and irrigation activities related to agriculture. El Paso is also close to mountains, and therefore, has relatively similar topographic patterns to those of Phoenix (see Figures 33 and 34). There is also a lot of irrigation in El Paso County associated with agriculture (Fullerton, 2006). Consequently, the positive average YOY annual precipitation change values across most of El Paso County could be attributed to similar factors to those Shepherd (2006) found in Phoenix. Hence, El Paso would be a good future case

study for Shepherd and other researchers to see if the patterns they found in Phoenix apply to other urban areas in the Southwest with profiles similar to that of Phoenix.

El Paso County Temperature Trends

El Paso County's average YOY mean annual temperature changes (see Figure 19) all show positive values. The southeast part of the City of El Paso and its surrounding suburbs as well as Fort Bliss Military Reservation (see Figure 16) are in the two highest average YOY mean annual temperature change brackets. These areas are also spread evenly across all but the highest elevation bracket (see Figure 17). Interestingly, all areas in the highest elevation bracket show the lowest average YOY mean annual temperature change. However, the cells on the west side of the City of El Paso and those in the southernmost part of El Paso County are in the three lowest elevation brackets as well as the lowest average YOY mean annual temperature change bracket. This does not suggest that elevation plays a role in predicting average YOY mean annual temperature change values.

**El Paso County PRISM Cell
Average YOY Mean Annual Temp. Changes (°F) 1979-2015**

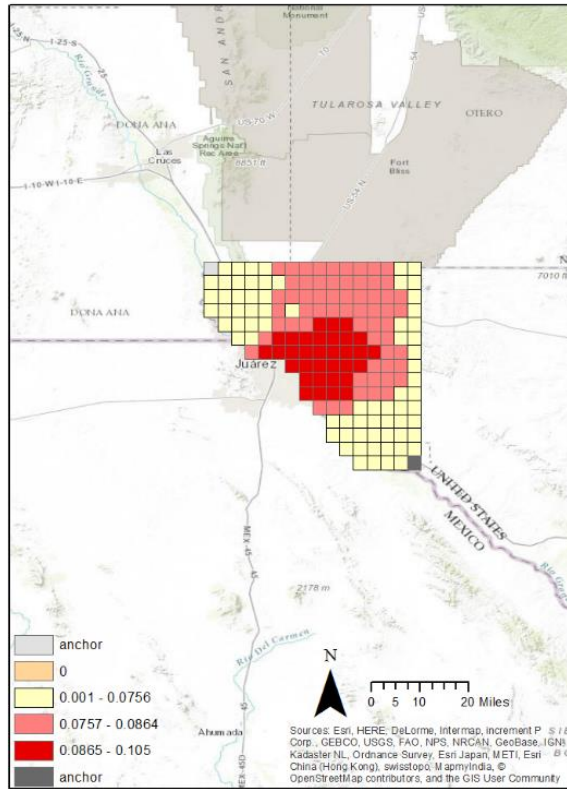


Figure 19 – Average YOY mean annual temperature changes in El Paso County from 1979-2015

The highest average YOY mean annual temperature changes in El Paso County are only between 0.076°F and 0.110°F. These are much less than the 0.37°C (0.66°F) increase in mean temperature per decade for the Southwest as a whole between 1982 and 2012 according to Sheng (2013). Unfortunately, Sheng did not specify the basis for this claim. More research is needed to convert my PRISM data to mean temperature increases per decade to ascertain if El Paso’s average temperature increases during this time period are lower relative to that for the entire Southwest. But, that research is beyond the scope of this thesis. Nonetheless, the PRISM data

do show evidence of slight temperature increases across El Paso County between 1979 and 2015, which indicates agreement with Nielsen-Gammon's (2011) temperature findings for far west Texas.

Comparison of El Paso County Precipitation Trends to Findings of Englehart & Douglas (2003)

Englehart and Douglas (2003) show statistically significant changes in minimum and maximum annual temperatures for all seasons between 1941-1970 and 1971-2000 across all stations regardless of class. They do not provide mean annual temperature increases but rather increases in winter minimum temperatures of $0.65^{\circ}\text{C}/\text{decade}$ and increases in summer minimum and maximum temperatures of $0.74^{\circ}\text{C}/\text{decade}$ and $0.62^{\circ}\text{C}/\text{decade}$, respectively, for the El Paso station (Englehart & Douglas, 2003). Their model also shows a statistically significant difference between the temperature increases of the stations in 'large urban' areas and those in 'rural' areas between the two aforementioned time periods (Englehart & Douglas, 2003). This phenomenon suggests the presence of an urban heat amplification effect (Englehart & Douglas, 2003). The PRISM cells in the two highest average YOY mean annual temperature increase brackets (see Figures 33 and 36) are not confined to the urbanized parts of El Paso County. This could indicate that the urban heat island effect from Englehart and Douglas (2003) extends to the rural areas immediately adjacent to an urban area, which could increase overall temperatures in the El Paso area and entire Southwest due to rapid urbanization trends. This is an important concept for future research to investigate.

Meaning of PRISM Model Findings

More research is needed to evaluate the meaning of my PRISM findings as well as how they compare with other measurements of precipitation and mean annual temperature trends in

El Paso County. This involves comparison with other models and methodologies that measure precipitation and mean annual temperature trends not only for El Paso specifically but also for the rest of the Southwest. This research also needs to look at factors that could influence El Paso's precipitation and temperature patterns differently from those of the greater Southwest. These include urban heat island effects, topographic influences, air pollution, and the conversion of desert scrubland to accommodate the expanding City of El Paso (Feddema et al., 2005; Nielsen-Gammon, 2011). Given El Paso's proximity to Juarez, a city that has twice El Paso's population and is growing even more quickly, future investigation must include Juarez's temperature and precipitation patterns as well as the aforementioned variables' effects on them because Juarez's growth and corresponding land use change could influence temperature and precipitation regimes in both cities (Fullerton, 2006; Pick, Viswanathan, & Hettrick, 2001).

The Southwest is expected to become more arid in the future due to increasing temperatures, which in turn increase evapotranspiration of water into the atmosphere (Liu et al., 2012; R Seager et al., 2007; Weiss et al., 2009). These events mean that the Southwest will also have to contend with the possible emergence of decreased precipitation and the increased likelihood of more erratic precipitation patterns (Liu et al., 2012; R Seager et al., 2007; Weiss et al., 2009). My PRISM model results point to increased temperatures and possibly more erratic precipitation patterns in El Paso. Given that such a scenario would require El Paso to depend more on increasingly saline groundwater supplies, increased desalination capacity and further water reduction measures such as limiting the filling and construction of backyard pools and golf courses may be necessary to help the city continue to exist in an increasingly water-scarce environment (EPW, 2015, 2016; Gober et al., 2011; MacDonald, 2010; Nielsen-Gammon, 2011).

Discussion

Applicability of WaterSim Model Findings to El Paso

Gober et al (2011) concluded that Phoenix would have to adopt policies that included restricting the construction of backyard swimming pools, restricting population growth, and restricting residential water consumption to available surface water supplies in order for the city to maintain a steady water supply in light of increasing temperatures due to climate change. Gober and others' (2011) findings are based on WaterSim model scenarios that predict that climate change will reduce surface water supplies from the Salt-Verde River system by 50% and Colorado River water supplies by 30% (Gober et al., 2011). With population growth between 100% and 150% of anticipated projections, groundwater would have to become 60-65% of Phoenix's water supplies in order to support current water consumption habits and population growth (Gober et al., 2011). These levels of groundwater withdrawal would lead to land subsidence and water quality problems that existed prior to the passage of Arizona's 1980 Groundwater Management Act (Connall, 1982; Gober et al., 2011). To avoid land subsidence and the problems associated with it, Phoenix would have to maintain average groundwater supplies at 227,000 acre-feet over five-year periods to accommodate expected population growth (Gober et al., 2011). If population growth rates reach 150% of current forecasts, per capita water consumption levels would need to fall from 848 liters per capita daily (LPCD) in 2010 to 148 LPCD by 2030 (Gober et al., 2011). If population growth rates stay at 100% of current projections or fall to 50% of current projections, then per capita water consumption would have to decline to 178 LPCD and 204 LPCD, respectively, by 2030 (Gober et al., 2011).

The City of El Paso already has stringent water conservation ordinances and penalties as well as water conservation incentives and educational programs, which are described in detail in section 2.1 (EPW, n.d., 2014). These include policies that restrict landscaping and car washing at residences (EPW, n.d., 2014). However, these policies do not include restricting the construction of backyard swimming pools, restricting population growth, or restricting residential water consumption to available surface water supplies (EPW, n.d., 2014). They also do not include incentives to encourage construction of high-density multifamily dwellings, which reduce per capita water consumption (EPW, n.d., 2014; Gober et al., 2011). The constant back-and-forth movement between residents of El Paso and Juarez would likely make restricting growth difficult for the City of El Paso and El Paso County (Lapeyrouse et al., 2011). However, the other policy measures Gober and others (2011) suggest could be viable options for El Paso to further conserve water. More research is required to analyze and address the obstacles within El Paso towards implementing such ambitious policies. Nevertheless, Juarez's growing population could undermine El Paso's conservation efforts because the two cities share the same surface and groundwater resources (see Figure 5) (Fullerton, 2006; Pick et al., 2001). This is a testament to the fact that water conservation policies in the El Paso area would require a sincere, collaborative effort with Juarez. Consequently, future research should also assess how El Paso and Juarez can collaborate on effective water conservation measures that adequately accommodate the water needs of a growing population on both sides of the border (Gober et al., 2011; Pick et al., 2001).

Influence of Climate Change on Role of Water Desalination in Phoenix and El Paso

Given the Phoenix area's warming temperatures and the Southwest's propensity for drought, Phoenix's groundwater resources face the possibility of increased salinization (Baker, Brazel, & Westerhoff, 2004; Sheng, 2013; Weiss et al., 2009). Just like El Paso, Phoenix would have to develop reverse osmosis (RO) plants to remove salts (Baker et al., 2004; EPW, 2015). The primary issues with RO is the high amount of energy required to remove salts and the fact that the process loses 10-20% of the intake water as brine (Baker et al., 2004; Khawaji, Kutubkhanah, & Wie, 2008). Brine disposal is also a key environmental concern (Baker et al., 2004; Halder, Tandon, Chintalapalle, Roy, & Tarquin, 2015). The rise in water demand due to higher temperatures will require desalination to play a greater role in Phoenix, El Paso, and other parts of the Southwest, especially if precipitation patterns remain unpredictable (Baker et al., 2004; EPW, 2015, 2016; Nielsen-Gammon, 2011; Sheng, 2013; Weiss et al., 2009).

Because RO water desalination will form an increasing part of El Paso and Phoenix's water supplies, it is imperative to develop methods to improve the sustainability of RO. Ways to improve RO's sustainability portfolio include capturing brine and converting it into useful products such as mortar, improving the energy efficiency and freshwater production of RO membranes, and incorporating solar power into the energy supply of RO plants (El-Sayed, 2007; Fiorenza, Sharma, & Braccio, 2003; Greenlee, Lawler, Freeman, Marrot, & Moulin, 2009; Halder et al., 2015; MacDonald, 2010). The right balance of water conservation and new freshwater production through RO desalination will ensure that El Paso, Phoenix, and the rest of the Southwest will be able to endure the volatile water situations associated with climate change for many years to come.

Summary

The models appear to agree that climate change is leading to higher temperatures in El Paso and across the Southwest (Gober et al., 2011; Nielsen-Gammon, 2011; Sheng, 2013). But, they appear less conclusive about precipitation patterns for the same region (Liu et al., 2012; Nielsen-Gammon, 2011). My PRISM results provide valuable insight into the effects of climate change on El Paso's precipitation and temperature trends that neither completely agrees with the findings of other literature nor contradicts them. But, they are only the beginning of necessary further exploration to discern a complete understanding of how climate change will drive El Paso's future temperature and precipitation tendencies. Hence, it is vital that future studies analyze how global warming will affect the frequency of the precipitation-causing phases of ENSO, PDO, and AMO that bring precipitation to the Southwest (Anthes et al., 2006; Cane, 2005; St. Jacques et al., 2010; Weiss et al., 2009). Furthermore, El Paso's rapid urbanization calls for more studies into how urban temperature enhancements affect the city's precipitation as well as the temperature profile of the surrounding rural areas (Englehart & Douglas, 2003; Shepherd, 2006).

El Paso's increasingly precarious water situation due to warming temperatures and possibly increasingly variable precipitation patterns will increase the importance of RO desalination as a water supply source, which in turn opens opportunities for El Paso to lead in improving RO desalination's environmental footprint (Baker et al., 2004; El-Sayed, 2007; EPW, 2015, 2016; Fiorenza et al., 2003; Greenlee et al., 2009; Halder et al., 2015; Khawaji et al., 2008). The next two sections describe the important role the KBH plant plays in securing El

Paso's water supplies as well as the measures EPW is taking to minimize adverse environmental effects from the KBH plant.

2.3 THE HISTORY OF THE KBH DESALINATION PLANT & THE RO DESALINATION PROCESS

This section illustrates the important role the KBH desalination plant plays in El Paso's water supplies by providing an overview of why the plant was constructed. This section also explains reverse osmosis (RO), the process the KBH plant uses to desalinate water, through pictures of the plant that illustrate the various stages of RO (EPW, 2016).

The Reasons for the Construction of the KBH Plant

According to EPW and USGS reports, high water use from the Hueco Bolson Aquifer due to rapid growth in El Paso and Juarez from the late 1970s to the present day has depleted the aquifer's freshwater supplies and led to intrusion of brackish water from the nearby Tularosa Basin (see Figure 20) (Bredehoeft, Ford, Harden, Mace, & Rumbaugh, 2004; Heywood & Yager, 2003; Hutchison, 2006; Sheng, 2013).

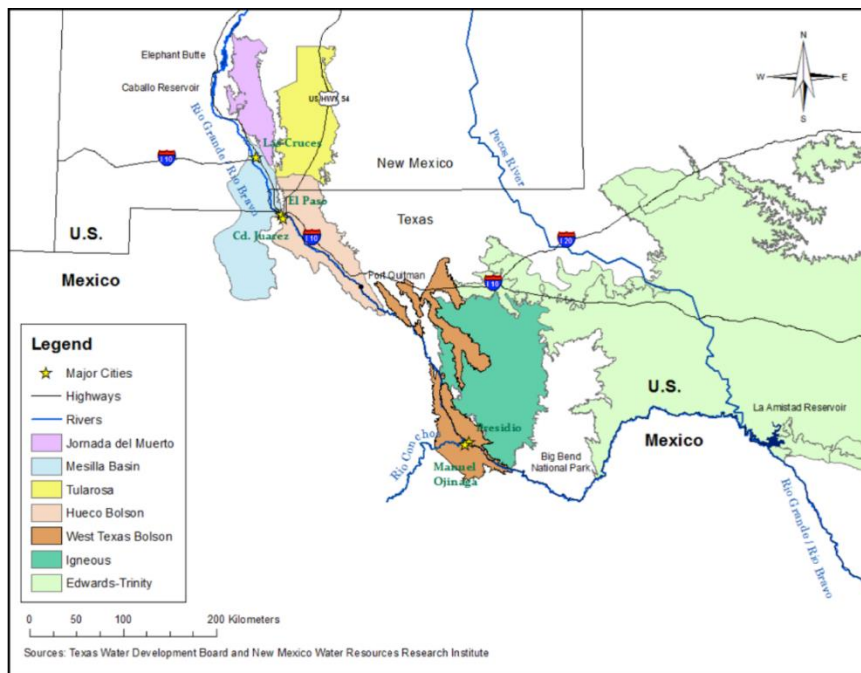


Figure 20 – Map of Hueco Bolson and nearby aquifers (Sheng, 2013).

In response to these reports, EPW and Fort Bliss embarked on a joint project to build the KBH plant, the world’s largest inland desalination plant (EPW, 2016). A 1997 USGS report coupled with extensive drilling of test wells led EPW to select the current location east of El Paso Airport as the plant’s site (see Figure 21) (EPW, 2016; White, Baker, & Sperka, 1997). The plant started operations in 2007 and can produce up to 27.5 million gallons of freshwater daily (MGD) through the RO process (EPW, 2016; M. Perez, personal communication, March 1, 2017). The KBH plant can increase EPW’s freshwater production by 25% based on current consumption patterns and it increases El Paso’s water supplies to accommodate growth for at least 50 years (EPW, 2016). Moreover, the KBH plant captures brackish groundwater flows from the north before they enter freshwater wells (EPW, 2016).

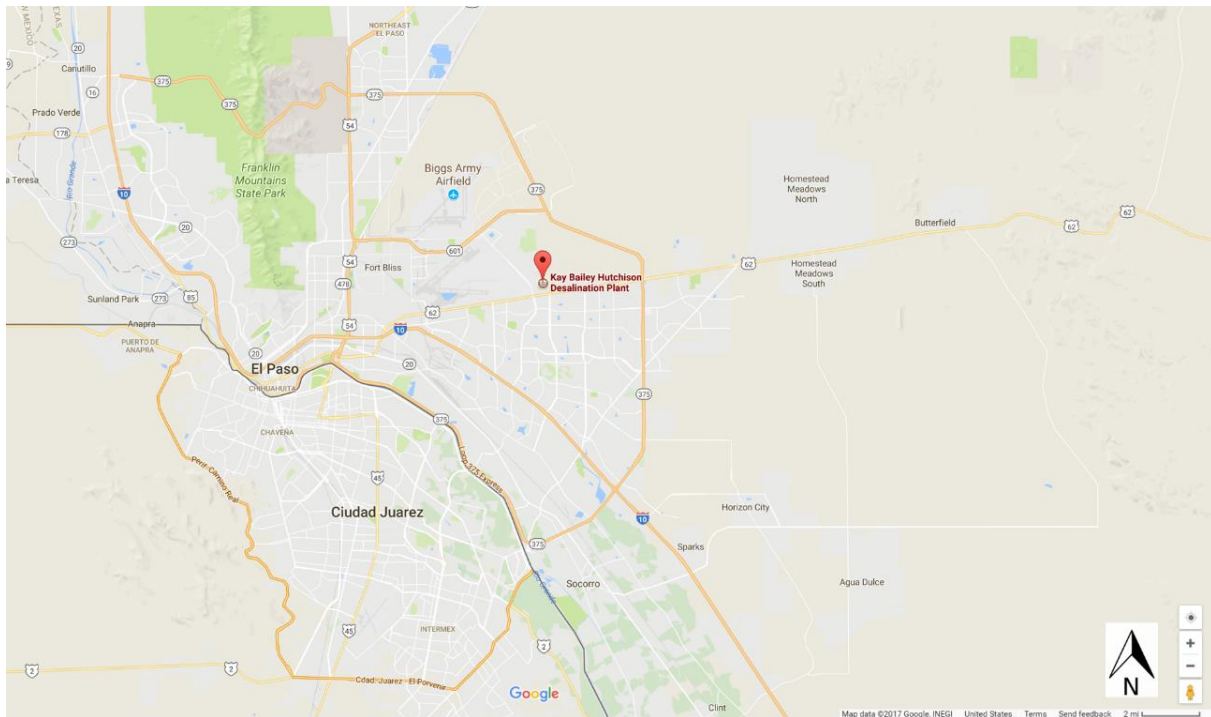


Figure 21 – Location of KBH desalination plant in El Paso (Bing Images, n.d.; Landsat & Google Maps, 2017)

How the KBH Plant Works – the RO Process

The KBH plant produces freshwater by blending desalted water with water drawn from freshwater wells nearby (EPW, 2016). The KBH plant’s production portfolio consists of up to 15.5 MGD of desalted water, or permeate, and up to 12 MGD of water from freshwater wells (EPW, 2016; A. Ruiz, personal communication, August 2, 2016). Up to 3 MGD of brine, or concentrate, is sent to injection wells approximately four thousand feet deep located 22 miles east of the KBH plant (EPW, 2016; A. Ruiz, personal communication, August 2, 2016). Approximately 80% of the brackish water that enters the plant emerges as permeate while the remaining 20% emerges as concentrate (A. Ruiz, personal communication, August, 2, 2016).

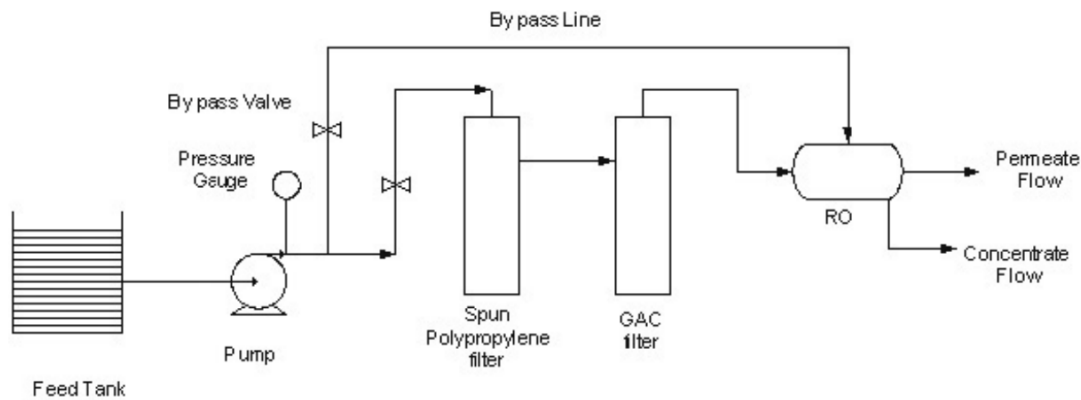


Figure 22 – A diagram of the RO process (Khawaji, Kutubkhanah, & Wie, 2008)

The RO process (see Figure 22) relies on applying an amount of pressure greater than the water’s osmotic pressure across a membrane (Khawaji et al., 2008). The process forces water across the membrane contrary to its natural flow direction at really high pressure, which leaves dissolved solids behind after the water clears the membrane (Khawaji et al., 2008). Although no heating is necessary for RO to work, the process uses enormous amounts of energy to build the

necessary reverse osmotic pressure (Khawaji et al., 2008). The four major steps of the RO process are: 1) pre-treatment of feed water to remove suspended solids and other large particles, 2) high pressure pumping, 3) separation of dissolved solids via a membrane, and 4) post-treatment of permeate (Khawaji et al., 2008).

Electricity Supply & Pre-treatment



Figure 23 – The transformers that power the KBH desalination plant (Photo Credit: Art Ruiz)

Figure 23 displays the two transformers connected to the EPE grid that power the KBH plant while Figure 24 shows the facility in which the feed water undergoes pre-treatment. This process removes debris and other heavy solids (Khawaji et al., 2008).



Figure 24 – Feed water pre-treatment facility (Photo Credit: William Delgado-Thompson)

High Pressure Feed Pump

The next step involves sending the water through a high-pressure feed pump (see Figure 25) to raise its pressure to an appropriate level before it passes through a set of membranes known as a treatment train (see Figure 26) (Khawaji et al., 2008; A. Ruiz, personal communication, August 2, 2016). The KBH plant has a total of five treatment trains (A. Ruiz, personal communication, August 2, 2016).



Figure 25 – High pressure feed pump that sends brackish water to membranes (Photo Credit: William Delgado-Thompson)

Treatment Train & Membrane



Figure 26 – A set of membranes through which brackish water passes known as a treatment train (Photo Credit: William Delgado-Thompson)

As the water goes through these trains, it is separated into permeate and concentrate (Khawaji et al., 2008; A. Ruiz, personal communication, August 2, 2016). Figure 27 displays the type of membrane through which the feed water passes during the RO process.



Figure 27 – The membrane in the trains through which feed water passes (Photo Credit: William Delgado-Thompson)

Feed Water, Permeate, & Concentrate

Figures 21 through 23 show the different levels of total dissolved solids (TDS) that the feed water, permeate, and concentrate contain. They are a testament to the effectiveness of the membranes at removing TDS from brackish water.



Figure 28 – TDS concentration of feed water before RO process (Photo Credit: Art Ruiz & William Delgado-Thompson)



Figure 29 – TDS concentration of permeate after RO process (Photo Credit: Art Ruiz & William Delgado-Thompson)



Figure 30 – TDS concentration of concentrate after RO process (Photo Credit: Art Ruiz & William Delgado-Thompson)

Freshwater Distribution & Concentrate Disposal Pipeline

After the water passes through the membranes, the permeate exits the facility (see Figure 31) and undergoes further treatment before becoming a part of EPW's drinking water supplies while the concentrate goes to the deep injection wells (see Figure 32) (A. Ruiz, personal communication, August 2, 2016). The next section describes the energy and environmental concerns related to the RO desalination process and the measures the KBH plant has adopted to address these issues.



Figure 31 – Permeate pumps that lead freshwater to EPW's distribution system (Photo Credit: William Delgado-Thompson)



Figure 32 – Pipes that take concentrate to the injection wells (Photo Credit: William Delgado-Thompson)

2.4 ENVIRONMENTAL CONCERNS OF DESALINATION

This section describes the environmental concerns associated with water desalination such as brine disposal and energy usage (Shahzad, Burhan, Ang, & Ng, 2017; Younos, 2005). To address these concerns, the KBH plant has taken a variety of measures such as building designs that maximize natural light during daylight hours, a partnership with a Enivro Water Minerals, a firm dedicated to recovering some of the plant's brine and processing it into useful products, and a project with Eaton, a power management company, to track energy usage at different stages of the RO process and improve the plant's energy efficiency (A. Ruiz, personal communication, August 2, 2016; M. Perez, personal communication, August 4, 2016).

KBH Plant Brine Disposal Policies

Before construction could begin on the KBH plant, EPW and Fort Bliss had to submit an environmental impact statement (EIS) to the Environmental Protection Agency (EPA) (S. Reinert, personal communication, September 12, 2016). The EIS is a report that project managers working with federal agencies compile that assesses potential negative effects of a proposed project on the surrounding area's land, air, and water quality (EPA, 2017). After the EPA approved the KBH plant's EIS in 2004, the plant's brine disposal policies were subject to the rules of the Texas Commission on Environmental Quality (TCEQ) (Jansky, 2004; A. Ruiz, personal communication, August 2, 2016; S. Reinert, personal communication, September 12, 2016). TCEQ rules allow brackish water desalination plant operators to dispose of brine in evaporation ponds or deep wells (TCEQ, 2008, 2010). According to Art Ruiz, using evaporation ponds would have required 1400 acres of land in order to accommodate one active pond and one

backup pond, which EPW deemed infeasible (personal communication, August 2, 2016). Hence, EPW decided to use deep injection wells to dispose of concentrate (A. Ruiz, personal communication, August 2, 2016; S. Reinert, personal communication, September 12, 2016).

TCEQ's guidelines for the disposal of brine in deep injection wells state that the wells must have a water supply with a TDS concentration of at least 10,000 mg/L (TCEQ, 2010). They also must be located at least half a mile away from usable drinking water supplies for humans or wildlife (TCEQ, 2010). EPW has to report any buildup of water in the wells to the TCEQ so that the TCEQ can ascertain if any pressure from the buildup will lead to possible environmental damage (S. Reinert, personal communication, September 12, 2016). Because concentrate enters the wells by gravity without any human-induced pressure, the process does not lead to seismic activity concerns (S. Reinert, personal communication, September 12, 2016).

EPW's assessments state that the deep injection wells could accept concentrate from the KBH plant for at least 50 years (EPW, 2016; S. Reinert, personal communication, September 12, 2016). According to Mr. Reinert, if the wells could not accept more injected concentrate, EPW would check the wells to see if they are clogged with scale (personal communication, September 12, 2016). If scale is the culprit, EPW would use acids to break the scale to restore the well's brine acceptance capabilities (S. Reinert, personal communication, September 12, 2016). If this process fails, EPW would consider drilling a new well (S. Reinert, personal communication, September 12, 2016). Although individual wells may need to be replaced or restored, EPW's current assessments state that the area in which the wells are located has the capability of accepting concentrate beyond 50 years (S. Reinert, personal communication, September 12, 2016).

EWM Brine Recovery Partnership

The KBH plant has partnered with Enviro Water Minerals (EWM), a company dedicated to improving the sustainability of water production, to recover some of the brine from the desalination process and convert it into useful products (Enviro Water Minerals Company, n.d.; A. Ruiz, personal communication, August 2, 2016). EWM uses RO and electrodialysis to extract 99% of brine from feed water and uses it to produce products such as gypsum, magnesium hydroxide, and hydrochloric acid (see Figures 33 and 34) (Enviro Water Minerals Company, n.d.). The KBH plant will supply EWM with 1.25 MGD of brine that would have otherwise gone to the injection wells (Enviro Water Minerals Company, n.d.). This constitutes a little more than a third of the plant's average daily brine production (A. Ruiz, personal communication, August 2, 2016). After EWM further extracts brine from the KBH Plant's concentrate, it sends the remaining freshwater back to the KBH plant to distribute into El Paso's water supplies (Enviro Water Minerals Company, n.d.; A. Ruiz, personal communication, August 2, 2016).

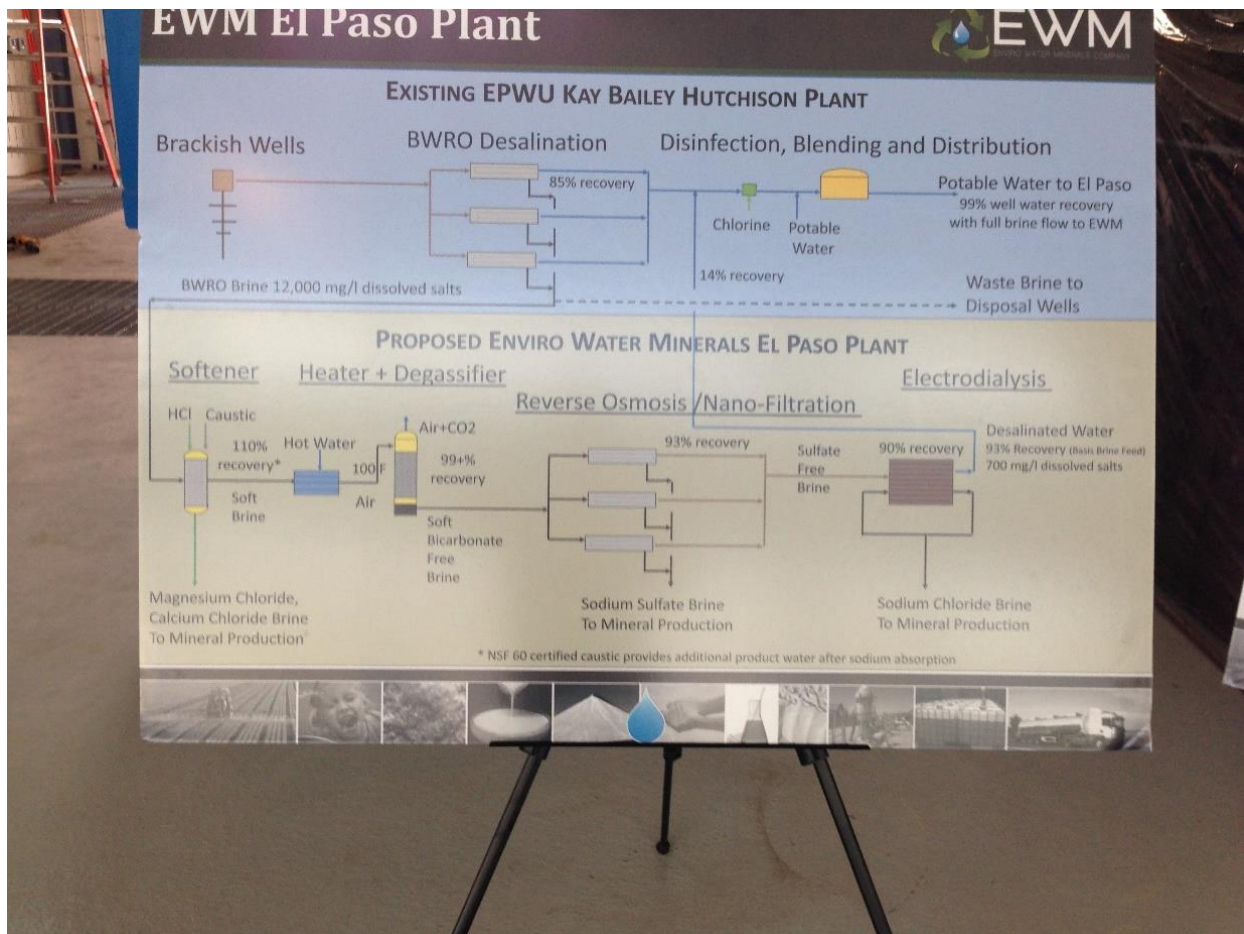


Figure 33 – Diagram of EWM’s brine recovery process (Enviro Water Minerals Company, n.d.) (Photo Credit: William Delgado-Thompson)

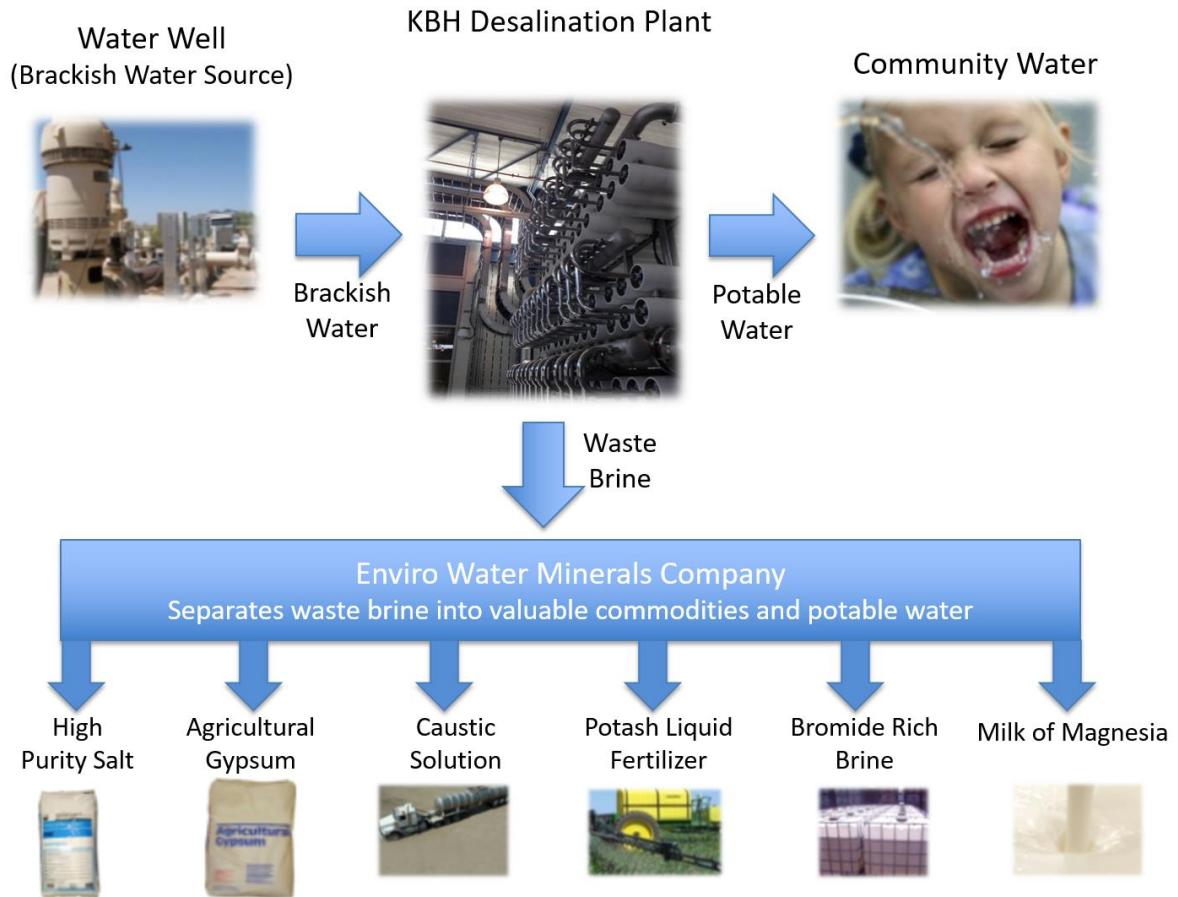


Figure 34 – Chart that illustrates the products EWM makes from its brine recovery process (Enviro Water Minerals Company, n.d.)

The EWM project attests to the difference innovation and investment can make in addressing the issues of brine disposal. Reducing the amount of brine disposed into wells through reuse mitigates some of the environmental concerns associated with brine disposal (Younos, 2005). Researchers are currently investigating methods to improve brine recovery and expand the number of products brine can be used to manufacture (Halder, Tandon, Chintalapalle, Roy, & Tarquin, 2015). If the EWM project is fruitful, it could expand the market for brine products, which could in turn spur a new method of recycling.

KBH Plant Energy Efficiency Policies

The KBH plant's building design consists of many windows in order to utilize natural light to the greatest extent possible (see Figure 35) (A. Ruiz, personal communication, August 2, 2016). The use of natural light ensures that as few electric lights as possible light the plant during daylight hours (A. Ruiz, personal communication, August 2, 2016). Furthermore, by this year, the KBH plant will further reduce energy consumption by equipping lights with LED bulbs (A. Ruiz, personal communication, August 2, 2016).



Figure 35 – Natural light plays a key part in illuminating the KBH plant (Photo Credit: William Delgado-Thompson)

Eaton Energy Tracking Project

The KBH plant's project with Eaton to track energy usage not only will show the energy different phases of the desalination process use but also will signal when treatment trains need flushing or other maintenance (M. Perez, personal communication, August 4, 2016). According to Mr. Perez, knowing which parts of the process use the greatest amount of energy is paramount to improving the energy efficiency of the RO process (personal communication, August 4, 2016). He also said that any sudden spikes in energy at different parts of the process could be valuable indicators of the need for maintenance (M. Perez, personal communication, August 4, 2016). Thus, data from Eaton's software could also help the KBH plant strategically perform preventive maintenance to minimize the chances of equipment failure while maintaining the highest level of energy efficiency (M. Perez, personal communication, August 4, 2016).

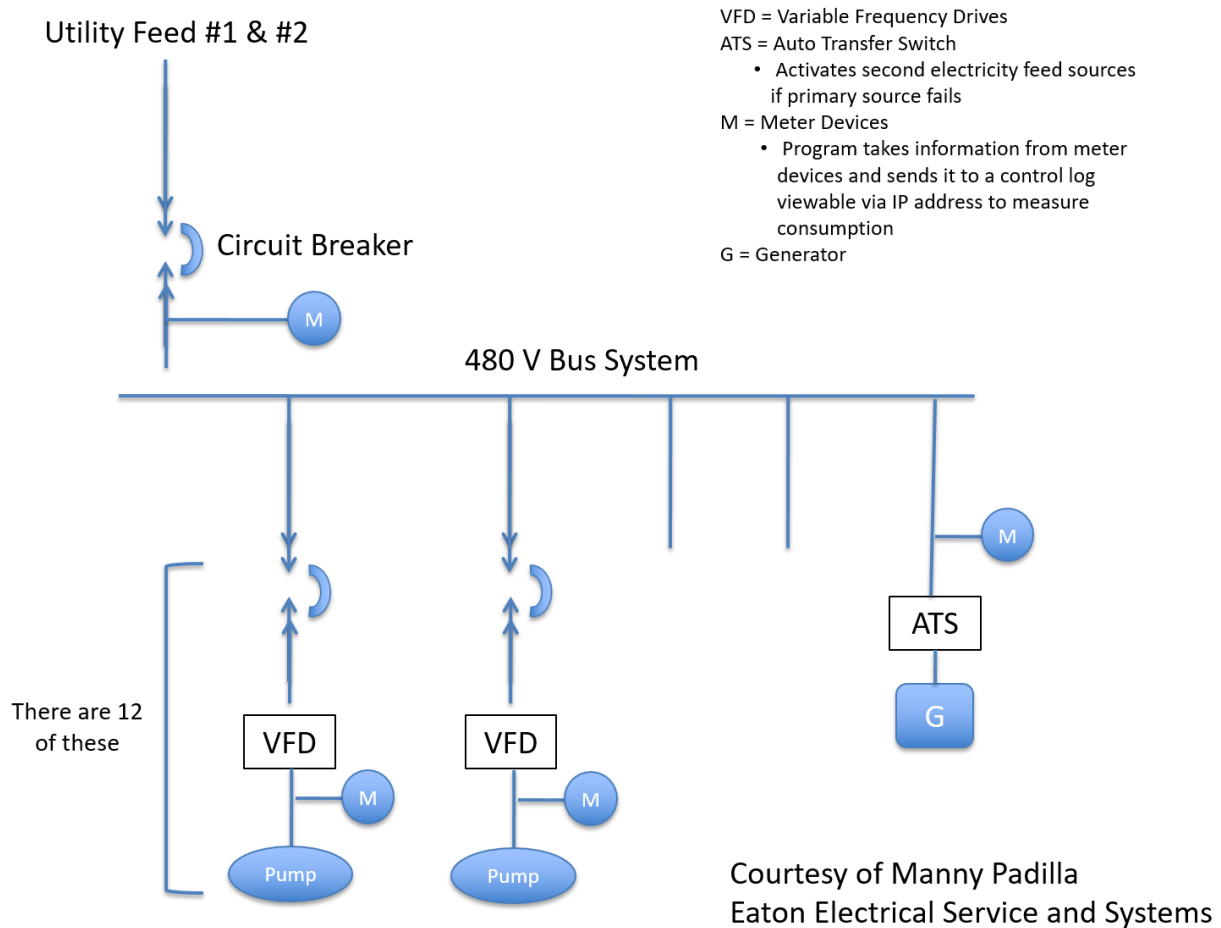


Figure 36 – A diagram showing how Eaton’s software will track energy usage (M. Padilla, personal communication, August 3, 2016).

Figure 36 illustrates how Eaton’s planned system would work. The proposed program monitors energy by logging information from each metering point, labeled ‘M’ in Figure 36. These metering devices exist but their measurements could not be read before this program (M. Padilla, personal communication, August 3, 2016). The metering devices send their readings to a computer program on an intranet network solely accessible to KBH plant personnel. This program converts the readings to Excel spreadsheet format for easy interpretation (M. Padilla, personal communication, August 3, 2016). The twelve variable frequency drives (VFDs)

regulate the voltage and RPM of the high-pressure pumps that send feed water across the membranes (M. Padilla, personal communication, August 3, 2016). The automatic transfer switch (ATS) activates the secondary power system if the primary system fails. The generator (G) is the KBH plant's secondary power source (M. Padilla, personal communication, August 3, 2016; A. Ruiz, personal communication, August 2, 2016). Lastly, the symbols in Figure 36 with two arrows pointing toward each other with a curved line between them represent circuit breakers (M. Padilla, personal communication, August 3, 2016).

Summary

Energy usage and brine disposal are key environmental concerns pertaining to desalination (Shahzad et al., 2017; Younos, 2005). The KBH plant's measures regarding these two issues represent meaningful steps toward addressing its environmental footprint. These are examples for both future and existing desalination plants to follow when considering their impacts on the environment. Furthermore, desalination plants around the world could play a key role in growing the economies of the countries in which they are located by stimulating the advancement of brine reuse and computer programs that improve energy efficiency. Additional measures the KBH plant and other desalination plants could take to further reduce their environmental impact include maintaining the latest, most-efficient membrane technology as well as ensuring that a greater share of the energy they use comes from solar power or other renewable energy sources (Fiorenza, Sharma, & Braccio, 2003; Khawaji, Kutubkhanah, & Wie, 2008). The next section details recent projects that studied incorporating renewable energy into

desalination. They provide some key benefits and concerns regarding the adoption of renewable energy into desalination for officials at the KBH plant to consider.

2.5 LITERATURE REVIEW

This section analyzes the literature about current endeavors to integrate solar energy and other renewable energy resources into water desalination. These case studies serve as a point of comparison to this thesis. They also delineate important concepts to consider when building or refitting desalination plants to run on solar energy or other renewable energy sources. The first case study describes the logistics of building a brackish water RO desalination plant in Texas powered by an onsite set of PV panels and the grid. The second case study takes place at the Brackish Groundwater Desalination Research Facility in Alamogordo, New Mexico. It involves utilizing HOMER to measure the economic feasibility of using renewable energy to power two separate off-grid desalination plants - one that uses the electrodialysis reversal (EDR) desalination process and another that uses the RO desalination process. The modeled desalination plants are located in places with arid climates similar to those of Alamogordo and El Paso. The third case study uses the H2RES model to analyze how increasing desalination capacity in Jordan can also increase the amount of solar and wind energy produced there. The last case study elaborates on the obstacles and opportunities of desalination with renewable energy by describing existing and planned desalination plants around the world that operate with renewable energy.

Benefits of a Grid-PV Hybrid Desalination Plant in Texas

Texas' abundant solar and wind resources provide excellent opportunities to construct desalination plants powered by these renewable resources (Gold & Webber, 2015). According to Gold and Webber (2015), PV modules could heat water before it goes through the desalination

process. This mutually beneficial arrangement would increase the efficiency of PV modules by cooling them down while the preheated water would require less energy to desalinate (Gold & Webber, 2015). Additionally, the excess electricity the PV modules sell to the grid could serve as another revenue source for a desalination plant when water sales are low (Gold & Webber, 2015).

Gold and Webber's (2015) modeled brackish water RO desalination plant is located in Abilene, Texas, a city that has plentiful wind and solar energy resources (Gold & Webber, 2015). Their approach to estimate the power required for a desalination plant sums the power required to withdraw water from the aquifers with that required to send the water through the desalination process (Gold & Webber, 2015). Equations 2 through 4 in Gold and Webber (2015) illustrate the variables required to estimate the energy consumed in these two parts. Key variables include the desalination capacity factor, the pump efficiency, the density of the water, and the depth of the aquifer (Gold & Webber, 2015). The desalination capacity factor refers to the ratio of the actual output of treated water to the potential output of treated water (Gold & Webber, 2015).

The desalination plant Gold and Webber (2015) modeled produces 790,000 gallons of water per day, which is enough to supply four thousand people with 195 gallons each day. This is significantly lower than the KBH plant's maximum daily production of 27.5 million gallons of water per day (EPW, 2016). But, 195 gallons per capita each day represents the average daily water use in the 40 largest cities in Texas (Gold & Webber, 2015).

Other key differences between Gold and Webber's (2015) model and this thesis is the use of a Generic Algebraic Modeling System (GAMS) to estimate electricity costs. The source for the GAMS electricity inputs comes from the average 2011 electricity costs for industrial

customers, which is \$0.068/kWh (Gold & Webber, 2015). These are for customers on the Electric Reliability Council of Texas (ERCOT) grid, which is the grid that supplies 90% of Texas' electricity customers (ERCOT, n.d.). These rates do not apply to El Paso because the city is outside of ERCOT's service area (ERCOT, n.d.). Moreover, Gold and Webber's (2015) model allows the plant to decide when to sell electricity from the PV modules to the grid when it is most profitable to do so and when to use that electricity to desalinate water when it is most economically wise to do so. This thesis allocates all electricity produced by the microgrid to desalination first and then sells the remainder to the grid. Their model also does not account for either the processes the grid may require to set up a PV-powered microgrid or the costs of maintaining the microgrid (Gold & Webber, 2015).

Utilizing HOMER to Power Off-Grid Desalination Plants

According to Karimi and others (2015), solar energy is not yet an economical energy source for larger desalination operations with access to grid electricity. But, they state that it is a cost-competitive energy source for smaller desalination plants in remote areas with really sunny or windy climates that are not connected to the grid (Karimi, Abkar, Aghajani, & Ghassemi, 2015). Their study proves this claim by using HOMER to illustrate the different net present cost (NPC) scenarios for various electricity supply combinations to power off-grid EDR and RO desalination plants (Karimi et al., 2015).

Karimi and others (2015) programmed HOMER to consider PV modules, wind turbines, diesel generators, and battery banks as potential energy sources for both modeled desalination plants. For the modeled EDR desalination plant, the best configuration included PV modules,

batteries, and inverters to convert AC current to DC current (Karimi et al., 2015). For the modeled RO desalination plant, the best combination consisted of PV modules, batteries, inverters, and a diesel generator (Karimi et al., 2015). But the diesel generator was predicted to supply a tiny portion of this plant's electricity load (Karimi et al., 2015). Figures 10a and 10b in Karimi and others (2015) illustrate the different NPCs for each combination; all configurations whose diesel generators were expected to supply a sizable share of the load had NPCs that were much higher than those in which the diesel generator played little or no role. However, Alamogordo's low average wind speeds caused HOMER to exclude wind turbines from the most economical electricity supply combination for both modeled desalination plants (Karimi et al., 2015). Nonetheless, Karimi and others' (2015) is further testament to the validity of the HOMER model and the potential of solar-powered desalination plants.

Increasing Renewable Energy Use in Jordan Via Desalination

Novosel and others (2014) state that Jordan is the fourth most water-deprived country in the world. Although Jordan has a large amount of solar and wind resources, most of the nation's energy comes from imported fossil fuels (Novosel et al., 2014). Jordan's abundant solar and wind energy potential combined with its scarce water resources signify that water desalination with solar and wind power could address the country's water situation while simultaneously setting it on a path to energy independence (Novosel et al., 2014).

The H2RES model that Novosel and others (2014) use to model renewable energy potential uses inputs similar to those HOMER uses. These include hourly solar and wind energy data, PV module and wind turbine expected energy production capacities, the price of grid

electricity, and the price of PV and wind electricity generation systems (Novosel et al., 2014). The main difference between HOMER and H2RES is that HOMER ranks configurations by the lowest NPC while H2RES ranks configurations by the least marginal cost of energy produced (Novosel et al., 2014). This methodology ranks solar and wind energy systems highly because they do not include the costs of the extra fuel required to generate one extra kilowatt-hour (kWh) of energy (Novosel et al., 2014).

Novosel and others' (2014) grid-connected modeled desalination plant uses the RO process to desalinate seawater from the Red Sea and pump it over the mountains to serve Jordan's water demand. PV and wind turbine installations are the primary energy sources for the plant with the assumption that some of the excess electricity these installations produce will supply Jordan's electricity grid (Novosel et al., 2014). Rather than use batteries to store excess energy from the renewable sources that does not supply the grid, their modeled desalination plant uses this excess energy pump brine into a reservoir (Novosel et al., 2014). When solar and wind energy resources are not sufficient to meet the plant's electricity demand, rather than draw electricity from the grid, the brine reservoir releases brine through a turbine to generate extra electricity for the plant; the brine then flows to the Dead Sea (Novosel et al., 2014). If necessary, the system can also pump briny water from the Dead Sea back to the reservoir to repeat the cycle (Novosel et al., 2014). Figures 4 and 5 in Novosel and others' (2014) report illustrate how such a desalination plant could significantly increase the presence of solar and wind energy in Jordan's electricity supplies.

Novosel and others' (2014) use of marginal cost per kWh produced is a pivotal measure to highlight the added value of renewable energy resources relative to fossil fuel-based energy

resources. This measure helps emphasize the fact that each kWh of energy produced from renewable resources is not at the mercy of fuel sources that are costly to extract, volatile in price, detrimental to the environment, and limited in availability (Al-Karaghoul, Renne, & Kazmerski, 2009; Shahzad, Burhan, Ang, & Ng, 2017; Shatat, Worall, & Riffat, 2013). Building a reservoir to store brine not only helps reuse a product that would otherwise have gone to waste but also further increases the role of renewable energy in Jordan's electric supply. Moreover, a brine reservoir is a clever plan to address energy storage issues while ensuring renewable energy can still meet Jordan's electricity needs when solar and wind energy are not available.

Challenges and Opportunities for Renewable Energy in Desalination

131 desalination plants around the world use renewable energy to supply their electricity demands (Shahzad et al., 2017). They represent less than one percent of the total number of the world's existing desalination plants (Shahzad et al., 2017). 43% of desalination plants that use renewable energy use PV modules, 27% convert solar energy to heat for the desalination process, 20% use wind energy, and the remaining 10% use a mix of renewable energy resources (Shahzad et al., 2017).

The main challenge for running desalination plants entirely on renewable energy sources is their intermittent availability (Karimi et al., 2015; Novosel et al., 2014). Battery banks and reservoirs can address this issue so that plants have an uninterrupted energy supply (Karimi et al., 2015; Novosel et al., 2014). But, these systems add to the cost of desalination with renewable energy, which in turn affect its economic feasibility relative to fossil fuel-based energy sources (Karagiannis & Soldatos, 2008; Karimi et al., 2015; Shatat et al., 2013).

Nonetheless, the rising price of fossil fuels combined with the rapid advancement and declining costs of battery technology are gradually addressing this challenge (Ardani et al., 2017; El-Sayed, 2007; Hadjipaschalis, Poullikkas, & Efthimiou, 2009).

Another option to guarantee continuous electricity for desalination plants that run on renewable energy involves interconnecting them with the grid (Gold & Webber, 2015; Shahzad et al., 2017). However, this would require addressing the concerns and terms of the grid electricity provider pertaining to interconnected distributed generation systems (El Paso Electric Company, 2016). But, these issues create further opportunities to ascertain the best methods to interconnect microgrids to the grid without damaging the grid.

The amount of land area PV module microgrids require is a challenge to utilizing PV modules to power desalination plants (Shahzad et al., 2017). To operate an RO desalination plant that produces 1 m³ of water daily with 8 kWh/m³ of water produced requires 26.5 to 28 m² of land (Shahzad et al., 2017). According to Ran Fu, a researcher at the National Renewable Energy Laboratory, this challenge becomes more of an issue if the PV modules have double axis trackers (personal communication, March 26, 2017). To address this obstacle, it is imperative that future solar technologies lower the amount of land area PV modules require and increase the amount of energy each PV panel generates.

Although desalination plants that run on renewable energy resources account for less than one percent of the world's desalination plants, their existence serves as a testament to the potential for future desalination plants to incorporate renewable energy (Shahzad et al., 2017). The world's largest desalination plant that uses renewable energy is located outside Perth, Australia (Shahzad et al., 2017; Water-Technology, n.d.). This plant, which started operating in

2007, uses wind energy and produces up to 66 million gallons of freshwater daily through the RO process (Shahzad et al., 2017; Water-Technology, n.d.). The plant's total output accounts for 17% of Perth's water needs (Water-Technology, n.d.).

Other RO desalination plants that use wind energy include one on Fuerteventura, one of the Canary Islands, and another on Therasia Island in Greece (Shahzad et al., 2017). Both of these plants have been operating since the mid 1990s (Shahzad et al., 2017). The Al-Khafji RO desalination plant in Saudi Arabia is expected to produce almost 16 million gallons of water daily using PV modules (Shahzad et al., 2017). IBM is currently developing a membrane distillation thermal desalination process that uses heat generated from concentrated PV panels to desalinate water (Shahzad et al., 2017). These examples are just a few of many that affirm the potential for renewable energy to play a more central role in water desalination. The next section describes the framework that the HOMER model uses in order to illustrate potential opportunities to equip the KBH plant with a solar-powered microgrid, and therefore further the prospects of expanding the role of solar energy and other renewable energy sources into water desalination.

Chapter 3

3.1 HOMER MODEL SETUP

This section defines the distinguishing and fixed parameters HOMER uses to provide the cost/benefit forecast that pertains to each of the twelve different configurations to meet the energy requirements of the Kay Bailey Hutchison (KBH) water desalination plant. Examples of fixed parameters for each iteration include solar radiation and temperature data, the discount rate, and the plant’s electric load profile, and prices for grid electricity. Examples of distinguishing parameters for each iteration include the PV modules’ price scale, the PV modules’ use of axis trackers, and the presence of net metering to calculate energy costs.

Initial Project Design Window

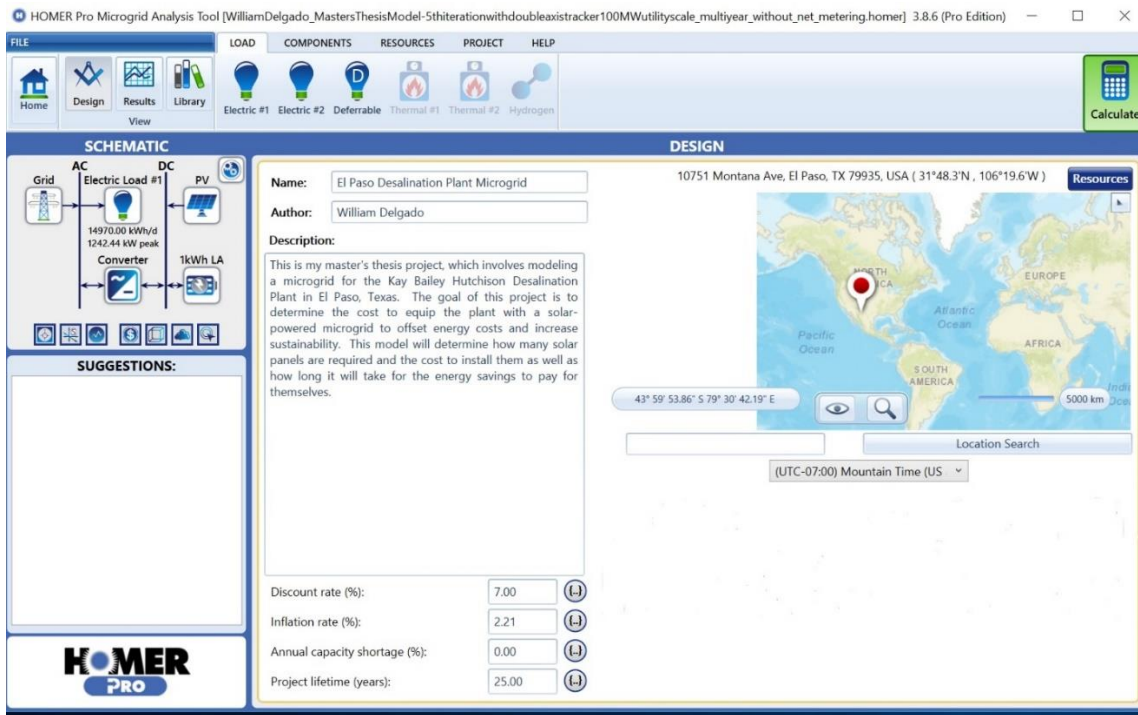


Figure 37 – Screenshot of initial project design window in HOMER

The first window to appear upon initializing HOMER is the design window as illustrated in Figure 37. The first step is to input your project location in HOMER, which for this project is the address of the KBH desalination plant. Upon clicking the ‘Location Search’ button, HOMER acquires the latitudinal and longitudinal coordinates for the address you inputted. These coordinates allow HOMER to download pertinent resource data for your project location such as solar radiation and temperature data.

Nominal Discount Rate, Capacity Shortage, and Project Lifetime

The next step in the project design process is to consider the nominal discount rate⁴, the expected inflation rate⁵, the annual capacity shortage, and the project lifetime (see Figure 37). The nominal discount rate is the interest rate or the cost to borrow money (HOMER Energy, 2016d). HOMER adjusts the nominal discount rate you input (see Figure 37) for inflation with the equation $I = (I^* - f)/(1 + f)$ where I equals the discount rate adjusted for inflation, or the real discount rate, while I* equals the nominal discount rate and f equals the expected inflation rate (HOMER Energy, 2016d). This process converts costs and savings in dollars from future years to 2016 dollars based on inflation and interest rates to provide a forecast of future costs and savings with 2016 dollars as the unit (HOMER Energy, 2016d, 2016e). I set the nominal discount rate as 7% based on a 2016 report compiled by the National Renewable Energy Laboratory (NREL) (Fu et al., 2016). I set the expected inflation rate as 2.21% based on the average inflation from the years 1995 to 2016 (“Consumer Price Index, 1913- | Federal Reserve Bank of Minneapolis,” n.d.). A nominal discount rate of 7% and an expected inflation rate of 2.21% lead to a real discount rate of 4.69% (see Figure 74). The annual capacity shortage is the

⁴ The nominal discount rate is listed as ‘discount rate’ in Figure 37.

⁵ The expected inflation rate is listed as ‘inflation rate’ in Figure 37.

anticipated demand in kWh that the model will not have to meet (HOMER Energy, 2016f). This project has the model meeting all demand with a mixture of solar panels and grid energy. Aleph Baumbach, the head support engineer at HOMER Energy, recommended that I set the project's lifetime as 25 years (personal communication, February 7, 2017), which equals the typical lifespan of solar panels (Pingel, Zemen, Frank, Geipel, & Berghold, 2009; Rodriguez & Amaratunga, 2008). I felt that this was appropriate given that rapidly changing solar technology will likely create a completely new cost and component profile, which would result in a complete revamp of the project 25 years from now (Feldman et al., 2015).

Hourly Solar Radiation Data

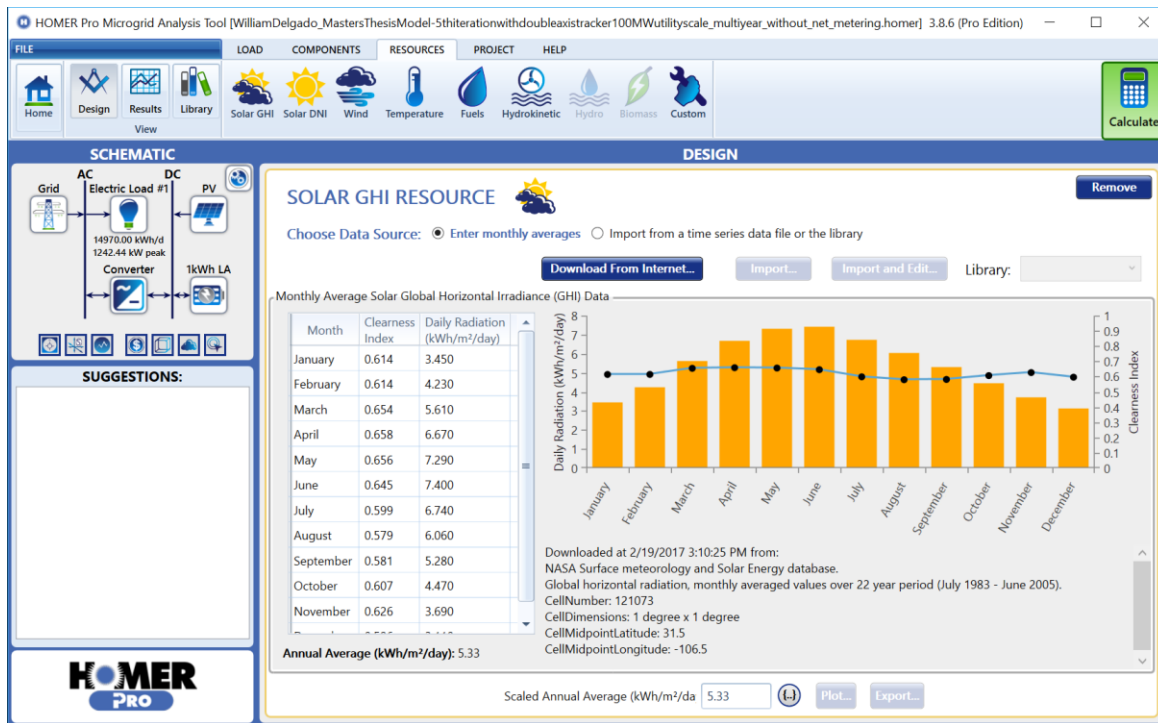


Figure 38 – Screenshot of project location's solar radiation data downloaded from SMSSED database

To acquire a realistic picture of available solar energy for the location of the plant, I used HOMER's ability to download solar radiation data for the plant's latitudinal and longitudinal coordinates directly from the internet. The solar radiation dataset (see Figure 38) I downloaded for the project comes from NASA's Surface Meteorology and Solar Energy Database (SMSSED), which uses satellites to measure solar radiation and average temperature at the surface of locations across the Earth (Stackhouse et al., 2016). This dataset displays average monthly solar radiation across the Earth's surface from July 1983 to June 2005 (Stackhouse et al., 2016).

HOMER uses the Graham Algorithm, created by V.A. Graham, and processes developed by John Duffie and William Beckman to model hourly solar radiation figures across all days of the year from the SMSSED data (Duffie & Beckman, 1991; Graham & Hollands, 1990; HOMER Energy, 2016g, 2016h). The figure in Article 5.16 of the HOMER model's user manual (see figure in Appendix) shows two charts, one with Seattle's hourly solar radiation for a year based on measured data, and another with Seattle's predicted hourly solar radiation for the same year based on the Graham Algorithm and Duffie and Beckman's methodology (HOMER Energy, 2016h). The two charts are effectively identical, which is a testament to the accuracy of the aforementioned hourly solar radiation modeling approaches.

HOMER's hourly solar radiation data are delineated in civil time, which corresponds to the local standard time at the project location relative to the prime meridian (HOMER Energy, 2016g). In El Paso's case, the local standard time is seven hours west of the prime meridian, which corresponds to the US Mountain Time Zone (see Figure 37). But, HOMER calculates hourly solar radiation data using solar time, which directly measures the sun's position across the sky based on a given latitude, the day of the year, and the time of day, which in solar time is the

difference between the angle of the sun relative to the Earth's surface at a given moment in the day and the angle of the sun relative to the Earth's surface when the sun is at its zenith (HOMER Energy, 2016g). Article 5.9 in the HOMER model user manual details the equations the model uses to convert civil time into solar time. These hourly solar radiation figures help HOMER provide a clear idea on the number of solar panels required for a microgrid system to supply a load based on the amount of available solar energy in the project area (HOMER Energy, 2016i).

Accounting for Cloud Cover

HOMER accounts for cloud cover and other phenomena that block the sun's rays from the Earth's surface via the clearness index (HOMER Energy, 2016j). HOMER calculates the clearness index at an hourly level by dividing the average hourly solar radiation at a point on the Earth's surface by the average hourly solar radiation at the top of Earth's atmosphere over said point (HOMER Energy, 2016g, 2016k). Articles 5.5 and 5.9 in the HOMER model user manual describe the equations used to calculate the hourly average solar radiation at the top of Earth's atmosphere. Important variables for these equations include the zenith angle of the sun, latitude, the day of the year, the hour of the day in solar time, and the solar declination, or the latitude at which the sun's rays are perpendicular to the Earth's surface at solar noon (HOMER Energy, 2016g).

Global Horizontal Irradiation (GHI) Data

Given that this project uses flat PV panels as opposed to concentrated PV panels, I used SMSSED's solar global horizontal irradiation (GHI) data to estimate PV panel output because HOMER recommends this type of data for flat PV panels (HOMER Energy, 2016i). GHI is defined as the sum of direct normal irradiance, or the amount of solar radiation coming from the

sun that hits a surface perpendicularly, diffuse irradiance, or the amount of solar radiation that the atmosphere reflects to a surface, and the amount of solar radiation that the ground reflects (HOMER Energy, 2016i; NREL, n.d.). HOMER utilizes methods developed by William Beckman and John Duffie to forecast hourly PV panel energy output from GHI data (Duffie & Beckman, 1991; HOMER Energy, 2016g). Important variables for the equations that Duffie and Beckman’s methods use are the panels’ azimuth and slope relative to the ground. Others include the time of day in solar time, the day of the year, the location’s latitude and longitude, PV temperature, and clearness index (Duffie & Beckman, 1991; HOMER Energy, 2016g).

Temperature Data

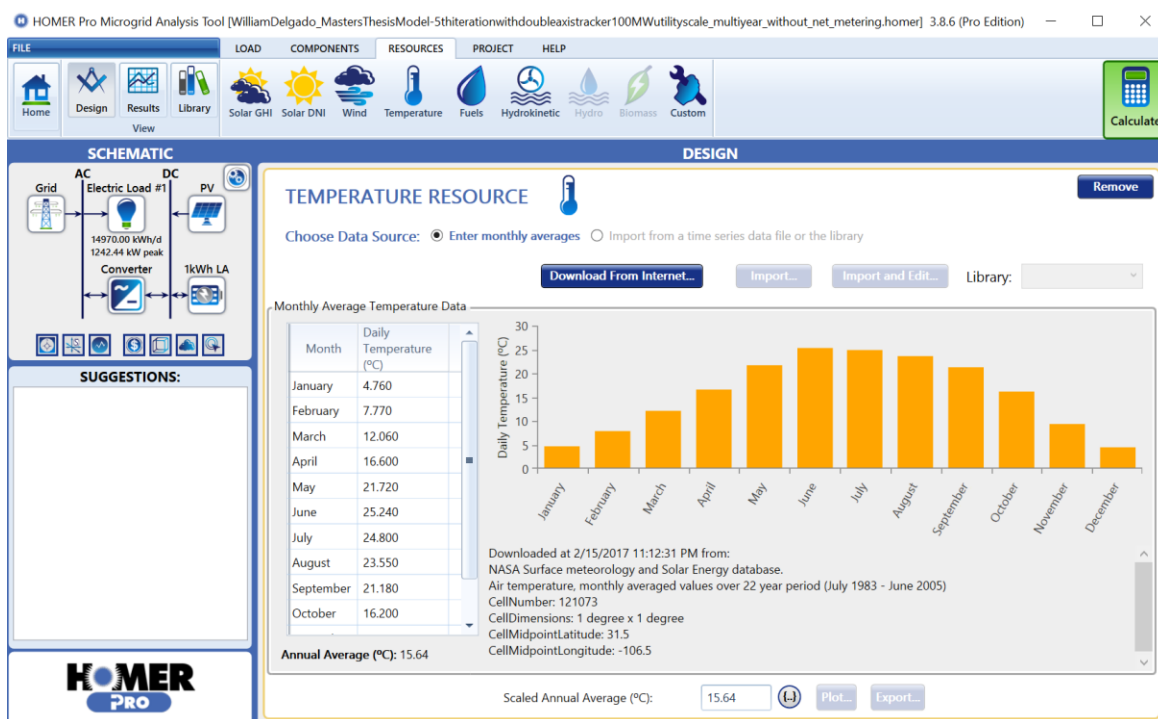


Figure 39 – Screenshot of project location’s average ambient daily temperature data downloaded from SMSRD database

Given that temperature also affects PV panels' efficiency, I also downloaded daily temperature data from the SMSED for the plant's location. This dataset provides average daily ambient temperatures that include daytime hours and nighttime hours. Just like the solar dataset, the temperature dataset is based on monthly averages from July 1983 to June 2005 (Stackhouse et al., 2016). For simplicity purposes, the dataset assumes that all days across a given month have the same average ambient temperature (HOMER Energy, 2016l). This temperature dataset plays an important part in determining the average operating temperature for the PV panels, which in turn affects their efficiency (HOMER Energy, 2016l). This concept will be explained later in this section.

KBH Plant Electric Load Profile

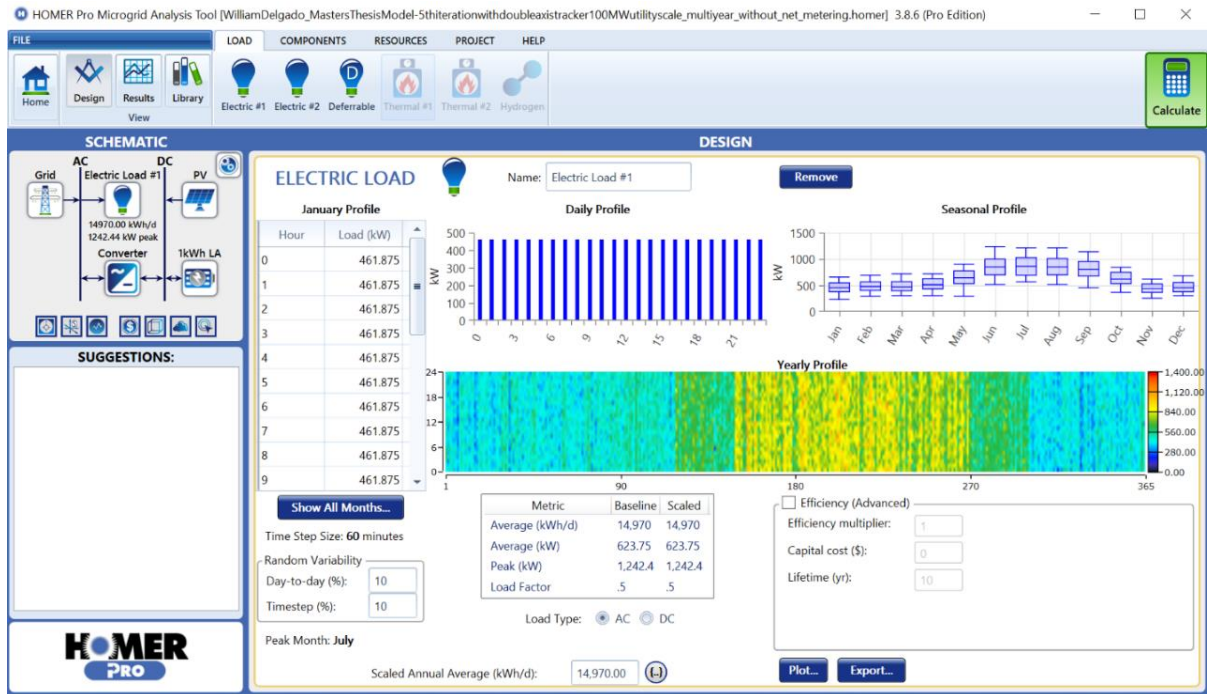


Figure 40 – Screenshot of KBH plant's electric load profile

The next step involves configuring the plant's electric load profile for the model as Figure 40 shows. This subsection describes each of the components that comprise the plant's electric load profile. The schematic section in the top left corner of Figure 40 illustrates the components that will meet the load. On the right side are the PV module and 1 kWh lead acid batteries that have arrows pointing left to a line with 'DC' at the top. This line indicates that PV modules and batteries will supply direct current. To the left of this line is a converter⁶ that will convert DC current to AC current. The converter has arrows coming from the 'DC' line to it and then another set of arrows that go from it to a line to its left with 'AC' at the top. These arrows indicate that the converter will convert the DC current the PV modules and batteries produce to AC current. To the left of the 'AC' line is the grid component, which indicates that the regular electric grid will play a part in meeting the KBH plant's load. The grid has an arrow pointing to the 'AC' line, which indicates that it will supply AC current. The blue lightbulb symbol to the right of the 'AC' line and above the converter symbolizes the KHB plant's load that the components have to meet. The fact that there is an arrow from the 'AC' to the lightbulb and not one from the 'DC' line indicates that the entirety of the KBH plant's electricity consumption will come from AC power. The icons below the schematic section represent other factors that will be described in later subsections.

HOMER bases electric load profiles on time steps that have a range of several values from one minute to sixty minutes (see Figure 40). Time steps are the amount of time in which a demand/load at a given moment remains constant (HOMER Energy, 2016m). Manuel Perez

⁶ In this project, the term 'inverter' will refer to the 'converter' in later subsections. Converters convert current from AC to DC while inverters convert current from DC to AC (Vignola et al., 2008). The inverter in this project converts the PV modules' and batteries' DC power to AC power.

stated that hourly energy consumption is the same across all days in a given month, which explains why all hours across all days in each month have the same load (personal communication, August 4, 2016). Consequently, I set the time step as 60 minutes in the ‘Optimization’ space under the ‘Project’ tab⁷.

The load data for all months (see Figure 43), entered upon clicking the blue ‘Show All Months’ button under the ‘January Profile’ table, come from the plant’s energy billing data spreadsheets that Mr. Perez compiled (personal communication, February 3, 2017). These spreadsheets have energy consumption data in kWh across all months for the years 2011 through 2016 (M. Perez, personal communication, February 3, 2017). I was going to include 2010 data, but some months have missing entries (M. Perez, personal communication, February 2, 2017). Hence, I used data from the years 2011 to 2016 because prior data may be limited due to 2010’s incomplete data and the fact that the plant opened in 2007 (M. Perez, personal communication, March 1, 2017). Furthermore, annual precipitation levels of 5.27”, 6.05”, 9.51”, 8.57”, 12.08”, and 9.34” for the years 2011, 2012, 2013, 2014, 2015, and 2016 respectively provide a representative precipitation range from drought to surplus rainfall for a city whose average annual precipitation is 8.71” (N. US Department of Commerce, NOAA, n.d.). Rainfall amounts play an important part in determining the volume of groundwater pumped, and therefore the production and energy usage of the KBH plant (EPW, 2015).

KBH Plant Monthly Average Energy Usage

To obtain the KBH plant’s average monthly energy usage across the six years of source data (see Figure 41), I averaged the monthly kWh consumption for each month of the year from

⁷ For more information, see the part of the ‘The Project Tab’ subsection entitled ‘Optimization Component’

the years 2011 to 2016. I then divided each monthly average kWh consumption figure by 730.5, the number of hours in a month, to get the average kW load at any moment across a given hour in a given month. This is important because kWh represent the amount of energy used across a given time period. For example, if a 1 kW appliance runs for one hour it uses 1 kWh of energy (Simpson & Mcpherson, 1998). In contrast, kW represent the demand, or load, needed for an appliance to run at any given moment (Simpson & Mcpherson, 1998).

The top third of Figure 41 shows the monthly kWh consumption for the years 2011 to 2016 while the middle third shows the average monthly consumption for each month of the year across the six years. Immediately adjacent to average monthly consumption figures are hourly loads across each month with the average hourly load of 624.82kW across all months in the far-right area. The bottom third shows the price per kWh from the grid for each of the six years and then the average of these prices for the six years. Data for Figure 41 come from the spreadsheets Mr. Perez compiled to represent energy consumption data (personal communication, February 3, 2017).

temperature profile was similar to that of April. Manuel Perez stated that EPE’s billing cycles do not directly match calendar months while KBH production data do. The explanation for these apparently anomalous energy consumption figures is that in some months energy consumed in one calendar month is billed in another, which can skew the monthly averages (M. Perez, personal communication, February 2, 2017).

Yearly Load Data												
		Weekdays						Weekends				
Hour	January	February	March	April	May	June	July	August	September	October	November	December
0	461.875	489.071	478.576	510.000	655.510	840.000	870.000	822.000	805.000	630.000	454.301	459.320
1	461.875	489.071	478.576	510.000	655.510	840.000	870.000	822.000	805.000	630.000	454.301	459.320
2	461.875	489.071	478.576	510.000	655.510	840.000	870.000	822.000	805.000	630.000	454.301	459.320
3	461.875	489.071	478.576	510.000	655.510	840.000	870.000	822.000	805.000	630.000	454.301	459.320
4	461.875	489.071	478.576	510.000	655.510	840.000	870.000	822.000	805.000	630.000	454.301	459.320
5	461.875	489.071	478.576	510.000	655.510	840.000	870.000	822.000	805.000	630.000	454.301	459.320
6	461.875	489.071	478.576	510.000	655.510	840.000	870.000	822.000	805.000	630.000	454.301	459.320
7	461.875	489.071	478.576	510.000	655.510	840.000	870.000	822.000	805.000	630.000	454.301	459.320
8	461.875	489.071	478.576	510.000	655.510	840.000	870.000	822.000	805.000	630.000	454.301	459.320
9	461.875	489.071	478.576	510.000	655.510	840.000	870.000	822.000	805.000	630.000	454.301	459.320
10	461.875	489.071	478.576	510.000	655.510	840.000	870.000	822.000	805.000	630.000	454.301	459.320
11	461.875	489.071	478.576	510.000	655.510	840.000	870.000	822.000	805.000	630.000	454.301	459.320
12	461.875	489.071	478.576	510.000	655.510	840.000	870.000	822.000	805.000	630.000	454.301	459.320
13	461.875	489.071	478.576	510.000	655.510	840.000	870.000	822.000	805.000	630.000	454.301	459.320
14	461.875	489.071	478.576	510.000	655.510	840.000	870.000	822.000	805.000	630.000	454.301	459.320
15	461.875	489.071	478.576	510.000	655.510	840.000	870.000	822.000	805.000	630.000	454.301	459.320
16	461.875	489.071	478.576	510.000	655.510	840.000	870.000	822.000	805.000	630.000	454.301	459.320
17	461.875	489.071	478.576	510.000	655.510	840.000	870.000	822.000	805.000	630.000	454.301	459.320
18	461.875	489.071	478.576	510.000	655.510	840.000	870.000	822.000	805.000	630.000	454.301	459.320
19	461.875	489.071	478.576	510.000	655.510	840.000	870.000	822.000	805.000	630.000	454.301	459.320
20	461.875	489.071	478.576	510.000	655.510	840.000	870.000	822.000	805.000	630.000	454.301	459.320
21	461.875	489.071	478.576	510.000	655.510	840.000	870.000	822.000	805.000	630.000	454.301	459.320
22	461.875	489.071	478.576	510.000	655.510	840.000	870.000	822.000	805.000	630.000	454.301	459.320
23	461.875	489.071	478.576	510.000	655.510	840.000	870.000	822.000	805.000	630.000	454.301	459.320

Figure 43 – Screenshot of adjusted hourly load profiles by month inputted into HOMER

This could potentially affect the accuracy of a typical annual load profile, which explains why I adjusted the load profiles across several months (see Figure 43). Per Aleph Baumbach’s recommendation, I reduced April and May’s load to 510 kW and 655.5 kW respectively to account for the approaching summer (personal communication, February 7, 2017). Baumbach recommended July as a peak month based on his experience helping other clients with projects in the Northern Hemisphere (personal communication, February 7, 2017). The temperature data

(see Figure 39) show July's average temperature almost as hot as June's which provides further justification for setting July as a peak. Consequently, I increased July's hourly load to 870 kW. Given that October's temperature profile is similar to that of April and it is the first month after the hot summer months, I concluded that its load profile should be between that of April and May. Thus, I reduced October's load to 630 kW. I spread the reduction from October's original load of 165 kW across June, July, August, and September to account for the higher temperature profiles of those months and any energy consumed in those months that showed up on October's bill. Because June's temperature profile closely mirrors that of July, I raised its load to 840 kW. Since August and September are still summer months but have lower temperature profiles than those of June and July, I raised their loads to 822 kW and 805 kW respectively. The load profiles for November through March remain unadjusted (see Figures 42 & 43).

Seasonal Load Profile

The seasonal profile (see Figure 44) uses a box and whisker plot to display each month's overall maximum load, overall minimum load, average daily maximum load, average daily minimum load, and overall average load (HOMER Energy, 2016n). The seasonal profile acquires its figures from the 'Random Variability' calculator⁸, which simulates load variability across all days and hours of a given month (HOMER Energy, 2016n). The top and bottom lines of the plot represent the overall maximum and minimum load for each month respectively (HOMER Energy, 2016n). The top and bottom of the blue boxes represent each month's average daily maximum and minimum loads respectively while the middle line of each plot

⁸ The subsection entitled '*Simulation of Daily and Hourly Electric Load Variability*' explains how the 'Random Variability' calculator simulates load variability across all days and hours of a month.

represents the month's overall average load (HOMER Energy, 2016n). Hovering the mouse over a plot will provide the numerical figures for the corresponding month.

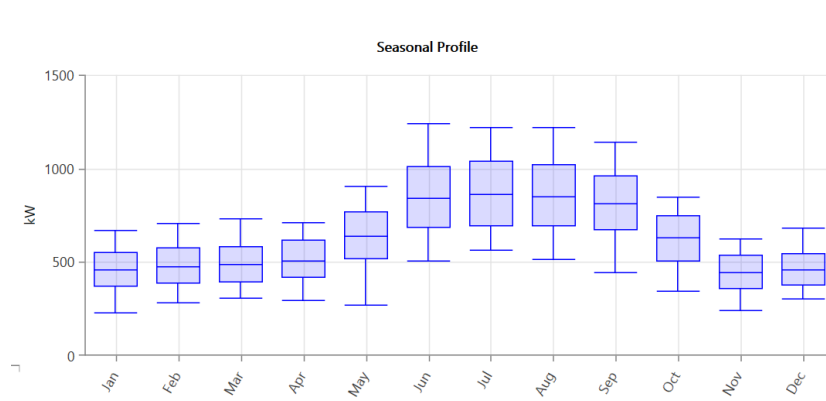


Figure 44 – Screenshot of zoomed-in view (of Figure 40) of seasonal load profile for each month

Yearly Load Profile

The yearly profile above the 'Metric Box' in Figure 40 uses a color-coded ramp to display the load for the plant across all hours and days of the year. The yearly load profile does simulate load variability across daily loads. The numbers on the x-axis represent the day of the year. For example, the number 180, represents the 180th day of the year, or June 29. The numbers on the left y-axis represent the hours of the day while those on the right y-axis represent the load in kW during any given hour. Hovering the mouse over a spot in the yearly profile graph provides information on the energy demand at the given hour and day to which the spot corresponds. Unsurprisingly, the days during the summer months have the brightest colors, signifying they have the highest energy load.

Daily Load Profile

The daily load profile (see Figure 40) shows the hourly load across all days of a given month⁹; HOMER uses the load from January's¹⁰ days to illustrate this concept. The daily load profile, unlike the yearly profile, only simulates slight load variability. The x-axis represents the hours of the day while the y-axis represents the load.

Simulation of Hourly and Daily Electric Load Variability

Although Mr. Perez said that the KBH plant's electric load remains constant across all hours in a given month, I felt it was important to simulate variabilities in the load to reflect possible sudden changes in energy demand associated with sudden spikes and drops in water production (personal communication, August 4, 2016). The 'random variability' section (see Figure 40) simulates load variations on a daily (see 'day-to-day' box in 'random variability' section) and hourly (see 'timestep' box in 'random variability' section) basis to account for load fluctuations (HOMER Energy, 2016o). The day-to-day variability alters the size of the load without altering its pattern while the time step variability alters the pattern of the load without altering its size (see Figures 46 and 47) (HOMER Energy, 2016o). The combination of these two effects provides a realistic picture of load variability across different days and hours. HOMER multiplies a perturbation factor, α , by each hourly load value to create a load with variability. The perturbation factor $\alpha = 1 + \delta_d + \delta_{ts}$ where δ_d represents the daily perturbation factor and δ_{ts} represents the hourly perturbation factor (HOMER Energy, 2016o). HOMER sets δ_d for each day by randomly selecting a value from a normal distribution with a mean of zero and

⁹ One cannot manually enter different hourly loads for each day of a given month; the random variability calculator accounts for these variations (A. Baumbach, personal communication, February 7, 2017).

¹⁰ Figure 50 shows the daily load profile for all months of the year.

a standard deviation equal to the value inputted into the ‘day-to-day’ variability box (see Figure 40) (HOMER Energy, 2016o). HOMER similarly sets δ_{ts} for each hour by randomly selecting a value from a normal distribution with a mean of zero and a standard deviation equal to the value inputted in the ‘timestep’ box (HOMER Energy, 2016o). Aleph Baumbach recommended 10% for both δ_d and δ_{ts} (personal communication, February 7, 2017). I felt this was appropriate given Mr. Perez’s statement that the plant’s load remains constant across all hours of the month (personal communication, August 4, 2016). Figures 45 through 48 illustrate how δ_d and δ_{ts} influence load variability (HOMER Energy, 2016o).

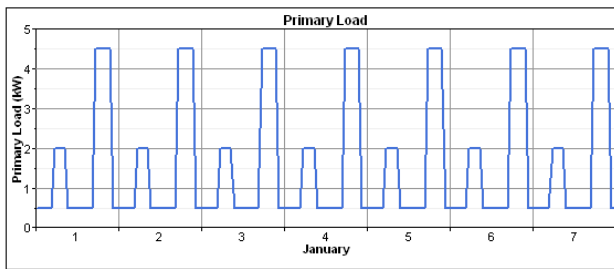


Figure 45 – Screenshot of sample primary load with no variability (HOMER Energy, 2016o)

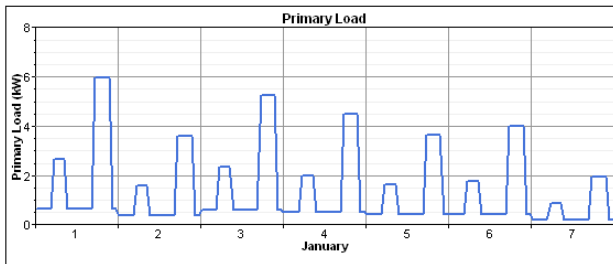


Figure 46 – Screenshot of sample primary load with size altered but not pattern to illustrate effects of δ_d (HOMER Energy, 2016o)

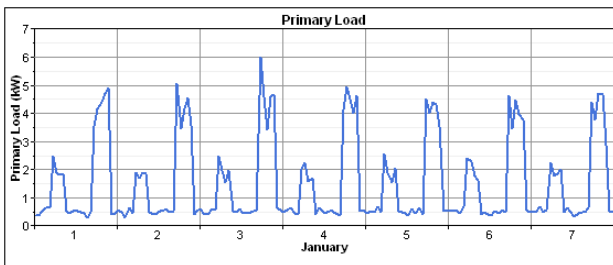


Figure 47 – Screenshot of sample primary load with pattern altered but not size to illustrate effects of δ_{ts} (HOMER Energy, 2016o)

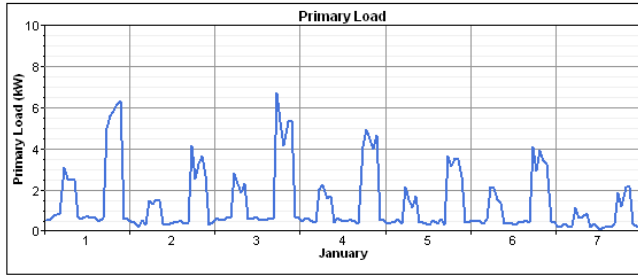


Figure 48 – Screenshot of sample primary load with full variability to illustrate effects of δ_d and δ_{ts} (HOMER Energy, 2016o)

Metric Box, Baseline Data, and Scaled Data

The ‘metric box,’ located to the right of the Random Variability box (see Figure 40), displays other load adjustment factors. The load factor is the average load divided by the peak load (HOMER Energy, 2016p). The baseline data are the raw data calculated based on the load data the user enters (HOMER Energy, n.d.). The scaled average allows the user to adjust the entire baseline load up or down; HOMER uses scaled data for its calculations (HOMER Energy, 2016q). Unlike with random variability, the adjustment is consistent across all days, hours, and months of the year (HOMER Energy, 2016q). Users typically add these types of scenarios to model future increases in loads in order to forecast necessary increases in micro grid capacity (HOMER Energy, n.d.). For simplicity and due to limited information about future load growth, I set the scaled data equal to the baseline data. The metric box also displays the average hourly load across the year as 623.75 kW. This is slightly different from the amount of 624.82 kW from Figure 41. This discrepancy is probably due to decimal rounding errors that occurred when I adjusted the load data for the model from that provided by Mr. Perez.

Plot Button

The plot button in Figure 40 displays a closer look at the scaled hourly load for each day and hour of the year as Figure 49 illustrates. The light gray lines represent each day’s boundaries

while points in between represent each day’s hours. Each peak or trough on the blue line represents the hourly load at a given hour on a given day. Straight lines between peaks and troughs illustrate differences and trends between hourly load values. But, some hourly loads are on points that interrupt the straight lines between peaks and troughs because their values are between those of the peak and trough that surround them. This variable display incorporates the parameters set in the ‘random variability’ box from Figure 40. In addition to a closer view of hourly loads, the plot button displays an amplified view of the seasonal and yearly profiles from Figure 40 through the ‘Monthly’ and ‘DMap’ tabs respectively. While the daily profile tab in Figure 40 only shows the hourly load profile for January’s days, the ‘Profile’ tab in Figure 50 shows the hourly load profile for all days of each month of the year with slight variability.

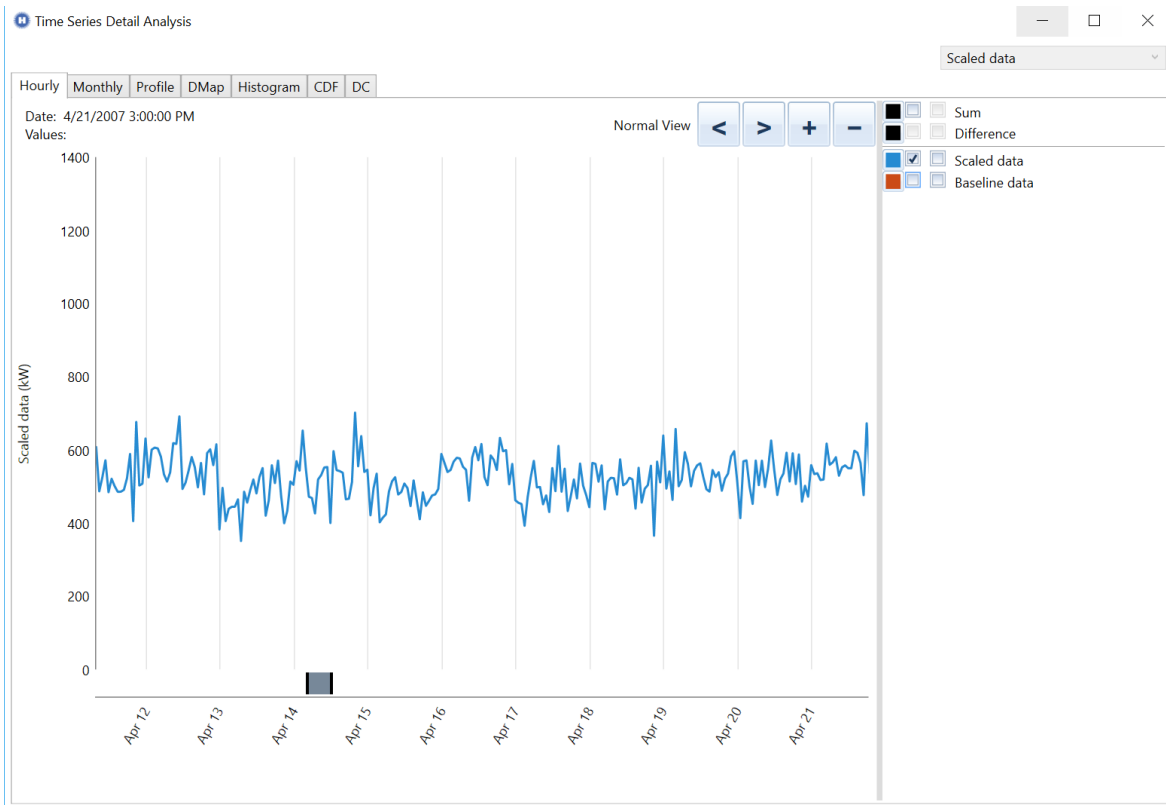


Figure 49 – Screenshot of zoomed hourly load for the KBH plant for each day of the year with simulated load variability

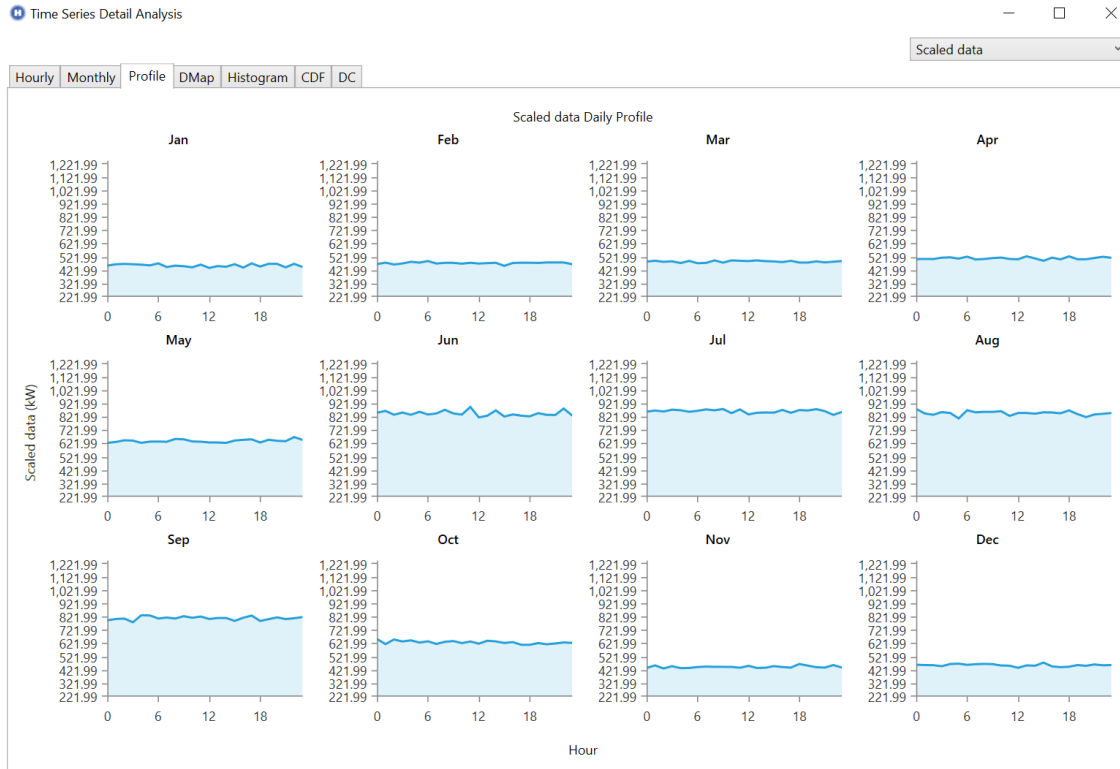


Figure 50 – Screenshot of daily load profile across all days for each month of the year with slight variability

Graphical Displays of KBH Plant Load Data – Histogram, Cumulative Distribution Function, and Load Duration Curve

Figure 49 also provides informative graphical displays of the plant’s hourly load values across the year in the form of a histogram, cumulative distribution function/ogive curve, and load duration curve via the ‘histogram,’ ‘CDF,’ and ‘DC’ tabs respectively. These graphs convey a clear picture of load distribution to show how often hourly load values fall into a given range. The histogram from Figure 51 has blue bars that each represent an interval with a 50-kW range. The height of each bar represents the percentage of the time the plant’s hourly load falls within that interval. For instance, the tallest bar in the histogram has a value of 14.59%, acquired through hovering the mouse over the bar. This means that 14.59% of the 8760 hourly load values in the distribution have a value between 450 kW and 500 kW. There are 8760 load values

in the distribution to represent the hourly load for each of the 8760 hours in a year. The sum of the values of four bars between 400 kW and 600 kW equals 46.84%, which signifies that 46.84% of the hourly load values during the year fall between 400 kW and 600 kW. This illustrates the fact that the plant’s load is between 400 kW and 600 kW for about half of the hours in a year.

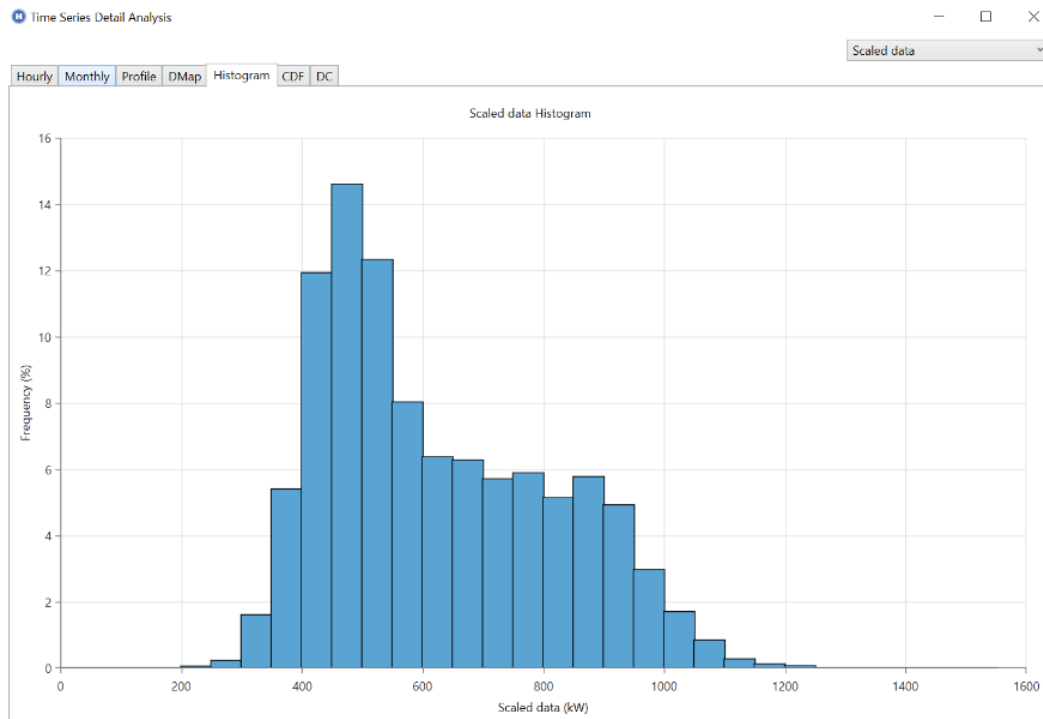


Figure 51 – Screenshot of histogram distribution of hourly load values across the year

The CDF graph in Figure 52 shows a broader picture of the histogram distribution by more clearly displaying the load distribution in terms of probabilities. The value on the y-axis of a CDF graph represents the probability that the corresponding value on the x-axis is less than or equal to the x value. For example, the x value of about 575 kW corresponds to the y value of 50%. This means that 50% of the hourly load values across the year will be less than or equal to 575 kW (National Institute of Standards and Technology, 2013). The mean hourly load across the year is 623.75 kW. The fact that it is slightly higher than the median hourly load of 575 kW

signifies that the load distribution is slightly skewed right from a normal distribution because there are some high load values that are not balanced out by equally low load values. (Earickson & Harlin, 1994). Accordingly, the CDF graph's shape deviates slightly from the true S-shape one with a normal distribution would possess. The CDF graph also shows that x values of 400 kW and 600 kW correspond to a y value of about 8% and 55% respectively. The difference between these two y values equals 47%, which is about the same as the sum of the values of the four histogram bars between 400 kW and 600 kW. The line between 400 kW and 600 kW is the steepest part of the CDF graph, which attests to the fact that the highest proportion of hourly load values across the year lies between these two quantities.

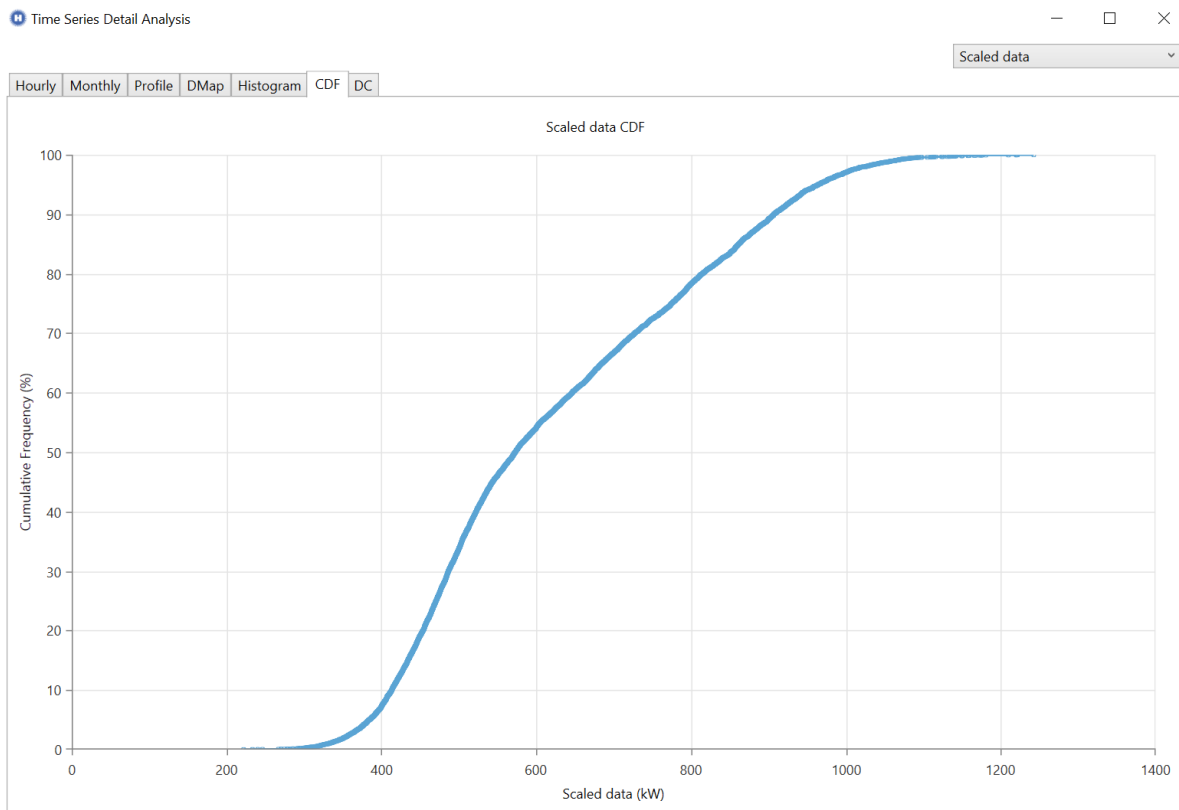


Figure 52 – Screenshot of cumulative distribution function of hourly load values

The duration curve (DC) in Figure 53 customizes a typical duration curve, which has probabilities on the x-axis and events on the y-axis, to portray the number of hours whose load values met or exceeded a given quantity (Vogel & Fennessey, 1994). The x-axis shows the 8760 hours in a year (listed as time steps) while the y-axis shows a load value. For example, the x value of 5000 time steps corresponds to a y value of about 540 kW. This means that for 5000 of the 8760 hours in a year, the hourly load value equals or exceeds 540 kW. The x value of 4380 time steps, which is equal to half of the 8760 time steps in a year, corresponds to a y value of about 575 kW. This means that 4380 time steps in a year have a load value greater than or equal to 575 kW, which in turn confirms 575 kW as the plant’s median hourly load for the year.

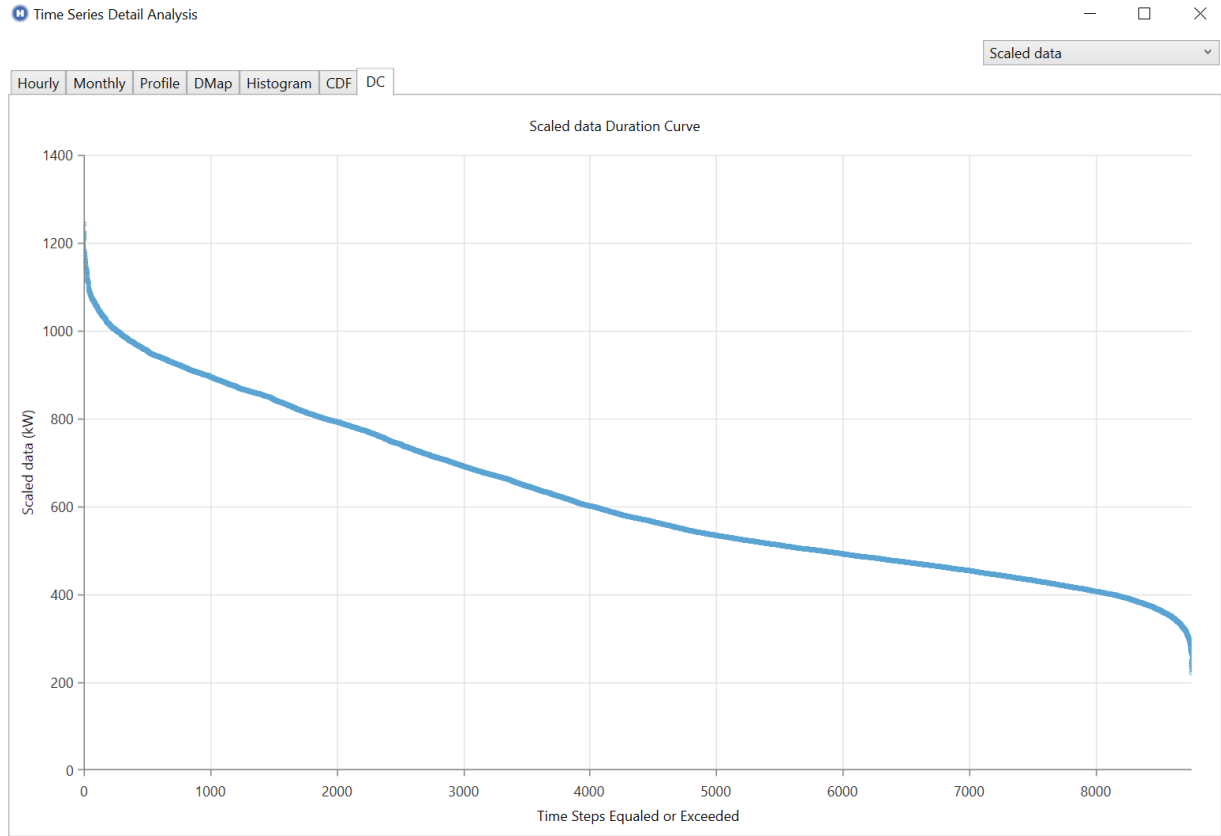


Figure 53 – Screenshot of load duration curve

'Efficiency (Advanced)' Box

The 'Efficiency (Advanced)' Box is the last part of the load setup (see Figure 40). This box allows the user to price the cost effectiveness of measures to reduce electric demand. For instance, a user could predict how long it would take for LED lights to yield electric bill savings that exceed the cost of switching from fluorescent lights (HOMER Energy, 2016r). Because this project does not cover potential electric load reduction measures, that box was not utilized.

Configuring Model Components: PV Module, Inverter, Battery, and Grid

The next part of the setup process involves setting the model's PV module parameters along with the inverter, battery, and grid. I had six rounds of model iterations to illustrate how the PV module's distinctive parameters influence the plant's ideal energy supply configuration. Energy policy recommendations for the plant come from the fifth and sixth rounds of iterations and are described in the 'results' section. Both the fifth and the sixth rounds have six iterations each. All twelve iterations use the load profile from Figure 40 and account for PV panel output degradation over the years, which is why each iteration has 'multiyear' in its name¹¹.

PV Module Configurations

Each Iteration's Distinguishing PV Module Parameters: Axis Trackers, Price Scales, and Net Metering

Three criteria distinguish the PV module parameters of each iteration: 1) the use of a single axis tracker, double axis tracker, or no axis tracker¹² 2) the price scale, and 3) the presence

¹¹ Iteration names are at the top of Figure 54 through 59

¹² Single axis trackers adjust to the sun's position on either a horizontal plane or a vertical one; dual axis trackers adjust maintain a perpendicular position relative to the sun throughout the day (Argeseanu et al., 2010).

or lack of net metering. Six of the iterations include net metering and are labeled as ‘with net metering’ while the other six do not include net metering and are labeled as ‘without net metering.’ The iterations with net metering comprise the sixth round of model iterations and have ‘6th iteration’ in their name. Those without net metering comprise the fifth round of model iterations and have ‘5th iteration’ in their name. For example, a file with ‘5th iteration,’ ‘single axis tracker,’ ‘100 MW utility scale,’ and ‘without net metering’ in its name signifies that it is from the fifth round of iterations, contains a single axis tracker¹³, uses the ‘100 MW utility’ price scale, and does not contain net metering. The two price scales, ‘100 MW utility scale’ and ‘500 kW commercial scale’ represent price profiles at different load levels. They originate from a 2016 report for the National Renewable Energy Laboratory (NREL) written by Fu and others that shows PV panel prices at different economies of scale based on different load quantities. This report describes prices for crystalline silicon PV modules (Fu et al., 2016). Therefore, I assume that each iteration’s ‘Generic flat plate PV’ is this type of PV module (see Figure 54). The two price scales are based on PV panels supplying a 100 MW load and a 500 kW load respectively (Fu et al., 2016). Because the plant’s mean hourly load across all months is 623.75 kW (see Figure 40), the ‘500 kW commercial scale’ pricing is the most appropriate and realistic for the plant. But, I included the ‘100 MW utility scale’ pricing to demonstrate how a reduction in prices can make a substantial difference in the capacity and monetary savings of a solar-powered micro grid. Furthermore, the results from the 100 MW utility scale could help make the case for governmental grants as well as illustrate a preview of the effects of future advancement and price declines of solar technology. Section 4.1 outlines the cost/benefit results of each

¹³ Iterations that do not contain axis trackers do not have ‘axis tracker’ in their name.

iteration and explains how net metering, axis trackers, and price scales influence the optimal PV-powered micro grid configuration and, consequently, the plant's energy expenses.

Net Metering

A utility that uses net metering bills a customer for the net energy consumed from the grid (Poullikkas, 2013). Net energy is defined as the difference between the energy consumed from the grid and the energy fed into the grid. Utilities that do not use net metering bill for the gross energy the customer consumes from the grid. Given that the expected production capacity of the micro grid is greater than 50 kW, El Paso Electric Company would not allow net metering for the plant (El Paso Electric Company, 2011a). Nonetheless, I included iterations with net metering to demonstrate how it could increase the plant's savings on energy expenditures. Net metering's effects will manifest in Section 4.1.

Justification for Source of PV Module and Inverter Pricing Across All Iterations

Javier Perea, the business line manager at Solar Smart Living stated that the figures in the 2016 NREL report prepared by Fu and others were representative of solar system installation costs in El Paso (personal communication, February 7, 2017). Thus, I used price figures from this report to represent the prices of generic PV panels and inverters for all model iterations. This report states that from the fourth quarter of 2009 to the first quarter of 2016, the cost of a 200-kW capacity commercial PV solar system per watt in 2016 US dollars has fallen from \$5.23 to \$2.13, which is a testament to the rapid advancement and increasing viability of solar power as an energy resource (Fu et al., 2016).

Initial Costs of PV Module with Double Axis Tracker, 100 MW Utility Price Scale, and No Net Metering

The iteration in Figure 54 comes from the fifth round of iterations and includes ‘100 MW utility scale’ pricing, a double solar axis tracker, and no net metering. The initial price of a generic PV module per watt at ‘100 MW utility scale’ pricing that includes a double axis tracker and an inverter is \$1.44, which corresponds to \$1440/kW. The price listed in the ‘Capital’ box in Figure 54 shows \$1350 because the \$90 inverter cost per kW at this scale, per page 39 of the 2016 NREL report by Fu and others¹⁴, is listed separately under the ‘Converter’ tab at the top of the figure. This price level, which applies to the iterations from the fifth and sixth rounds with ‘double axis tracker’ and ‘100 MW utility scale’ in their names, derives from the chart on page 43 of the 2016 NREL report by Fu and others. This chart shows the cost of a PV module without an axis tracker per watt in San Antonio, Texas as \$1.32 while the cost of one with a single axis tracker per watt in San Antonio, Texas is \$1.38. Per Javier Perea’s earlier recommendation, I assume that these costs are the same for El Paso.

¹⁴ This page shows the inverter price per kW for a single axis PV module at the ‘100 MW utility’ scale; with Ran Fu’s approval I assumed that the corresponding inverter price for a dual axis PV module per kW is the same (personal communication, June 4, 2017).

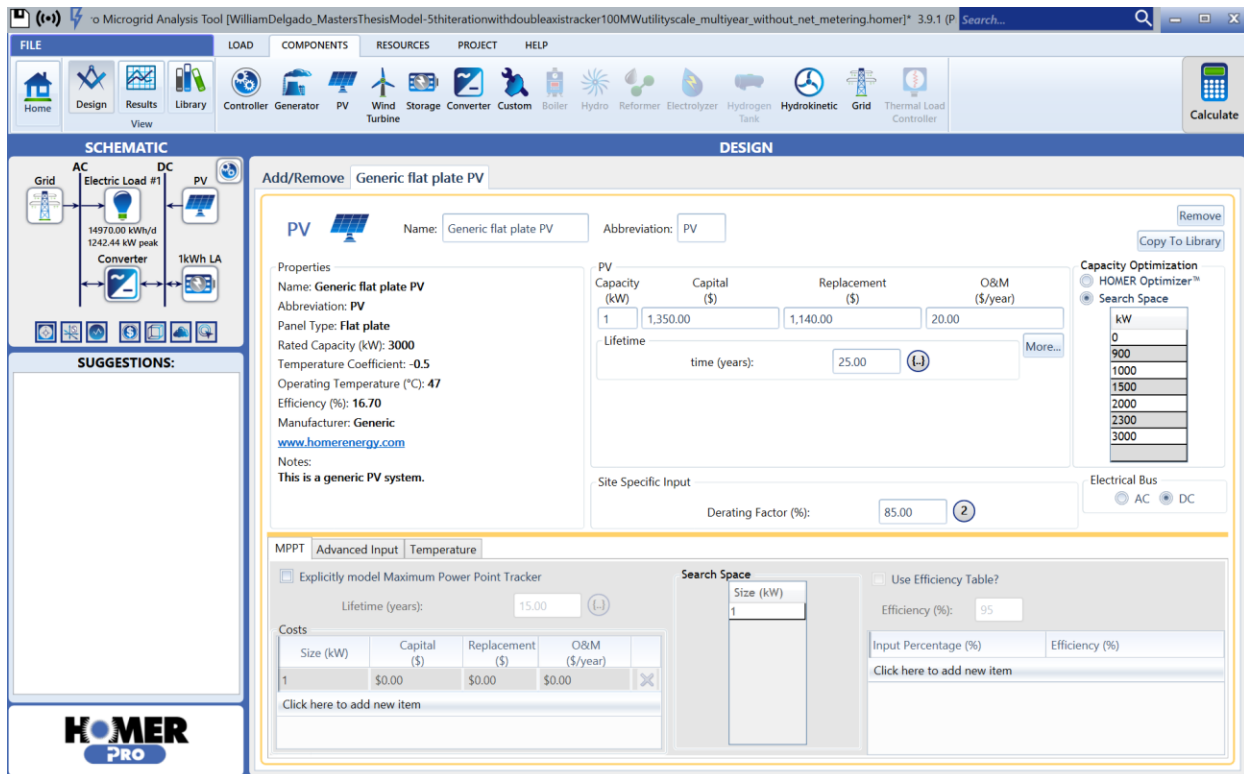


Figure 54 – Screenshot of generic PV module design parameters from fifth round of iterations with ‘100 MW utility scale’ pricing, double solar axis tracker, and no net metering

The difference between the cost of a PV module without an axis tracker and one with an axis tracker for Texas is \$0.06/W. Because I was unable to find literature that stated otherwise, I assume the difference between the cost of a PV module with a double axis tracker and one with a single axis tracker is also \$0.06/W. I consider this a conservative estimate given that economies of scale, the concept that the price per unit of a good produced falls as more units of said good are produced, would probably reduce the cost of incorporating a second axis tracker (Christensen & Greene, 1976). Ran Fu, the lead author of the 2016 NREL report by Fu and others cited above stated that he thought my assumption was appropriate (personal communication, March 26, 2017). But, he did not believe it was a conservative estimate because the costs of land required for PV modules with double axis trackers would probably outweigh the effects of economies of

scale (personal communication, March 26, 2017). As a result, I set the price of a PV module with a double axis tracker in Texas as \$1.44/W.

Replacement Cost Components of PV Module with Double Axis Tracker at 100 MW Utility Pricing Scale

The chart on page 39 of the 2016 NREL report by Fu and others delineates each of the components that account for the price of a PV system per watt at the ‘100 MW utility scale’. I decided to factor some of these into the replacement cost (see ‘Replacement’ box in Figure 54) of a double axis PV solar system per watt at the ‘100 MW utility scale’ pricing given that the others are likely to apply only at the initial stage of the project. These include interconnection fees, structural components, land acquisition, transmission lines, and construction permit fees (Fu et al., 2016). The components that I believed would factor into the panels’ replacement cost at the ‘100 MW utility’ price scale. are: 1) the module price, 2) the electrical balance of system (BOS) price, 3) labor costs, 4) the engineering, procurement, and construction (EPC) overhead costs, 5) the total price difference between a new module with a double axis tracker and a new one without an axis tracker, and 6) contingency. I included the total price differences between new modules with either one or two axis trackers and new ones without axis trackers in the replacement costs for all iterations that contain at least one axis tracker¹⁵. I did this to account for the difference in costs of individual replacement components for modules with axis trackers and those without. But, these total price differences account for components that are not factored into replacement costs. However, they provide a conservative estimate that creates a further layer of contingency. The BOS refers to equipment such as fuses, switches, conductors, and

¹⁵ These are the differences between the prices listed in the ‘Capital’ boxes of iterations with either one or two axis trackers and those without axis trackers.

conduits (Fu et al., 2016). EPC overhead refers to the costs of shipping and handling equipment while contingency accounts for costs that are higher than the estimated price (Fu et al., 2016). Because inverters are covered under a separate tab, their costs are counted separately and described later in this section. The replacement costs for a solar PV module at the ‘100 MW utility scale’ with a double axis tracker are \$640/kW for the module, \$100/kW for the electrical BOS, \$160/kW for labor, \$80/kW for EPC overhead, \$120/kW for the price difference between a module without an axis tracker and one with a double axis tracker, and \$40/kW for contingency (Fu et al., 2016). This totals \$1140/kW, which is the quantity in the ‘Replacement’ box of Figure 54. This replacement price applies to iterations from the fifth and sixth rounds with ‘double axis tracker’ and ‘100 MW utility scale’ in their names.

It is important to note that the PV module cost delineation from page 39 of the 2016 NREL report by Fu and others is at the nationwide level. Given that prices for initial PV modules are lower in Texas (see page 43 of 2016 NREL report) compared to the nation as a whole, it is likely that the replacement costs are overstated. The inclusion of the total price differences between the price of new modules with at least one axis tracker and that of new modules without axis trackers provides an even more conservative estimate of the replacement costs of PV modules with axis trackers. Replacement costs are also likely to be overstated given solar technology’s rapid advancement and decreasing costs (Feldman et al., 2015). For example, page 8 of the 2016 NREL report by Fu and others shows substantial decreases in the cost per watt of solar systems at residential, commercial, and utility price scales between 2009 and 2016. Page 13 of the same report shows sizable gains in PV panel efficiency at all three aforementioned scales between 2010 and 2015 (Fu et al., 2016). Efficiency refers to the

percentage of sunlight PV panels into electricity at their maximum power output level under standard test conditions (HOMER Energy, 2016s). These facts attest to the unpredictability of solar technology advancement by the year 2042, 25 years from the year 2017. Consequently, I felt it was most appropriate to use the aforementioned conservative estimate and to provide a clearer picture on replacement costs when there is a clearer idea of the progress and cost of solar technology for the year 2042.

Aarabi Madhavan, a renewable energy analyst at HOMER Energy, stated that HOMER will only include replacement costs in iterations if components have to be replaced before the lifetime of the project is over (personal communication, March 16, 2017). I set the lifetime of the solar panels as 25 years (see Figure 54) based on the fact that today's solar panels in general have a lifetime of 25 years (Pingel et al., 2009; Rodriguez & Amaratunga, 2008). Furthermore, Larry Perea mentioned that solar panels in general have a 25-year warranty but are expected to produce electricity for 30 to 50 years (personal communication, September 26, 2016). Given that I set the lifetime of the solar panels to 25 years (see Figure 54) and the project's lifetime as 25 years (see Figure 37), their replacement costs are not factored into the project. If axis components are not under the same 25-year warranty, I assumed that the operation and maintenance costs account for the replacement cost of these components.

Operation and Maintenance Costs of PV Module with Double Axis Tracker at 100 MW Utility Pricing Scale

The 'O&M' box in Figure 54 reflects the annual operation and maintenance (O&M) costs for a generic PV module per kW (HOMER Energy, 2016t). The \$20/kW O&M costs in Figure 54 are for the iterations from the fifth and sixth rounds with 'double axis tracker' and '100 MW utility scale' in their names. I set these costs based on the 2016 NREL report by Fu and others

and another NREL report from 2016 titled “Distributed Generation Renewable Energy Estimate of Costs” (Fu et al., 2016; NREL, 2016). The latter NREL report showed O&M costs as \$19/kW with a standard deviation of \$15 at the national level (NREL, 2016). Page 43 of the 2016 NREL report by Fu and others showed the annual O&M costs for a module without an axis tracker as \$15/kW and the O&M costs for a module with a single axis tracker as \$18/kW. Based on this information and the fact that Texas’ costs are below the national average (see pages 39 and 43 of the 2016 NREL report by Fu and others), I set the annual O&M costs for a PV module without an axis tracker as \$10/kW. I added \$5/kW to this O&M cost for a PV module with a single axis tracker to provide a conservative estimate and account for a potential margin of error for the O&M cost differences between a module without an axis tracker and one with a single axis tracker from the 2016 NREL report by Fu and others. With Ran Fu’s validation, I added another \$5/kW to the annual O&M costs for a dual axis PV module with the same logic I utilized for deriving the initial price of a dual axis PV module (personal communication, April 12, 2017). Consequently, the annual O&M costs for a double axis PV module at the ‘100 MW utility’ pricing scale are \$20/kW (see Figure 54).

Initial Costs of PV Module with Single Axis Tracker, 100 MW Utility Price Scale, and No Net Metering

The iteration in Figure 55 uses PV design criteria from the fifth round of iterations and includes ‘100 MW utility scale’ pricing, a single solar axis tracker, and no net metering. The initial price of a generic PV module per watt at a ‘100 MW utility scale’ pricing that includes a single axis tracker and an inverter is \$1.38, which corresponds to \$1380/kW. This price level, which applies to the iterations from the fifth and sixth rounds with ‘single axis tracker’ and ‘100 MW utility scale’ in their names, also reflects the figures for Texas from the chart on page 43 of

the 2016 NREL report by Fu and others. The reasoning behind this price setting is explained in the paragraph after Figure 54 that delineates the initial cost of a generic PV module with a dual axis tracker. The price listed in the ‘Capital’ box in Figure 55 shows \$1290 because the \$90 inverter cost per kW at this scale, per page 39 of the 2016 NREL report by Fu and others, is listed separately under the ‘Converter’ tab at the top of the figure.

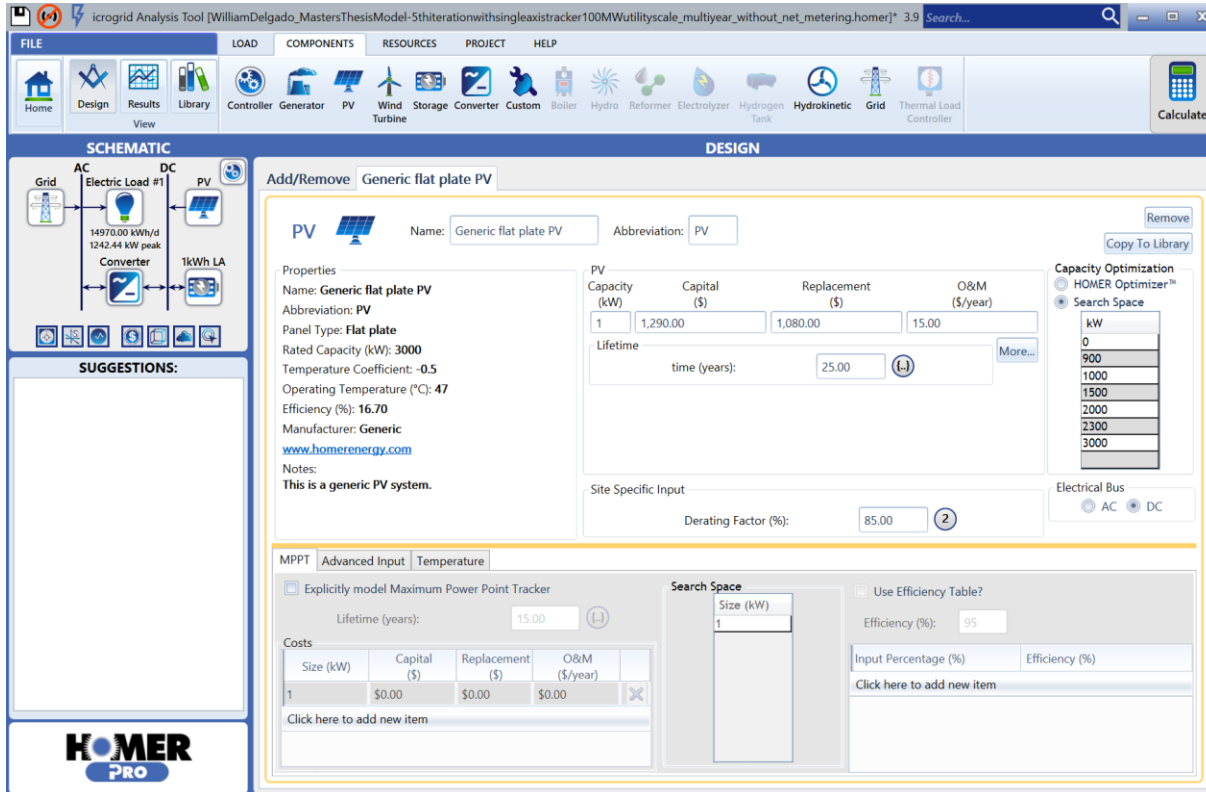


Figure 55 – Screenshot of generic PV design parameters from fifth round of iterations with ‘100 MW utility scale’ pricing, single solar axis tracker, and no net metering

Replacement Cost Components of PV Module with Single Axis Tracker at 100 MW Utility Pricing Scale

Just like with its double axis counterpart, I used the same components from the chart on page 39 of the 2016 NREL report by Fu and others to calculate the replacement costs for a PV module with a single axis tracker at the ‘100 MW utility scale.’ These are: 1) the module price, 2) the electrical BOS price, 3) labor costs, 4) EPC overhead costs, 5) the price difference per watt

between a new PV module with a single axis tracker and a new one without an axis tracker, and 6) contingency. The replacement costs for a solar PV module at the ‘100 MW utility scale’ with a single axis tracker are \$640/kW for the module, \$100/kW for the electrical BOS, \$160/kW for labor, \$80/kW for EPC overhead, \$60/kW for the price difference between a new module without an axis tracker and a new one with a single axis tracker, and \$40/kW for contingency. This totals \$1080/kW, which is the quantity in the ‘Replacement’ box of Figure 55. The costs of all components that factor into replacement costs for a PV module with a single axis tracker are the same as those for a PV module with a dual axis tracker, except the price difference between a new PV module with a single axis tracker and a new one without an axis tracker.

Operation and Maintenance Costs of PV Module with Single Axis Tracker at 100 MW Utility Pricing Scale

The \$15/kW annual O&M costs in the ‘O&M’ box in Figure 55 are for the iterations from the fifth and sixth rounds with ‘single axis tracker’ and ‘100 MW utility scale’ in their names. I used the same two NREL reports to set these costs as I did to set the O&M costs for a PV module with a double axis tracker (see Figure 54) (Fu et al., 2016; NREL, 2016). As I explained earlier, I set the annual O&M costs for a PV module without an axis tracker as \$10/kW and added \$5/kW to the annual O&M costs for a PV module with a single axis tracker. As a result, the annual costs in the ‘O&M’ box in Figure 55 are \$15/kW.

Initial Costs of PV Module Without Axis Tracker, 100 MW Utility Price Scale, and No Net Metering

The iteration in Figure 56 uses PV design criteria from the fifth round of iterations and includes ‘100 MW utility scale’ pricing. It does not include an axis tracker or net metering. The initial price of a generic PV module per watt at ‘100 MW utility scale’ pricing that includes an

inverter but does not include an axis tracker is \$1.32, which corresponds to a price of \$1320/kW. This price level, which applies to the iterations from the fifth and sixth rounds with ‘100 MW utility scale¹⁶’ in their names, also reflects the figures for Texas from the chart on page 43 of the 2016 NREL report by Fu and others. I explained the justification for this pricing in the paragraph after Figure 54 that delineates the initial cost of a generic PV module with a dual axis tracker. The price listed in the ‘Capital’ box in Figure 56 shows \$1220 because the \$100 inverter cost per kW at this scale, per page 39 of the 2016 NREL report by Fu and others, is listed separately under the ‘Converter’ tab at the top of the figure.

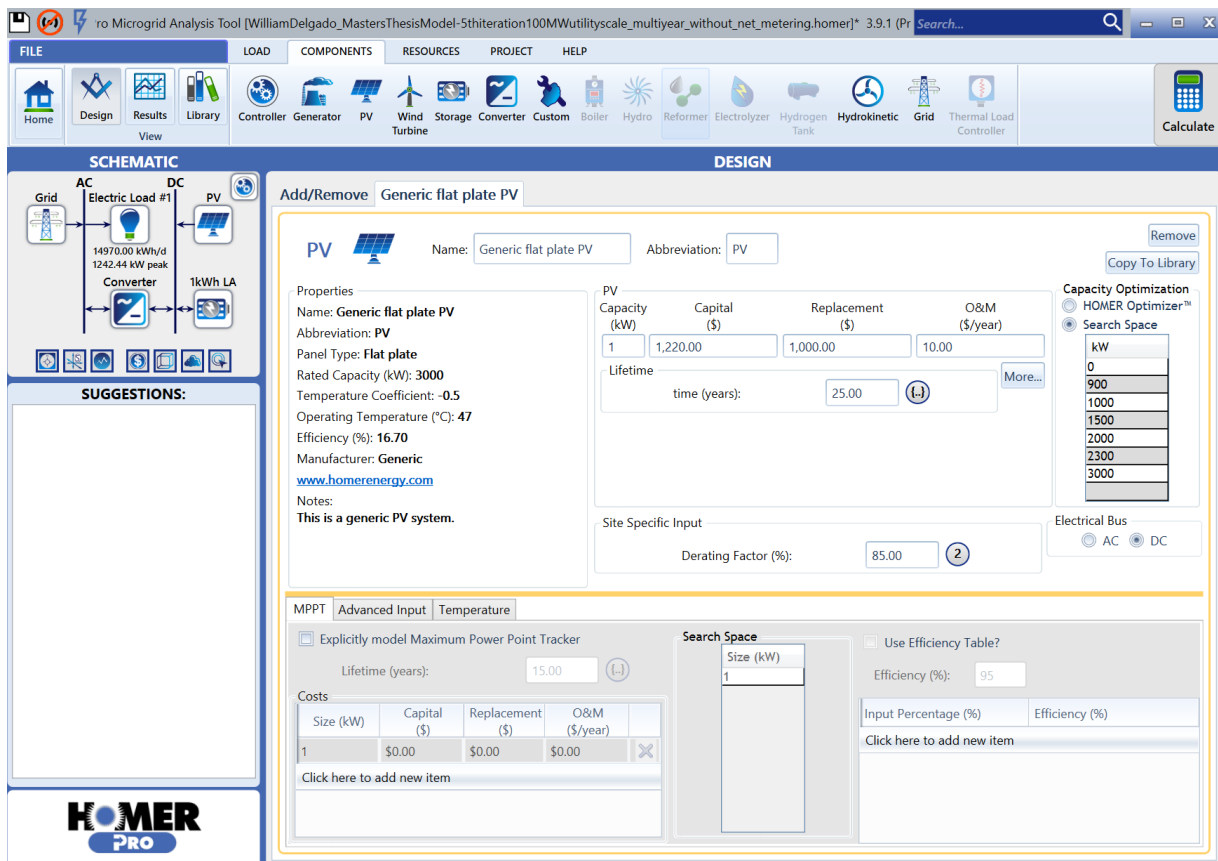


Figure 56 – Screenshot of generic PV design parameters from fifth round of iterations with ‘100 MW utility scale’ pricing, no axis trackers, and no net metering

¹⁶ Since these iterations do not include axis trackers, neither the words ‘single axis tracker’ nor ‘double axis tracker’ are present in their names.

Replacement Cost Components of PV Module Without Axis Tracker at 100 MW Utility Pricing Scale

I used the same components from the chart on page 39 of the 2016 NREL report by Fu and others to calculate the replacement costs of a PV module without an axis tracker at the ‘100 MW utility scale’ as I did to calculate those of PV modules with single axis trackers and double axis trackers at the same price scale. The one exception is the fact that the replacement costs of a PV module without an axis tracker do not include the total price difference between a new PV module with axis trackers and a new one without. These components are: 1) the module price, 2) the electrical BOS price, 3) labor costs, 4) EPC overhead costs, and 5) contingency. The replacement costs for a solar PV module at the ‘100 MW utility scale’ without an axis tracker are \$640/kW for the module, \$100/kW for the electric BOS, \$150/kW for labor, \$70/kW for EPC overhead, and \$40/kW for contingency. This totals \$1000/kW, which is the quantity in the ‘Replacement’ box of Figure 56. The labor and EPC overhead replacement cost components are slightly lower for PV modules without axis trackers than they are for PV modules with either one or two axis trackers (Fu et al., 2016).

Operation and Maintenance Costs of PV Module Without Axis Tracker at 100 MW Utility Pricing Scale

The \$10/kW annual O&M costs in the ‘O&M’ box in Figure 56 are for the iterations from the fifth and sixth rounds whose names have ‘100 MW utility scale’ but do not have ‘single axis tracker’ or ‘double axis tracker.’ I used the two NREL reports that I used to set the O&M costs for PV modules with single and double axis trackers (See Figures 54 and 55) (Fu et al., 2016; NREL, 2016). Using the reasoning I outlined in the paragraph in which I set the annual O&M costs for a PV module with a double axis tracker at the ‘100 MW utility scale’, I set the

annual O&M costs for a PV module without axis trackers at the ‘100 MW utility scale’ as \$10/kW.

Initial Costs of PV Module with Double Axis Tracker, 500 kW Commercial Price Scale, and No Net Metering

The iteration in Figure 57 uses PV design criteria from the fifth round of iterations and includes ‘500 kW commercial scale’ pricing, a double solar axis tracker, and no net metering. The initial price of a generic PV module per watt at the ‘500 kW commercial scale’ that includes a double axis tracker is \$1.99, which corresponds to \$1990/kW. This price level, which applies to the iterations from the fifth and sixth rounds with ‘double axis tracker’ and ‘500 kW commercial scale’ in their names, derives from the charts on pages 32 and 33 of the 2016 NREL report by Fu and others. Page 32 of this same report shows the price per watt of a 200-kW and 500-kW commercial PV system at the nationwide level. The prices for these systems per watt at the national level are \$2.13 and \$2.06 respectively (Fu et al., 2016). Page 33 of the 2016 NREL report by Fu and others shows the price per watt of a 200-kW commercial PV system in Texas as \$1.99. The difference between the price of a 200-kW commercial PV system per watt at the national level and one at the Texas level is \$0.14. Given this fact, I assumed that the difference between the price of a 500-kW commercial PV system per watt at the national level and one at the Texas level is also \$0.14; Ran Fu approved of this reasoning (personal communication, March 29, 2017). This means that the price per watt of a 500-kW commercial PV system in Texas is \$1.92, which corresponds to \$1920/kW. But, this price includes \$0.13/watt for an inverter (see page 32 of Fu et al 2016¹⁷). Given that the \$130/kW price for an inverter at the

¹⁷ This page shows the inverter price per kW for a single axis PV module at the ‘500 kW scale; with Ran Fu’s approval, I assumed that the corresponding inverter price for a dual axis PV module per kW is the same (personal communication, June 4, 2017).

'500 kW commercial scale' is listed separately under the 'Converter' tab in Figure 57, the initial price of a 500 kW PV system in Texas without solar axis trackers is \$1790/kW.

Unfortunately, Fu and others (2016) did not have prices for PV modules with a single axis tracker at the '500 kW commercial scale.' To approximate the difference in price between a PV module without an axis tracker and one with a single axis tracker at the '500 kW commercial scale,' I used the difference in price between these two types of modules at the '5 MW utility scale.' Per page 39 of Fu and others (2016), the price difference between a PV module without an axis tracker and one with a single axis tracker at the '5 MW utility scale' is \$0.10/watt or \$100/kW (Fu et al., 2016). I contacted Ran Fu to seek his opinion about this reasoning, and he confirmed that it was appropriate (personal communication, March 28, 2017). I used the same rationale for setting the price difference between a PV module with a single axis tracker and one with a double axis tracker at the '100 MW utility scale' to set the price difference between a PV module with a double axis tracker and one with a single axis tracker at the '500 kW commercial scale.' I outlined this rationale in the first paragraph after Figure 54. Per this rationale, the price difference of a PV module with a double axis tracker and one without an axis tracker at the '500 kW commercial scale' is \$0.20/watt or \$200/kW. I added the \$200/kW to the price of \$1790/kW for a PV module without an axis tracker at the '500 kW commercial scale' to set the total initial price of a PV module with a double axis tracker at the '500 kW commercial scale' in Texas as \$1990/kW, which is the price displayed in the 'Capital' box of Figure 57.

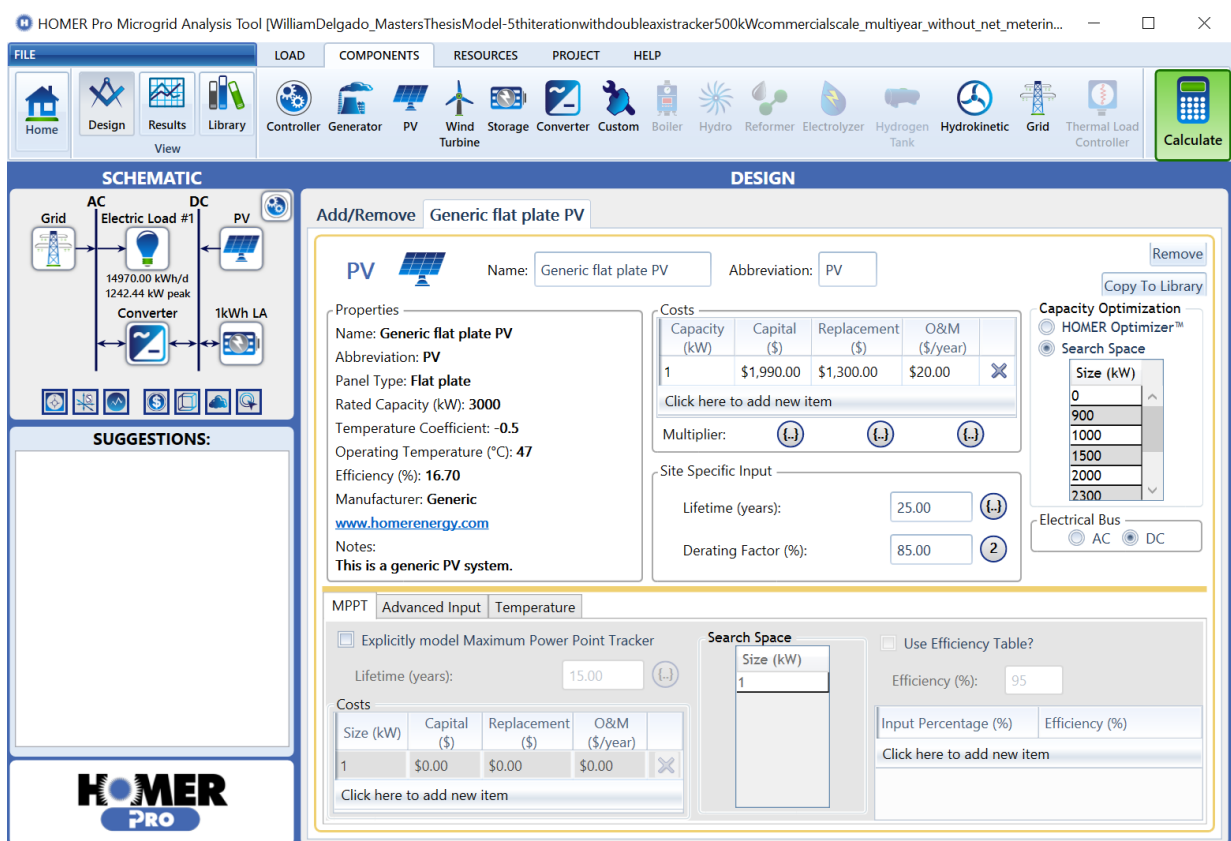


Figure 57 – Screenshot of generic PV design parameters from fifth round of iterations with ‘500 kW commercial scale’ pricing, double solar axis tracker, and no net metering

Replacement Cost Components of PV Module with Double Axis Tracker at 500kW Commercial Pricing Scale

The chart on page 32 of the 2016 NREL by Fu and others report delineates each of the components that account for the price of a PV system per watt at the ‘500 kW commercial scale.’ I factored the same components into the replacement costs for the iterations at the ‘500 kW commercial scale’ as I did for those at the ‘100 MW utility scale.’ I explained the reasoning behind selecting these components in the second paragraph after Figure 54. These components are: 1) the module price, 2) electrical BOS price, 3) labor costs, 4) EPC overhead costs, 5) total price difference between a new PV module with a dual axis tracker and a new one without an axis tracker, and 6) contingency. The replacement costs for a PV module with a double axis

tracker at the '500 kW commercial scale' are \$640/kW for the module, \$150/kW for the electrical BOS, \$100/kW for labor, \$150/kW for EPC overhead, \$200/kW for the price difference between a new PV module with a dual axis tracker and a new one without an axis tracker, and \$60/kW for contingency. This totals \$1300/kW, which is the quantity in the 'Replacement' box of Figure 57.

The chart on page 33 of the 2016 NREL report by Fu and others shows that labor costs for a 200-kW commercial PV system in Texas are \$0.06/watt less than the labor costs for a 200-kW commercial PV system at the national level. This same chart shows that EPC overhead costs for a 200-kW commercial PV system in Texas are \$0.04/watt less than EPC overhead costs for a 200-kW commercial PV system at the national level. In light of these facts, I assumed that the difference in labor costs for a 500-kW commercial PV system in Texas and those of a 500-kW commercial PV system at the national level is also \$0.06/watt. Given that the labor costs for a 500-kW commercial PV system at the national level are \$0.16/watt per the chart on page 32 of Fu and others (2016), I calculated that the labor costs for a 500-kW commercial PV system in Texas are \$0.10/watt, or \$100/kW. I also assumed that the difference in EPC overhead costs for a 500-kW PV commercial system in Texas and those of a 500-kW commercial PV system at the national level is also \$0.04/watt. Given that the EPC overhead costs for a 500-kW commercial PV system at the national level are \$0.19/watt, I calculated that the EPC overhead costs for a 500-kW commercial PV system in Texas are \$0.15/watt, or \$150/kW (Fu et al., 2016). Ran Fu agreed with the logic behind the aforementioned settings (personal communication, March 29, 2017).

Operation and Maintenance Costs of PV Module with Double Axis Tracker at 500 kW Commercial Pricing Scale

The \$20/kW annual O&M costs in the ‘O&M’ box in Figure 57 are for the iterations from the fifth and sixth rounds with ‘double axis tracker’ and ‘500 kW commercial scale’ in their names. I used the same two NREL reports to set these costs as I did for those in Figures 54 through 56 (Fu et al., 2016; NREL, 2016). With Ran Fu’s assent, I used the same rationale to set the annual O&M costs as \$20/kW for a PV module with a dual axis tracker at the ‘500 kW commercial scale’ as I did to set those for a PV module with a dual axis tracker at the ‘100 MW utility scale’ (personal communication, April 12, 2017).

Initial Costs of PV Module with Single Axis Tracker, 500 kW Commercial Price Scale, and No Net Metering

The iteration in Figure 58 uses PV design criteria from the fifth round of iterations and includes ‘500 kW commercial scale’ pricing, a single solar axis tracker, and no net metering. The initial price of a generic PV module per watt at the ‘500 kW commercial scale’ that includes a single axis tracker is \$1.89, which corresponds to \$1890/kW. This price level, which applies to the iterations from the fifth and sixth rounds with ‘single axis tracker’ and ‘500 kW commercial scale’ in their names, derives from the charts on pages 32 and 33 of the 2016 NREL report by Fu and others. I explained in the paragraph before Figure 57 the logic behind the initial price of \$1790/kW for a 500 kW PV system without axis trackers in Texas. Subsequently, I added \$100/kW to the price of \$1790/kW for a PV module without an axis tracker at the ‘500 kW commercial scale’ to set the total initial price of a PV module with a single axis tracker at the ‘500 kW commercial scale’ in Texas as \$1890/kW, which is the price displayed in the ‘Capital’

box of Figure 58. I explained the basis for adding \$100 to \$1790 in order to represent the price per kW of a 500 kW PV system with a single axis tracker in the first paragraph after Figure 57.

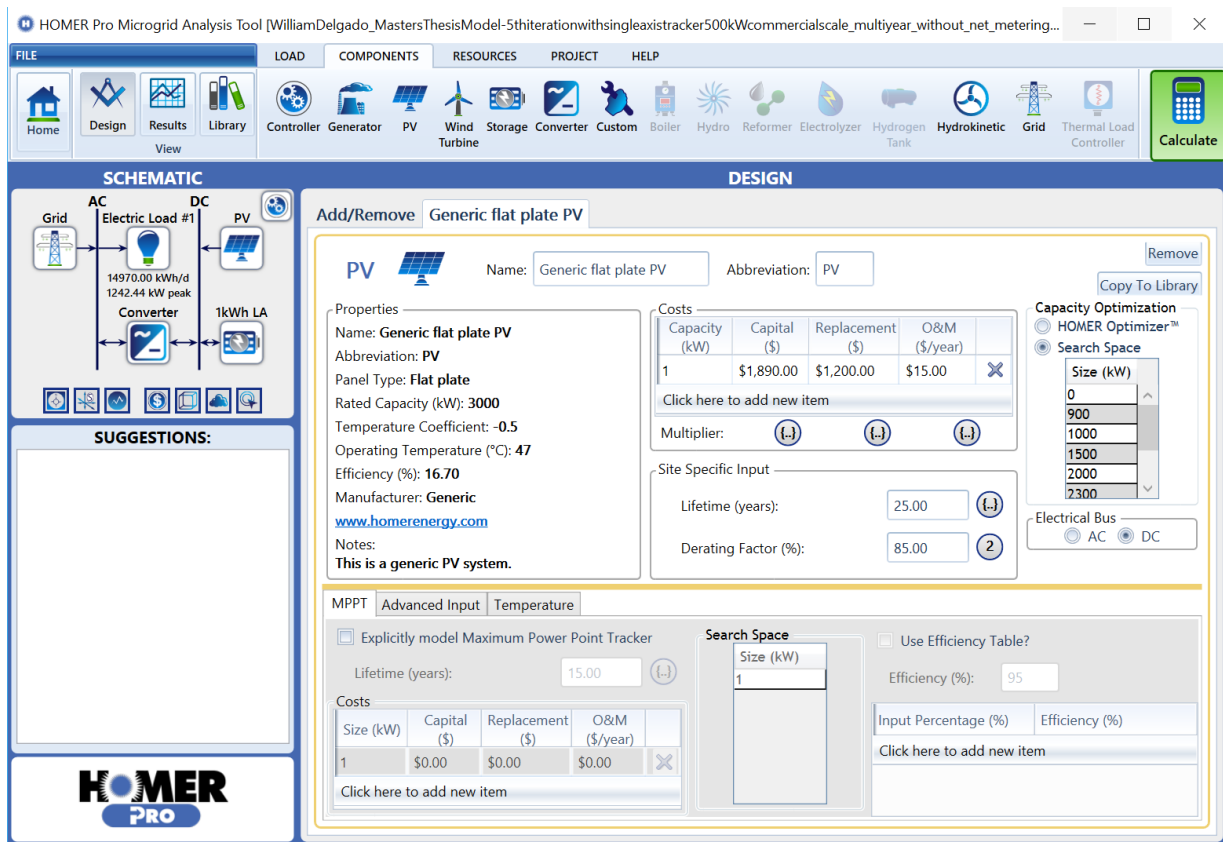


Figure 58 – Screenshot of generic PV design parameters from fifth round of iterations with ‘500 kW commercial scale’ pricing, single solar axis tracker, and no net metering

Replacement Cost Components of PV Module with Single Axis Tracker at 500kW Commercial Pricing Scale

I factored in the same components from the chart on page 32 of the 2016 NREL by Fu and others report to calculate the replacement costs for a PV module with a single axis tracker at the ‘500 kW commercial scale’ as I did for its double axis counterpart at this scale. These are: 1) the module price, 2) the electrical BOS price, 3) labor costs, 4) EPC overhead costs, 5) the price difference per watt between a new PV module with a single axis tracker and a new one without an axis tracker, and 6) contingency. The replacement costs for a PV module with a single axis

tracker at the ‘500 kW commercial scale’ are \$640/kW for the module, \$150/kW for the electrical BOS, \$100/kW for labor, \$150/kW for EPC overhead, \$100/kW for the price difference between a PV module with a single axis tracker and one without an axis tracker, and \$60/kW for contingency. This totals \$1200/kW, which is the quantity in the ‘Replacement’ box of Figure 58.

Operation and Maintenance Costs of PV Module with Single Axis Tracker at 500 kW Commercial Pricing Scale

The \$15/kW annual O&M costs in the ‘O&M’ box in Figure 58 are for the iterations from the fifth and sixth rounds with ‘single axis tracker’ and ‘500 kW commercial scale’ in their names. I used the same two NREL reports to set these costs as I did for those in Figures 54 through 56 (Fu et al., 2016; NREL, 2016). With Ran Fu’s approval, I used the same rationale to set the annual O&M costs as \$15/kW for a PV module with a single axis tracker at the ‘500 kW commercial scale’ as I did to set those for a PV module with a single axis tracker at the ‘100 MW utility scale’ (personal communication, April 12, 2017).

Initial Costs of PV Module Without Axis Tracker, 500 kW Commercial Price Scale, and No Net Metering

The iteration in Figure 59 uses PV design criteria from the fifth round of iterations and includes ‘500 kW commercial scale’ pricing. It does not include an axis tracker or net metering. The initial price of a generic PV module per watt at the ‘500 kW commercial scale’ without an axis tracker is \$1.79, which corresponds to \$1790/kW. This price level, which applies to the iterations from the fifth and sixth rounds with ‘500 kW commercial scale’ in their names, derives from the charts on pages 32 and 33 of the 2016 NREL report by Fu and others. I explained in the paragraph before Figure 57 the logic behind the initial price of \$1790/kW for a 500 kW PV

system without axis trackers in Texas. This is the price displayed in the ‘Capital’ box of Figure 59.

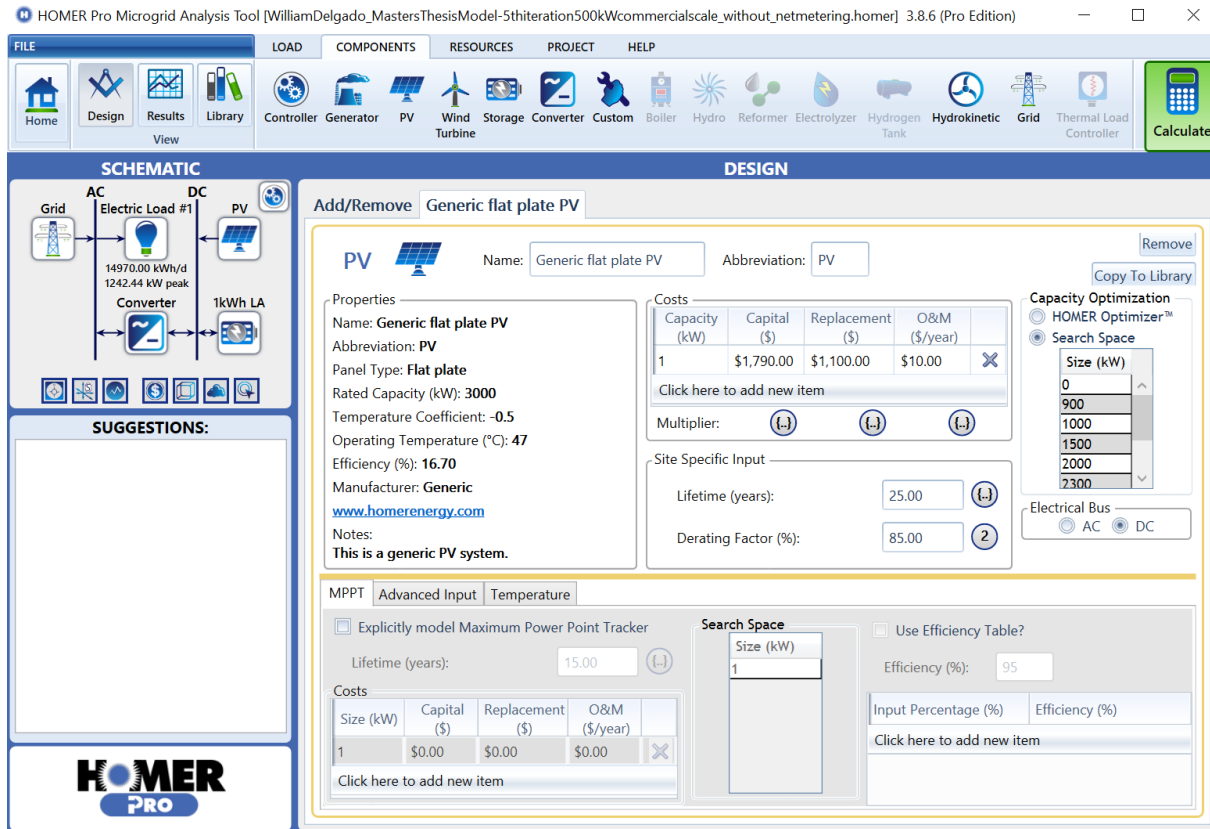


Figure 59 – Screenshot of generic PV design parameters from fifth round of iterations with ‘500 kW commercial scale’ pricing, no axis trackers, and no net metering

Replacement Cost Components of PV Module Without Axis Tracker at 500kW Commercial Pricing Scale

I used the same components from the chart on page 32 of the 2016 NREL report by Fu and others to calculate the replacement costs of a PV module without an axis tracker at the ‘500 kW commercial scale’ as I did to calculate those of PV modules with single axis trackers and double axis trackers at the same scale. The one exception is the fact that the replacement costs of a PV module without an axis tracker do not include the total price difference between a new PV module with axis trackers and a new one without. These components are: 1) the module price, 2)

the electrical BOS price, 3) labor costs, 4) EPC overhead costs, and 5) contingency. The replacement costs for a solar PV module at the ‘500 kW commercial scale’ without an axis tracker are \$640/kW for the module, \$150/kW for the electric BOS, \$100/kW for labor, \$150/kW for EPC overhead, and \$60/kW for contingency. This totals \$1100/kW, which is the quantity in the ‘Replacement’ box of Figure 59.

Operation and Maintenance Costs of PV Module Without Axis Tracker at 500 kW Commercial Pricing Scale

The \$10/kW annual O&M costs in the ‘O&M’ box in Figure 59 are for the iterations from the fifth and sixth rounds with ‘500 kW commercial scale’ in their names. I used the same two NREL reports to set these costs as I did for those in Figures 54 through 56 (Fu et al., 2016; NREL, 2016). I used the same rationale to set the annual O&M costs as \$10/kW for a PV module without axis trackers at the ‘500 kW commercial scale’ as I did to set those for a PV module without axis trackers at the ‘100 MW utility scale.’

PV Module Capacity Optimization

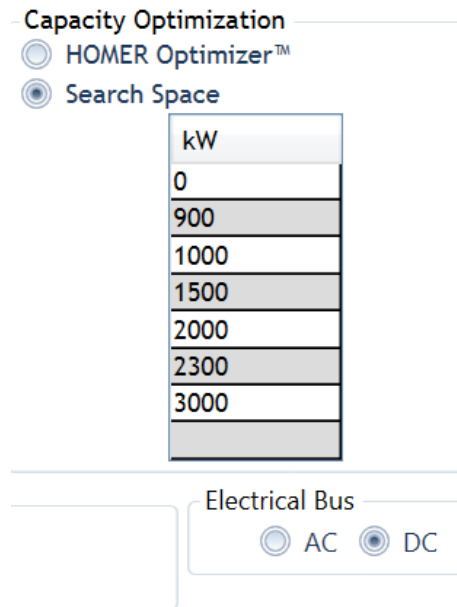


Figure 60 – Screenshot of PV module capacity search space

Figure 60, which is a magnified part of each of Figures 54 through 59, illustrates the PV module capacity optimization search space. The PV module capacity optimization search space allows the user to test different PV module kW capacities to maximize PV electricity production and lead to the most economically feasible PV/grid energy combination to power the KBH plant. The HOMER optimizer allows the user to enter an upper and lower limit of PV capacities; the lower limit should be zero to allow the model to designate a grid-only configuration as the best energy source while the upper limit should be significantly higher than the greatest anticipated load in order for HOMER to have an ideal range of PV module capacities (HOMER Energy, 2016c; A. Baumbach, personal communication, February 7, 2017). The optimizer uses an algorithm, based on factors such as PV module pricing, battery pricing, inverter pricing, and grid energy pricing, as well as grid interconnection costs and PV production based on available solar radiation to find the energy source combination that results in the least amount of energy costs for the plant over the course of the project's lifetime (HOMER Energy, 2016c; A. Baumbach, personal communication, February 7, 2017).

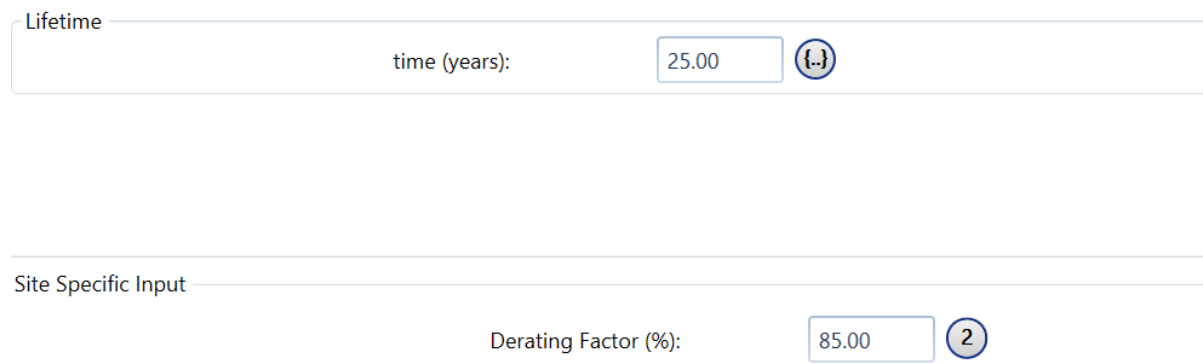
Given that this project explicitly accounts for PV module output degradation over the years,¹⁸ the iterations from the fifth and sixth rounds do not use the optimizer. The optimizer's algorithm extrapolates on the best energy configurations over the lifetime of the project without explicitly accounting for user-inputted rates of decline of the PV module output over the project's lifetime (A. Madhavan, personal communication, March 16, 2017). The optimizer is unable to account for user-inputted rates of decline of the PV module output because HOMER does not have the capacity to reoptimize the best configuration for every year of the project's

¹⁸ The 'Multi-Year' calculator is where the user enters PV module output decline rates over the project's lifetime; these rates are described in a later subsection.

lifetime based on these rates of PV module output decline (A. Madhavan, personal communication, March 16, 2017). Without the optimizer, the user has to manually create his or her own variety of PV module capacities (A. Madhavan, personal communication, March 16, 2017). Furthermore, without the optimizer, HOMER will only test the capacity values that you enter into the search space and provide results based on those capacity values (see Figure 60) (A. Madhavan, personal communication, March 16, 2017).

To find the ideal variety of PV module capacities, I followed Ms. Madhavan’s recommendation of running each iteration with the optimizer and without the ‘Multi-Year’ calculator (personal communication, March 16, 2017). Interestingly, the optimizer found the same variety of PV module capacities for each iteration. This variety of PV module capacities is depicted in the search space area of Figure 60. The electrical bus, located below the search space area in Figure 60, is set to DC to illustrate that the PV panels produce DC power that is immediately sent to an inverter that’s separate from the PV module (HOMER Energy, 2016t).

PV Module Lifetime and Derating Factor



The screenshot shows two input fields. The first field is labeled 'Lifetime' and contains the text 'time (years):' followed by a text box with the value '25.00' and a blue circular icon with a minus sign. The second field is labeled 'Site Specific Input' and contains the text 'Derating Factor (%):' followed by a text box with the value '85.00' and a blue circular icon with the number '2'.

Figure 61 – Screenshot of PV module lifetime and derating factor

Figure 61, which is a magnified part of Figures 54 through 59, displays the PV module lifetime and derating factor. I set the PV module lifetime to 25 years based on the findings of

Pingel and others (2009) and Rodriguez and Amaratunga (2008). The derating factor accounts for reduced PV module output in real-world operating conditions, which include dust, loss of energy in transmission, and temperatures, compared to the output for which it was rated at testing conditions (Ma, Yang, Lu, & Peng, 2015). For example, a PV module that is rated to produce 2000 kW of electricity at testing conditions will produce 1600 kW of electricity in real-world operating conditions if it has an 80% derating factor. All iterations have sensitivity cases that use 85% and 90% as derating factors. Other case studies that use HOMER to model a solar-powered microgrid use 90% as their derating factor (Givler & Lilienthal, 2005; Su, Yuan, & Chow, 2010). But, I also included 85% as a derating factor to adequately consider the effects of dust and high summer temperatures in El Paso’s desert climate that might reduce PV module output.

Temperature Effects on PV Module Performance

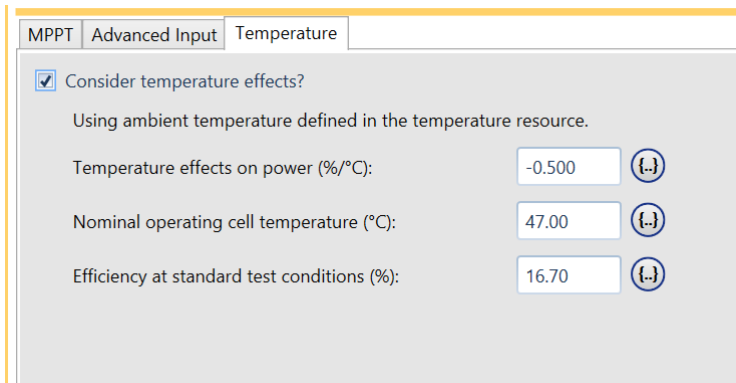


Figure 62 – Screenshot of parameters related to temperature effects on PV module performance

Figure 62, which is a magnified view of the ‘Temperature’ tab from Figures 54 through 59, displays the measures that take into account the effects of temperature PV module performance. These factors apply to the PV modules used in all twelve iterations. The temperature coefficient refers to the percentage decrease of a PV module’s output in kW for each

degree Celsius the temperature of the PV module's surface increases above the ambient air temperature (Brhimat & Mekhtoub, 2014; HOMER Energy, 2016u, 2016v). I set the temperature coefficient as $-0.5\%/^{\circ}\text{C}$ based on the findings for silicon PV panels of Brhimat and Mekhtoub (2014). Article 5.8 in the HOMER model user manual outlines the equations HOMER uses to calculate the PV cell surface temperature at each time step in order to incorporate the effects of increased surface temperatures on PV module performance based on the aforementioned temperature coefficient. Key variables include the quantity of solar radiation striking the module at each time step, the percentage of solar radiation that the ground absorbs at each time step, the temperature coefficient, the ambient air temperature, and the nominal operating cell temperature (NOCT) (HOMER Energy, 2016u). The NOCT is defined as the surface temperature that PV modules would reach if exposed to the following conditions: 1) an ambient air temperature of 20°C , 2) 0.8 kW/m^2 of solar radiation, 3) a wind speed of 1 m/s , and 4) a minimal electrical load (García & Balenzategui, 2004). The NOCT is a factor that illustrates that allows researchers to predict how the ambient air temperature influences the surface temperature of a PV module (HOMER Energy, 2016u). However, the NOCT varies based on changes in the aforementioned conditions and on PV module materials such as types of glass that influence the module's conversion of solar radiation into heat (García & Balenzategui, 2004; Muller, 2010). I set the NOCT as 47°C for silicon PV modules based on the results of a 2010 NREL study (Muller, 2010). This study contains the equation that calculates the NOCT (Muller, 2010).

Unfortunately, HOMER does not use the temperature data from NASA's SMSSED to model the ambient air temperature, or the NOCT, for each time step (A. Madhavan, personal

communication, March 16, 2017). Instead, HOMER bases the ambient air temperature and the NOCT for each time step on the average daily ambient air temperature of a given month from NASA's SMSED (see subsection on temperature data). Therefore, HOMER assumes that the ambient air temperature, and thus the NOCT, is the same across all hours of all days in a given month. In order to model temperatures at the time step level, users have to upload their own temperature datasets. This fact undermines HOMER's ability to accurately account for the effect of temperatures from the hottest hours of the day on PV module performance. This is especially true during the summer. But, Steffi Klawiter, a technician at HOMER Energy, mentioned that including a temperature coefficient and a derating factor can lead to redundant counting of PV module energy losses as both variables account for declines in output performance due to temperature (personal communication, February 17, 2017). Furthermore, the 2005 NREL case study in Sri Lanka by Givler and Lilienthal did not use a temperature coefficient to account for temperature's effects on PV module performance. Instead, they felt that a derating factor of 90% was sufficient to consider temperature's influence on PV module output (Givler & Lilienthal, 2005). Given these facts, I am confident that derating factors of 85% and 90% will adequately incorporate the effects of El Paso's high summertime temperatures on PV module energy production.

PV Module Efficiency at Standard Test Conditions

The efficiency of the PV modules at standard test conditions (see Figure 62) refers to the percentage of photons from sunlight that the module converts into electricity when the module is producing electricity at its maximum rated capacity (HOMER Energy, 2016s). Standard test conditions for PV modules have a solar radiation level of 1 kW/m^2 and a PV module temperature

of 25°C (Park, Kang, Kim, Yu, & Kim, 2009). I set the PV module efficiency for the modules in all twelve iterations based on the results of the 2016 NREL study by Fu and others, which, as of 2015, found 16.7% to be the efficiency for PV modules at the commercial and utility scales.

Advanced Inputs and MPPT

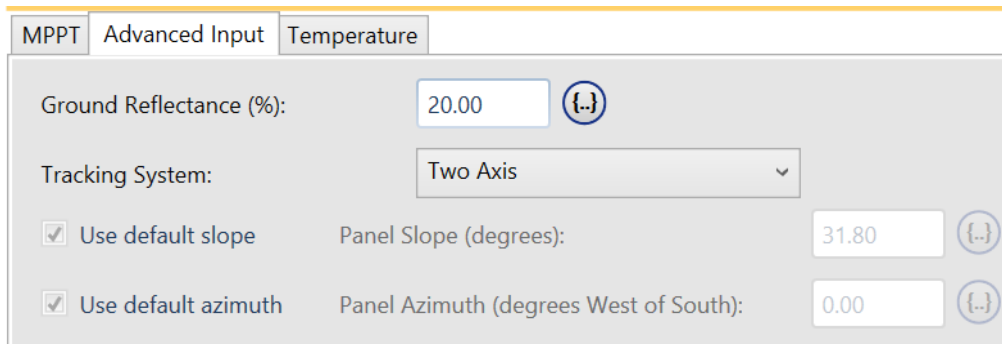


Figure 63 – Screenshot of advanced generic PV module design parameters for iterations with double solar axis trackers

Figure 63, which is a magnified view of the ‘Advanced Inputs’ tab from Figures 54 through 59, displays the measures that consider the influence of sunlight reflected from the ground, axis tracking systems, and slope orientation on PV module output. The ground reflectance factor in Figure 63 applies to all iterations. The ground reflectance factor, or albedo, refers to the percentage of solar radiation that hits the ground and is reflected (HOMER Energy, 2016w). This factor modestly affects the amount of radiation that hits the panels, which in turn slightly affects their operating temperature (HOMER Energy, 2016u, 2016w). The albedo for El Paso is about 20% (Coakley, 2003).

The tracking system component in Figure 63 illustrates the type of tracking system the PV modules in different iterations contain. The tracking system factors in Figure 63 apply to all iterations whose PV modules have double solar axis trackers. Given that Figure 63 applies to

iterations with double solar axis trackers, it displays a ‘Two Axis’ tracking system¹⁹. The slope refers to the angle at which panels are mounted relative to the horizon (HOMER Energy, 2016x). The azimuth is the direction the PV panels face; a 0° azimuth corresponds to due south, a 180° azimuth corresponds to due north, and -90° and 90° azimuths are due east and due west respectively (HOMER Energy, 2016y). Because double axis trackers maintain a perpendicular position relative to the sun throughout the day by rotating on a horizontal and vertical axis, the user is not allowed to input the slope and azimuth orientations because the PV module is constantly shifting with the sun (Argeseanu, Ritchie, & Leban, 2010; HOMER Energy, 2016x, 2016y, 2016z).

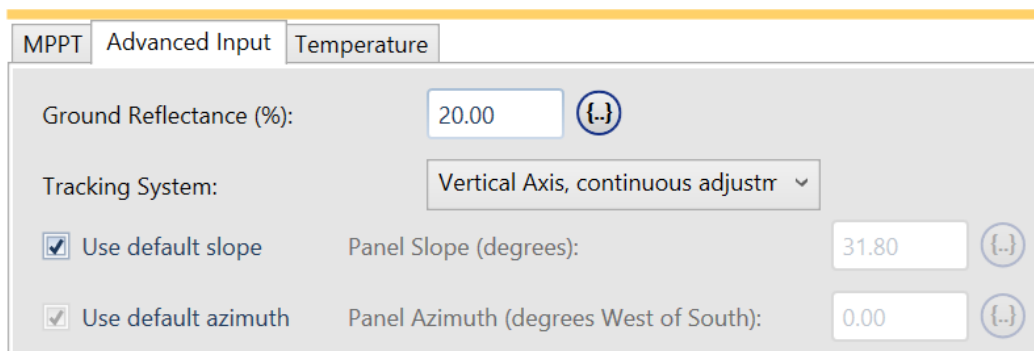


Figure 64 – Screenshot of advanced generic PV module design parameters for iterations with single solar axis trackers and a vertical axis that its continually adjusted

Figure 64, also a magnified view of the ‘Advanced Inputs’ tab from Figures 54 through 59, shows the tracking system configuration of all iterations that contain PV modules with single axis solar trackers. All iterations whose PV modules have single axis solar trackers have a tracking system that continually adjusts the PV module along a vertical axis of rotation. I

¹⁹ HOMER models dual axis and single axis tracking systems based on the changing position of the sun during each hour the day (HOMER Energy, 2016x, 2016y, 2016z). See the subsection entitled ‘Hourly Solar Radiation’ data, Articles 5.9 and 7.129 in the HOMER model user manual, and Duffie and Beckman (1991) for more details.

applied this type of system to these iterations because it is the most common system type for PV modules with single axis trackers (Lubitz, 2010). This type of system maintains a fixed slope but continually adjusts the azimuth with each time step (HOMER Energy, 2016y, 2016z).

Consequently, the user is not allowed to enter the azimuth but is allowed to enter the slope (HOMER Energy, 2016y). HOMER sets PV modules' default slope to the latitude of the KBH Plant's location, which is 31.80° north of the equator (HOMER Energy, 2016x). I left the slope at the default angle because it is most likely to maximize annual solar energy production (HOMER Energy, 2016x).

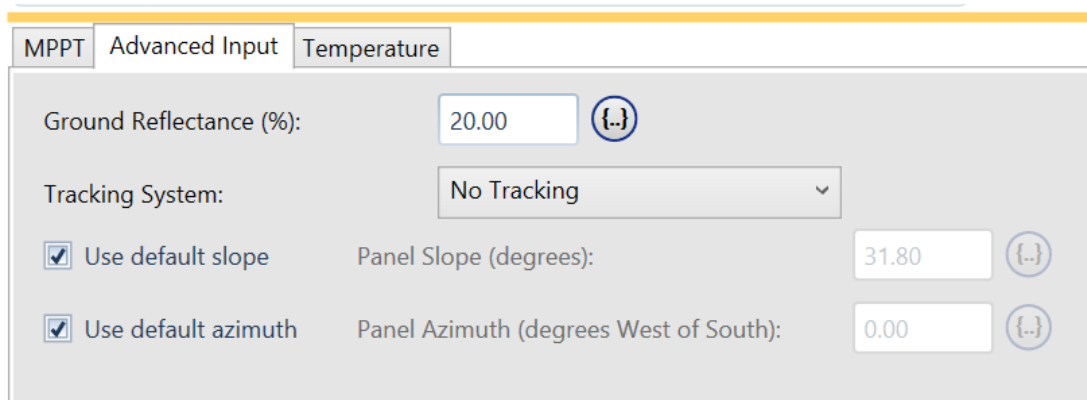


Figure 65 – Screenshot of advanced generic PV module design parameters for iterations without solar axis trackers

Figure 65, also a magnified view of the 'Advanced Inputs' tab from Figure 54 through 59, shows the tracking system configuration of all iterations that contain PV modules without solar axis trackers. PV modules without solar axis trackers have a fixed slope and fixed azimuth that the user can adjust (HOMER Energy, 2016z). Just like with the iterations whose PV modules have single axis trackers, I set the panels' slope to 31.80° . I set the panels' azimuth to 0° because solar panels with a fixed azimuth should be oriented towards the equator, which signifies their azimuth should be 0° in the northern hemisphere (HOMER Energy, 2016y).

Lastly, the MPPT tab in Figures 62 through 65 stands for maximum power point tracker (HOMER Energy, 2016t). The MPPT is a type of inverter built into the PV module system rather than a stand-alone inverter (HOMER Energy, 2016r; A. Baumbach, personal communication, February 7, 2017). The MPPT has the exact same parameters as a stand-alone inverter (HOMER Energy, 2016t). Per Aleph Baumbach's recommendation, I modeled a stand-alone inverter, which I will describe in the next subsection (personal communication, February 7, 2017).

PV Module Inverter Configurations

All PV modules that supply an AC electric load such as that of the KBH plant require an inverter to convert the DC current they produce to AC current (Vignola, Mavromatakis, & Krumsick, 2008). Figures 66 through 68 illustrate the values of the four parameters that define the inverter's configuration: 1) initial and replacement costs, 2) capacity in kW, 3) inverter lifetime, and 4) inverter efficiency. I based the inverter's initial and replacement costs in all iterations on the findings of the 2016 NREL report by Fu and others. This report displays the price of a generic inverter, which explains my decision to include a generic inverter in this project.

Fu and others' 2016 report finds that the pricing scale of PV modules influences the price of inverters per kW. But, this report also finds that the presence of solar axis trackers on PV modules at 'utility-scale' pricing reduces the price of inverters per kW compared to the price of inverters on PV modules at 'utility-scale' pricing without solar axis trackers (Fu et al., 2016). Just like with the PV modules, I followed Aarabi Madhavan's recommendation of running each iteration with the optimizer and without the 'Multi-Year' calculator to find the optimal variety of

inverter capacities (personal communication, March 16, 2017). The inverter capacity variety box is located to the right of the 'Costs' box in Figure 66. As with the PV module capacity variety, the optimizer found the same inverter capacity variety in all iterations. Hence, the inverter capacity variety remains constant across all iterations.

The inverter efficiency and lifetime also do not vary across iterations. These factors are listed just below the 'Costs' box in Figure 66. The checkbox below the inverter lifetime and efficiency settings that states 'Parallel with AC Generator?' asks whether the inverter is allowed to run in tandem with the grid, the only AC energy producer in this project. I have the box checked because I assume that the PV modules will work with the grid simultaneously to meet the KBH plant's electricity demands. The inverter's efficiency refers to the percentage of energy in DC current that the PV modules produce in kWh that the inverters convert to AC current (HOMER Energy, 2016aa). The typical average efficiency of an inverter is around 95%, which is the value I set for this project (EL-Shimy, 2012). An inverter's electric load primarily affects its level of efficiency²⁰, although the ambient air temperature is a lesser factor (Faranda, Hafezi, Leva, Mussetta, & Ogliari, 2015; Fedkin, 2015). However, HOMER assumes that the inverter's efficiency remains constant (HOMER Energy, 2016aa). Inverter lifetimes typically last fifteen years (Givler & Lilienthal, 2005). Consequently, I set the inverter lifetime for this project to fifteen years, which means that the inverters will have to be replaced once during the project's lifetime.

The 'Rectifier Input' box lies below the 'Inverter Input' box in Figure 66. A rectifier converts AC electricity to DC electricity (HOMER Energy, 2016aa). I forewent a rectifier for

²⁰ See Figure 4 in Faranda and others (2015) and Figure 11.8 in Fedkin (2015) for more information on inverter efficiencies.

this project in all iterations because it does not include components that require an AC to DC converter. In order to exclude a rectifier from the model, HOMER requires the user to set the rectifier's relative capacity, which is the capacity relative to that of the inverter, to 0% (HOMER Energy, 2016a, 2016aa).

Inverter Costs for PV Modules with Single or Double Axis Trackers at '100 MW utility' Price Scale

The initial price for inverters for PV modules with single or double axis trackers at the '100 MW utility' price scale is \$0.09/watt, which equals \$90/kW. This figure is listed in the 'Capital' column of the 'Costs' box in Figure 66. This price comes from page 39 of the 2016 NREL report by Fu and others and applies to all iterations from the fifth and sixth rounds with '100 MW utility scale' and 'single axis tracker' or 'double axis tracker' in their names.

Unfortunately, this report did not explicitly state the cost of inverters for PV modules with double axis trackers. However, Ran Fu stated that I could use the same inverter price for PV modules with single axis trackers for PV modules with double axis trackers because the inverter-load²¹ ratios for PV modules with single and dual axis trackers at the '100 MW utility' pricing scale in both the fifth and sixth rounds of iterations are about equal (personal communication, June 5, 2017). To maintain a conservative estimate, I left the inverter's replacement cost at \$90/kW. Inverter O&M costs are typically bundled with the O&M costs of the whole PV module since they are considered a part of it (Cambell, 2008; EL-Shimy, 2012; Givler & Lilienthal, 2005). Thus, I set the inverter's O&M costs to \$0 because I included them with the O&M costs of the PV module (see Figure 54 through 59).

²¹ The inverter-load ratio (ILR) refers to the ratio of the maximum PV module capacity in kW to the maximum inverter efficiency capacity in kW (Blue Oak Energy, n.d.).

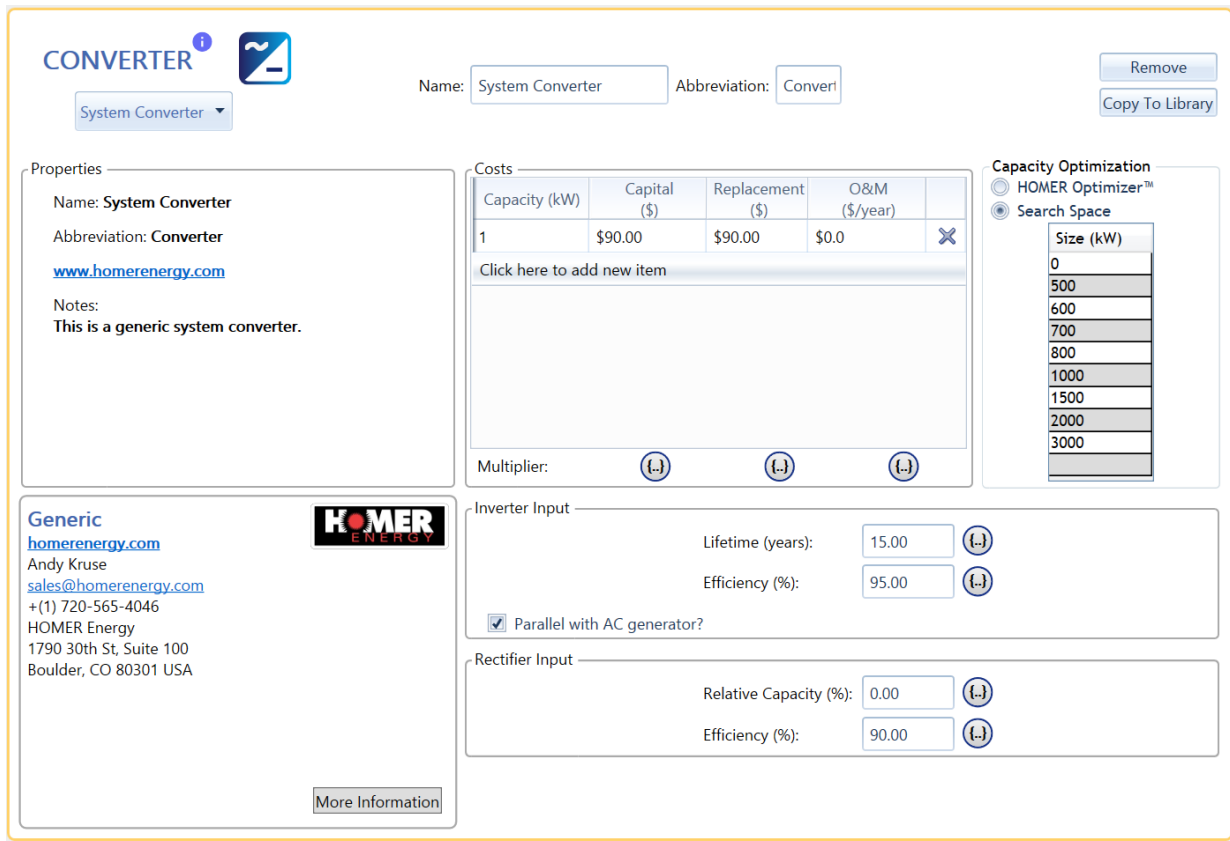


Figure 66 – Screenshot of inverter configurations for PV modules with single or double axis trackers priced at the ‘100 MW utility’ price scale

Inverter Costs for PV Modules Without Trackers at ‘100 MW utility’ Price Scale

Figure 67 displays the costs of an inverter for PV modules without axis trackers at the ‘100 MW utility’ price scale. This price is \$0.10/watt or \$100/kW with a conservative estimated replacement cost of \$100/kW. Price data also come from page 39 of the 2016 NREL report by Fu and others. They apply to all iterations from the fifth and sixth rounds with ‘100 MW utility scale’ and without ‘single axis tracker’ or ‘double axis tracker’ in their names. O&M costs are also set to \$0 because they are included with those of the PV module as a whole.

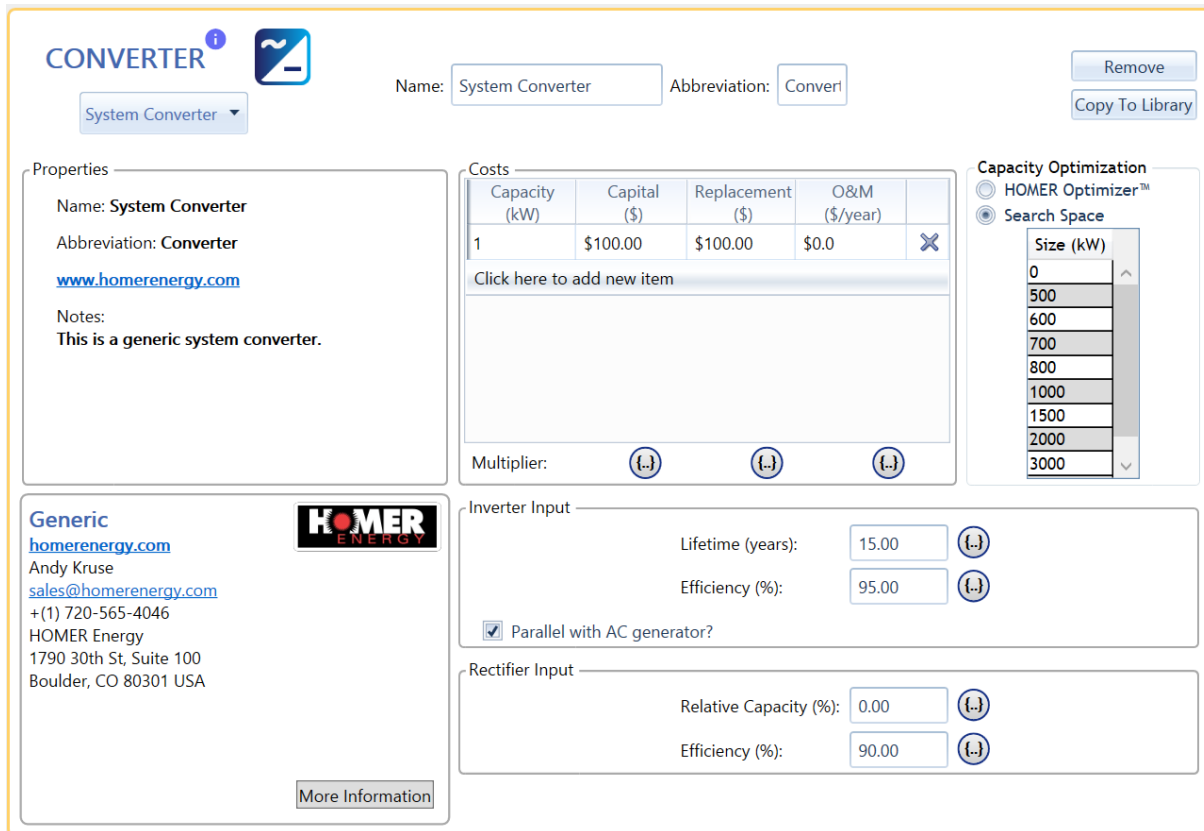


Figure 67 – Screenshot of inverter configurations for PV modules without axis trackers at the ‘100 MW utility’ price scale

Inverter Costs for All PV Modules at ‘500 kW Commercial’ Price Scale

Figure 68 displays the costs of an inverter for all PV modules at the ‘500 kW commercial’ price scale regardless of the presence of solar axis trackers. Ran Fu confirmed that the initial inverter price for all PV modules at ‘500 kW commercial’ pricing scale does not vary with the presence of solar axis trackers given that fact that the inverter load ratio is about the same across all iterations at this price scale (personal communication, June 5, 2017). This price is \$0.13/watt or \$130/kW with a conservative replacement cost also equal to \$130/kW. Price data come from pages 32 and 33 of the 2016 NREL report by Fu and others. They apply to all iterations from the fifth and sixth rounds with ‘500 kW commercial scale’ in their names. O&M costs are also set to \$0 because they are included with those of the PV module as a whole.

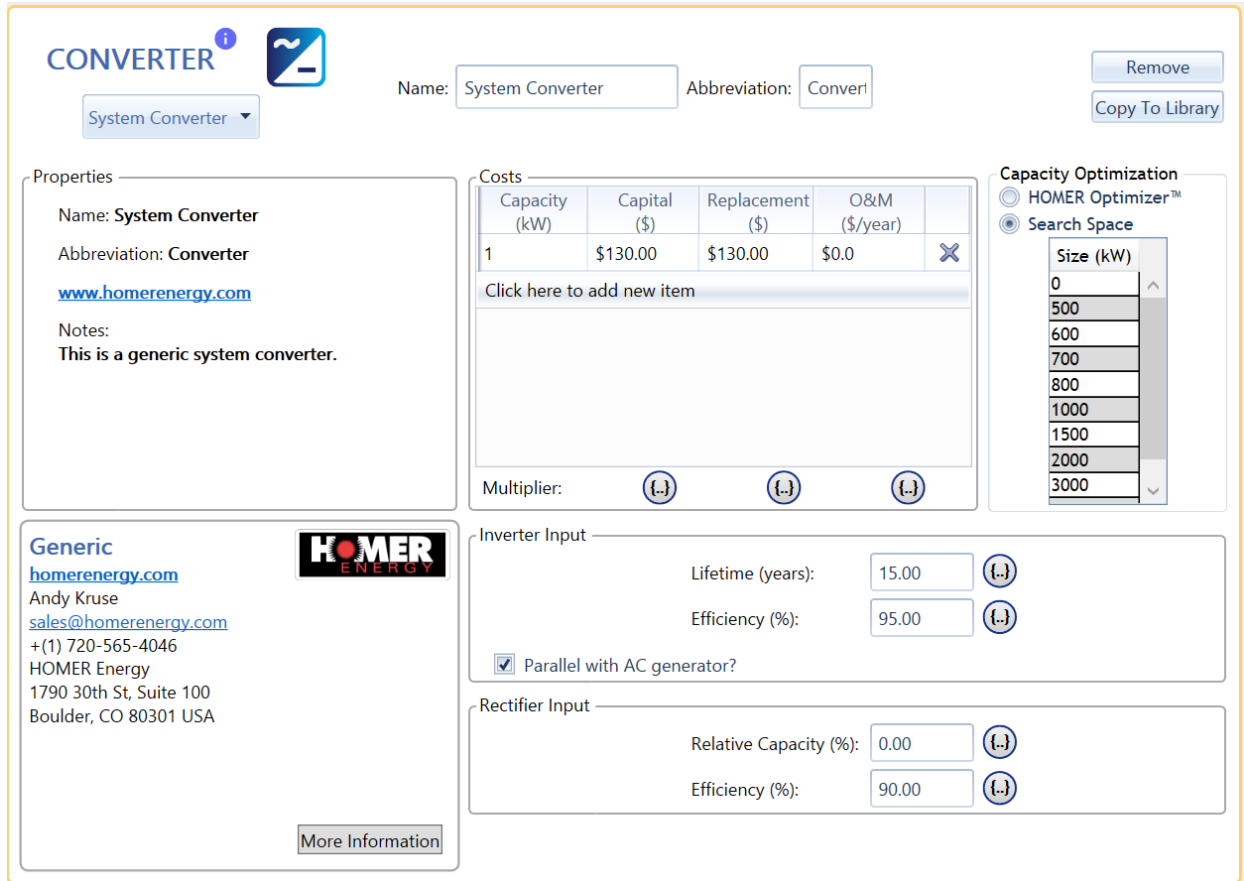


Figure 68 – Screenshot of inverter configurations for PV modules at the ‘500 kW commercial’ price scale regardless of the presence of axis trackers

PV Module Battery Configurations

I equipped all iterations with a lead acid battery to assess the feasibility of powering the KBH plant at night with stored excess solar energy generated during the day. I selected a generic lead acid battery that can output up to 1kWh of energy instead of a generic lithium ion one because a lead acid battery’s cost is only \$255/kWh versus \$300/kWh for a lithium ion battery (Albright, Edie, & Al-Hallaj, 2012). Lithium ion battery technology also has yet to develop beyond its role in portable technology to one in stationary technology (Albright et al., 2012). Figure 69 displays the battery’s configurations, which apply to all twelve model iterations in the project.

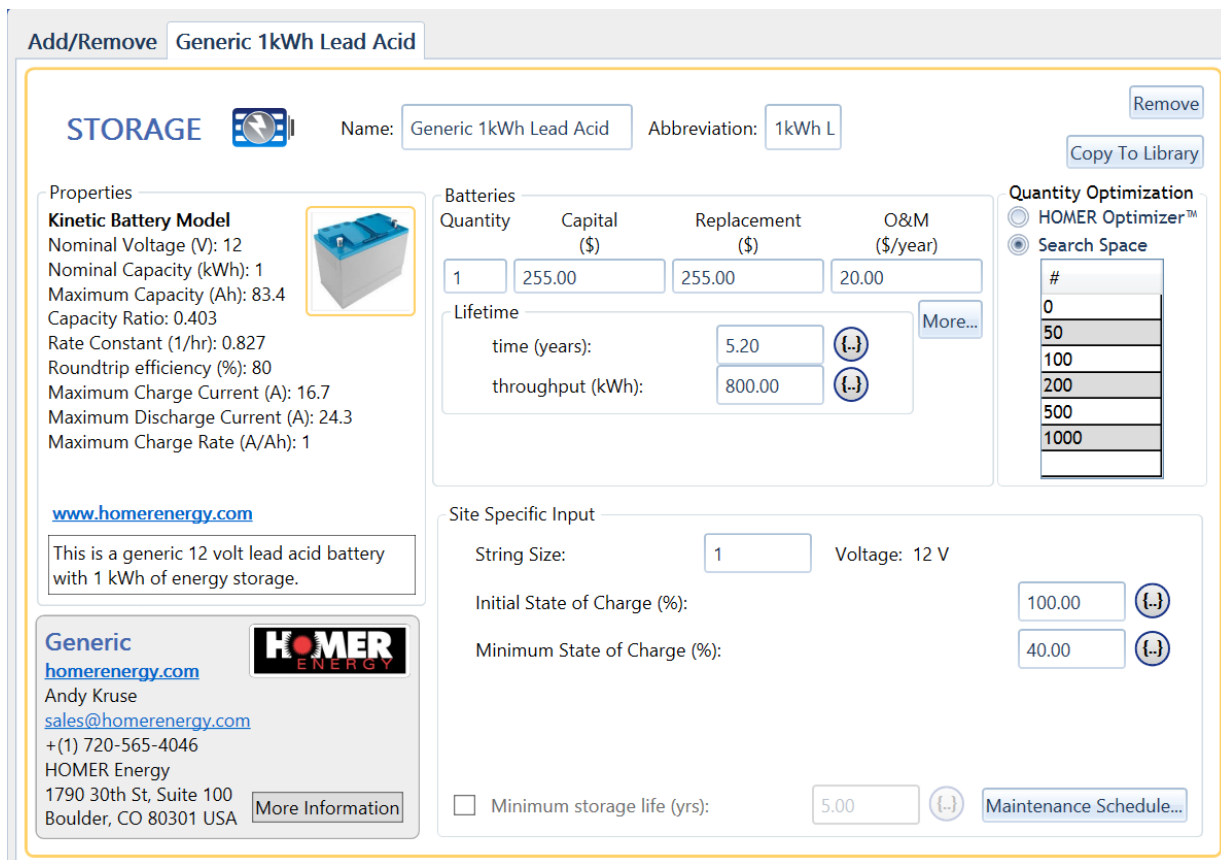


Figure 69 – Screenshot of battery configurations for PV modules in all iterations

The ‘Properties’ box in the top left corner of Figure 69 shows the characteristics of a generic 1 kWh lead acid battery, which is based on the most common values from different brands of the same type of battery (A. Baumbach, personal communication, June 2, 2017). To the right of this box is the ‘Batteries’ box, which shows the initial capital costs and replacement costs per battery as well as each battery’s O&M costs. The initial capital costs of a generic 1 kWh lead acid battery are \$255 per battery and the O&M costs are \$20/year for each battery (Diorio, Dobos, & Janzou, 2015). I kept the replacement costs at \$255 per battery to maintain a conservative estimate.

The battery's lifetime parameters are below the 'Batteries' box in the 'Lifetime' box. HOMER assumes that a battery's lifetime is primarily based on the number of discharge cycles a battery goes through before it fails²² and the depth of discharge in a discharge cycle (A. Baumbach, personal communication, June 2, 2017). The depth of discharge refers to the percentage of energy capacity a battery expends before it is recharged to full capacity (A. Baumbach, personal communication, June 2, 2017). However, the user can override this parameter by setting a fixed calendar-year period after which the batteries will be replaced in the 'time' entry area of the 'Lifetime' box in Figure 69. Given the fact that El Paso's ambient air temperatures routinely rise above 30 °C in the summer, it was most appropriate for me to reduce the battery lifetime to 5.2 years, which means the batteries will have to be replaced four times during the course of the project (Albright et al., 2012; N. W. S. US Department of Commerce, NOAA, n.d.).

²² Displayed in the 'Cycles to Failure' axis in the graph in Figure 70

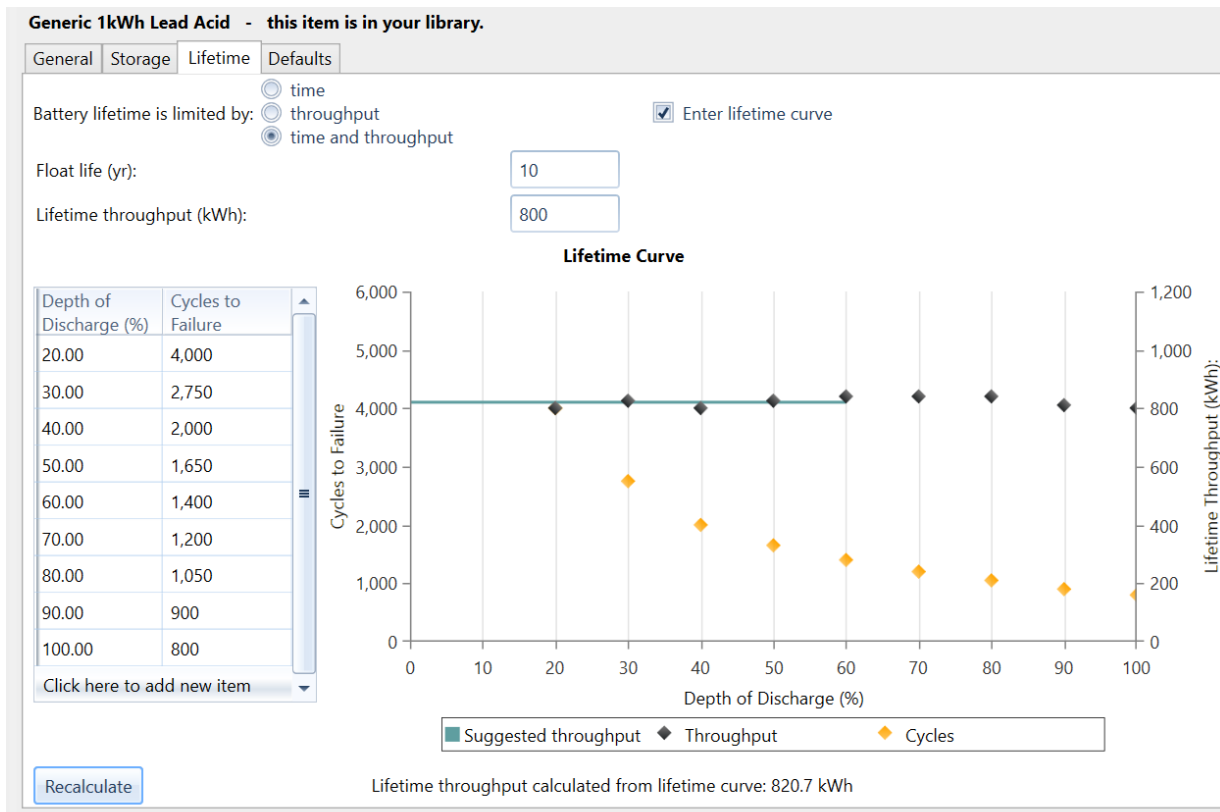


Figure 70 – Screenshot of the battery’s lifetime in ‘cycles to failure’ as a function of the battery’s depth of discharge

The axis entitled ‘Cycles to Failure’ in Figure 70 illustrates that lead acid batteries will last for more discharge cycles if the depth of discharge is deeper. However, they will fail completely if they are discharged below 20% capacity (A. Baumbach, personal communication, June 2, 2017). The battery’s lifetime throughput refers to the total amount of energy the battery discharges in kWh over its time of operation (HOMER Energy, 2016z; A. Baumbach, personal communication, June 2, 2017). HOMER uses the equation $\text{Throughput (kWh)} = C_{\text{batt}} * (\text{DOD}/100) * N * V / 1000$ to calculate throughput where C_{batt} refers to the maximum capacity of the battery in amp-hours, DOD equals the depth of discharge, N equals the number of discharge cycles, and V stands for the voltage of the battery (A. Baumbach, personal

communication, June 2, 2017). This equation finds that the battery's average lifetime throughput based on a variety of DOD scenarios in Figure 70 is 800 kWh, which is the value I set in the 'throughput' entry of the 'Lifetime' box in Figure 69.

The battery capacity variety box is located to the right of the 'Costs' box in Figure 69. Just like with the PV modules and inverters, I followed Aarabi Madhavan's recommendation of running each iteration with the optimizer and without the 'Multi-Year' calculator to find the optimal variety of inverter capacities (personal communication, March 16, 2017). As with the PV module capacity variety and inverters, the optimizer found the same battery capacity variety in all iterations. Therefore, the battery capacity variety remains constant across all iterations.

The 'string' entry below the 'Site Specific Input' box, located below the 'Lifetime' box, in Figure 69 refers to the number of batteries connected to each other (HOMER Energy, 2016ab). I assume that all batteries are independent of each other per Aleph Baumbach's recommendation, which explains why the 'string' value equals one (personal communication, February 7, 2017). I also assume that each battery starts a discharge cycle at 100% capacity, which explains why I set the 'Initial State of Charge' entry to 100%. Aleph Baumbach also recommended leaving the batteries' 'Minimum State of Charge' entry at 40% in order to minimize the risk that the charge level will drop below 20% (personal communication, June 2, 2017). The minimum state of charge ensures that batteries will stop discharging energy at the set level. Lastly, my project does not consider a minimum storage life or maintenance schedule for batteries because it assumes that the batteries will operate and be maintained as needed.

Grid Power Configurations

This project incorporates the grid as one of the sources of power for the KBH plant because its primary objective is to ascertain the energy cost savings a grid/PV hybrid power system would provide the plant as opposed to the current grid-only power supply system. Consequently, the project includes the grid as a power source in all simulations. The KBH plant's current supplier of grid electricity is El Paso Electric Company (EPE), which is the sole electricity provider for El Paso (El Paso Electric Company, n.d.-b). The Public Utility Commission of Texas (PUCT) regulates EPE as a regulated monopoly, which means that it has to approve EPE's electricity rate changes (El Paso Electric Company, n.d.-b; PUCT, n.d.).

Grid Parameters

Figure 71 shows the main parameters behind the grid component's configurations. All parameters in Figure 71 apply to all iterations with the exception of net metering, which only applies to sixth round iterations. Given that EPE tabulates net metering on a monthly basis, all from the sixth round have net metering purchases calculated monthly (El Paso Electric Company, 2011a). The first step in setting grid parameters is to decide which type of rates the grid is going to use. The 'simple rates' configuration assumes that the price for electricity from the grid and the price at which the grid buys a customer's excess electricity are constant (HOMER Energy, 2016ac). The 'real time rates' setting allows users to model a grid whose purchase and sellback rates constantly change over each time step (HOMER Energy, 2016ad). The 'scheduled rates' module, which this project uses, is designed for rates that vary based on the time of year, day of the week, and hour of the day (HOMER Energy, 2016ae). Lastly, the

‘grid extension’ program is for modeling the cost of extending the grid to a remote location that it does not already serve (HOMER Energy, 2016af).

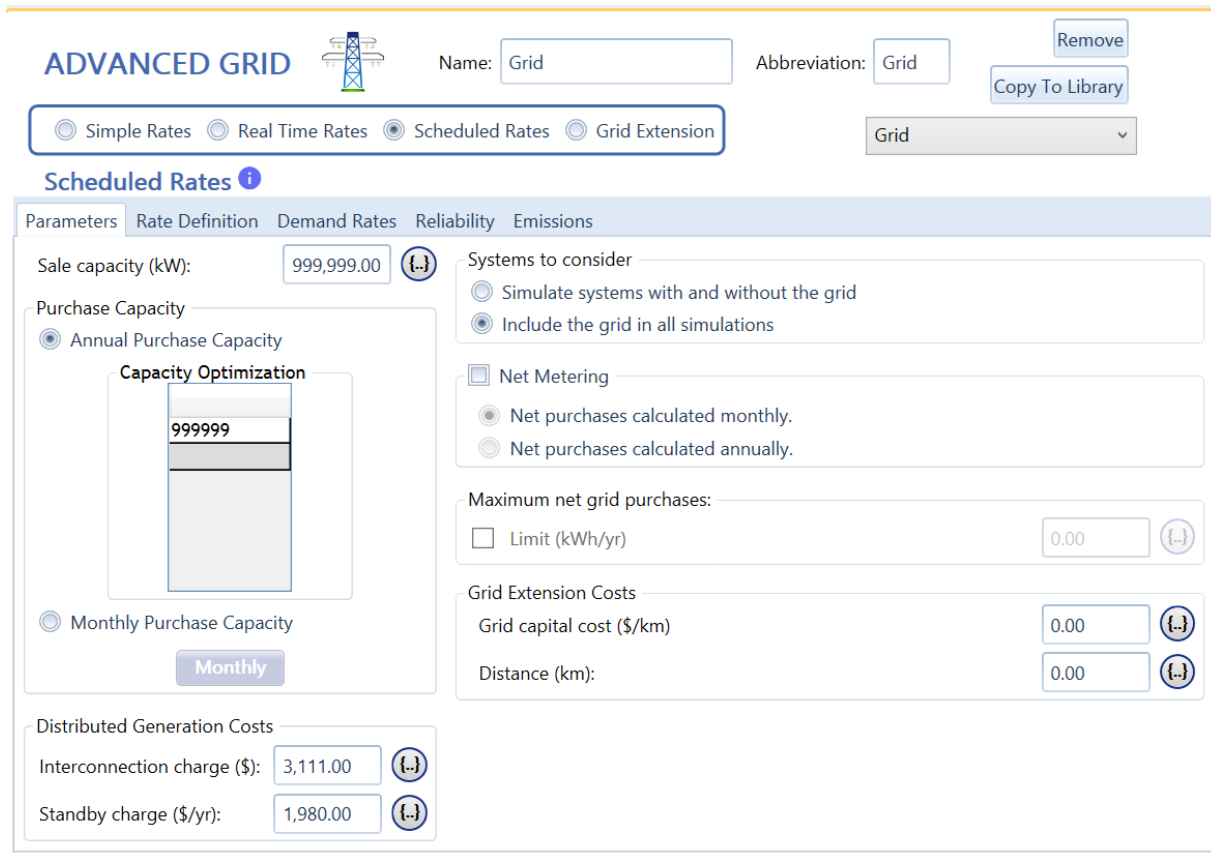


Figure 71 – Screenshot of grid component’s main configurations

EPE charges scheduled electricity rates for entities that pump water for municipal consumption under rate schedule 11 – Time of Use (TOU) (El Paso Electric Company, 2016d). Rate schedule 11 – TOU contains three rate categories: 1) off-peak, 2) shoulder-peak, and 3) on-peak. Off-peak rates apply at all times during the months of October through May. Shoulder-peak rates apply from 10 am through 1 pm and 5 pm through 8 pm on weekdays from June through September. On-peak rates apply from 1 pm through 5 pm on weekdays from June through September. Off-peak rates apply from June through September on weekends and at all

times not covered by the shoulder-peak and on-peak rates (El Paso Electric Company, 2016d). Per EPE's schedule 11– TOU rates, HOMER calculates that the KBH plant currently pays an average of \$0.0890/kWh for electricity (see Figure 82). But, Figure 41 shows that the KBH plant paid an average of \$0.08086/kWh for electricity from 2011 through 2016. This discrepancy indicates that the average electricity rate the KBH plant pays does not completely follow EPE's schedule 11 – TOU. Unfortunately, Mr. Perez does not track the hourly electricity rates for the plant because he is only interested in the cumulative annual electricity costs to operate the plant (personal communication, January 12, 2017). For customer privacy reasons, Paul Garcia, an EPE representative could not share the specific electricity rates for the KBH plant (personal communication, February 10, 2017). Thus, EPE's schedule 11 – TOU rates are the closest approximation I could find for the KBH plant's current electricity rates and are used in this project.

The sale capacity refers to the maximum amount of energy in kWh that an off-grid system can sell to the grid in a timestep (HOMER Energy, 2016ag). 999,999 is the maximum value HOMER can model and is its way of indicating that there is no limit to sales to the grid in a timestep (A. Baumbach, personal communication, February 7, 2017). EPE's allows generating systems that can produce up to 10 MW of power to be interconnected with the grid with no limit to the amount of power that can be sold to the grid (El Paso Electric Company, 2011b, 2016e). Hence, I did not set a limit to the sale capacity or the maximum net grid purchases in Figure 71. The purchase capacity refers to the maximum amount of energy that the grid is allowed to supply (HOMER Energy, 2016ag). To provide the optimum cost-effective combination of PV and grid power, this project does not limit the amount of energy that originates from the grid.

The interconnection charge is a one-time fee that the electric utility assesses on all customers who would like to have a separate power generation system that works simultaneously with the grid (HOMER Energy, 2016ah). EPE's interconnection charge funds an pre-interconnection study that assesses whether the proposed generation system could potentially cause adverse impacts to the grid's stability and reliability (El Paso Electric Company, 2016e). This fee is based on the system's electricity production capacity and whether the system has been pre-certified for safety and reliability by the PUCT according to its codes before the system is proposed to EPE (El Paso Electric Company, 2016e; PUCT, 2017). EPE's interconnection charge also includes a base fee of \$100 for a system with a production capacity of at least 100 kW of power plus \$1 for each additional 100 kW of power in the system's predicted production capacity (El Paso Electric Company, 2016e). To provide a conservative estimate, this project assumes that the PV module system will not have been pre-certified by the PUCT before the plant submits an application for interconnection. For the purposes of the interconnection fee, I set the expected production capacity of the PV modules to 624 kW, which is the KBH plant's approximate average electric load. The total interconnection fee is \$3111, which includes \$3006 for a system with a production capacity between 500 kW and 2000 kW that is not pre-certified by the PUCT, \$100 for the system's first 100 kW of expected power generation, and \$5 for the system's additional 500 kW of expected power production between 100 kW and 624 kW.

But, the interconnection charge also consists of the estimated costs EPE incurs to install an interconnected system such as parts, labor, and the extra expenses for the company to build the system compared to if they had purchased the total amount of electricity the system is expected to generate from other sources (El Paso Electric Company, 2011b). This fee is separate

from the pre-interconnection study and instead reflects the estimated costs of building a future interconnected system (El Paso Electric Company, 2011b, 2016e). To tabulate these estimated costs, EPE conducts a month-long study after it approves a customer's application for interconnection that yields variable results depending on the customer's proposed system (El Paso Electric Company, 2011b). Because there is no definite estimated amount for these costs unless EPE conducts a study, I excluded these costs from the interconnection charge.

The standby charge is the annual fee the electric utility levies to customers with separate electricity generation systems that are connected to the grid in order to provide backup power should their system fail (HOMER Energy, 2016ai). EPE charges customers a standby fee of \$165/month or \$1980/year for grid-interconnected systems with a generation capacity greater than 100 kW (El Paso Electric Company, 2011b). Customers whose systems have a capacity to generate at least 100 kW of power pay 5.3178% of the interconnection costs annual to cover O&M expenses related to the interconnected system (El Paso Electric Company, 2011b). I also excluded these costs from the standby charge because there is no definite estimated amount until the costs of interconnection study is complete.

Lastly, EPE may require customers with interconnected systems to go onto backup power service rates as described in rate schedules 46 and 47 (El Paso Electric Company, 2016a, 2016b, 2016e). The implementation of these rates is subject to negotiation with EPE and the PUCT; EPE did not specify the circumstances that increase the likelihood that these rates will be implemented (El Paso Electric Company, 2016a, 2016b, 2016e). These rate schedules charge customers based on their estimated consumption from the grid (El Paso Electric Company,

2016a, 2016b). Because these rates may not apply to the project’s proposed system, I excluded them from the grid component’s parameters.

Grid Rate Definitions

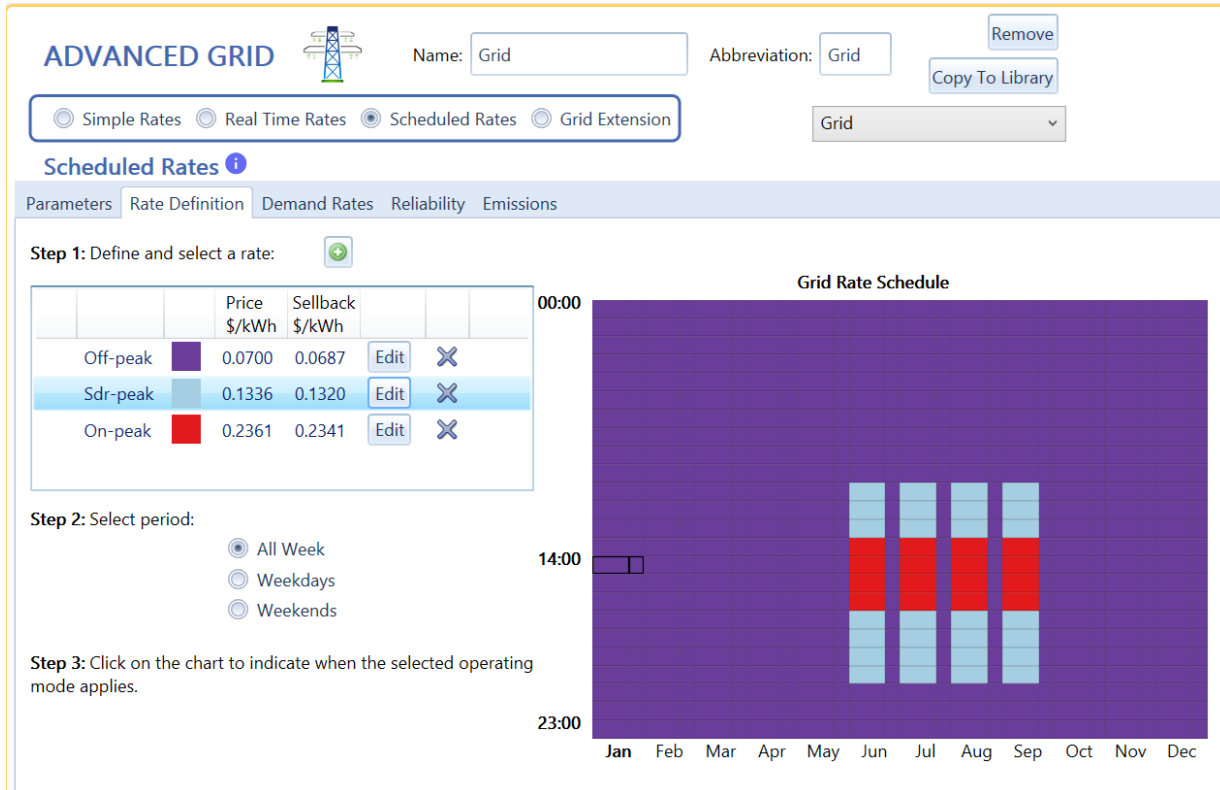


Figure 72 – Screenshot of grid component’s scheduled rates

The graph in Figure 72 depicts the months of the year on the x-axis and hours of day on the y-axis during which different scheduled rates apply. Wide rectangular blocks represent weekdays in a month while narrow ones represent all weekends. The different size blocks are more clearly visible during the times when shoulder peak and on peak rates apply. Red colored blocks represent times when on-peak rates apply, sky blue blocks represent times when shoulder-peak rates apply, and purple blocks represent times when off-peak rates apply. The factors that form the price at which EPE sells electricity are: 1) energy charge, 2) fixed fuel factor (FFF), 3)

military base discount recovery factor (MBDRF), and 4) energy efficiency cost recovery factor (EECRF) (El Paso Electric Company, 2016d) The energy charge is the market price for electricity while the FFF covers the costs of paying for the fuel that generates the electricity (El Paso Electric Company, 2017b). The EECRF incorporates EPE's costs of providing energy efficiency programs while the MBDRF recovers the costs of providing Fort Bliss with electricity at discounted prices (El Paso Electric Company, 2016c, 2017a).

The electricity rate the KBH plant pays during on-peak times is \$0.236149/kWh, which includes \$0.20820/kWh for the energy charge, \$0.025881/kWh for the FFF, \$0.000947/kWh for the MBDRF, and \$0.00121/kWh for the EECRF (El Paso Electric Company, 2016c, 2016d, 2017a, 2017b). During shoulder-peak times, the KBH plant pays \$0.133645/kWh, which includes \$0.106160/kWh for the energy charge, \$0.025881/kWh for the FFF, \$0.000483/kWh for the MBDRF, and \$0.00121/kWh for the EECRF (El Paso Electric Company, 2016c, 2016d, 2017a, 2017b). Lastly, during off-peak times the KBH plant pays \$0.069977/kWh, which includes \$0.042780/kWh for the energy charge, \$0.025881/kWh for the FFF, \$0.000195/kWh for the MBDRF, and \$0.00121/kWh for the EECRF (El Paso Electric Company, 2016c, 2016d, 2017a, 2017b). These prices associated with these rates appear next to their respective color blocks in the 'Price' column of Figure 72.

EPE pays customers with interconnected generation systems the equivalent amount of energy charge and fuel costs EPE avoided by accepting the system's excess kWh into the grid during all scheduled rate categories described earlier (El Paso Electric Company, 2011b). This means that EPE would pay the KBH plant the total of the energy charge and FFF for each kWh the PV modules feed into the grid (El Paso Electric Company, 2011b). The rate at which EPE

would pay the KBH plant for excess electricity at peak times is \$0.234081/kWh, which includes \$0.20820/kWh for the energy charge and \$0.025881/kWh for the FFF (El Paso Electric Company, 2011b, 2017b). During shoulder-peak times, EPE would pay the KBH plant \$0.132041/kWh, which includes \$0.106160/kWh for the energy charge and \$0.025881/kWh for the FFF (El Paso Electric Company, 2011b, 2017b). Lastly, during off-peak times the EPE would pay the KBH plant \$0.068661/kWh, which includes \$0.042780/kWh for the energy charge and \$0.025881/kWh for the FFF (El Paso Electric Company, 2011b, 2017b). These sellback rates and their associated prices appear next to their respective color blocks in the ‘Sellback’ column of Figure 72.

Demand Rates, Reliability, and Emissions

The ‘Demand Rates’ tab in Figure 72 is the monthly fee a utility charges during the peak demand month for the expected monthly load in kW (HOMER Energy, 2016aj). Because EPE does not specify when demand rates apply, this project does not incorporate them (El Paso Electric Company, n.d.-a). The ‘Reliability’ tab in the same figure allows the user to model the reliability of the grid’s power supply. This project does not use that tab because it assumes that grid power is always available. The ‘Emissions’ tab, also located in Figure 72, allows the user to model the amount of emissions grid power generates in order to quantify emissions savings with a renewable energy system. Because I could not find a definite source on the types of energy that EPE procures to supply its customers and those energy types’ associated emissions, I did not model potential emissions savings in this project.

The Project Tab



Figure 73 – Screenshot of project tab components

Figure 73 displays the components, which are encircled in red, associated with the project tab in the HOMER model. The 'input report' provides an explanation of the iteration's current results in word or PDF format while the 'estimate' button approximates the length of time for the model to run new calculations. Other components provide the user with an overview of the key variables that will influence the results that the model produces. These variables are known as sensitivity variables because the user can program multiple values into them simultaneously so that the model can provide a side by side comparison to illustrate how the model's results change with different variable values (HOMER Energy, 2016ak, 2016al). The project tab does not

display all of the sensitivity variables that comprise the HOMER model. These are explained in earlier subsections. Instead, the project tab’s summary of key sensitivity variables allows the user an opportunity to comprehensively review the model’s crucial settings before running calculations.

Economics Component

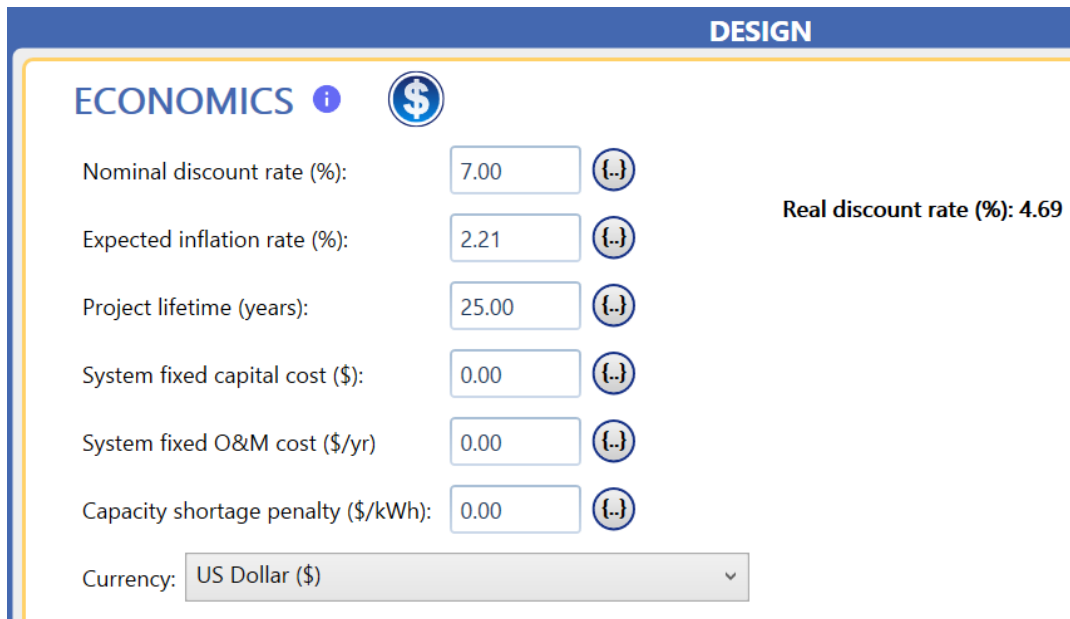


Figure 74 – Screenshot of the economics component of the project tab

The economics component of the project tab displays the model’s primary economic parameters, which are also present in the initial project design window (see Figure 37). These parameters are explained in the subsection entitled ‘Initial Project Design Window’ and apply to all twelve iterations. This project does not model fixed capital costs or fixed O&M costs but rather assumes that the capital and O&M costs for PV modules, inverters, and batteries cover the total capital and O&M costs. Additionally, because this project does not model capacity shortages (see subsection entitled ‘Initial Project Design Window’), there is no capacity shortage

penalty. Lastly, HOMER allows the user to set prices based on many different world currencies. Given that this project is located in the United States, I set the currency to the US dollar.

Constraints Component

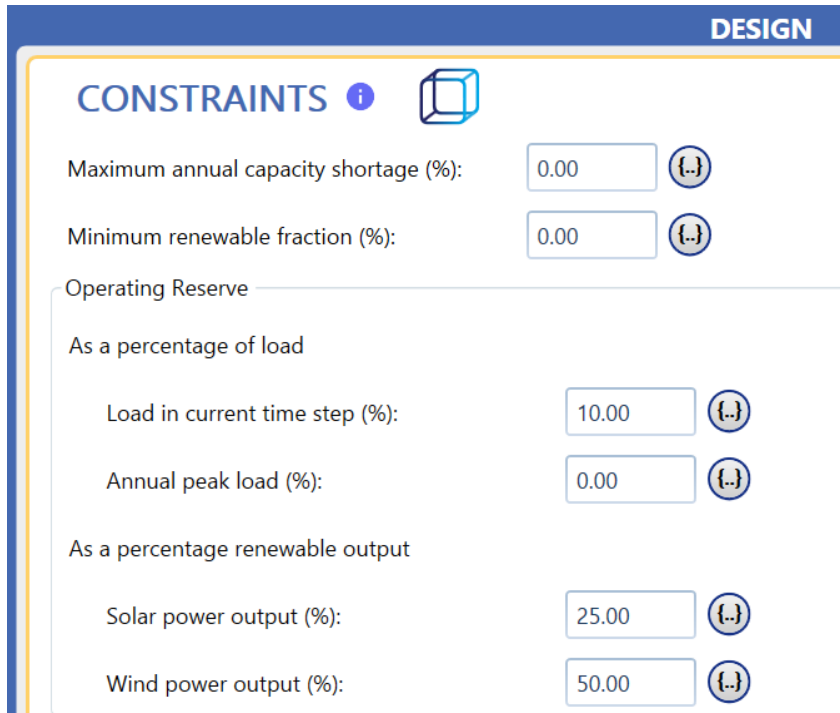


Figure 75 – Screenshot of the constraints component of the project tab

The constraints component of the project tab allows the user to set limitations and guidelines for the model to follow. These constraints apply to all twelve iterations. The ‘Minimum renewable fraction’ variable permits the user to impose a minimum percentage of renewable energy in microgrid configurations. To provide the clearest picture on the economic efficacy of solar energy as a power source for the KBH plant, this project does not impose minimum renewable energy fractions.

The ‘Maximum annual capacity shortage’ settings area relates to the capacity shortage fraction (HOMER Energy, 2016am, 2016an, 2016ao). The capacity shortage fraction is the total

annual capacity shortage²³ in kWh divided by the total annual electrical demand in kWh (HOMER Energy, 2016a). The maximum annual capacity shortage fraction is the greatest capacity shortage fraction that a configuration is allowed to have before HOMER discards it as a potential candidate to meet an electrical load (HOMER Energy, 2016a). For example, HOMER might generate a simulation that contains 400 kW of PV panels and two 100-kW generators to serve a 600-kW electrical load with a maximum annual capacity shortage fraction of 0.15. This particular configuration provides the lowest overall cost to meet the electrical load over the lifetime of the project. But, given the fact that the PV modules will not always produce 400 kW of electricity due to overcast days and the possibility of a technical failures within the PV modules, this configuration will not always be able to supply a 600-kW electrical load. For instance, if the PV modules consistently produce only 300 kW of electricity and both generators operate at full capacity, this configuration will meet 500 kW of the 600-kW load, which means the capacity shortage is 100 kW. This translates into a capacity shortage fraction of 100 kW/600 kW, or 0.16667. With a maximum annual capacity shortage fraction for the load of 0.15, HOMER will discard this configuration as a potential option to support the load (HOMER Energy, 2016a).

Instead, HOMER would select a configuration that costs more such as one that includes 600 kW of PV panels and two 100-kW generators. This configuration costs more initially because it requires expenditures on both the PV modules and the generators due to the fact that the PV modules will sometimes produce less than 600 kW of electricity. However, assuming the PV panels never produce less than 310 kW of electricity, this configuration has a better chance

²³ See the subsection entitled 'Initial Project Design Window' for an explanation of capacity shortage

of generating 510 kW, the minimum electricity amount required to meet a maximum annual capacity shortage fraction of 0.15 due to the higher PV module electrical production capacity. Consequently, HOMER will select this configuration although its costs more than the first one (HOMER Energy, 2016an). But, a maximum annual capacity shortage fraction does not factor into this project because it has set the model to meet the KBH plant's electricity demands at all times.

The operating reserve is the extra operating capacity that is available to instantly serve a sudden increase in the electrical load or a sudden decrease in renewable power output (HOMER Energy, 2016am, 2016ap). The operating reserve is equal to the operating capacity minus the electrical load at a given time step (HOMER Energy, 2016ap). The operating capacity refers to the largest possible electrical load that a system could serve at a moment's notice (HOMER Energy, 2016aq). In order to maintain a reliable supply of electricity, the operating capacity should always be greater than the electrical load (HOMER Energy, 2016aq). HOMER adds the values from the four boxes in the 'Operating Reserve' area in Figure 75 to determine the total required operating reserve for each time step (HOMER Energy, 2016am).

The first part of the 'Operating Reserve' settings area allows the user to configure the required operating reserve based on a percentage of the load. The value of the 'Load in current time step' box is the percentage of the primary load that HOMER adds to the primary load to obtain a required operating reserve (HOMER Energy, 2016am). The 10% value means that the model's operating capacity must be large enough to serve a sudden increase in the electrical load of 10% (HOMER Energy, 2016am). I selected this value based on the 10% value in the 'time step' and 'day-to-day' boxes in the 'Random Variability' section in Figure 40. The value of the

‘Annual peak load’ box sets an operating reserve based on the peak load throughout the year to each time step (HOMER Energy, 2016am). This allows the model to have a constant operating reserve for each time step based on the annual peak load in addition to the operating reserve calculated for the load at each time step (HOMER Energy, 2016am). I left this value blank because I felt that the combination of the values in the ‘Random Variability’ section of Figure 40 and the operating reserve based on each time step was more than sufficient to account for sudden increases in the electrical load.

The second part of the ‘Operating Reserve’ settings area in Figure 75 allows the user to set an operating reserve based on sudden decreases in output from renewable energy sources. The value of the ‘Solar power output’ and ‘Wind power output’ boxes is the percentage of the PV module and wind turbine capacity that HOMER adds to the operating reserve should their output suddenly decrease by that percentage (HOMER Energy, 2016am). A value of 25% in the ‘Solar power output’ box signifies that the system must have enough operating reserve available to supply the load if the PV modules’ output suddenly decreases by 25% of their current operating output (HOMER Energy, 2016am).

The ‘Solar power output’ and ‘Wind power output’ parts of the required operating reserve only matter if the system is not connected to the grid or has a limited purchase capacity from the grid. If this were the case, generators and other more consistent sources of energy would be crucial parts of the electricity configuration even if HOMER forecasts that they will only operate if renewable energy output suddenly declines. In this project, the grid does not have an exclusively backup role to meet the KBH plant’s electricity demand. Instead, the grid is always expected to supply part of or all of the KBH plant’s load at any given moment, including

when sudden declines in PV module output occur. Furthermore, this project assumes that the grid is always operational and that the KBH plant can purchase as much electricity from the grid as necessary to account for sudden decreases in power production from the PV modules. As a result, the ‘Solar power output’ and ‘Wind power output’ parts of the required operating reserve are redundant and will not affect the outcome of simulations. Thus, I found it acceptable to leave both of these parts with their default values pictured in Figure 75.

Emissions Component

The screenshot displays the 'EMISSIONS' component interface, which is divided into two main sections: 'Emissions Penalties' and 'Limits on Emissions'. The 'Emissions Penalties' section on the left lists six pollutants with their respective penalty values in dollars per ton (\$/t), all set to 0.00. The 'Limits on Emissions' section on the right lists the same six pollutants with checkboxes and input fields for limits in kilograms per year (kg/yr), all set to 0.00. The interface includes a title bar with the word 'EMISSIONS' and a cloud icon, and a header for each section.

Emissions Penalties		Limits on Emissions	
Carbon dioxide (\$/t):	0.00	<input type="checkbox"/> Carbon dioxide (kg/yr):	0.00
Carbon monoxide (\$/t):	0.00	<input type="checkbox"/> Carbon monoxide (kg/yr):	0.00
Unburned hydrocarbons (\$/t):	0.00	<input type="checkbox"/> Unburned hydrocarbons (kg/yr):	0.00
Particulate matter (\$/t):	0.00	<input type="checkbox"/> Particulate matter (kg/yr):	0.00
Sulfur dioxide (\$/t):	0.00	<input type="checkbox"/> Sulfur dioxide (kg/yr):	0.00
Nitrogen oxides (\$/t):	0.00	<input type="checkbox"/> Nitrogen oxides (kg/yr):	0.00

Figure 76 – Screenshot of the emissions component of the project tab

The emissions component depicted in Figure 76 allows the user to incorporate limits and penalties on emissions for using energy sources that produce greenhouse gases and other pollutants. None of the iterations in this project incorporates emissions penalties or limits.

HOMER models emissions penalties in dollars per ton and adds these costs to the operating costs for systems that emit pollutants depicted in Figure 76 (HOMER Energy, 2016ar). If the user decides to impose emission limits, HOMER discards combinations of energy sources that include systems that exceed emission limits (HOMER Energy, 2016ar). The grid is the only electricity source in this project that produces emissions directly. Given that I was unable to find clear data on the mix of energy sources from which EPE supplies its customers, I decided not to incorporate emissions constraints in this project. However, I will model emissions constraints in future studies.

Optimization Component

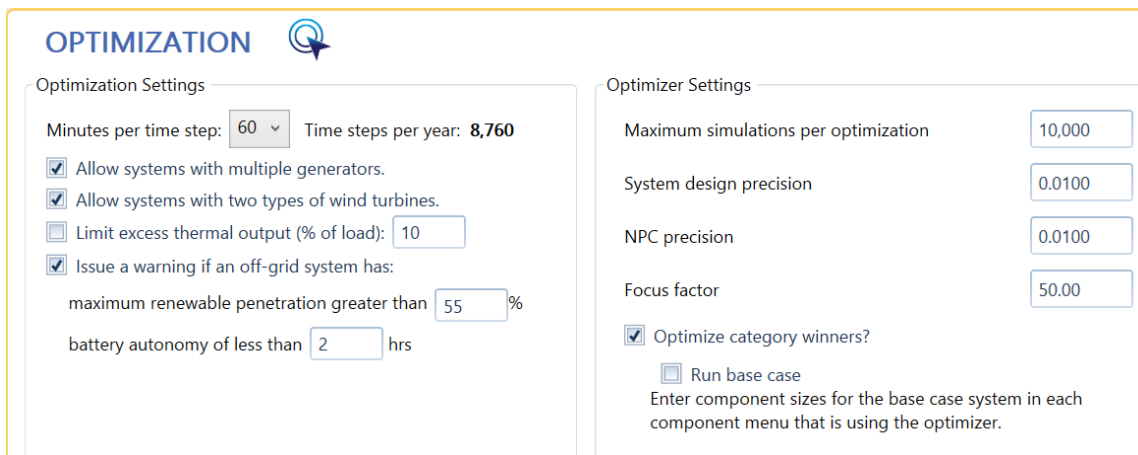


Figure 77 – Screenshot of the optimization component of the project tab

The optimization component in the project tab is where the user sets the time step length and restricts the types of systems that configurations can use and configures the optimizer if it is used in a project (HOMER Energy, 2016m). These time step configurations apply to all twelve iterations. The definition of a time step and the justification for setting time steps to sixty minutes for this project are explained in the subsection entitled ‘KBH Plant Electric Load Profile.’ Because this project does not incorporate any of the generation systems in the

‘Optimization Settings’ area of Figure 77, HOMER ignores the checkboxes next to these parameters. The checkbox entitled ‘Limit excess thermal output’ excludes thermal systems from combinations that produce excess electricity outputs greater than the percentage of the load that the user sets (HOMER Energy, 2016m). For example, HOMER would exclude a thermal heat system from a combination of energy sources that supplies more than 60 kW of excess electricity for a 600-kW load if the user sets the excess thermal output limit to 10% of the load. HOMER ignores the ‘Optimizer Settings’ area for this project because it does not use the optimizer. Article 33 in the HOMER model user manual contains more information on the optimizer’s parameters.

Search Space Component

Search Space

This table displays the values of all optimization variables. HOMER simulates the set of all possible combinations of these variables. You can also edit the search space for each component individually in the Component Input menus.

Converter Capacity (kW)	Grid Purchase Capac (kW)	1kWh LA Strings (#)	PV Size (kW)
0	999999	0	0
500		50	900
600		100	1000
700		200	1500
800		500	2000
1000		1000	2300
1500			3000
2000			
3000			

Winning Sizes Overall Winner Category Winner Calculate OK Cancel

Converter Capacity (kW)	Grid Purchase Capac (kW)	1kWh LA Strings (#)	PV Size (kW)
0	999999	0	0
500		50	900
600		100	1000
700		200	1500
800		500	2000
1000		1000	2300
1500			3000
2000			
3000			

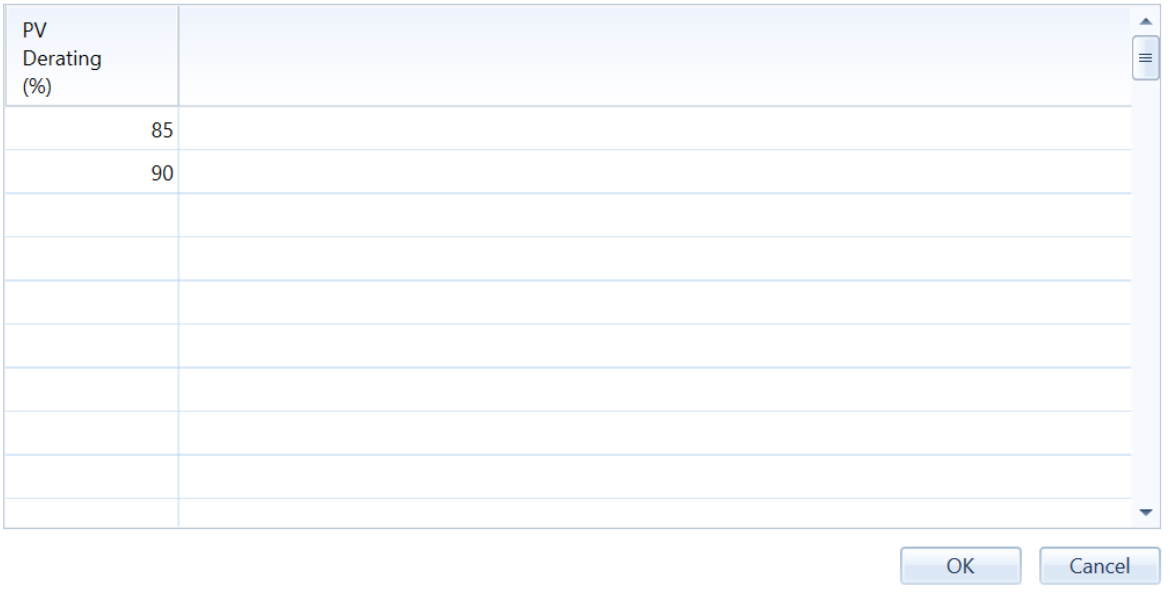
Figure 78 – Screenshot of the search space component of the project tab

The top half of the search space component of the project tab in Figure 78, which applies to all iterations, displays the different capacities of each component that could supply the electricity load in a HOMER simulation (HOMER Energy, 2016as). This display illustrates an overview of the variety of capacities for each component that the user entered earlier in the setup process. The bottom half of the search space component shows the overall best energy configuration as well as the best energy configuration for each variety of energy sources. Component capacities that are highlighted in yellow signify that those component capacities form part of the overall most ideal combination of energy sources to meet the load. Component capacities that are highlighted in blue signify that those component capacities form part of the most ideal configuration for each possible combination of energy sources even if that combination is not the most cost-effective for the load as a whole. The ‘Results Page’ subsection provides further explanation of this concept with a clearer illustration. These highlighted areas vary with an iteration’s pricing scale, the presence of axis trackers, and the presence of net metering.

Sensitivity Component

Sensitivity Inputs

This table displays the values of each sensitivity variable (variable for which you have specified multiple values). Columns with a star are using HOMER Optimizer™ and showing the range of values for that variable. Columns without a star are showing all of the values of that variable that HOMER will simulate. These columns are also editable in the Component Input views where the HOMER Optimizer™ can be turned on and off.



PV Derating (%)
85
90

Figure 79 – Screenshot of the sensitivity component of the project tab

The sensitivity component in Figure 79 displays all sensitivity variables for each component that will supply the load except for the capacity varieties that the user sets for these components (HOMER Energy, 2016a). The sensitivity component does not display capacity varieties for each component because they are already displayed in the ‘search space’ component (see Figure 78). The PV module is the only component that has sensitivity variables in this project; the batteries and the grid do not have multiple values programmed into their sensitivity variables except for their capacity varieties. The key sensitivity variables for the PV module are 1) the price scale, 2) the quantity of axis trackers, 3) the presence of net metering, and 4) the derating factor. The first three sensitivity variables each have their own iteration because

HOMER does not allow a side-by-side comparison of either of net metering or different quantities of axis trackers in one iteration. This concept is explained in the subsection on PV module configuration. In contrast, HOMER allows a side-by-side comparison of PV module derating factors, which explains why the two values for the derating factor this project uses are present in Figure 79. The ‘Results Page’ subsection and the ‘Results’ section further demonstrate how the derating factor influences the best energy combination and potential monetary savings.

Multi-Year Inputs Component

Multi-Year Inputs
×

Enable

Project lifetime (years):

Grid: GridPrice (%/year): <input style="width: 40px;" type="text" value="0.5"/> <input style="width: 40px;" type="button" value="Years"/>	System Fixed O&M Cost (%/year): <input style="width: 40px;" type="text" value="0"/> <input style="width: 40px;" type="button" value="Years"/>	PV: Degradation (%/year): <input style="width: 40px;" type="text"/> <input style="width: 40px;" type="button" value="Years"/>
Diesel: Fuel Price (%/year): <input style="width: 40px;" type="text" value="0"/> <input style="width: 40px;" type="button" value="Years"/>	Electric Load #1: Scaled Ave (%/year): <input style="width: 40px;" type="text" value="0"/> <input style="width: 40px;" type="button" value="Years"/>	

Figure 80 – Screenshot of the multi-year inputs component of the project tab

The multi-year input component allows the user to incorporate increases in prices of inputs such as grid energy and diesel fuel as well as increases in the electric load and PV module output degradation (HOMER Energy, 2016au). Aarabi Madhavan clarified that these price

increases apply in addition to the general inflation set in the initial project window (see Figure 37) (personal communication, March 16, 2017). I set the rise in electricity prices on top of inflation to 0.5% based on Bureau of Labor Statistics data as of late 2016 that show that grid electricity prices are rising by this percentage above the rate of general inflation, which leads to a total grid electricity price increase of 2.71% per year over the course of this project (BLS, 2017). Unfortunately, according to Aarabi Madhavan, HOMER increases grid sellback prices only by general inflation (personal communication, March 16, 2017). Because EPE pays customers with interconnected systems the equivalent amount of energy charge and fuel costs EPE avoided by accepting the system's excess kWh into the grid, the yearly percentage increases in electricity prices should also apply to the grid sellback rates (El Paso Electric Company, 2011b). Consequently, HOMER will slightly underestimate the monetary value of electricity sold to the grid when adjusted for inflation.

PV Module Output Degradation Rates

The PV degradation input of the multi-year inputs component is blank because it reflects the fact that I set custom degradation rates that are not consistent over the course of the project. These degradation rates apply to all twelve iterations. Figure 81 shows the specific PV module output degradation rates for each year of the project. According to Larry Perea, PV modules have a warranty to produce 90% of their original expected production capacity after 10 years of operation (personal communication, September 2, 2016). After the next 15 years, they have a warranty to produce 80% of their original expected production capacity (L. Perea, personal communication, September 2, 2016). These findings are similar to those of a 2012 NREL study

on output degradation of PV modules in arid climates such as that of El Paso (Jordan & Kurtz, 2012).

As Figure 81 shows, I set the PV modules' output degradation rate based on Mr. Perea's insight to 1% per year relative to the original expected production capacity for the first ten years and 0.667% per year relative to the original expected production capacity for the next fifteen years. I set these constant rates given that annual PV module degradation rates in dry climates are more or less constant (Jordan & Kurtz, 2012). For example, after five years of operation, I set the PV modules to produce 95% of their original expected production capacity to reflect the 1% per year decline of the first ten years of operation. After eleven years of operation, I set the PV modules to produce 89.333% of their original expected production capacity to reflect the 0.667% per year decline of the next fifteen years of operation.

Year	Multiplier
1	0.99
2	0.98
3	0.97
4	0.96
5	0.95
6	0.94
7	0.93
8	0.92
9	0.91
10	0.90
11	0.8933
12	0.8866
13	0.8799
14	0.8732
15	0.8665
16	0.8598
17	0.8531
18	0.8464
19	0.8397
20	0.8330
21	0.8263
22	0.8196
23	0.8129
24	0.8062
25	0.80

Figure 81 – Screenshot of PV module production rates over the course of the project relative to the original expected production capacity

The Results Page

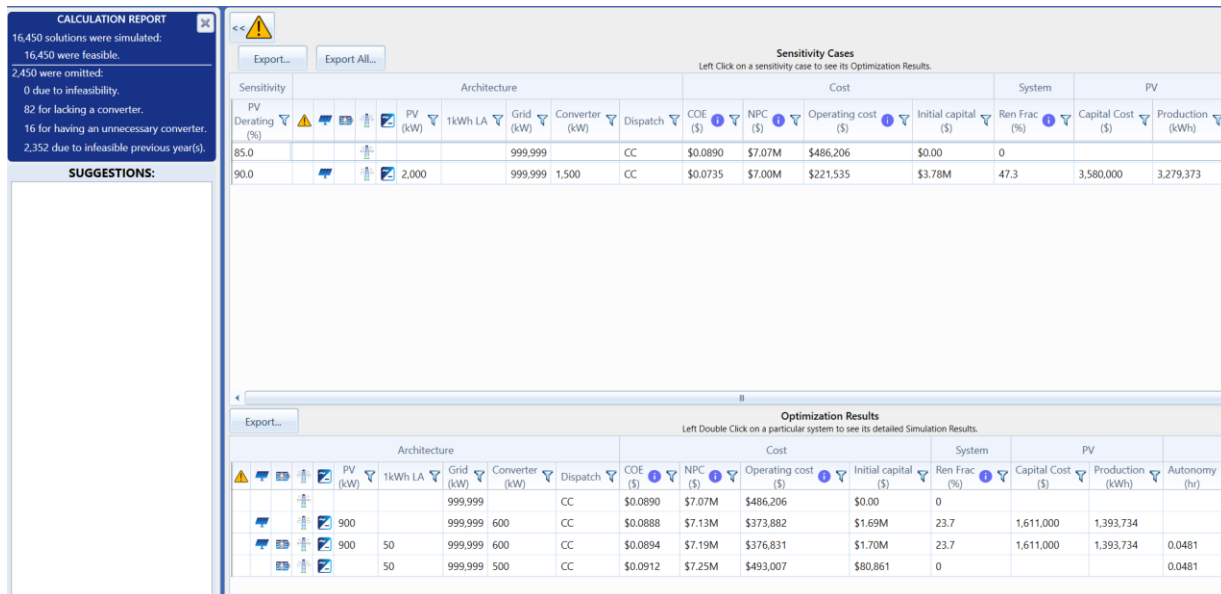


Figure 82 – Screenshot of the left half of the results page from fifth round of iterations with ‘500 kW commercial scale’ pricing, no axis trackers, and no net metering

Sensitivity Cases

The top half of Figure 82 lays out the most cost-effective electricity source combination for each sensitivity case. This particular results page applies to the iteration from the fifth round of iterations with ‘500 kW commercial scale’ pricing, no axis trackers, and no net metering. I selected this iteration for Figure 82 to illustrate the fact that HOMER does sometimes find that a grid-only electricity supply is the most cost-effective combination for a given sensitivity case.

The blue box in the top left corner of this figure shows a calculation report that describes how many simulations HOMER ran to find the most cost-effective electricity supply combination and as well as the simulations that were omitted for various reasons. As explained in the description of the ‘Sensitivity Component’ in the ‘Project Tab’ subsection, the key sensitivity variables for each iteration pertain to the PV modules. These are: 1) the price scale, 2) the quantity of axis trackers, 3) the presence of net metering, and 4) the derating factor.

The first sensitivity case considers all of the components and their associated capacity varieties described in Figure 78 as potential suppliers of the KBH plant's electricity load. But, all PV modules in this sensitivity case have a derating factor of 85%. The second sensitivity case also considers all of the components and their associated capacity varieties described in Figure 78 as potential suppliers of the KBH plant's electricity load. However, all PV modules in this sensitivity case have a derating factor of 90%. The most cost-effective electricity supply combination for the first sensitivity case is solely the grid. In contrast, the most cost-effective electricity supply combination for the second sensitivity case consists of mixture of PV modules with inverters in addition to the grid.

These results show that for the first sensitivity case, PV modules with an 85% derating factor, at the '500 kW commercial' price scale without either solar axis trackers or net metering will not produce electricity with a high enough monetary value in the form of savings from grid-purchased power and excess electricity sold to the grid over the course of the project to offset the PV modules' installation costs, O&M costs, and the expenses of purchasing electricity from the grid. But, as the second sensitivity case shows, PV modules with a 90% derating factor without axis trackers or net metering at the aforementioned price scale will produce enough electricity to make PV modules a part of the most cost-effective electricity supply combination for the KBH plant.

Parameters of Sensitivity Cases

The column titles in the top half of Figure 82 depict the components and their associated costs that could potentially form part of each sensitivity case. The first column on the left side of this figure shows the factors that distinguish each sensitivity case, which in this project consists

of the variable derating factors for the PV modules. The yellow triangle icon to the right signals if a system's renewable electricity production volume is high enough such that neither the inverters, the storage devices, nor the load in general can absorb that excessively large amount of energy (HOMER Energy, 2016b). This icon appears in the row of a sensitivity case when the user fails to configure the model to have storage, grid purchases, or other measures to absorb this surplus energy (HOMER Energy, 2016b). Fortunately, the yellow triangle icon does not appear in any of the iterations in this project. The next four icons represent the potential components that could supply electricity for the load. The first of these icons represents the PV modules while the next one represents battery storage. The next two represent the grid and the inverters, respectively. The appearance of an icon in the sensitivity case's row signifies that that component is one of the electricity suppliers for that particular sensitivity case. For example, the appearance of the PV module, grid, and inverter icons in the sensitivity case whose PV modules have a derating factor of 90% indicates that the electricity supply for that sensitivity case will come from PV modules and inverters as well as the grid.

The columns to the right of the icons in the top half of Figure 82 entitled 'PV (kW),' '1 kWh LA,' 'Grid,' and 'Converter (kW)' depict the capacities of each electricity supply component. For example, these columns in the second sensitivity case in Figure 82 show 2000 kW of the PV modules, nothing for the lead acid batteries²⁴, 999,999 kW for the grid, and 1500 kW for the converter/inverter. These figures reveal that the most cost-effective combination to supply the load for that particular sensitivity case will include PV modules with a production

²⁴ Any of these columns that displays a blank numerical amount indicates that the component associated with that column does not form a part of the electricity supply combination for that particular sensitivity case.

capacity of 2000 kW, no lead acid batteries, as much electricity from the grid as needed when the PV modules cannot fully supply the load, and inverters with a production capacity of 1500 kW.

The column in the top half of Figure 82 entitled 'Dispatch' refers to the dispatch strategy HOMER uses to supply the load. The dispatch strategy is the set of rules that determines how generators in the system operate in relation to the other components that supply the load (Barley & Winn, 1996; HOMER Energy, 2016am). The CC stands for cycle charging strategy, which means that the generator will always operate at full capacity provided it can either supply the full load or charge battery banks (HOMER Energy, 2016av). Otherwise, the generator does not run (HOMER Energy, 2016av). The other dispatch strategy type is LF, or load following. An LF dispatch strategy allows the generator to supply the primary load and relies on other sources such as renewable energy sources to charge battery banks (HOMER Energy, 2016aw). Dispatch strategies do not apply in this project because it does not incorporate generators as a potential electricity supply sources.

The COE, or cost of energy, is the average cost per kWh in current dollars²⁵ of the system's energy production and consumption over the course of the project (HOMER Energy, 2016ax). The COE's role is to spread the costs of setting up a system with PV modules such as the capital costs and O&M costs as well as the grid energy costs over each kWh the PV modules produce (HOMER Energy, 2016e, 2016ax, 2016ay, 2016az). The equation for the COE is the total annualized cost of the system in dollars per year divided by the total annual electrical load served in kWh per year (HOMER Energy, 2016ax). The total annualized cost reflects the total

²⁵ In this project, 2016 dollars are current dollars; I selected 2016 dollars as current dollars because the price data I used for the PV modules and grid electricity prices are in 2016 dollars (El Paso Electric Company, 2016d; Fu et al., 2016).

net present cost spread over the project's lifetime (HOMER Energy, 2016ay, 2016ba). The equation for the total annualized cost is $C_{\text{ann, tot}} = \text{CRF}(i, R_{\text{proj}}) * C_{\text{NPC, tot}}$ where $C_{\text{ann, tot}}$ is the total annualized cost, CRF is the capital recovery factor, i is the annual real discount rate, R_{proj} is the project lifetime, and $C_{\text{NPC, tot}}$ is the total net present cost (HOMER Energy, 2016ay, 2016ba). The project lifetime equals 25 years while i equals 4.69% (see Figure 74). The CRF is a ratio to calculate the amount of each annual payment to repay a loan to buy capital in current dollars after accounting for the annual real discount rate and the loan's payback period (HOMER Energy, 2016bb).

The total net present cost (NPC) is the total costs in current dollars the project incurs over its lifetime minus the total revenues in current dollars the project incurs over its lifetime (HOMER Energy, 2016e, 2016az). The NPC column is located next to the COE column in the top half of Figure 82. The NPC is the primary economic factor HOMER uses as a point of comparison to determine the most cost-effective combination of energy sources for a load (HOMER Energy, 2016az) HOMER calculates the total net present cost by adding the costs and revenues for the project for each year, discounting them by synthesizing the annual real discount rate and the number of years since the project began, and compiling the total adjusted costs and revenues for the project over its lifetime in terms of current dollars (HOMER Energy, 2016e, 2016az). Examples of costs that go into the NPC calculations include initial capital costs for the PV modules, grid energy costs, and PV module O&M costs while examples of revenues include those from sales to the grid (HOMER Energy, 2016az).

The operating cost (OC) reflects all annualized costs and revenues to operate the system except for initial capital costs (HOMER Energy, 2016bc). The OC equals the total annualized

cost in dollars per year ($C_{ann, tot}$) minus the total annualized capital cost in dollars per year ($C_{ann, cap}$) (HOMER Energy, 2016bc). The $C_{ann, cap}$ equals the total initial cost multiplied by the CRF; it reflects the amount of the annual payments in current dollars for the initial capital investment (HOMER Energy, 2016bc). The total initial capital cost reflects the initial price of PV modules, inverters, and batteries multiplied by the ideal capacity that HOMER finds for each component at the beginning of the project (see Figure 82) (HOMER Energy, 2016bd).

Lastly, the renewable fraction is the average annual fraction of the load's energy consumed over the project's lifetime that originated from renewable sources (HOMER Energy, 2016be). The equation for the renewable fraction for each year is $f_{ren} = 1 - (E_{nonren}/E_{served})$ where f_{ren} is the renewable fraction, E_{nonren} is the total energy supplying the load from nonrenewable sources in kWh/year, and E_{served} is the total energy in kWh/year the KBH plant consumes in a given year (HOMER Energy, 2016be). Subtracting the fraction of energy supplied from nonrenewable energy sources to find the fraction of energy supplied from renewable sources reflects the production of the inverters rather than the direct PV module production. This is important because only the PV modules' energy that the inverters convert to AC current directly supplies the KBH plant's load.

The top half of Figure 83 shows the other column titles and their corresponding data (see Figure 82) that appear in the 'sensitivity cases' and 'optimization results' areas of each iteration. I had to create two figures to display all of these column titles because my computer screen could not capture all of them in one frame. For the sensitivity case whose PV modules have a 90% derating factor, the initial capital cost of the PV modules and inverters together is \$3,580,000. The average annual PV energy production over the course of the project is approximately 3.3

million kWh/year. The columns describing data about the 1 kWh lead acid batteries are blank because HOMER did not find that batteries could be part of the most cost-effective electricity supply combination. The converter column group shows that the inverter’s average power output at a given time step over each year of the project is 354 kW. Finally, the grid column group shows for this sensitivity case that the KBH plant’s average annual grid energy purchases over the course of the project will total 3.45 million kWh/year while the plant’s average annual energy sold to the grid over the course of the project is approximately 1 million kWh/year.

Sensitivity Cases
 Click on a sensitivity case to see its Optimization Results. Compare Economics Column Choices...

PV		1kWh LA		Converter		Grid	
Capital Cost (\$)	Production (kWh)	Autonomy (hr)	Annual Throughput (kWh)	Rectifier Mean Output (kW)	Inverter Mean Output (kW)	Energy Purchased (kWh)	Energy Sold (kWh)
						5,464,050	0
3,580,000	3,279,373			0	354	3,449,955	1,087,354

Optimization Results
 Click on a particular system to see its detailed Simulation Results. Categorized Overall

PV		1kWh LA		Converter		Grid	
Capital Cost (\$)	Production (kWh)	Autonomy (hr)	Annual Throughput (kWh)	Rectifier Mean Output (kW)	Inverter Mean Output (kW)	Energy Purchased (kWh)	Energy Sold (kWh)
						5,464,050	0
1,611,000	1,393,734			0	150	4,212,550	59,286
1,611,000	1,393,734	0.0481	0	0	150	4,212,550	59,286
		0.0481	0	0	0	5,464,050	0

Figure 83 – Screenshot of the right half of the results page of iteration in Figure 82

Optimization Results

The optimization results, depicted in bottom half of Figures 82 and 83, lay out the most cost-effective configuration for each possible combination of electricity sources laid out in Figure 78 for a given sensitivity case. The first type of view in the optimization results is known as a ‘categorized’ view (HOMER Energy, 2016bf). The other view, known as the ‘overall’ view, shows every possible combination of electricity supply sources for a given sensitivity case with each possible capacity configuration for each electricity supply component outlined in Figure 78 (HOMER Energy, 2016bf). These combinations are ranked in the order of least NPC to most NPC. Figure 84 illustrates part of the ‘overall’ view of the optimization results section for the sensitivity case whose PV modules have a derating factor of 85%. Figures 85 and 86 provide a clearer ‘categorized’ view of each sensitivity case and its corresponding electricity source combinations. These combinations are also ranked in the order of least NPC to most NPC.

Overall View of Optimization Results

Sensitivity		Architecture				Cost				System	PV		1kWh LA		Converter		Grid	
PV Derating (%)		PV (kW)	1kWh LA	Grid (kW)	Converter (kW)	Dispatch	COE (\$)	NPC (\$)	Operating cost (\$)	Initial capital (\$)	Ren. Frac. (%)	Capital Cost (\$)	Production (kWh)	Autonomy (hr)	Annual Throughput (kWh)	Rectifier Mean Output (kW)	Inverter Mean Output (kW)	Energy Purchased (kWh)
85.0				999.999	CC		\$0.0890	\$7.07M	\$486,206	\$0.00	0							5,464,050
90.0		2,000		999.999	1,500	CC	\$0.0735	\$7.00M	\$221,535	\$3.78M	47.3	3,580,000	3,279,373			0	354	3,449,955

Optimization Results																			
Left Double Click on a particular system to see its detailed Simulation Results																			
Architecture		Cost				System	PV		1kWh LA		Converter		Grid						
PV (kW)	1kWh LA	Grid (kW)	Converter (kW)	Dispatch	COE (\$)	NPC (\$)	Operating cost (\$)	Initial capital (\$)	Ren. Frac. (%)	Capital Cost (\$)	Production (kWh)	Autonomy (hr)	Annual Throughput (kWh)	Rectifier Mean Output (kW)	Inverter Mean Output (kW)	Energy Purchased (kWh)			
900	50	999.999	800	CC	\$0.0895	\$7.20M	\$376,287	\$1.73M	23.9	1,611,000	1,393,734	0.0481	0	0	151	4,210,940			
1,000	50	999.999	600	CC	\$0.0895	\$7.22M	\$366,580	\$1.88M	25.8	1,790,000	1,548,593	0.0481	0	0	163	4,114,970			
2,000	50	999.999	1,500	CC	\$0.0772	\$7.22M	\$236,576	\$3.78M	45.7	3,580,000	3,097,186	0.0481	0	0	335	3,488,853			
1,500	50	999.999	1,000	CC	\$0.0842	\$7.23M	\$302,220	\$2.83M	37.0	2,685,000	2,322,890	0.0481	0	0	249	3,716,209			

Figure 84 – Screenshot of the ‘overall’ view of the optimization results of iteration with 85% derating factor in Figure 82

The main message that the ‘overall’ view conveys is that batteries are not a cost effective component for the KBH plant’s electricity supply. For instance, the top combination enclosed in the red rectangle of Figure 84 contains PV modules with 2000 kW of capacity with inverters that have a capacity of 1500 kW in addition to the grid. This combination has a COE of \$0.0772/kWh, an NPC of \$7.22 million, and an OC of approximately \$237,000. The bottom combination enclosed in this same rectangle contains PV modules with 1500 kW of capacity, inverters that have a capacity of 1000 kW, 50 1 kWh lead acid batteries, and the grid. This combination has a COE of \$0.0842/kWh, an NPC of \$7.23 million, and an OC of approximately \$302,000. The fact that the bottom combination contains a smaller capacity of PV modules and inverters yet its OC is higher than that of the top combination demonstrates that batteries are not economically worthwhile to supply the KBH plant’s load. This is probably due to the fact that

HOMER finds it cheaper for the grid to supply when the PV modules are unavailable. Evidence for this rests in the fact that the batteries’ annual running time (autonomy) in this combination is only 0.0481 hours and their annual energy production (throughput) in kWh is zero.

Categorized View of Optimization Results

Sensitivity	Architecture					Cost				System	PV	
PV Derating (%)	PV (kW)	1kWh LA	Grid (kW)	Converter (kW)	Dispatch	COE (\$)	NPC (\$)	Operating cost (\$)	Initial capital (\$)	Ren Frac (%)	Capital Cost (\$)	Production (kWh)
85.0			999,999		CC	\$0.0890	\$7.07M	\$486,206	\$0.00	0		
90.0	2,000		999,999	1,500	CC	\$0.0735	\$7.00M	\$221,535	\$3.78M	47.3	3,580,000	

Optimization Results												
Left Double Click on a particular system to see its detailed Simulation Results.												
Architecture					Cost				System	PV		
PV (kW)	1kWh LA	Grid (kW)	Converter (kW)	Dispatch	COE (\$)	NPC (\$)	Operating cost (\$)	Initial capital (\$)	Ren Frac (%)	Capital Cost (\$)	Production (kWh)	
		999,999		CC	\$0.0890	\$7.07M	\$486,206	\$0.00	0			
900		999,999	600	CC	\$0.0888	\$7.13M	\$373,882	\$1.69M	23.7	1,611,000	1,393,734	
900	50	999,999	600	CC	\$0.0894	\$7.19M	\$376,831	\$1.70M	23.7	1,611,000	1,393,734	
	50	999,999	500	CC	\$0.0912	\$7.25M	\$493,007	\$80,861	0			

Figure 85 – Screenshot of the ‘categorized’ view of the optimization results of iteration with 85% derating factor in Figure 82

The sensitivity case that contains PV modules with a derating factor of 85% is highlighted in Figure 85 to indicate that the corresponding combinations in the optimization results area of the figure pertain to that sensitivity case. The optimization results confirm that the grid-only combination with an NPC of \$7.07 million is the most cost-effective for this sensitivity case. The second most cost-effective combination for this sensitivity case contains 900 kW of PV modules, 600 kW of inverters, no batteries, and the grid. This combination’s NPC is \$7.13 million, which is \$60,000 more than the grid-only combination’s NPC. Interestingly, this

combination’s COE is slightly lower than that of the grid-only combination while its OC is more than \$100,000 lower. Yet, these savings are not enough to offset the initial capital cost of \$1.69 million to pay for the PV modules and inverters. Furthermore, the combinations with batteries contain the highest NPCs, which further confirms the earlier findings that batteries in this project do not produce enough electricity and savings to offset their initial capital and O&M costs.

Sensitivity	Architecture							Cost				System	PV
PV Derating (%)	PV (kW)	1kWh LA	Grid (kW)	Converter (kW)	Dispatch	COE (\$)	NPC (\$)	Operating cost (\$)	Initial capital (\$)	Ren Frac (%)	Capital Cost (\$)		
85.0			999,999		CC	\$0.0890	\$7.07M	\$486,206	\$0.00	0			
90.0	2,000		999,999	1,500	CC	\$0.0735	\$7.00M	\$221,535	\$3.78M	47.3	3,580,000		

Optimization Results													
Left Double Click on a particular system to see its detailed Simulation Results.													
Architecture							Cost				System	PV	
PV (kW)	1kWh LA	Grid (kW)	Converter (kW)	Dispatch	COE (\$)	NPC (\$)	Operating cost (\$)	Initial capital (\$)	Ren Frac (%)	Capital Cost (\$)	Production (kWh)		
2,000		999,999	1,500	CC	\$0.0735	\$7.00M	\$221,535	\$3.78M	47.3	3,580,000	3,279,373		
2,000	50	999,999	1,500	CC	\$0.0740	\$7.06M	\$224,484	\$3.79M	47.3	3,580,000	3,279,373		
		999,999		CC	\$0.0890	\$7.07M	\$486,206	\$0.00	0				
	50	999,999	500	CC	\$0.0912	\$7.25M	\$493,007	\$80,861	0				

Figure 86 – Screenshot of the ‘categorized’ view of the optimization results of iteration with 90% derating factor from Figure 82

The sensitivity case that contains PV modules with a derating factor of 90% is highlighted in Figure 86 to indicate that the corresponding combinations in the optimization results area of the figure pertain to that sensitivity case. Upon increasing the derating factor to 90%, HOMER finds that the most cost-effective combination of electricity suppliers includes 2000 kW of PV modules, 1500 kW of inverters, and the grid. These increased capacities of PV

modules and inverters raise initial capital costs to \$3.78 million from \$1.69 million for the corresponding combination in the other sensitivity case.

Despite these higher initial capital costs, this combination's NPC is only \$7 million as opposed to \$7.07 million for the grid-only combination, and \$7.13 million for the combination that contains the grid and PV modules with a derating factor of 85%. Additionally, this combination's COE is \$0.0735/kWh as opposed to \$0.0890/kWh for the grid-only combination while its OC is about \$222,000, which is less than half the OC for the grid-only combination. These facts demonstrate that an increase in the PV modules' derating factor can make a substantial difference in the most cost-effective capacity of PV modules and inverters, and therefore in the total savings over the project's lifetime.

Interestingly, HOMER finds for this sensitivity case that a combination of PV modules, inverters, batteries, and the grid is more cost-effective than a grid-only combination because it has an NPC of \$7.06 million as opposed to \$7.07 million. But, this combination's NPC, COE, and OC are higher than that of the combination for this sensitivity case that includes all the aforementioned components except for batteries. Furthermore, the combination that omits PV modules but contains batteries, inverters, and the grid has a higher NPC, COE, and OC than the grid-only combination. This is further confirmation that batteries in this project do not produce enough electricity and savings to offset their initial capital and O&M costs.

Graphical Representations of the Results Page

In addition to tabular format, HOMER also displays the results from its calculations in various graphical formats that allow the user to visually compare different factors. These include a summary of costs, expected PV module output over the course of the project, expected grid

purchases and sales, and the amount of time to recover the initial capital costs. The following graphical representations are the results graphs of the combination that supplies the KBH load with PV modules, inverters, and grid energy from the iteration with ‘100 MW utility scale’ pricing, double axis trackers, no net metering and a derating factor of 85%. I selected the graphs from that combination in this iteration to demonstrate how PV modules at ‘100 MW utility’ price scale with double axis trackers can substantially increase the amount of savings in energy costs compared to a grid-only system despite a derating factor of 85%.

Cost Summary Graph

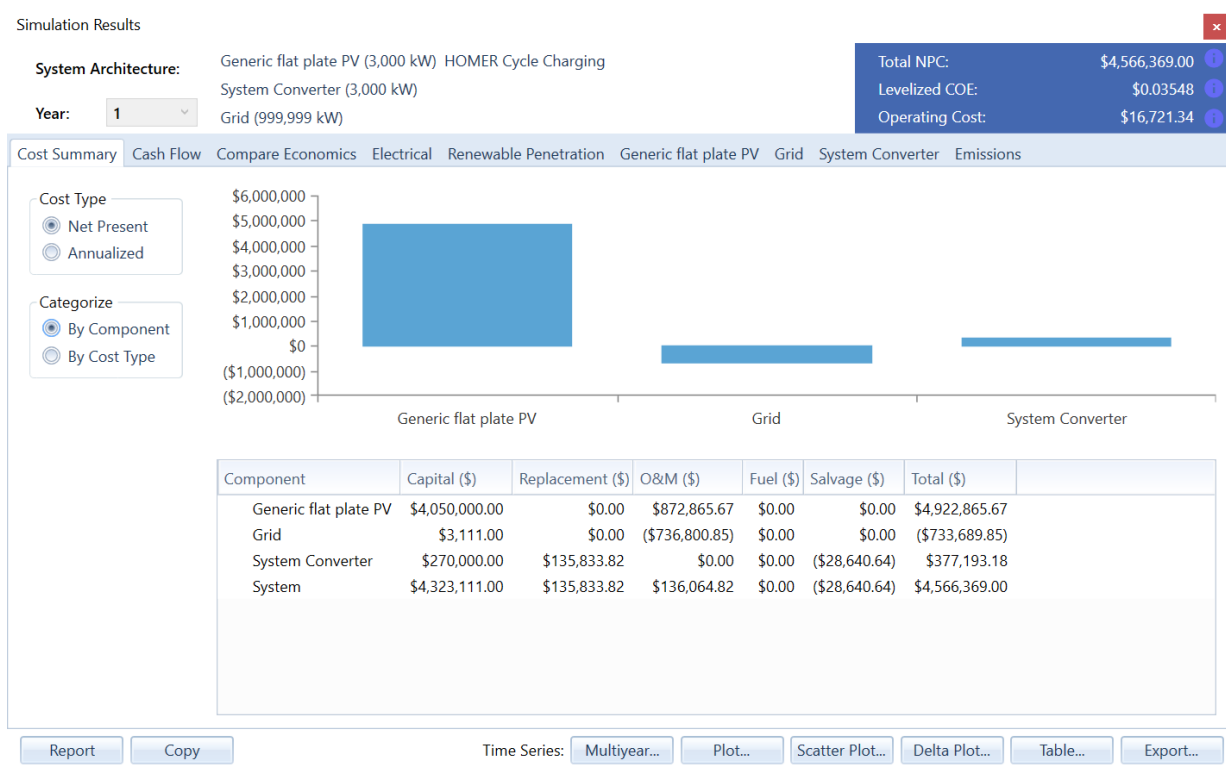


Figure 87 – Screenshot of cost summary graph of combination with PV modules, inverters, and grid energy from fifth round of iterations with ‘100 MW utility scale’ pricing, double axis trackers, no net metering, and an 85% derating factor

The graphical results in the ‘cost summary’ tab in Figure 87 show an overview of the costs the project will incur over its lifetime. The area labeled ‘system architecture’ displays the

ideal capacity of each of the components that supply the electricity load for this iteration. To the right of this area is a summary of the project's NPC, COE, and OC. The set of radio buttons labeled 'cost type' permits the user to set view the project's lifetime costs as net present costs or as annualized costs. The set of radio buttons labeled 'categorize' lets the user see costs by project component such as the total costs to install and run the PV modules or by type such as total initial capital costs or total O&M costs for all components.

The bar graphs reflect the total initial capital costs and O&M costs of each component and the entire system (see the row labeled 'system') over the course of the project in terms of current dollars. The grid's initial capital costs reflect the interconnection fee described in the 'grid power configurations' part of the 'configuring model components' subsection. The grid's O&M costs are negative because the microgrid over the course of the project will sell more power to the grid than it will purchase (HOMER Energy, 2016bg). The project's other revenue source is the salvage value of the inverters (labeled as 'system converter'), which reflects the value they will possess when the project ends but still have years of service remaining. HOMER assumes that components' values depreciate linearly, which signifies that salvage values are proportional to a component's remaining years of service (HOMER Energy, 2016bg, 2016bh). For example, the inverters that were replaced at year 15 will still have five years of service left at the end of the project. The salvage value reflects these inverters' five remaining years of service (HOMER Energy, 2016bg). Apart from the remaining life of a component, the other two key variables that HOMER uses to calculate salvage values are the component's replacement cost and the project's lifetime (HOMER Energy, 2016bg, 2016bh). Article 7.142 in the HOMER model user manual shows the equations and variables HOMER uses to determine a component's

salvage value. But, HOMER only calculates a salvage value for components that have years of service left the end of the project, which explains why the PV modules do not have a salvage value (HOMER Energy, 2016bg).

Time Series Graph

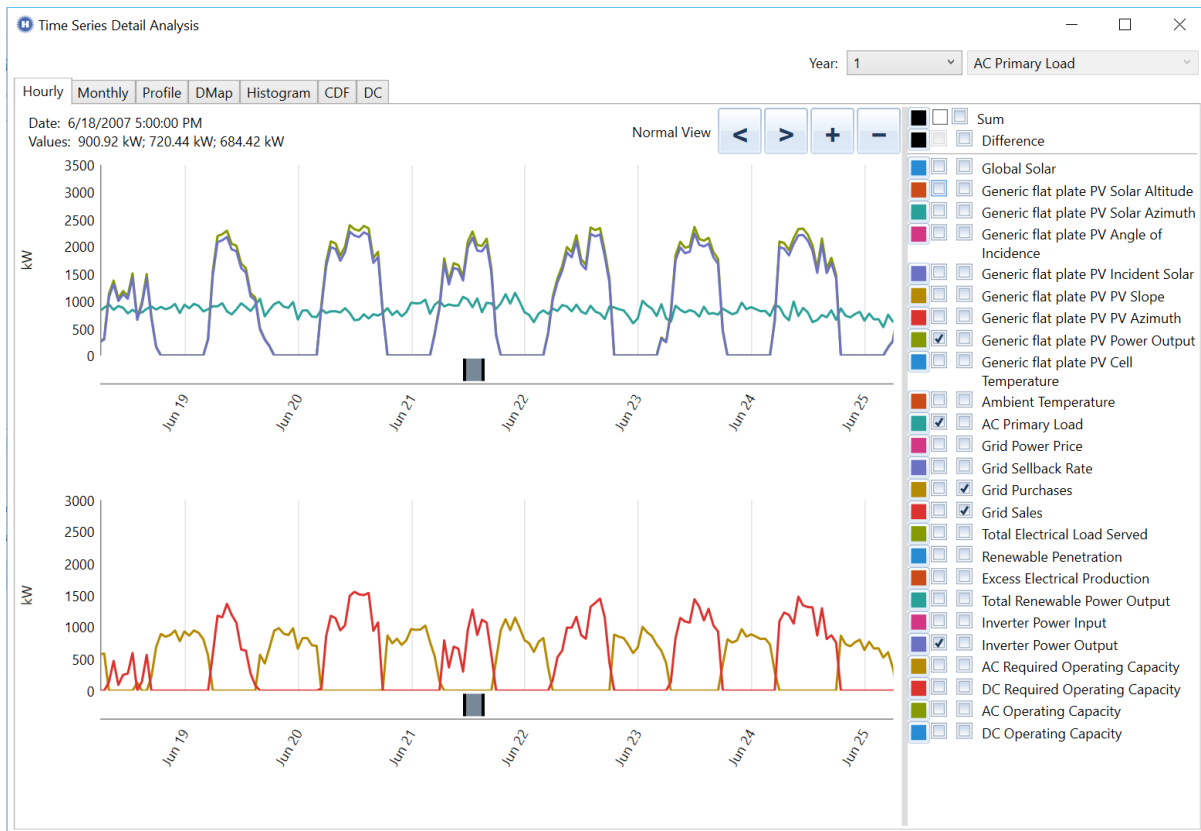


Figure 88 – Screenshot of time series plot that shows the predicted output values for various factors for each hour of each day of the year for the combination from Figure 87

Figure 88 portrays a time series graph that can show the expected values of many variables at each time step for every day of the year. These include the PV module output, the inverter output, the current load, and expected solar radiation. This time series graph can be accessed by clicking on the ‘plot’ button in Figure 87. Figure 88 is zoomed into the June 19 – June 25 time period to provide a closer view of the forecasted values for each variable at the

daily level at a time when the load is highest. Just like in Figure 49, the light gray lines represent each day's boundaries while points in between represent each day's hours. Hovering the mouse at a point between the gray lines shows the values for each variable at that time step.

The x-axis in both graphs in Figure 88 represents the hours and days of the year while the y-axis in these graphs represents the load or output in kW. The teal line in the top graph represents the variable AC primary load in kW at each hour across the year as outlined in the subsection entitled 'KBH Plant Electric Load Profile.' To display this line in the top graph, the user must click on the left checkbox by the object labeled 'AC primary load.' The forest green and purple lines, which are also in the top graph of Figure 88, reflect the PV module output and inverter output in kW, respectively. The slightly lower inverter output compared to the PV module output reflects the inverter's efficiency at converting DC current to AC current.

The difference between the inverter output and the load value at each time step is reflected in the bottom graph of Figure 88. When the red line is above zero, it indicates that the PV modules with their inverters are producing more electricity than the plant's load, and therefore the microgrid is selling excess energy to the grid. When the golden line is above zero, it indicates that the PV modules with their inverters are producing less electricity than the plant's load, and therefore the microgrid is purchasing the remaining energy to cover the load from the grid. To display these lines in the bottom graph, the user must click on the right checkbox by the objects labeled 'Grid purchases' and 'Grid sales.' Although this graph can display many more variables simultaneously, I decided that these ones provided the clearest picture of expected PV module output relative to the load at each time step across the year.

Multiyear Time Series Graph

In addition to the time series graph, the buttons at the bottom of Figure 87 shows the results page in other graphical formats such as a delta plot, a scatter plot, a multiyear plot, and a table format. Figure 89 uses the multiyear plot to illustrate the declining PV module output over the course of the project, which in turn reflects the PV module degradation rates set in Figure 81.

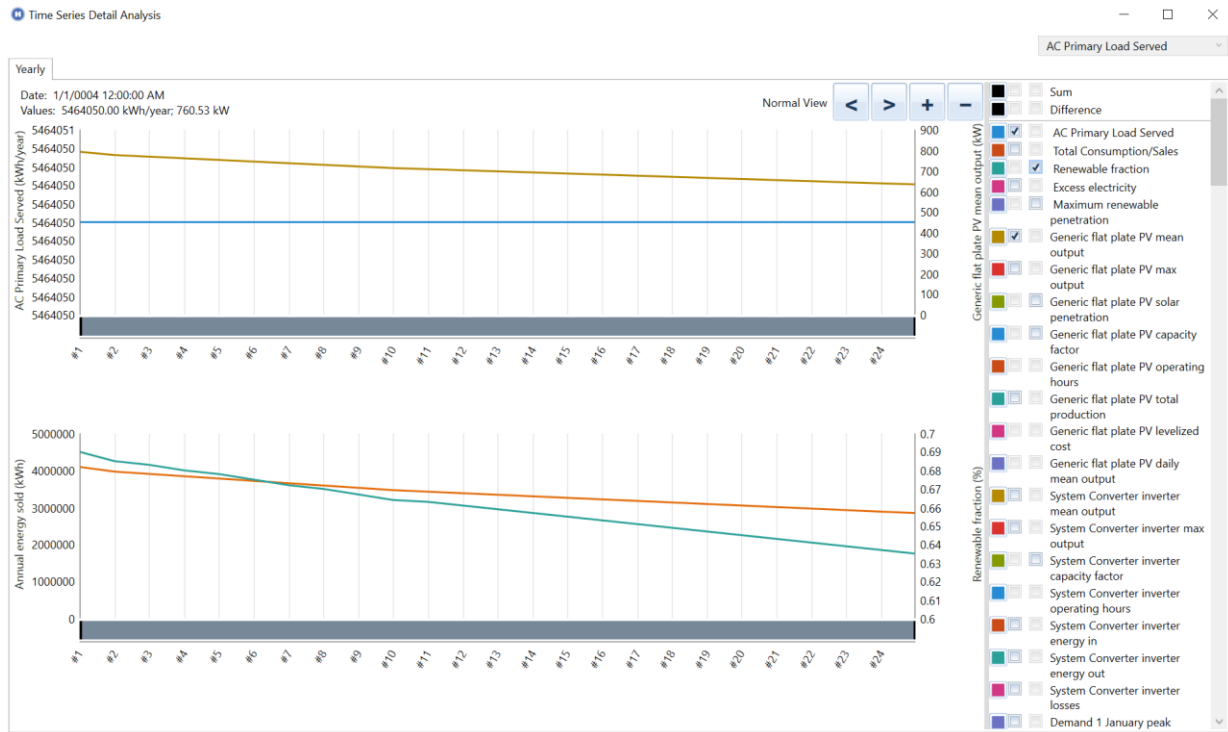


Figure 89 – Screenshot of multiyear series plot that shows the predicted output values for the primary AC load, PV module output, the fraction of the load served by renewable energy, and the amount of energy sold to the grid for the combination from Figure 87

The multiyear series plot in Figure 89 can show many more variables, all of which cannot fit into the screen's frame. The x-axis in both graphs reflects the year of the project's lifetime. The right y-axis in the top graph shows the mean output of the PV modules for a given year in kW while the left y-axis shows the annual AC primary load, which equals the KBH plant's load, served in kWh. The right y-axis in the bottom graph shows the fraction of the load served by

renewable energy while the left y-axis shows the annual amount of energy the microgrid sells to the grid in kWh.

The blue line in the top graph represents the AC primary load across the project's lifetime. It remains flat to reflect this project's assumption that the KBH plant's load remains constant for the duration of the project. The golden line in the top graph represents the mean PV module output for each year and shows the decline in PV module output over the course of the project. Both the teal and the orange²⁶ lines in the bottom graph further reflect the reduction in PV module energy generation during the project's lifetime. The teal line represents the declining fraction of the load served by renewable energy for each year of the project while the orange line represents the declining quantity of energy sold to the grid over each year of the project.

²⁶ All of the keys for variables displayed in Figure 89 are visible in the legend except for the key linked to the declining quantity of energy sold to the grid (orange line). Because the orange line's key is farther from the other keys than the frame can capture, it is not visible in Figure 89.

Cash Flow Graph



Figure 90 – Screenshot of cash flow graph of from Figure 87

The cash flow graph in Figure 90 displays the various costs associated with the project over each year of its lifetime in either tabular or chart format. The first year (year 0) reflects the major expense of the project, which is the initial capital costs (HOMER Energy, 2016bg). From year 2 through year 15, the overall costs of the project are zero or almost zero due to the fact that they consist solely of O&M costs. This occurs because of the graph’s scale and the fact that HOMER subtracts revenues from grid sales to calculate total O&M costs (see Figure 87), which in the case of this iteration, returns a result close to zero (HOMER Energy, 2016bg). Lastly, the salvage value for any components with remaining years of service at the end of the project is displayed in year 25 (HOMER Energy, 2016bg). For this project, the only components that fit these criteria are the inverters that will have been in service since year 15.

Compare Economics Graph

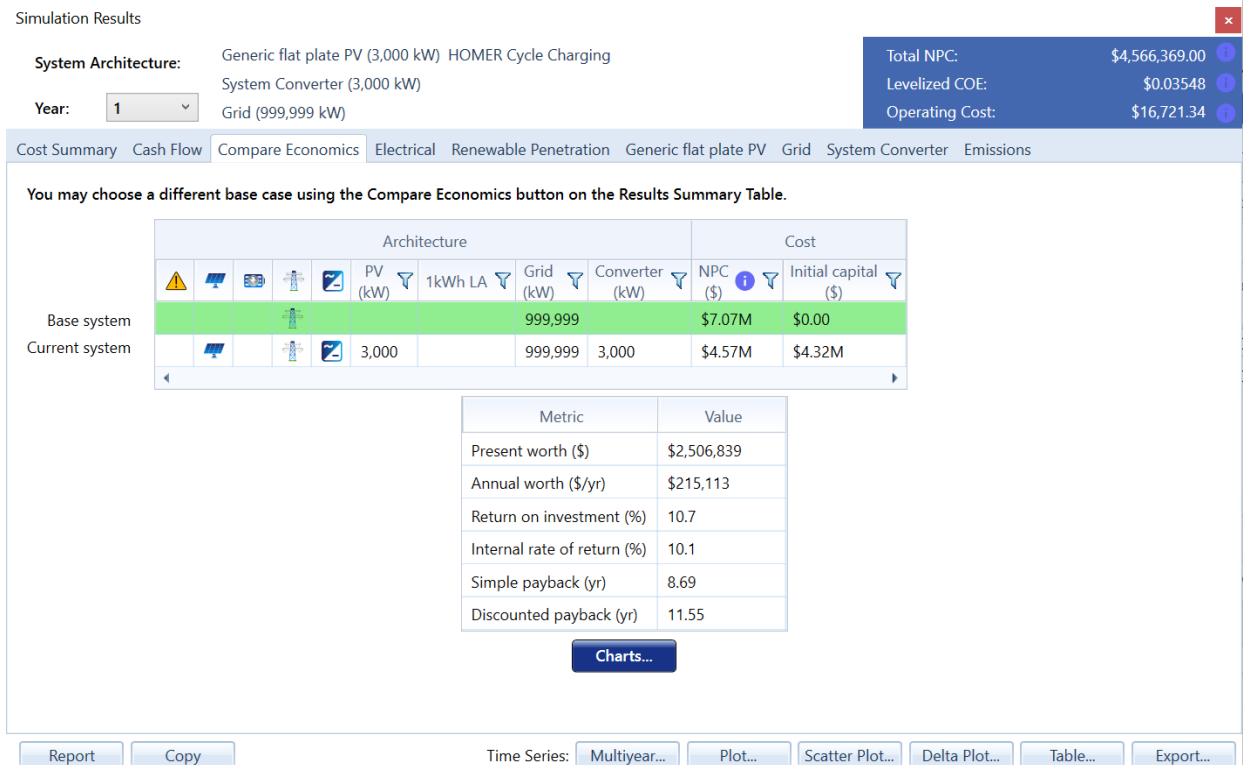


Figure 91 – Screenshot of compare economics graph of combination from Figure 87

The compare economics graph in Figure 91 shows a side-by-side economic comparison of the base system, which is the grid-only combination, and the current system, which is the combination described in the same figure. The present worth is the difference between the net present cost of the base system and that of the current system (HOMER Energy, 2016bi). The present worth's value reveals the quantity of money that the current system will save compared to the base system. If that quantity is positive, the current system saves money over the lifetime of the project compared to the base system; the opposite is true if that quantity is negative (HOMER Energy, 2016bi).

The simple payback point is the number of years required for the costs of operating the current system to generate a cumulative quantity of total net savings compared to the costs of

operating the base system that exceeds the amount of the initial investment into the current system (HOMER Energy, 2016bi). The current system's initial investment consists of the initial capital costs for PV modules and inverters plus the grid interconnection fee (See the 'Capital' column of Figure 87). The total net savings for each year for the current system's costs compared to the base system's costs is $(E_{\text{grid, avoid}} + E_{\text{grid sales}}) - (E_{\text{grid, purchase}} + \text{O\&M}_{\text{PV modules \& inverters}} + \text{the standby charge})$. $E_{\text{grid, avoid}}$ represents the value of the energy the current system generated from the PV modules that otherwise would have been acquired from the grid. $E_{\text{grid sales}}$ represents the value of the energy sold to the grid. $E_{\text{grid, purchase}}$ stands for the value of the energy the current system has to purchase from the grid when the PV modules are not generating power. $\text{O\&M}_{\text{PV modules \& inverters}}$ stands for the total O&M costs for the PV modules and their inverters. The standby charge refers to the fee the grid charges for its availability as a backup power source. But, the simple payback point does not account for inflation (HOMER Energy, 2016bi).

Figure 92, obtained by clicking on the 'Charts' button in Figure 91, explains the simple payback point using cash flows for both systems. In this figure, HOMER labels the base system's expenses at the beginning of the project (year 0) as zero because the base system does not have any initial cash flows. HOMER labels the current system's cash flows at the beginning of the project as \$4.3 million. These represent the current system's initial investment costs. As the project progresses, the base system's cash flows move downward because the system's cash flows only reflect payments to the grid. In contrast, the current system's cash flows are more stable because they reflect its total net savings relative to the base system. The point at which the two system's cash flows intersect represents the simple payback point. Beyond the simple

payback point, the KBH plant would spend more on energy costs using the base system compared to if they invested in the current system.

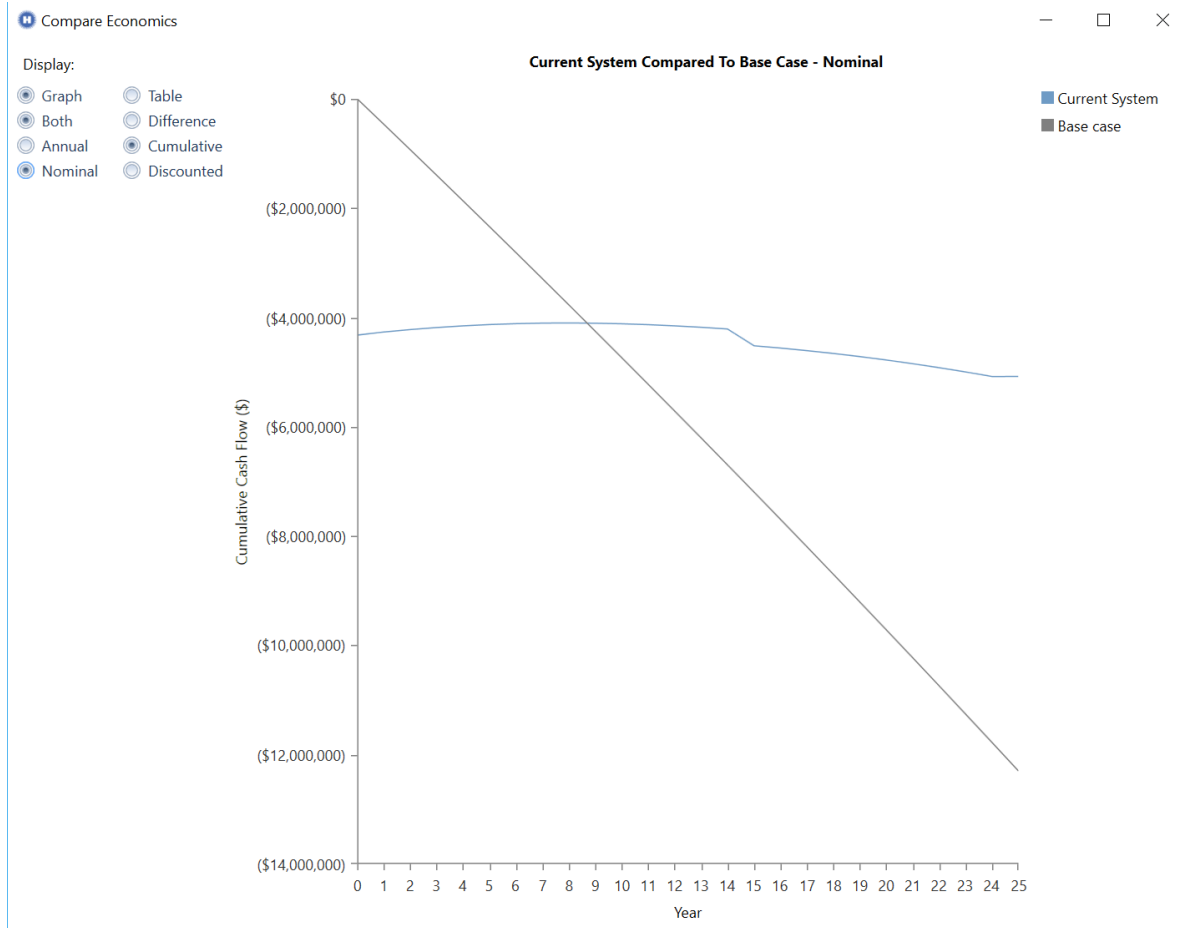


Figure 92 – Screenshot of nominal cash flows of current system and base system to illustrate simple payback point of combination from Figure 87

However, the simple payback point does not account for inflation (HOMER Energy, 2016bi). The discounted payback point tracks the same measures as the simple payback point but incorporates the inflation rate set in Figure 37 (HOMER Energy, 2016bi). Thus, the discounted payback point compares discounted cash flows between the base system and the current system. As a result, the discounted payback point is higher than the simple payback

point. Figure 93, also obtained by clicking on the ‘Charts’ button in Figure 91, illustrates the discounted payback point.

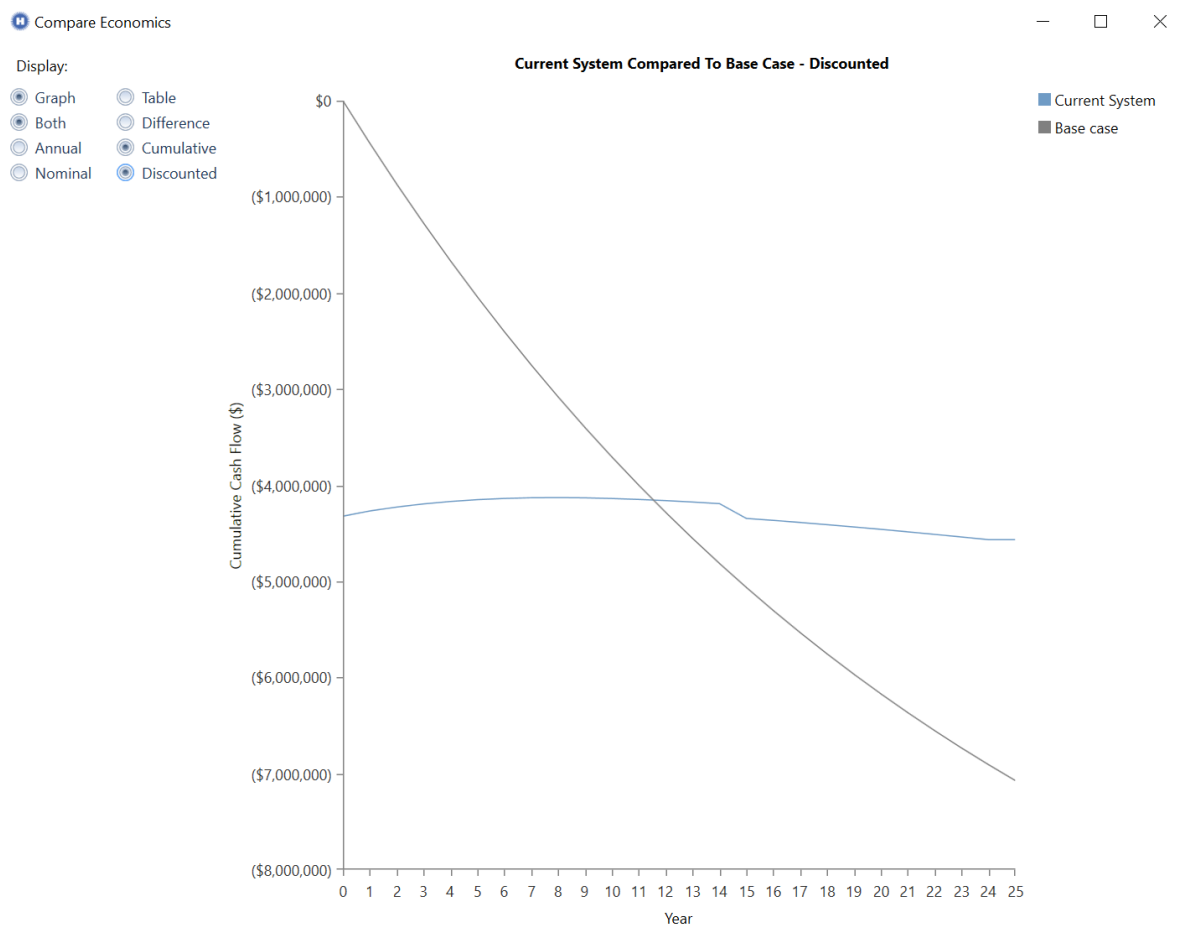


Figure 93 – Screenshot of discounted cash flows of current system and base system to illustrate discounted payback point of combination from Figure 87

The annual worth equals the present worth multiplied by the CRF (HOMER Energy, 2016bi). The annual worth is a ratio that illustrates the quantity of the present worth relative to the project’s annual loan repayments to purchase capital after discounting for interest and inflation (HOMER Energy, 2016bb, 2016bi). The internal rate of return (IRR) is the real discount rate at which the NPC of the base system equals the NPC of the current system (HOMER Energy, 2016bi). The IRR shows the maximum real discount rate at which the current

system will be able to recover its initial investment before the end of the project’s lifetime. The current system’s return on investment (ROI) reflects its annual cost savings over the base system relative to its initial investment (HOMER Energy, 2016bj). Article 7.141 in the HOMER model user manual explains the equation HOMER uses to calculate the ROI. Key variables are the project’s lifetime, the nominal annual cash flow for the current and base systems, and the capital costs for both systems (HOMER Energy, 2016bj).

Electrical Production Graph



Figure 94 – Screenshot of electrical production graph of combination from Figure 87

The electrical production graph in Figure 94 presents an overview of the annual electricity production profiles of the PV modules and the grid and the allocation of energy

produced to different sources during the project's first year²⁷. The production table displays the total annual energy output of the grid and the total energy output of the PV modules before accounting for losses to the inverters. This table also displays these two components' combined output while the chart below displays each component's average daily output for each month (HOMER Energy, 2016bk). The consumption table illustrates the fraction of the total annual energy that the system produced that went to serving the AC primary load, or the KBH plant's electricity needs, and the fraction sold to the grid (HOMER Energy, 2016bk).

The term 'excess electricity' in the top quantity table refers to the amount of electricity that the PV modules produced that the inverters could not process (HOMER Energy, 2016bl). This energy load is known as a dump load, and it has to be dissipated in order to prevent damage to the system (HOMER Energy, 2016bl; Roy, Kedare, & Bandyopadhyay, 2010; Solomon, Faiman, & Meron, 2010). Methods to dissipate dump loads include channeling the load to the ground, sending it to resistors, or funneling it to a bank of lightbulbs (Blume, 2011; Haque et al., 2010; HOMER Energy, 2016bl; McGowan & Manwell, 1988; Solomon et al., 2010).

The bottom quantity table shows that for the first year of the project, 69% of the KBH plant's electricity needs are expected to come from the PV modules (HOMER Energy, 2016bk). The current system is also expected to have a maximum renewable penetration of 105% for the first year. The renewable penetration equals the total electricity output from renewable sources in a given time step divided by the total load in the same time step (HOMER Energy, 2016bm). During the first year of the project, the maximum renewable penetration across all time steps is expected to be 105% of the load served at that time step.

²⁷ The user can see electricity production profiles for other years by using the dropdown menu labeled 'Year' in the top left corner of Figure 94.

Renewable Penetration Graph

The renewable penetration graph in Figure 95 provides a variety of charts and measures to assess PV modules’ capabilities to supply the load at different times of the year. The nominal renewable capacity divided by total nominal capacity in the ‘Capacity-based metrics’ box shows the potential fraction of the load that the PV modules could serve at any time step across the year if they had no derating factor, temperature coefficient, or energy losses to the inverters (HOMER Energy, 2016bn). The usable renewable capacity divided by total capacity reflects the potential fraction of the load that the PV modules could serve at any time step across the year after accounting for their derating factor, temperature coefficient, and energy losses to the inverters. A value of 100% means for both means that the PV modules’ nominal capacity and usable capacity could supply the entirety of the KBH plant’s electricity needs.



Figure 95 – Screenshot of renewable penetration graph of combination from Figure 87

The first measure in the ‘Energy-based metrics’ table reflects the PV modules’ total energy production for the first year in kWh divided by the plant’s total annual electricity consumption (HOMER Energy, 2016bn). The second measure in this table reflects the PV modules’ total energy production for the first year in kWh divided by the system’s total annual electricity production (HOMER Energy, 2016bn). But, these measures do not account for the PV modules’ energy that is lost when converted from DC current to AC current. The third measure does account for these losses because it subtracts the nonrenewable, or grid, output from the number one. This reveals the quantity produced by the only other source of energy directly supplying the load, which is the AC current from the inverters. Consequently, this measure is the most appropriate to determine the percentage of the plant’s electricity consumption that the PV modules can supply. The three charts below the ‘Energy-based metrics’ table show each of this table’s metrics for each time step across the year. Lastly, the ‘Peak values’ table assesses the peak value of the measures from the ‘Energy-based metrics’ table compared to the plant’s total annual electricity generation and the system’s total annual electricity production.

Generic Flat Plate PV Module Output Graph

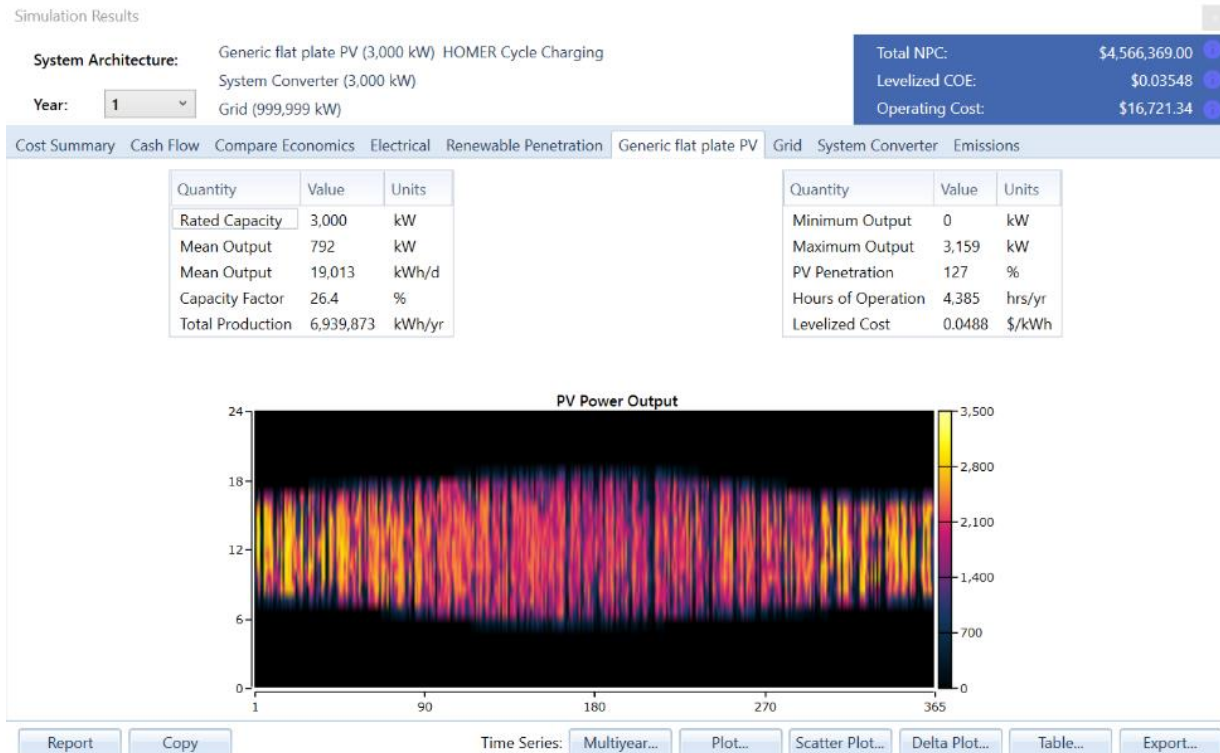


Figure 96 – Screenshot of generic flat plate PV output graph of combination from Figure 87

Figure 96 provides the statistics on PV module output across all timesteps of the year before accounting for energy lost to the inverters. This figure also shows the PV modules' minimum and maximum output over the course of the first year of the project. Three important measures from this graph are the PV penetration, the capacity factor, and PV modules' COE. The PV penetration is the PV modules' average annual output divided by the KBH plant's average annual load (HOMER Energy, 2016bo). The capacity factor equals the PV modules' average annual output divided by their rated capacity (HOMER Energy, 2016bo). The PV modules' COE represents the COE of the PV modules' electricity output without incorporating the value of energy sold to the grid (HOMER Energy, 2016bo).

Grid Statistics Graph

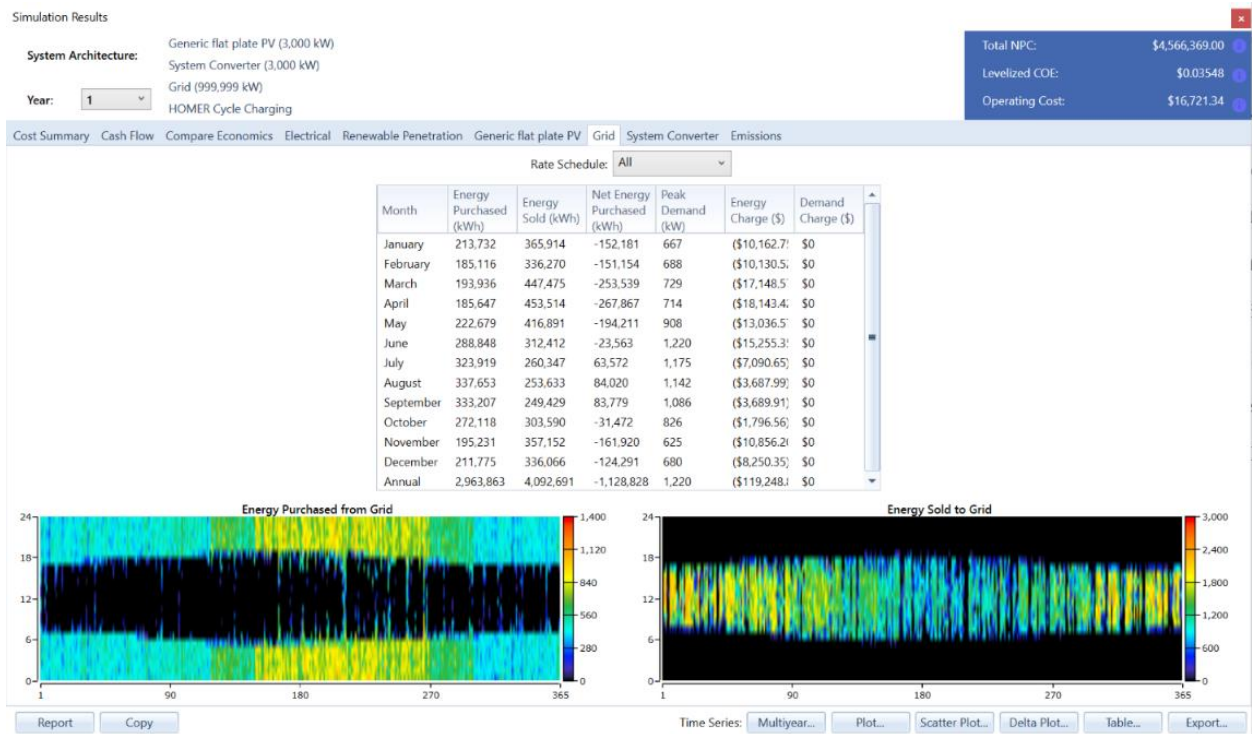


Figure 97 – Screenshot of grid statistics output graph of combination from Figure 87

The grid statistics graph in Figure 97 shows the monthly energy sales to the grid and energy purchases from the grid for the first year of the project. The two charts show the amount of energy purchased from the grid and sold to the grid at each hour for every day of the year. The days of the year are one the x-axis of both charts while the load level in kW is on the right y-axis and the hours of the day are on the left y-axis of both charts.

Inverter Output Graph

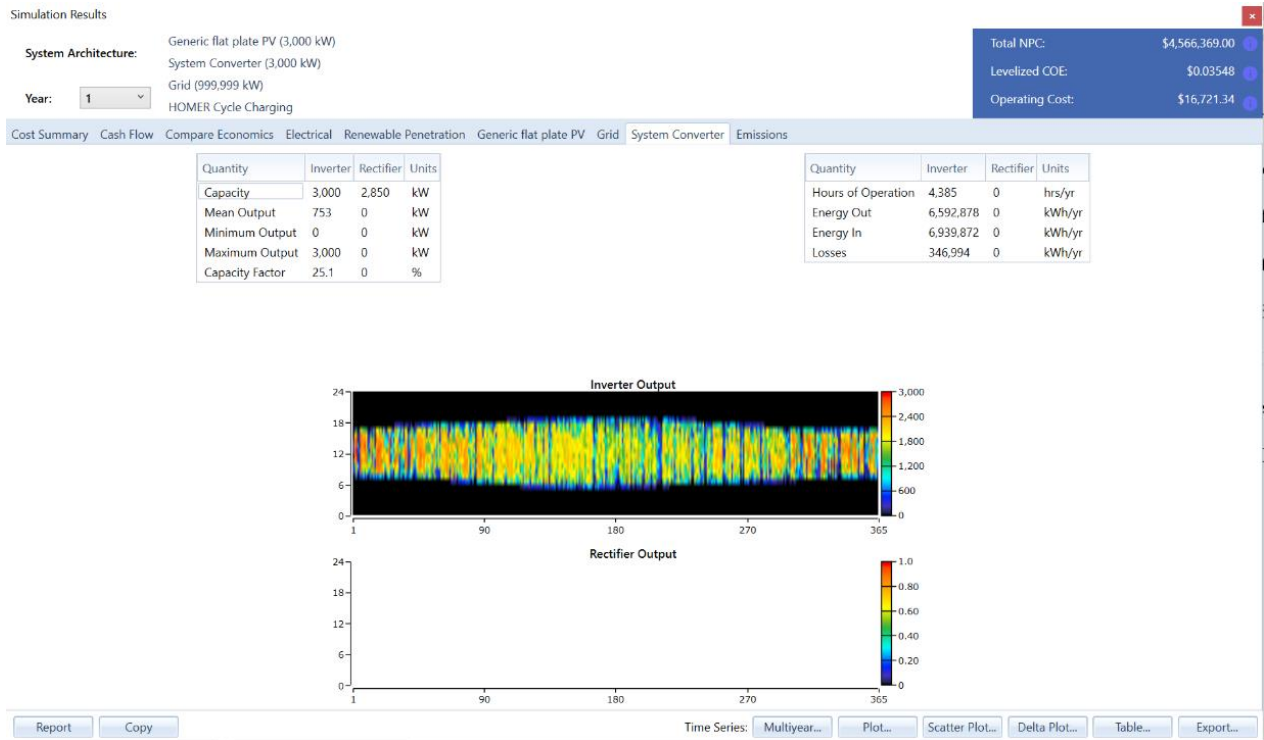


Figure 98 – Screenshot of inverter output graph of combination from Figure 87

The inverter output graph in Figure 98 displays the inverters’ output across all timesteps for the first year of the project as well as production factors such as the minimum and maximum output over the course of the year. The ‘Energy In’ field represents the annual amount incoming energy from the PV modules while the ‘Energy Out’ field represents annual amount of energy the inverters send to KBH plant or to the grid (HOMER Energy, 2016bp). The inverters also have a capacity factor that equals their average annual output divided by their rated capacity (HOMER Energy, 2016bp). The inverters’ capacity factor of 25.1% divided by the PV modules’ capacity factor of 26.4% equals 0.95, which represents the inverters’ efficiency of 95%.

Summary

The fixed and variable parameters that HOMER utilizes to generate its results help the model provide a comprehensive assessment on the feasibility of partially powering the KBH plant with a solar-powered microgrid. Though there are many, all of these parameters play an integral role in determining the economic assessments this thesis provides regarding the installation of a solar-powered microgrid at the KBH plant. The next section illustrates the way these parameters, particularly the ones that vary across iterations, shape the results HOMER gives and how they make an important difference in determining the level of energy cost savings a solar-powered microgrid could provide for the KBH plant.

Chapter 4

4.1 RESULTS OF THE HOMER MODEL

This section outlines the results of the HOMER model's cost/benefit forecast of the twelve energy supply configurations to meet the Kay Bailey Hutchison (KBH) desalination plant's electricity demand by using charts created in Microsoft Excel to compare their costs and savings. These charts evaluate the costs and benefits of each iteration based on the following measures: 1) initial capital cost, 2) energy produced, 3) renewable fraction, 4) energy sold, 5) annualized operating costs (OC), 6) cost of energy (COE), 7) net present cost (NPC), and 8) the discounted payback point (DPP). These charts also illustrate the influence of the key sensitivity variables pertaining to each iteration's PV modules on the aforementioned measures. These variables include: 1) the presence of axis trackers, 2) price scale, 3) net metering, and 4) the derating factor. There are separate charts for the configurations whose PV modules have a derating factor of 85% and those with a derating factor of 90% for clearer comparison; each iteration has the same capacity variety²⁸ for each component for both derating factors.

The most economical electricity supply source for ten of the twelve iterations whose PV modules have a derating factor of 85% consists of a combination of the grid and PV modules. The two exceptions were the iterations priced at the '500 kW commercial' scale without axis trackers. Solely the grid was the most cost-effective electricity supply source for these two

²⁸ See part about 'PV Module Capacity Optimization' in subsection entitled "Configuring Model Components: PV Module, Inverter, Battery, and Grid" in Section 3.1 for explanation about capacity varieties

iterations. In contrast, the most economical electricity supply combination for all twelve iterations whose PV modules have a derating factor of 90% includes a mix of the grid and PV modules. Interestingly, regardless of their PV modules' derating factor, not one of the iterations' most economical electricity supply configuration included batteries.

Initial Capital Cost

PV Module Configurations with 85% Derating Factor

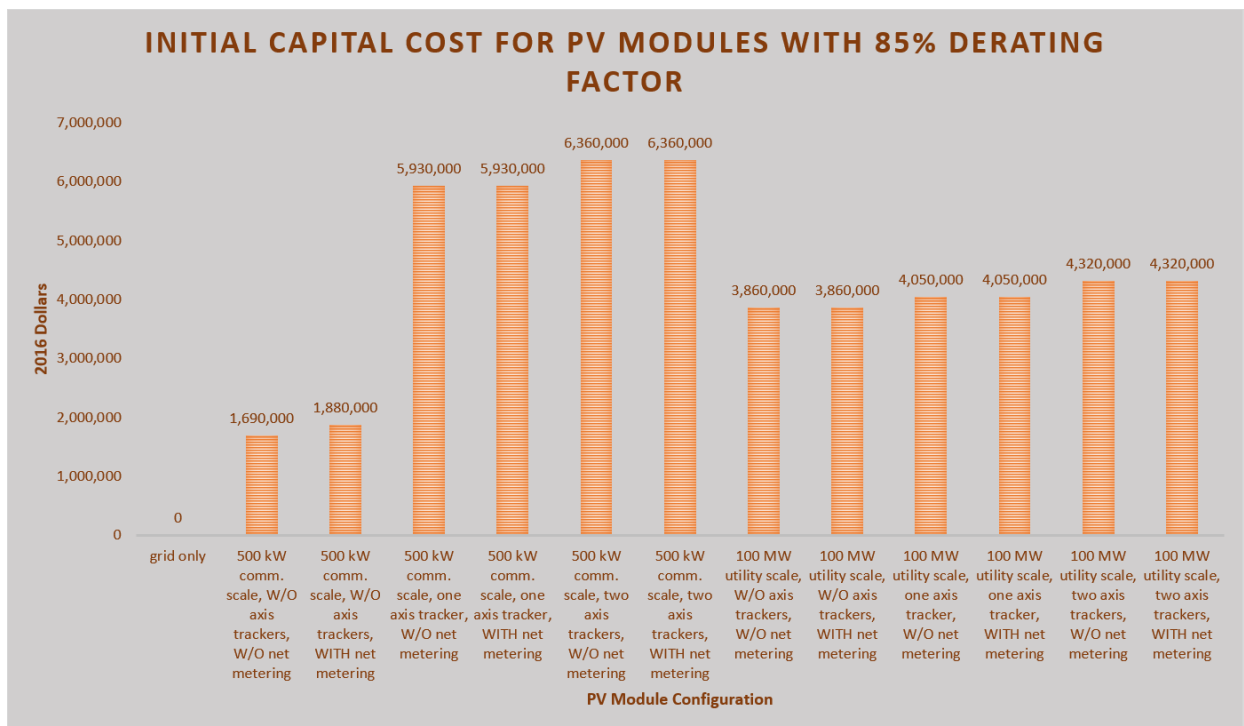


Figure 99 – Screenshot of Excel chart showing initial capital costs of PV module configurations with derating factor of 85%

The combinations with the lowest initial capital cost are those without axis trackers at the '500 kW commercial' price scale. This occurs because HOMER predicts that these combinations' lack of axis trackers will not allow them to produce enough energy to create a quantity of savings that overcomes the higher capital investment costs at this price scale.

Consequently, HOMER ascertains that the most cost-effective configuration for these combinations will have a lower capacity of PV modules, and therefore, a lower initial capital cost. Interestingly, upon adding net metering, HOMER determines that the most cost-effective combination will include a slightly higher capacity of PV modules, which leads to a slightly higher initial capital cost. Adding one axis tracker to PV modules priced at the ‘500 kW commercial’ scale substantially increases expected energy production (see Figure 101) compared to PV modules without axis trackers. As a result, HOMER sets these iterations’ ideal PV capacity to a significantly higher level, which is reflected in their initial capital costs in Figure 99. Dual axis trackers further increase the optimal PV module capacity, and therefore, the initial capital cost, albeit by a decidedly lower amount. But, the addition of net metering to the iterations with axis trackers at this price scale does not render an amount of savings that is sufficient to further increase the ideal PV module capacity.

An intriguing contrast between the combinations priced at the ‘500 kW commercial’ scale and those priced at the ‘100 MW utility’ scale is the sizable discrepancy between the differences in initial capital costs of each price scale’s iterations with corresponding numbers of axis trackers. The initial capital cost of the combinations without axis trackers at the ‘100 MW utility’ price scale is about two million dollars greater than that of their counterparts at the ‘500 kW commercial’ price scale. This is a testament to the monumental difference a hefty reduction in price per kW for PV modules can make in determining the appropriate PV module capacity and, accordingly, the extent of solar energy in the KBH plant’s electricity load. In comparison, the difference between the initial capital costs of the configurations with one axis tracker priced at the ‘100 MW utility’ scale is about two million dollars less than that of their counterparts at

the ‘500 kW commercial’ price scale. The same holds true for the combinations with two axis trackers. Additionally, at the ‘100 MW utility’ price scale, net metering does not change the optimal PV module capacity for any of the combinations. However, the notably smaller difference in initial capital costs between the iterations without axis trackers, those with one axis tracker, and those with two axis trackers at the ‘100 MW utility’ price scale compared to that of their corresponding counterparts at the ‘500 kW commercial’ price scale indicates that the presence of axis trackers on iterations at the ‘100 MW utility’ price scale does not yield as proportionate an increase in savings from solar energy production in order to warrant a comparable increase in PV module capacity.

PV Module Configurations with 90% Derating Factor

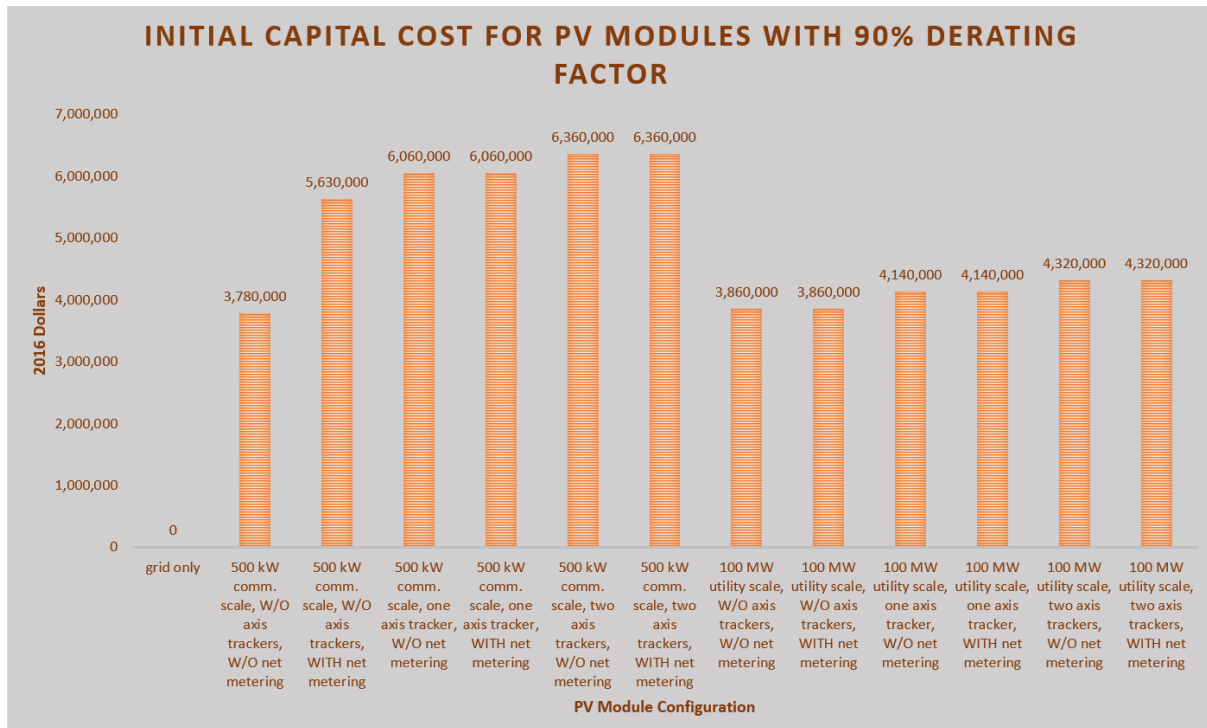


Figure 100 – Screenshot of Excel chart showing initial capital costs of PV module configurations with derating factor of 90%

Raising the PV modules' derating factor to 90% notably increases the initial capital cost of the iterations without axis trackers priced at the '500 kW commercial' scale. Additionally, incrementing the PV modules' derating factor to 90% further amplifies the effect of net metering for these combinations. When the PV modules' derating factor is 85%, including net metering adds \$200,000 to the initial capital cost of the configuration priced at the '500 kW commercial' scale whose PV modules do not include axis trackers. In comparison, when the PV modules' derating factor is 90%, adding net metering increases the initial capital cost of this configuration by nearly two million dollars.

But, augmenting the PV modules' derating factor to 90% only raises the initial capital cost of the iterations with one axis tracker priced at the '500 kW commercial' scale by \$130,000; adding net metering does not affect these costs. Neither the increase of the PV modules' derating factor to 90% nor the addition of net metering changes the initial capital cost of iterations with two axis trackers at this price scale. Interestingly, this phenomenon also applies to all the iterations priced at the '100 MW utility' scale. For instance, neither the initial capital cost of the iterations without axis trackers nor that of the iterations with two axis trackers changes upon increasing the derating factor to 90%. Additionally, the initial capital cost of the iterations with one axis tracker only rises by \$90,000. Net metering does not change the initial capital cost of any of the iterations priced at the '100 MW utility' scale. However, increasing the PV modules' derating factor to 90% noticeably reduces the differences in initial capital costs of the iterations without axis trackers, those with one axis tracker, and those with two axis trackers at the '500kW commercial' price scale.

Energy Produced

PV Module Configurations with 85% Derating Factor

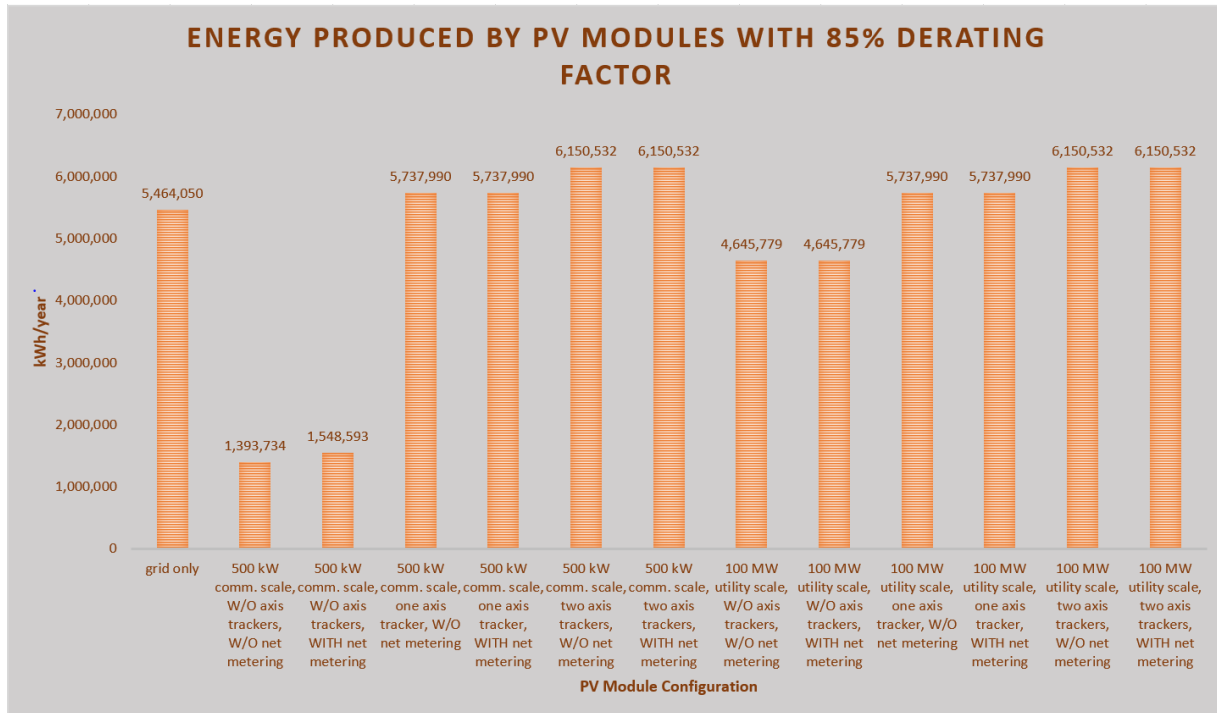


Figure 101 – Screenshot of Excel chart showing energy produced of PV module configurations with derating factor of 85%

The grid-only configuration in Figures 101 and 102 reflects the KBH plant’s average annual electricity consumption from the grid over the 2011-2016 period. This quantity differs slightly from that in Figure 41 in section 3.1 due to rounding errors related to adjustments to the load²⁹. The significantly lower expected energy production of the iteration without axis trackers or net metering at the ‘500 kW commercial’ price scale compared to the expected energy production of other iterations confirms that axis trackers substantially influence expected energy production. Net metering increases this combination’s most cost-effective PV capacity slightly,

²⁹ See parts entitled ‘KBH Plant Monthly Average Energy Usage’ and ‘Adjustments to KBH Plant’s Monthly Electric Load’ in subsection entitled “KBH Plant Electric Load Profile” in section 3.1 for more information.

which in turn increases its predicted energy production modestly. However, net metering does not affect either the ideal PV capacity or the energy production of any of the other iterations.

The results in Figure 101 prove that, without axis trackers, it is not economical to invest in a larger number of PV modules with an 85% derating factor at the ‘500 kW commercial’ price scale. Consequently, these iterations’ predicted energy output is much lower compared to that of the others. Yet, the much higher expected energy production of the iterations without axis trackers at the ‘100 MW utility’ price scale demonstrates the influence of price scale on iterations’ predicted energy output. But, price scale’s influence on energy production disappears upon adding one or two axis trackers to PV modules. This is illustrated in the fact that the expected energy production for the iterations with one axis tracker at both the ‘100 MW utility’ price scale and the ‘500 kW commercial’ price scale is equal. This also holds true for the iterations with two axis trackers at both price scales.

PV modules with single axis trackers produce 118% more energy than PV modules without axis trackers (Helwa, Baghat, & El-Shafee, 2000; Lubitz, 2010). Those with dual axis trackers produce 130% more energy than those without axis trackers (Helwa et al., 2000; Lubitz, 2010). These findings show that PV modules with a single axis tracker substantially increase energy production relative to those without axis trackers (Lubitz, 2010). Adding a second axis tracker further increases PV module output compared to that of PV modules without axis trackers, albeit to a much lesser degree (Lubitz, 2010). The expected energy production of the iterations with axis trackers at the ‘500 kW commercial’ price scale compared to that of their counterparts without axis trackers at the same price scale follows this pattern. But, the stark differences in ideal PV capacities between the iterations with axis trackers and those without axis

trackers results in a much greater difference in predicted energy production between these iterations. This corroborates the combined influence of price scale and axis trackers on expected energy production.

In comparison, the differences in expected energy output of the iterations without axis trackers, those with one axis tracker, and those with two axis trackers at the ‘100 MW utility’ price scale more closely resemble the findings of Helwa and others (2000) and Lubitz (2010). The iterations with one axis tracker at this price scale are expected to produce 124% more energy than those without axis trackers while those with two axis trackers are expected to produce 132% more energy than those without axis trackers. This illustrates that, for this project, the ‘100 MW utility’ price scale produces ideal PV capacities for each iteration whose predicted energy output more closely parallels the typical added energy output of one and two axis trackers.

PV Module Configurations with 90% Derating Factor

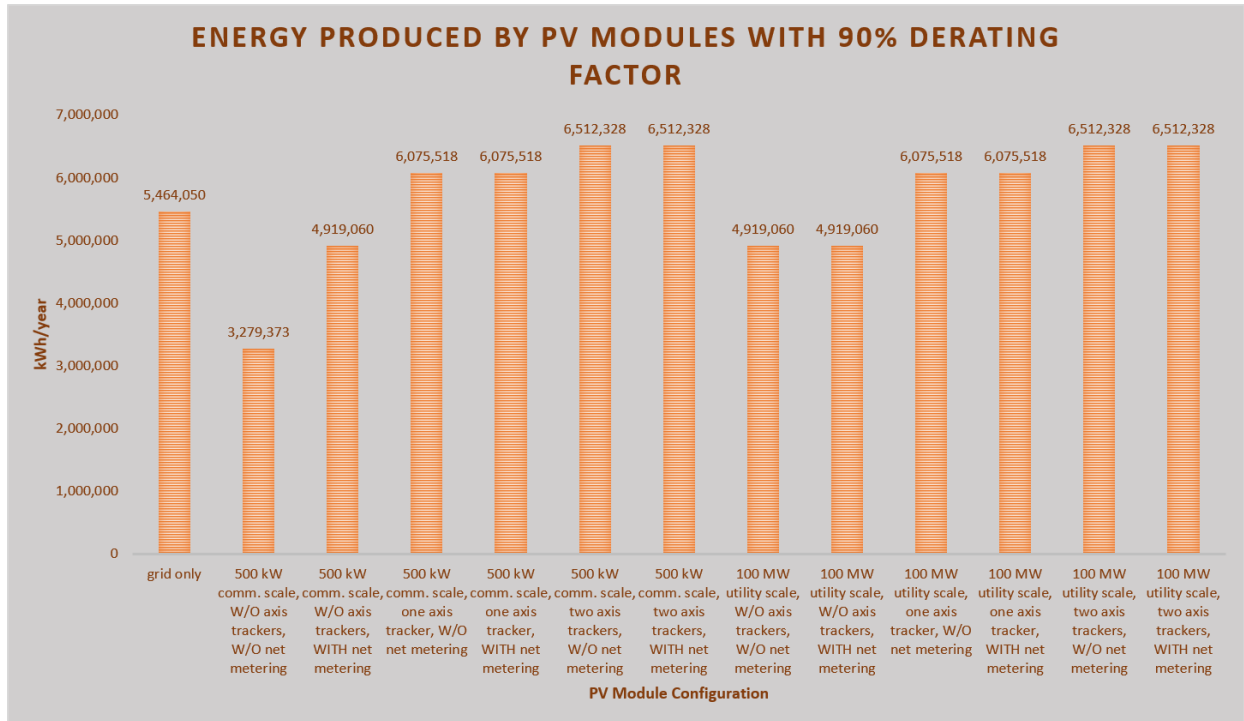


Figure 102 – Screenshot of Excel chart showing energy produced of PV module configurations with derating factor of 90%

Increasing the PV modules’ derating factor to 90% increases the expected energy production of the iterations without axis trackers at the ‘500 kW commercial’ price scale the most. Figure 102 shows that even a slight increase in the derating factor yields a considerably higher amount of expected energy production for the iterations without axis trackers at this price scale. Net metering’s influence on this iteration is also notably greater than the 85% derating factor. At the 90% derating factor, net metering raises this iteration’s predicted energy output by approximately 1.6 million kWh as opposed to an increase of approximately 150,000 kWh at the 85% derating factor. Net metering also raises this iteration’s expected energy production to an amount on par with that of the iterations without axis trackers at the ‘100 MW utility’ price scale.

However, at this derating factor, net metering also does not change the expected energy production of any other the other iterations.

But, increasing the PV modules' derating factor to 90% only raises the expected energy production of the iterations with either one or two axis trackers at the '500 kW commercial' scale by about 400,000 kWh; adding net metering does not affect these figures. This also applies to these iterations at the '100 MW utility' price scale. Additionally, the expected energy production of these iterations at the '100 MW utility' price scale equals that of their corresponding counterparts at the '500 kW commercial' price scale. Moreover, the expected energy production of the iterations without axis trackers with a 90% derating factor at the '100 MW utility' price scale is only about 300,000 kWh greater than that of their counterparts at this price scale with an 85% derating factor. This indicates that the derating factor and net metering do not have the same degree of influence on the energy output of iterations with one or two axis trackers or those without axis trackers at the '100 MW utility' price scale compared to the iterations without axis trackers at the '500 kW commercial' price scale.

The differences in expected energy production between the iterations without axis trackers, those with one axis tracker, and those with two axis trackers at the '100 MW utility' price scale with a 90% derating factor still resemble the findings of Helwa and others (2000) and Lubitz (2010). The iterations with one axis tracker at this price scale are also expected to produce 124% more energy than those without axis trackers while those with two axis trackers are also expected to produce 132% more energy than those without axis trackers.

However, with a 90% derating factor, the addition of net metering causes the differences in energy production between the iteration without axis trackers at the '500 kW commercial'

price scale and those with one or two axis trackers at this same price scale to also mirror the findings of Helwa and others (2000) and Lubitz (2010). This fact, combined with the greater expected energy production of the iteration either axis trackers or net metering, indicates that an increased derating factor leads to a more even distribution of expected energy production across iterations.

Renewable Fraction & Energy Sold

PV Module Configurations with 85% Derating Factor

Renewable Fraction

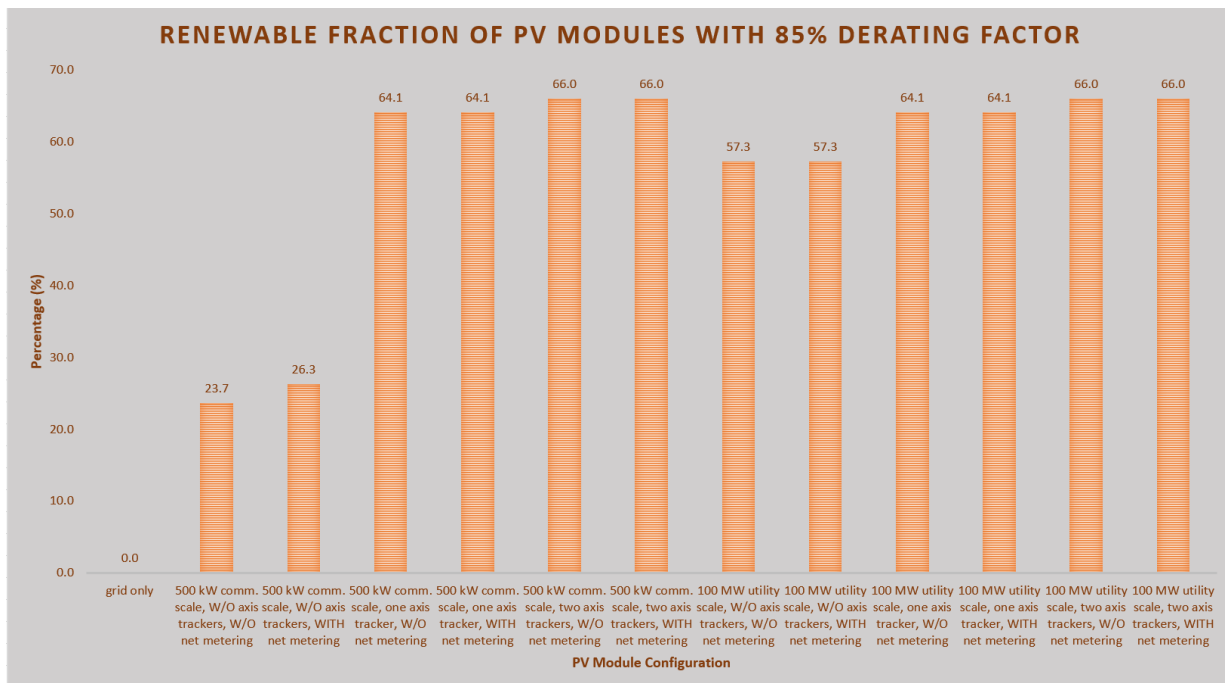


Figure 103 – Screenshot of Excel chart showing renewable fraction of PV module configurations with derating factor of 85%

Each iteration’s renewable fraction mirrors its expected energy production (see Figure 101). As a result, the presence of axis trackers, price scale, net metering, and the derating factor influence each iteration’s renewable fraction in the same way they influence their expected

energy production. The iterations without axis trackers at the ‘500 kW commercial’ price scale have a noticeably smaller renewable fraction due to their smaller ideal PV capacities. As Figure 103 confirms, these renewable fractions reflect a renewable energy resource that is only available during daylight hours and varies by time of day and time of year

Energy Sold

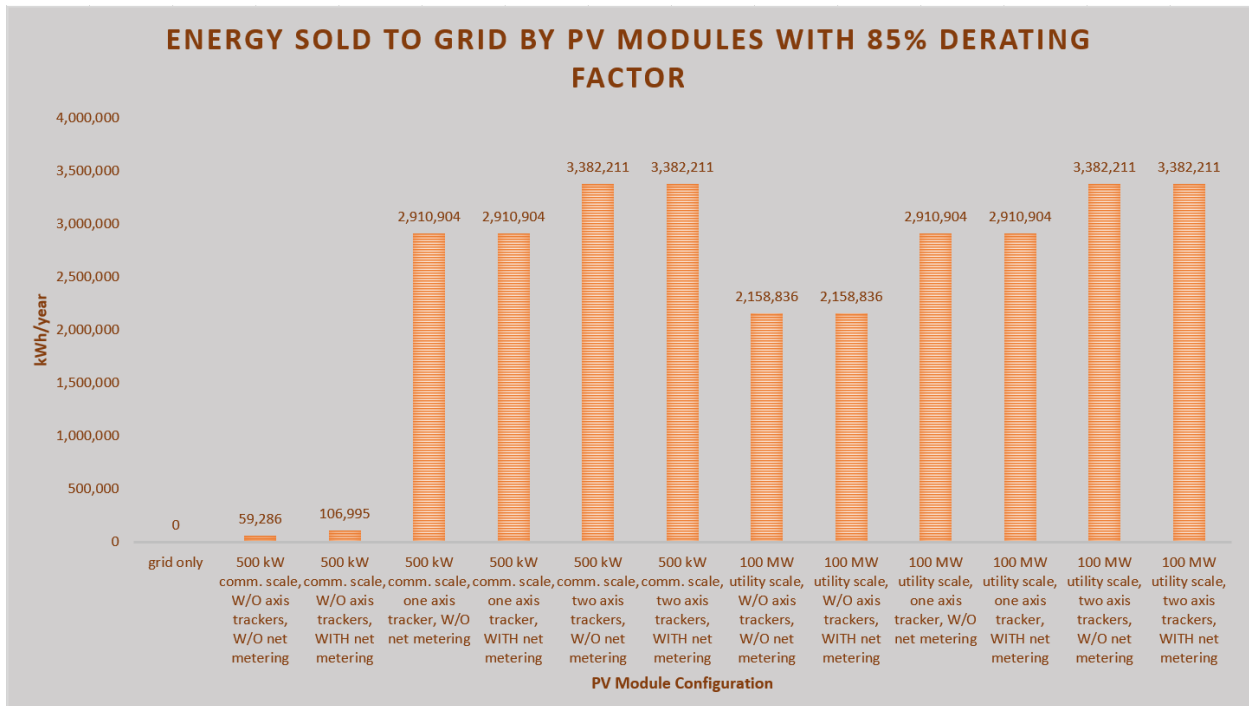


Figure 104 – Screenshot of Excel chart showing energy sold to grid of PV module configurations with derating factor of 85%

The amount of energy each iteration sells to the grid reflects its renewable fraction. This amount also illustrates that iterations with greater ideal PV capacities sell more energy to the grid. These quantities also confirm that with the right PV capacity, solar power could supply much more energy than the KBH plant requires over the course of the year. But, because solar energy varies by time of day, time of year, and the weather, the PV modules will never supply the KBH plant’s load 100% of the time unless it becomes economically feasible to install and

maintain a battery bank powerful enough to supply the plant’s load when the PV modules cannot. Figures 101 through 104 indicate that larger PV capacities, especially if the modules contain axis trackers, could provide a greater share of the KBH plant’s annual electricity demand. This is especially true during sunrise and sunset because larger PV arrays could capture more of the sun’s dimmer light to power the plant. Nevertheless, a larger PV array would require more investment, which may not prove economically wise. Hence, until there is an economically viable way to overcome the issues of energy storage and higher costs for bigger PV arrays, the renewable fraction will inevitably have a ceiling.

PV Module Configurations with 90% Derating Factor

Renewable Fraction

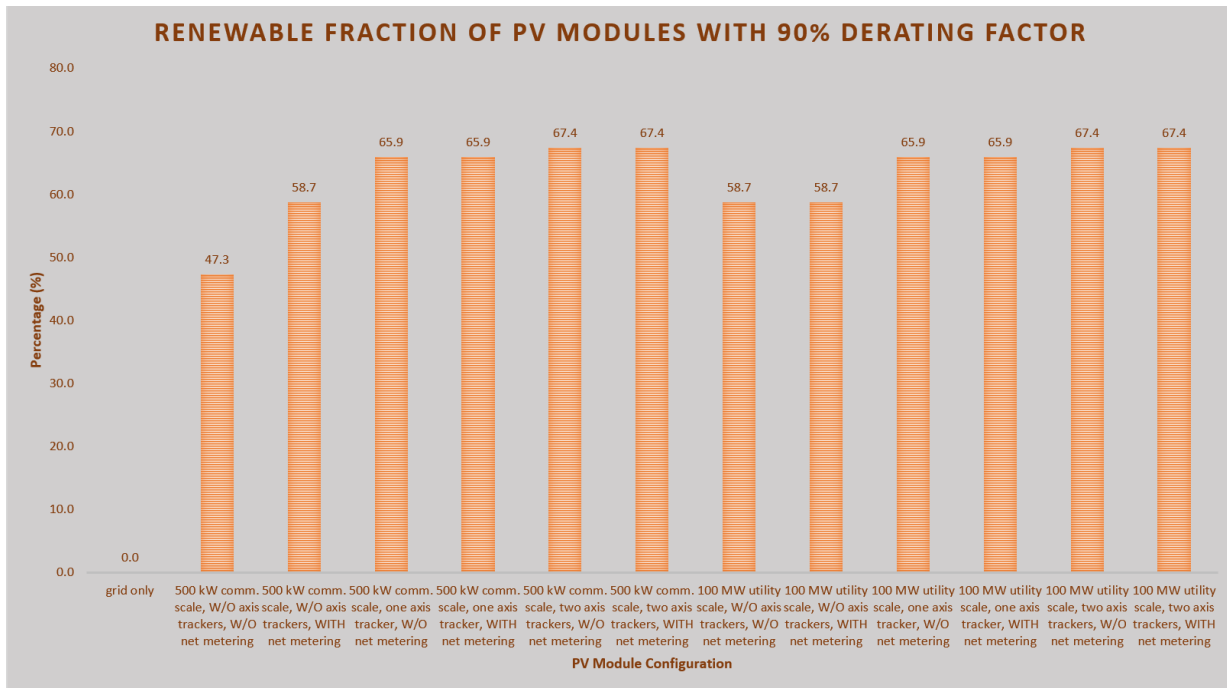


Figure 105 – Screenshot of Excel chart showing renewable fraction of PV module configurations with derating factor of 90%

Increasing the derating factor to 90% percent does not change the fact that each iteration’s renewable fraction follows its expected energy production (see Figure 102). Consequently, the presence of axis trackers, price scale, net metering, and the derating factor continue to affect each iteration’s renewable fraction in the same way they affect their expected energy production. But, the increased derating factor has the most notable effect on the renewable fraction of the iterations at the ‘500 kW commercial’ price scale without axis trackers. Hence, Figure 105 provides further evidence that just a marginal increase in the derating factor leads to a significantly greater amount of expected energy production for the iterations without axis trackers at this price scale.

Energy Sold

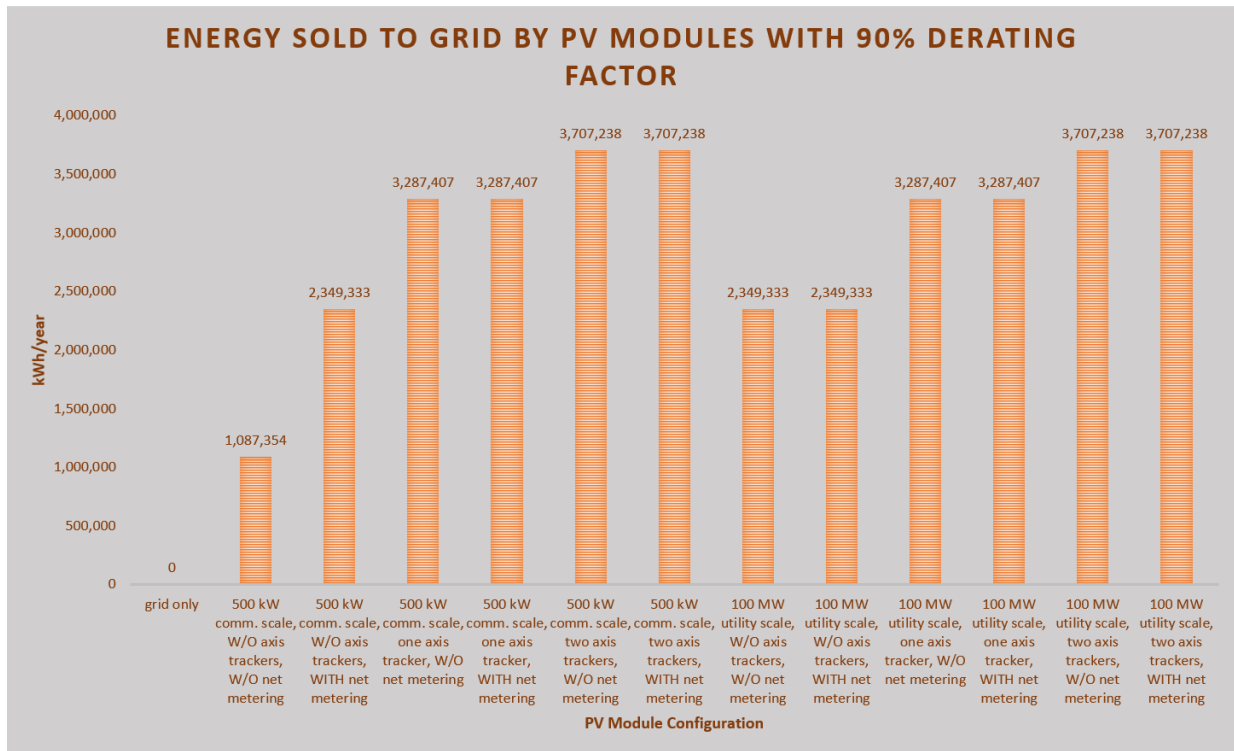


Figure 106 – Screenshot of Excel chart showing energy sold to grid of PV module configurations with derating factor of 90%

Raising the derating factor to 90% does not change the fact that each iteration's energy sold also follows its renewable fraction. Figures 105 and 106 prove that a greater derating factor can lead to ideal PV capacities that could supply an even greater proportion of the KBH plant's electricity demand. They also prove that a higher derating factor can produce even greater quantities of energy sold to the grid compared to PV modules with an 85% derating factor. Nonetheless, an increased derating factor does not change the fact that PV modules will never support the KBH plant's load all of the time unless the cost to install and maintain battery banks with an adequate capacity becomes economically viable as opposed to using grid energy when the PV modules cannot meet the load. Yet, the increased derating factor undeniably helps PV modules supply a larger share of the load, which further increases PV modules' economic viability to power water desalination plants.

Operating Cost & Cost of Energy

PV Module Configurations with 85% Derating Factor

Operating Cost

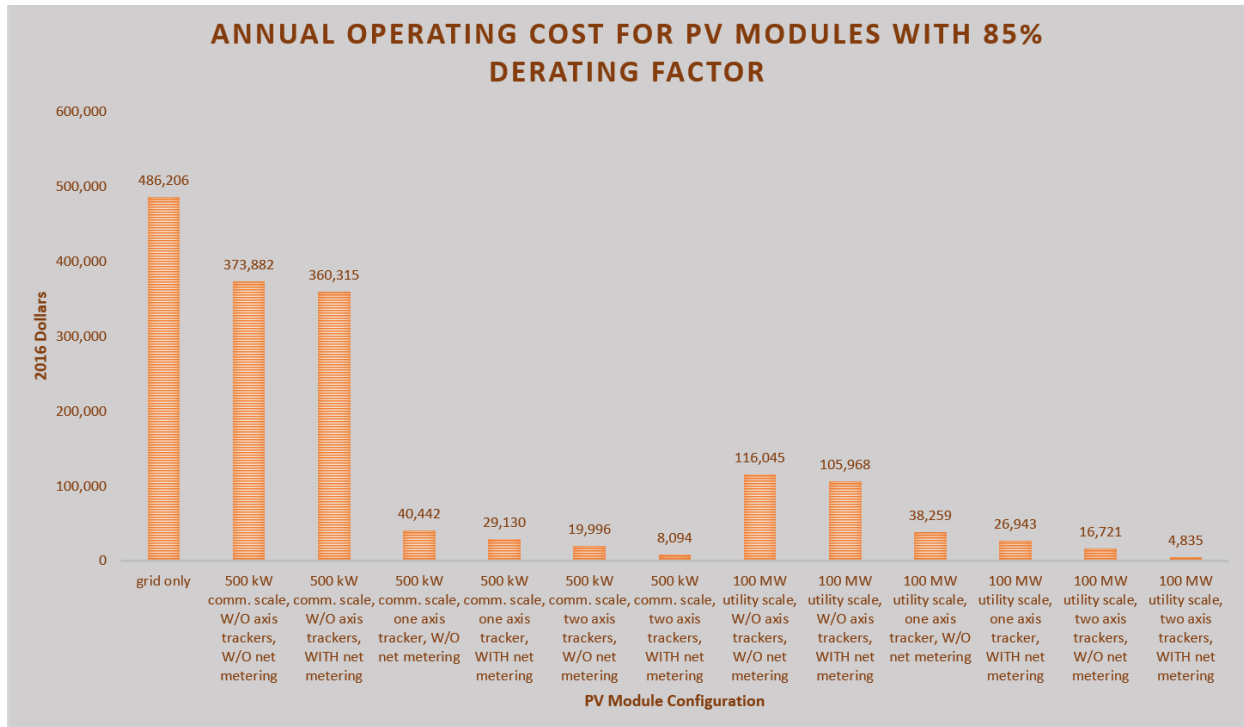


Figure 107 – Screenshot of Excel chart showing annual operating cost of PV module configurations with derating factor of 85%

The grid-only OC depicts the current average annual costs the KBH plant paid for grid electricity from 2011-2016. The quantity is higher than that in Figure 41 in section 3.1 due to the slight discrepancy in the grid-only electricity rates that HOMER calculates and those displayed in Figure 41³⁰. These effects cause the approximately \$43,000 difference between the grid-only configuration’s OC in Figure 41 and that in HOMER’s calculations.

³⁰ See part entitled ‘Grid Power Configurations’ in the subsection called “Configuring Model Components: PV Module, Inverter, Battery, and Grid” in section 3.1 for explanation

All iterations with PV modules display an OC lower than that of the grid-only configuration. This suggests that even the iterations without axis trackers at the '500 kW commercial' price scale would be more cost-effective than a grid-only configuration if there were no initial capital costs associated with the PV modules. Net metering also has a greater effect on the OC compared to other variables due to the fact that it alters the OC of iterations with the same quantity of axis trackers across both price scales. The addition of axis trackers to PV modules also substantially reduces each iteration's OC, especially at the '500 kW commercial' price scale. But adding one axis tracker to the iterations without axis trackers reduces the OC by a greater amount compared to adding another axis tracker to the iterations with one axis tracker. This applies to both price scales. Interestingly, price scale does not affect the OC of iterations with axis trackers to the same degree as iterations without axis trackers. For instance, the OC of the iterations without axis trackers at the '100 MW utility' price scale is about \$250,000 less than that of their counterparts at the '500 kW commercial' price scale. But, the OC of iterations with one or two axis trackers at the '100 MW utility' price scale is only between two thousand dollars and four thousand dollars less than that of their corresponding counterparts at the '500 kW commercial' price scale.

Cost of Energy

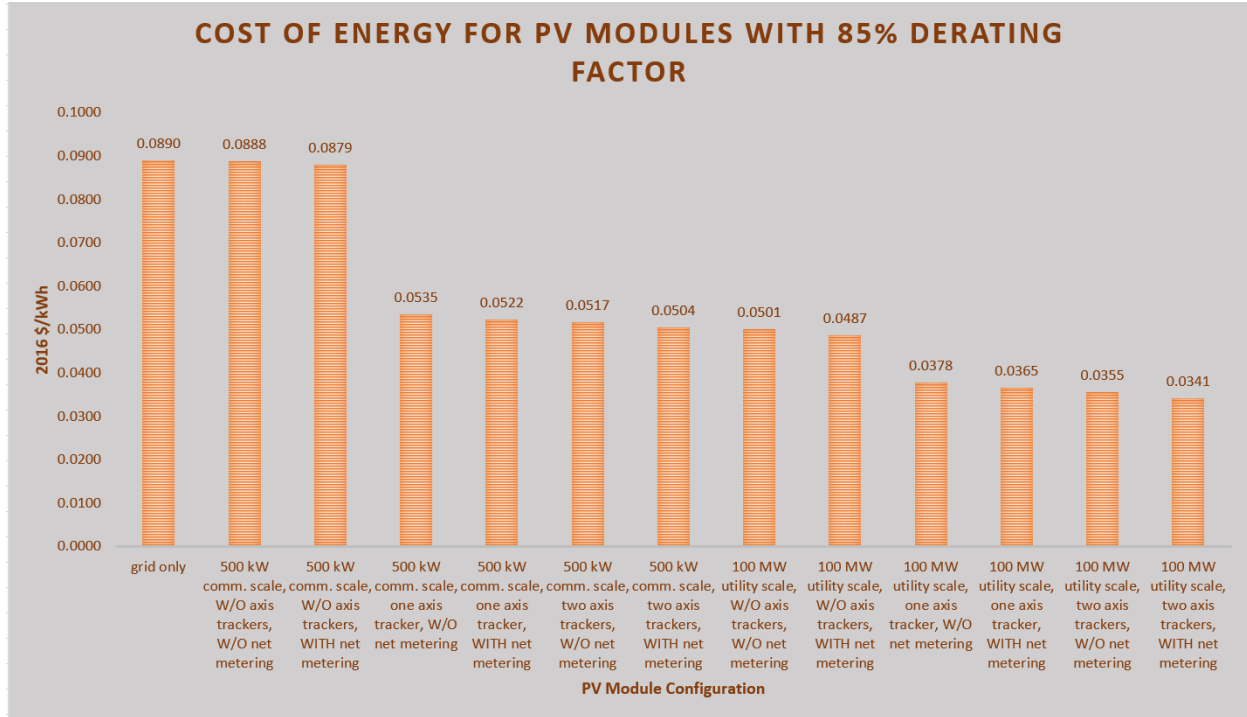


Figure 108 – Screenshot of Excel chart showing the cost of energy of PV module configurations with derating factor of 85%

The COE of the iterations without axis trackers at the ‘500 kW commercial’ price scale nearly equals that of the grid-only configuration. This provides evidence that these iterations are not likely to be cost-effective compared to the grid-only configuration. The fact that the COE of the grid-only configuration is slightly higher than that in Figure 41 further validates this claim. But, adding axis trackers to these iterations drops their COE considerably. This proves that each iteration’s COE is directly tied to its ideal PV capacity and expected energy production.

Net metering has a marginal effect on COE given that it only reduces each iteration’s COE by about 1/10 of a cent. At the ‘500 kW commercial’ price scale, adding one axis tracker to iterations without axis trackers reduces their COE by about \$0.03/kWh. At the ‘100 MW utility’ price scale, adding one axis tracker to iterations without axis trackers reduces their COE

by about \$0.01/kWh. Adding a second axis tracker at both price scales further reduces the COE, albeit by a much smaller amount. This further confirms the fact that adding one axis tracker to PV modules without axis trackers increases energy production to a greater degree than adding another axis tracker to PV modules with one axis tracker (Helwa et al., 2000; Lubitz, 2010).

The influence of price scale is most notable on the COE of the iterations without axis trackers. At the '500 kW commercial' price scale these iterations have a COE of about \$0.088/kWh if they have net metering and \$0.089/kWh if they do not. Their counterparts at the '100 MW utility' price scale have a COE of about \$0.049/kWh if they have net metering and \$0.050/kWh if they do not. But, price scale also has a sizable influence on the COE of iterations with axis trackers. The iterations with one axis tracker at the '500 kW commercial' price scale have a COE of about \$0.052/kWh if they have net metering and about \$0.054/kWh if they do not. Their counterparts at the '100 MW utility' price scale have a COE of about \$0.037/kWh if they have net metering and a COE of \$0.038/kWh if they do not (see Figure 108). The iterations with two axis trackers at the '500 kW commercial' price scale have a COE of about \$0.049/kWh if they have net metering and a COE of about \$0.050/kWh if they do not. Their counterparts at the '100 MW utility' price scale have a COE of about \$0.034/kWh if they do have net metering and \$0.036/kWh if they do not.

PV Module Configurations with 90% Derating Factor

Operating Cost

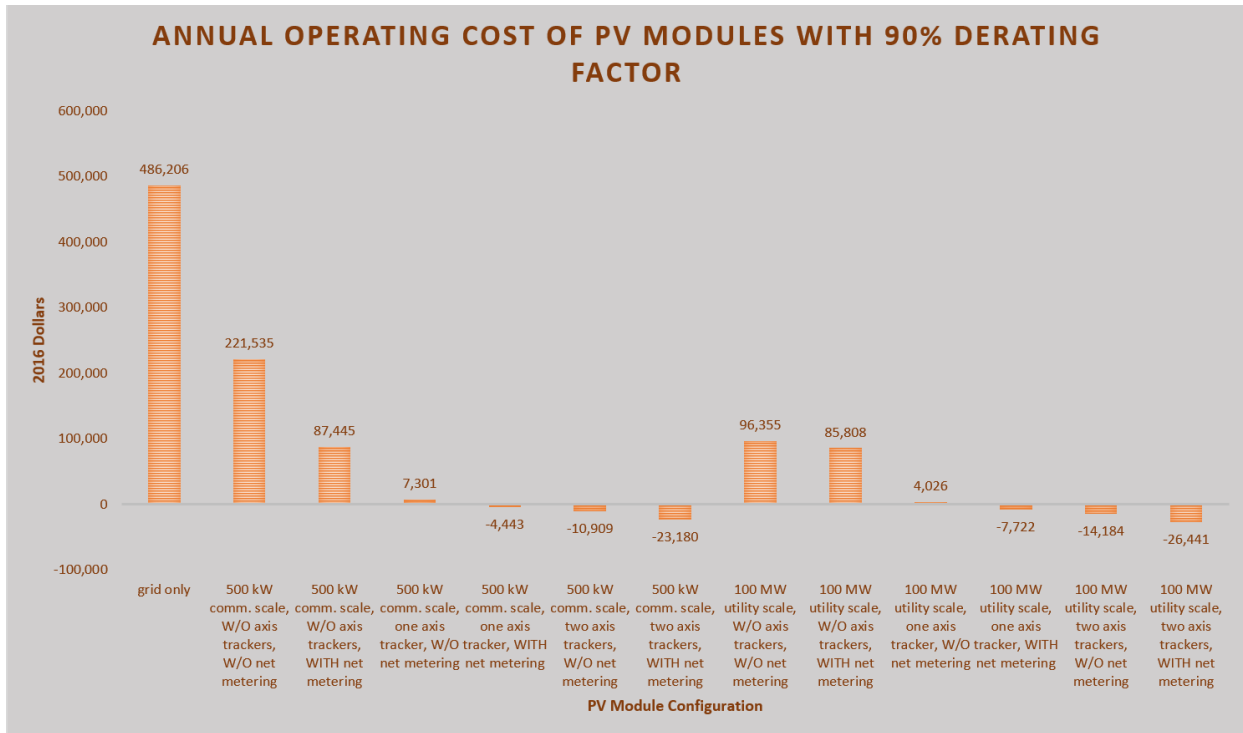


Figure 109 – Screenshot of Excel chart showing annual operating cost of PV module configurations with derating factor of 90%

Raising the derating factor to 90% reduces the OC of the iteration without axis trackers or net metering at the ‘500 kW commercial’ price scale by almost half. The higher derating factor also amplifies the effect of net metering on this iteration. This is true given the fact that at this derating factor, net metering reduces this iteration’s OC by about \$133,000 as opposed to just \$13,000. Furthermore, the 90% derating factor yields a negative OC for many of the iterations. This means that the revenue from energy sales to the grid and the avoided costs of grid energy that would have otherwise been consumed exceed the O&M expenses for these iterations. This provides a clear manifestation of the savings some PV-grid hybrid configurations can provide.

Besides the aforementioned changes, a 90% derating factor does not change the way the presence of axis trackers, net metering, and price scale shape each iteration’s OC.

Cost of Energy

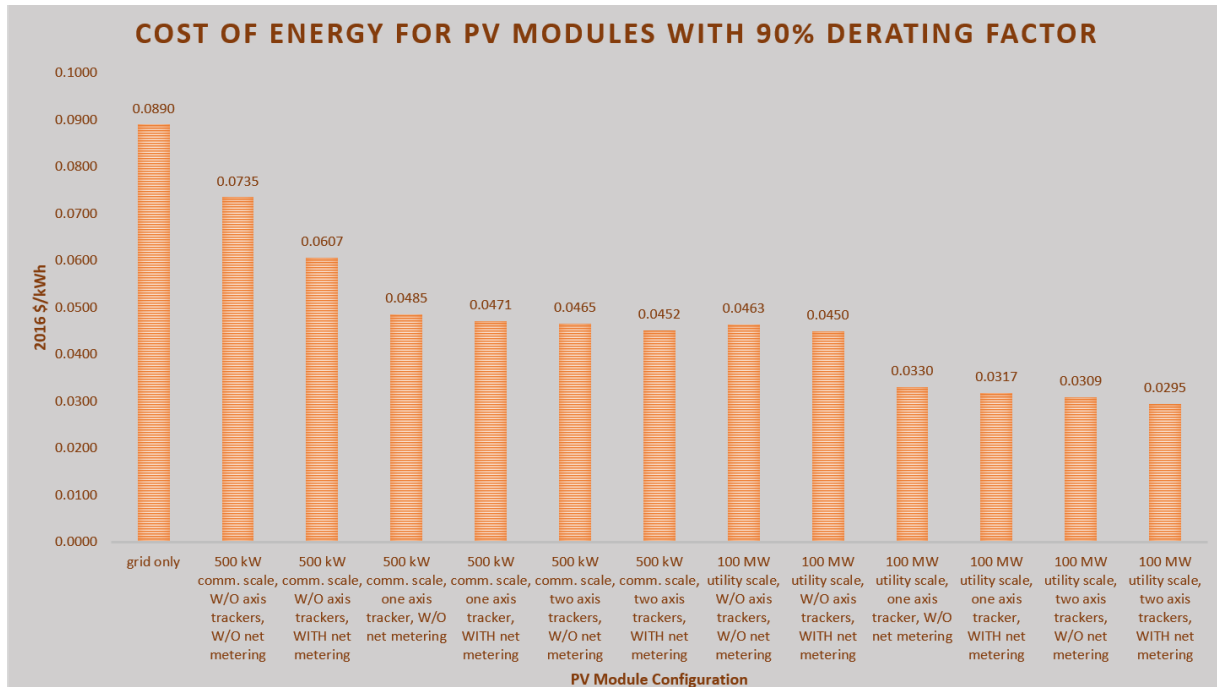


Figure 110 – Screenshot of Excel chart showing the cost of energy of PV module configurations with derating factor of 90%

Augmenting the derating factor to 90% reduces the COE for the iterations without axis trackers at the ‘500 kW commercial’ price scale considerably. At this derating factor, net metering also has a much more amplified effect on the COE of this iteration. Net metering lowers this iteration’s derating factor by nearly 1.5 cents as opposed to just 1/10 of a cent at the 85% derating factor. However, these effects do not apply to the other iterations. Instead, the higher derating factor only reduces the COE of the other iterations by about half of a cent. Furthermore, the influence of the presence of axis trackers, net metering, and price scale on each iteration’s COE does not vary under a 90% derating factor.

Net Present Cost & Discounted Payback Point

PV Module Configurations with 85% Derating Factor

Net Present Cost

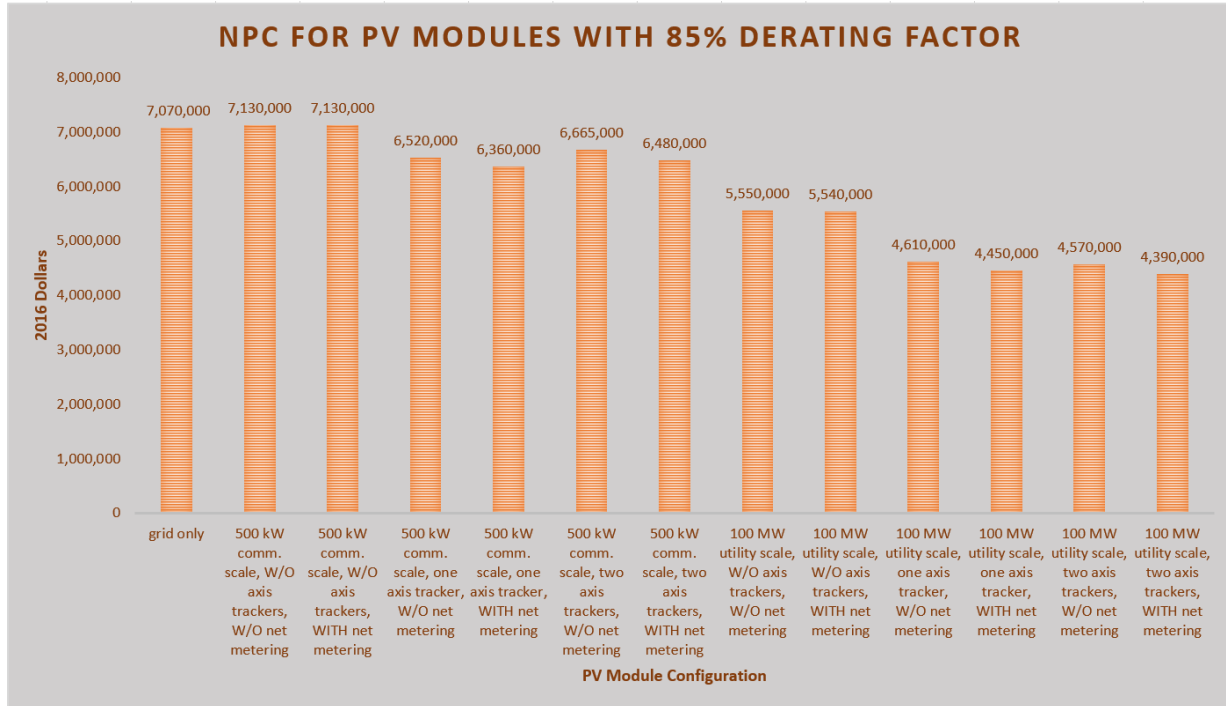


Figure 111 – Screenshot of Excel chart showing the net present cost of PV module configurations with derating factor of 85%

Figure 111 affirms that the iterations without axis trackers with an 85% derating factor at the ‘500 kW commercial’ price scale, regardless of whether they have net metering, are not cost-effective given that their NPC is greater than that of the grid-only configuration. Despite these iterations’ lower OC and COE, their ideal capacity and expected energy production at this price scale do not produce a quantity of savings and revenues that offsets either the initial capital costs and O&M costs or the costs of keeping a grid-only system. This is especially true given the fact

that the grid-only configuration's slightly overstated COE and OC leads to a slightly overstated NPC.

Adding one axis tracker to these iterations lowers the NPC by about \$600,000, which is well below the NPC of the grid-only configuration. Including net metering reduces the NPC by a further \$160,000. Interestingly, adding a second axis tracker at this price scale increases the NPC by \$145,000 relative to that of the iteration with one axis tracker. Although net metering reduces this difference to \$120,000, it still does not make adding a second axis tracker economical. This proves that the additional expected energy production and lower OC and COE that result from adding a second axis tracker are not enough to overcome the additional costs. As a result, the most cost-effective configuration at this price scale includes PV modules with single axis trackers and grid energy. However, the grid-only configuration's overstated NPC as a result of a COE slightly higher than that in Figure 41, could render all combinations at this price scale uneconomical.

The '100 MW utility' price scale vastly lowers the NPC of all PV module configurations, which in turn strengthens their economic viability. At this price scale, net metering lowers the NPC of all configurations with the same number of axis trackers. The degree to which net metering lowers the NPC of each configuration at this price scale increases with the number of axis trackers. For example, net metering lowers the NPC of the iterations without axis trackers by \$10,000. In contrast, net metering lowers the NPC of iterations with one axis tracker and two axis trackers by \$160,000 and \$180,000 respectively.

Adding one axis tracker reduces the NPC of the iteration without axis trackers by \$940,000 if both iterations do not have net metering. If both include net metering, this difference

rises to just over one million dollars. Unlike, at the ‘500 kW commercial’ price scale, including a second axis tracker decreases the NPC of the iteration without axis trackers by a further \$40,000 if both iterations do not have net metering and by a further \$60,000 if they do. Thus, the ‘100 MW utility’ price scale renders the combination with two axis trackers as the most economical.

Discounted Payback Point

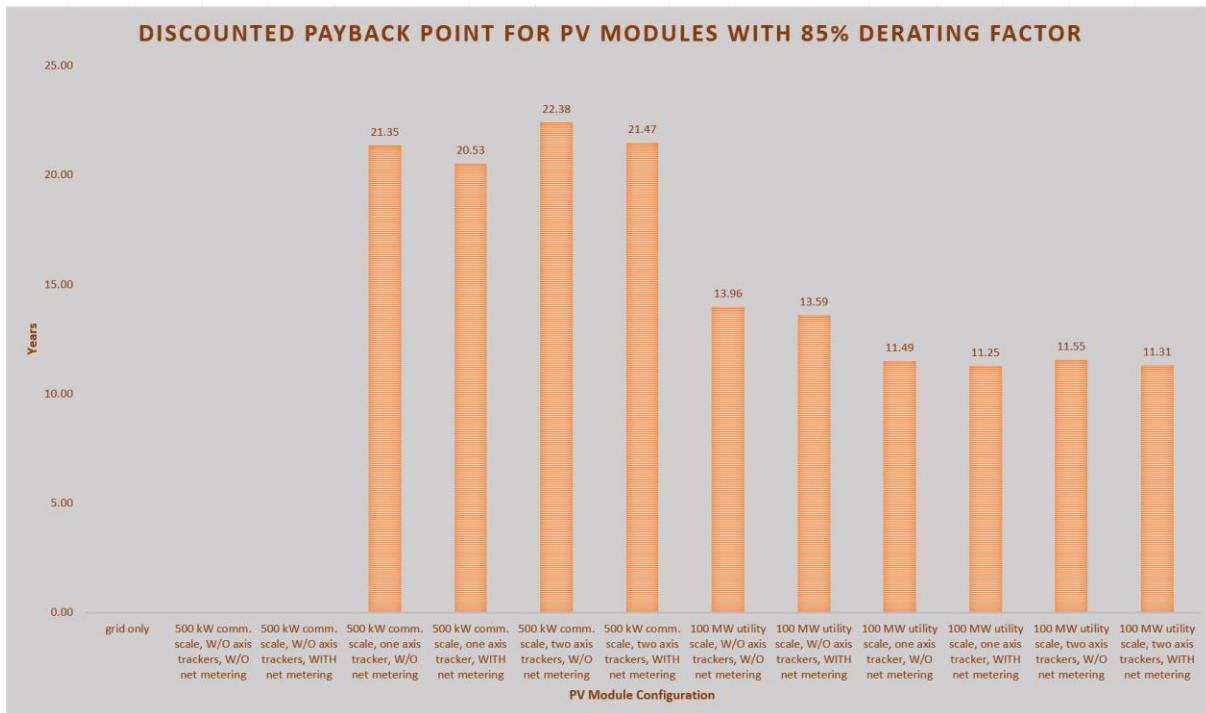


Figure 112 – Screenshot of Excel chart showing the discounted payback point of PV module configurations with a derating factor of 85%

The iterations without axis trackers at the ‘500 kW commercial’ price scale lack a DPP because HOMER predicts that they will not produce savings and revenues that exceed the discounted costs over the project’s lifetime. This is more evidence that these combinations are not economical. Adding one axis tracker produces a DPP of around 21 years; net metering lowers this DPP by about one year. The iteration with two axis trackers and no net metering at

this price scale has a DPP that is about one year longer than that of the iteration with one axis tracker and no net metering. This difference also applies to the iteration with two axis trackers and net metering. The higher DPP for the iterations with two axis trackers mirrors their higher NPC, which in turn illustrates that they are not the most economical configurations.

Price scale has a consequential effect on the DPP. Not only does the ‘100 MW utility’ price scale render the iterations without axis trackers to be economically competitive, it also reduces the DPP of the iterations with one and two axis trackers by about ten years. These findings show that smaller initial capital costs play a monumental role in reducing the time needed for solar-powered microgrids to recoup the initial investment and provide savings. But, the ‘100 MW utility’ price scale reduces the influence of net metering. At this price scale, net metering reduces each iteration’s DPP by less than half a year as opposed to almost a year.

An interesting observation regarding the PV modules with two axis trackers at the ‘100 MW utility’ price scale is the disagreement between their DPP and their NPC compared to those of the iterations with one axis tracker at this price scale. The iterations with two axis trackers have an NPC that is lower than that of their counterparts with one axis tracker. Yet, their DPP is marginally higher than that of iterations with one axis tracker. This creates a fascinating situation in which the iterations with two axis trackers will deliver more savings but will take a little longer to yield those savings.

PV Module Configurations with 90% Derating Factor

Net Present Cost

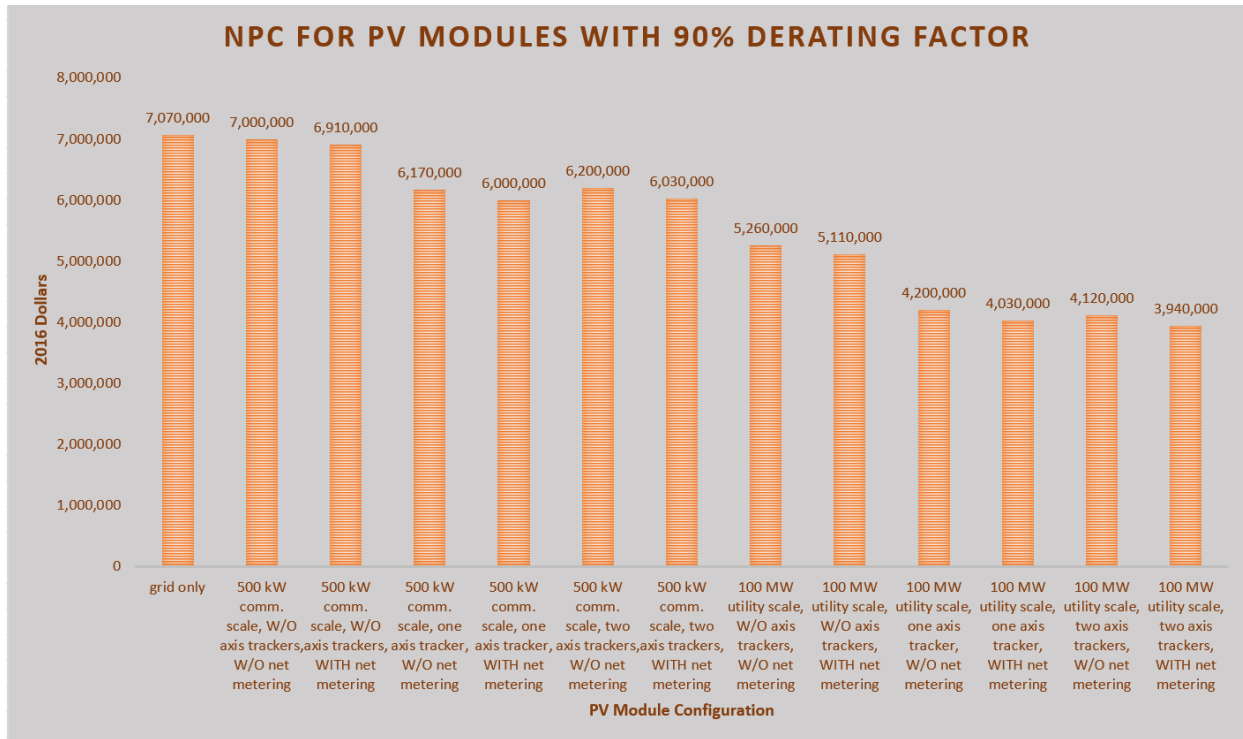


Figure 113 – Screenshot of Excel chart showing net present cost of PV module configurations with a derating factor of 90%

Increasing the derating factor to 90% has the greatest effect on the NPC of iterations without axis trackers at the ‘500 kW commercial’ price scale. At this price scale, regardless of the presence of net metering, they are economically competitive with the grid-only configuration. Given the overstated value of the grid-only configuration’s NPC, net metering is likely to provide a more solid degree of economic competitiveness for this configuration. But, the higher derating factor also reduces the other iterations’ NPC between \$400,000 and \$500,000.

The higher derating factor does not alter net metering’s influence on the NPC of the iterations with one or two axis trackers at the ‘500 kW commercial’ price scale. However, at the

‘100 MW utility’ price scale, the higher derating factor equalizes net metering’s influence on iterations with corresponding numbers of axis trackers. Adding net metering reduces the NPC of the iterations without axis trackers by around \$200,000. This difference in NPC also applies to the iterations with one tracker and those with two axis trackers.

A 90% derating factor increases the difference in NPC between iterations with one axis tracker and those without axis trackers at the ‘500 kW commercial’ price scale to about one million dollars, regardless of net metering (see Figure 113). This compares to a difference of about \$700,000 at the 85% derating factor if the iterations have net metering and \$600,000 if they do not (see Figure 111). Other than these changes, the 90% derating factor does not change the influence of axis trackers. At the ‘500 kW commercial’ price scale, the most economical combination uses PV modules with single axis trackers and grid energy. At the ‘100 MW utility’ price scale, the most cost-effective configuration utilizes PV modules with double axis trackers and grid energy. Moreover, the 90% derating factor does not adjust the influence of price scale on the iterations.

Discounted Payback Point

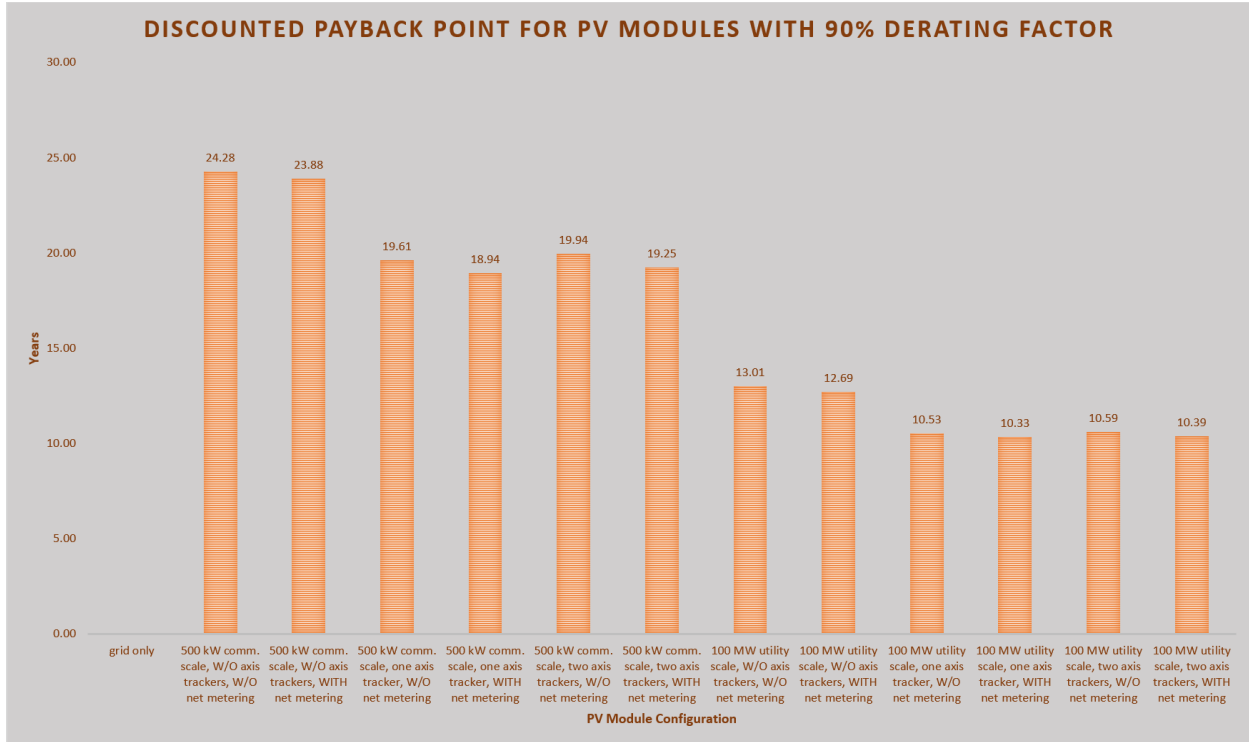


Figure 114 – Screenshot of Excel chat showing discounted payback point of PV module configurations with derating factor of 90%

The 90% derating factor produces a DPP of around 24 years for the iteration without axis trackers at the ‘500 kW commercial’ price scale. Adding net metering to this iteration reduces its DPP by a little under half of a year. For the iterations at this price scale with one axis tracker, the increased derating factor lowers their DPP by about two years compared to that at the 85% derating factor. This reduction also applies to the iterations with two axis trackers at this price scale. In comparison, the higher derating factor reduces the DPP of all iterations at the ‘100 MW utility’ price scale by only around one year compared to that at the 85% derating factor. However, raising the derating factor to 90% does not change the way price scale, the presence of axis trackers, or net metering shape the DPP of any of the iterations.

Summary

The KBH plant's current energy demands indicate that the '500 kW commercial' price scale is the most appropriate. Furthermore, given El Paso's high summertime temperatures, a derating factor of 85% is most likely to provide the most conservative and realistic predictions (US Department of Commerce, NOAA, n.d.). Despite this higher price scale and lower derating factor, the HOMER model shows great potential for solar energy to play a strong role in powering the plant. If the plant were to decide to install a solar-powered microgrid, the best electricity supply combination includes PV modules with single axis trackers in addition to the grid given that it produces the lowest NPC. However, the grid-only configuration's actual NPC may be lower enough to only allow combinations at the '100 MW utility' price scale to be cost effective. If this is true, further improvements in solar technology and a continuing downward trend in solar system costs are needed to make a solar-powered microgrid economically viable.

But, the rapid decline in costs for solar energy combined with breakneck improvement in solar technology signifies that PV modules with a 90% derating factor and prices closer to those at the '100 MW utility' scale are within reach (Feldman et al., 2015). These advancements only increase the viability of solar energy as a source to power the KBH plant and other desalination plants worldwide. As solar technology progresses, more research is needed to successfully integrate solar energy generated on site with grid power. This involves devising a system that thoroughly accounts for the variable nature of solar energy so that the microgrid does not affect either the operation of the plant or the stability of the grid. Improvements in energy storage would greatly address these issues (Hadjipaschalis, Poullikkas, & Efthimiou, 2009). As soon as technological improvements and policy shifts manage to comprehensively address these

concerns, solar energy will have a greater chance of becoming the primary energy source for water desalination. As a result, the costs and environmental impact of desalination will markedly improve.

The HOMER model provides a promising outlook regarding the feasibility of installing a solar-powered microgrid to reduce the KBH plant's electricity costs. But, as with all models, HOMER has its strengths and limitations. The next section details these strengths and limitations in the context of this project through my experience and assessments from the literature and Diego Cruz. Furthermore, other renewable energy modeling software tools can provide a different perspective on predicting the output of microgrids. The next section also describes some of these programs and how they compare to the HOMER model.

Chapter 5

5.1 HOMER STRENGTHS AND WEAKNESSES

This section outlines the strengths and weaknesses of the HOMER model based to determine the economic viability of equipping the KBH plant with a solar-powered microgrid based on my experience using the model for this thesis while using outside sources to complement my claims. These sources consist of a report written by electrical engineers at the University of Port Harcourt in Nigeria and insight from Diego Cruz. This section also describes other renewable energy modeling software tools and compares them to the HOMER model.

HOMER Strengths

HOMER's multiyear module allowed this project to account for the degradation in PV module output over the years, which further enhanced the validity of the PV module output predictions. HOMER's inflation and interest rate inputs also allow the user to account for borrowing costs and the future value of money. Additionally, HOMER's optimizer played a crucial part in configuring the ideal capacities for each of the component's in this project. HOMER's user manual thoroughly explains the terminology involved in configuring the model. HOMER's technical support also did an excellent job assisting with the setup of the model. Lastly, HOMER can quickly generate a detailed report on its results in word or PDF format to help users present the model's results.

Furthermore, one of HOMER's key strengths is its ability to consider a wide array of energy and technology configurations and costs as well as to provide a clear side by side

comparison of the pros and cons of each configuration (Okedu & Uzunmwangho, 2014). HOMER also contains a large database with pricing and performance information of different brands of components (D. Cruz, personal communication, August 8, 2016). HOMER also has access to accurate estimates of solar and wind energy at any location in the world, which in turn provides a realistic idea on the availability of these resources at a given location (D. Cruz, personal communication, August 8, 2016).

HOMER Weaknesses

Although HOMER's multiyear module proved really useful for this project, its inability to work with the optimizer greatly increases the time required for the model to make its calculations. Furthermore, the optimizer can only extrapolate on costs and outputs for future years. This extrapolation is limited given the fact that the results from the multiyear module were considerably different from those the optimizer produced. Lastly, the rise in electricity costs that the user enters into the 'Multi-Year Inputs' box does not apply to electricity buyback rates³¹ (A. Madhavan, personal communication, March 16, 2017). EPE's policy of paying the avoided cost for electricity generated by distributed generation systems suggests that this rate should be included in the buyback rates as well (El Paso Electric Company, 2011, 2017a).

Moreover, one of HOMER's key weaknesses is the model's inability to prompt the user to input key parameters for components such as a PV module's number of axis trackers (Okedu & Uzunmwangho, 2014). If the user fails to spot inputs such as these, the model's results could be incomplete and inaccurate (Okedu & Uzunmwangho, 2014). HOMER also does not provide

³¹ See part about 'Multi-Year Inputs' in the "Project Tab" subsection of section 3.1 for more information.

suggestions as to how to arrange a microgrid nor does it account for objects on the ground such as trees that could obstruct solar radiation (D. Cruz, personal communication, August 8, 2016). Additionally, HOMER does not allow the user to configure solutions for excess electricity nor does it predict how excess electricity could undermine the stability of the grid (D. Cruz, personal communication, August 8, 2016).

Other Renewable Energy Modeling Programs

HYBRID2

HYBRID2 was developed at the University of Massachusetts' Renewable Energy Research Laboratory (Ayodele & Ogunjuyigbe, 2014). HYBRID2 uses the same methodology as HOMER to estimate solar radiation during different time periods (Duffie & Beckman, 1991). HYBRID2 uses a probabilistic time series approach to make its predictions (Ayodele & Ogunjuyigbe, 2014; Klise & Stein, 2009). Although HYBRID2 provides the same outputs as HOMER, it can only model on-grid or off-grid systems with PV modules, generators, batteries, and wind turbines (Klise & Stein, 2009). HOMER, on the other hand, can incorporate other energy sources such as biomass, hydroelectric turbines, and thermal energy (HOMER Energy, 2014). Furthermore, while HOMER's developers continue to improve the model, HYBRID2's last update was in 2004 (HOMER Energy, 2014; Okedu & Uhunmwangho, 2014; UMass-Amherst, n.d.).

RETScreen

Natural Resources Canada developed RETScreen to assess the financial and environmental costs and benefits of renewable energy around the world (Klise & Stein, 2009;

Natural Resources Canada, n.d.). RETScreen's energy sources and outputs are similar to those found in HOMER (Klise & Stein, 2009). But, it uses an isotropic sky model created by professors at the University of Minnesota to estimate available solar energy at different locations (Klise & Stein, 2009; Liu & Jordan, 1963). Natural Resources Canada continues to update and improve RETScreen (Natural Resources Canada, n.d.).

RAPSIM

RAPSIM was created at Alpen Adria University in Klagenfurt, Austria (Pöchacker, Khatib, & Elmenreich, 2014). RAPSIM simulates on-grid and off-grid configurations with PV modules, batteries, wind turbines, and other renewable energy sources (Pöchacker et al., 2014). RAPSIM's main advantage over other modeling software is its ability to model the power flow of each of its components (Pöchacker et al., 2014). This tool allows RAPSIM to predict how the output from each component will affect the stability of the load's power supply and, if applicable, the grid (Pöchacker et al., 2014). Furthermore, RAPSIM operates on Mac and Windows operating systems while HOMER solely operates on Windows operating systems (HOMER Energy, 2014; Pöchacker et al., 2014). RAPSIM is also free to use; its last update took place at the end of 2016 (Pöchacker et al., 2014; SourceForge, n.d.).

Summary

HOMER and the other aforementioned renewable energy modeling software programs provide an insightful picture on the feasibility of supporting electricity demands such as those of the KBH plant at the microgrid scale. But, every location in which a microgrid could operate has unique limiting factors to microgrid construction and operation that these models cannot take into

account. The next section delineates some of the barriers related to constructing a solar-powered microgrid that apply to the KBH plant and El Paso in general.

5.2 LIMITATIONS TO SOLAR ENERGY VIA MICROGRIDS IN EL PASO

This section outlines the difficulties of powering the KBH plant with solar energy via a microgrid through the expert opinions of David Torres, Manuel Perez, and Larry Perea. To illustrate these difficulties in the context of the KBH plant, this section also describes the reasons a previous solar microgrid project for the plant failed according to Ed Archuleta.

David Torres Interview

The primary limitations to implementing microgrid systems in El Paso involve policies³² from EPE that are unfavorable to microgrids (D. Torres, personal communication, August 8, 2016). These policies include standby rates in case the microgrid system fails and fees to recover the cost of buying excess electricity sold to the grid (D. Torres, personal communication, August 8, 2016). If El Paso's electricity market becomes deregulated, the competition would help customers with grid-interconnected microgrids find more favorable policies for excess electricity their systems generate (D. Torres, personal communication, August 8, 2016). EPE's schedules entitled 'Backup Power Service for Qualifying Facilities', 'Maintenance Power Service for Qualifying Facilities', and 'Non-Firm Purchased Power From Distributed Generators' describe these policies in detail (El Paso Electric Company, 2011, 2016a, 2016b). As explained in section 3.1, these rates vary with the plant's contracted capacity of electricity purchased from the grid and may not apply at all (El Paso Electric Company, 2011, 2016c). But, if and to what extent these policies apply, the economics of a solar-powered microgrid for the

³² EPE's policies on distributed generation systems interconnected with the grid apply to those that use renewable energy sources and those that use non-renewable energy sources (El Paso Electric Company, 2016c).

KBH plant could change entirely. Consequently, the existence of these policies would require EPW to engage in a partnership with EPE to build this type of project (D. Torres, personal communication, August 8, 2016).

Other limitations to building a solar-powered microgrid pertain to the costs and efficiencies of current solar technology (D. Torres, personal communication, August 8, 2016). According to Mr. Torres, a solar-powered microgrid would be more feasible if each PV module could produce three times its current amount of electricity (personal communication, August 8, 2016). Furthermore, Mr. Torres stated that current costs to produce electricity with a microgrid powered by PV modules, especially those related to electricity storage, would require an increase in water rates (personal communication, August 8, 2016). In order to keep water rates constant, Mr. Torres' calculations showed that solar-powered electricity would need to be subsidized by at least \$0.10/kWh; current federal incentives are not enough (personal communication, August 8, 2016). Thus, with EPE's current policies and the current costs to maintain PV modules, not even PV modules that were purchased and installed at no cost to EPW would be economical (D. Torres, personal communication, August 8, 2016).

Manuel Perez Interview

Energy storage technology needs to improve in order to make solar and other renewable energy sources more cost competitive (M. Perez, personal communication, August 4, 2016). Energy storage would help address EPE's concerns about sudden shifts in the load related to microgrid failures for which EPE would have to fill the gap (M. Perez, personal communication, August 4, 2016). But, this could lead to full disconnection from the grid, which in turn would

incur extra costs for EPW to install and maintain emergency diesel generators (M. Perez, personal communication, August 4, 2016). As a result, Mr. Perez agrees with Mr. Torres' view that a partnership with EPE for a solar-powered microgrid that benefits both EPW and EPE is the best option (personal communication, August 4, 2016). This partnership would center on the most beneficial plan for both firms regarding EPE's purchase of excess electricity from the microgrid (M. Perez, personal communication, August 4, 2016).

Other difficulties related to building a solar-powered microgrid for the KBH plant is its location on federal land adjacent to Fort Bliss Military Reservation (M. Perez, personal communication, August 4, 2016). EPW's leasing costs of the federal land on which the KBH plant is situated would rise if EPW were to install a solar farm (M. Perez, personal communication, August 4, 2016). Mr. Torres added that the large amount of land PV modules require EPW to purchase or lease more land, which would drive up costs further (personal communication, August 8, 2016).

The KBH plant is more likely to invest in a solar-powered microgrid if Texas state policies and incentives for renewable energy from distributed generation systems were stronger (M. Perez, personal communication, August 4, 2016). Currently, statewide incentives for renewable energy generated by distributed generation systems are limited to property tax exemptions; other incentives vary by utility and municipality (US Department of Energy & North Carolina State University, n.d.). The state property tax exemption would not help the KBH plant because federal land is exempt from property taxes (US Department of the Interior, 1982). Improvements to Texas' renewable energy policies could include binding mandates such

as those in New Mexico to generate a certain percentage of the state's energy from renewable resources by a certain year (New Mexico Public Regulation Commission, n.d.)

Larry Perea Interview

In recent years, electric utilities have had greater difficulty covering costs to maintain their infrastructure due to increased energy efficiency and incentives to reduce consumption (L. Perea, personal communication, September 2, 2016). As a result, utilities have to raise rates in order to cover these and other costs associated with distributing electricity (L. Perea, personal communication, September 2, 2016). For example, EPE charges an energy efficiency cost recovery factor to make up for more efficient energy consumption (El Paso Electric Company, 2017). Distributed generation systems further decrease the amount of revenue electric utilities accrue, which in turn raises their aversion to these systems (L. Perea, personal communication, September 2, 2016). According to Mr. Perea, EPE has levied demand, or standby, charges on commercial customers who install solar energy systems as a way to render solar systems economically infeasible (personal communication, September 2, 2016). Thus, Mr. Perea's experience installing small solar energy systems is further testament to the importance of working with electric utilities in order to incorporate microgrids in a way that is fair to them and their customers.

Ed Archuleta Interview – Unsuccessful Solar Project at KBH Plant

Around 2010, Mr. Archuleta spearheaded a project to equip the KBH plant with a solar-powered microgrid (personal communication, July 28, 2016). The microgrid would have

supplied power to two out of the five RO treatment trains (E. Archuleta, personal communication, July 28, 2016). EPW embarked on this project because EPE decided to charge the plant expensive rates that varied by time of day (E. Archuleta, personal communication, July 28, 2016). The project failed because it was denied federal funding and none of the contractors who submitted bids had proposals that were cost-effective (E. Archuleta, personal communication, July 28, 2016). Additionally, EPE sought to implement capacity charges for users with their own solar energy systems when their solar panels do not produce power (E. Archuleta, personal communication, July 28, 2016). This policy further discouraged EPW from executing this project (E. Archuleta, personal communication, July 28, 2016). In order to make solar power cost-effective for the plant, Mr. Archuleta believes that more incentives for solar energy systems are needed (personal communication, July 28, 2016).

Summary

Current policies from EPE as well as solar technology limit the possibilities of installing a solar-powered microgrid to meet some of the KBH plant's electricity needs. A partnership between EPE and EPW would facilitate the process of building such a microgrid. But, the KBH plant's increased future role in El Paso's water supplies combined with decreasing solar technology costs and greater adoption of solar power enhances future opportunities for solar power to meet the KBH plant's electricity demand. The next section elaborates on these factors and explains how a solar-powered microgrid at the KBH plant could be a net benefit to EPE's distribution system.

5.3 FUTURE ROLE OF DESALINATION AND RENEWABLE ENERGY IN EL PASO

This section explains the importance of desalination in El Paso's future water supplies by describing current plans for the KBH plant and the development of other desalination technologies at UTEP. This section also delineates how solar energy will play an important part in El Paso's future desalination capacity and why a solar-powered microgrid could be a net benefit to EPW and EPE.

Future Role of Desalination in El Paso's Water Supplies

Recent USGS and EPW reports on the Hueco Bolson Aquifer indicate that the growing population in both El Paso and Juarez will further limit this aquifer's ability to supply freshwater for El Paso (Bredehoeft, Ford, Harden, Mace, & Rumbaugh, 2004; Heywood & Yager, 2003). Therefore, desalination is likely to play a more pivotal role in El Paso's future water supplies (Bredehoeft et al., 2004). Art Ruiz's prediction that the KBH plant is likely to become more of a primary water supplier for El Paso rather than just a backup, on-demand producer further validates these reports (personal communication, August 2, 2016). He based his view on the volatile available water supplies from the Rio Grande, which constrain El Paso to groundwater supplies from November through February (A. Ruiz, personal communication, August 2, 2016). Mr. Ruiz also confirmed that EPW does have plans to expand the KBH plant and increase its average production (personal communication, August 2, 2016). The debate rests on whether to build a second plant or solely expand the KBH plant (A. Ruiz, personal communication, August 2, 2016). But, concerns about the cost to build a second plant as well as the impact drilling new

wells may have on water chemistry could reduce the likelihood of a second desalination plant (A. Ruiz, personal communication, August 2, 2016).

Mr. Ruiz also mentioned that the falling costs of desalination will increase its role in El Paso and around the world (personal communication, August 2, 2016). A greater selection of membrane brands coupled with improvement in membrane efficiency and costs will increase the economic viability of desalination as a water source (A. Ruiz, personal communication, August 2, 2016). Additionally, if brine recovery projects like that administered by EWM are successful, the cost of brine disposal will fall dramatically (A. Ruiz, personal communication, August 2, 2016). Projects like this could spur a new industry in brine recovery, which would in turn reduce costs further and increase the appeal of desalination (A. Ruiz, personal communication, August 2, 2016).

Other ways desalination's role could increase in El Paso is through the development of new desalination processes. Dr. Shane Walker and his team at UTEP's CIDS are developing a new desalination process funded by the NSF called electro dialysis metathesis (EDM) (personal communication, July 29, 2016). EDM passes an electric current through brackish water and uses a cathode and an anode to attract and separate the positive and negative ions in salts (S. Walker, personal communication, July 29, 2016). The remaining salt-free water is then extracted (S. Walker, personal communication, July 29, 2016). EDM's advantages include its lower energy usage and its ability to neutralize calcium sulfate, an insoluble compound that damages RO membranes (S. Walker, personal communication, July 29, 2016). Calcium sulfate is commonly present in the El Paso area's groundwater supplies (Walton & Ohlmacher, 2000). EDM converts calcium sulfate through ion exchange into more soluble salt compounds that are more easily

discarded as brine (S. Walker, personal communication, July 29, 2016). Although EDM still requires more testing and development before it can move to a large scale, it could potentially revolutionize water desalination technology for El Paso and the world by providing cheaper, cleaner water for more communities (S. Walker, personal communication, July 29, 2016).

Future Role of Solar Energy in El Paso's Desalination Operations

El Paso's location in the sunny American Southwest combined with rapid increases in demand for solar power and swift improvements in solar technology will substantially increase the role solar energy plays in El Paso's electricity supplies (M. Perez, personal communication, August 4, 2016; L. Perea, personal communication, September 2, 2016). Increased grid energy prices could further accelerate this demand. As more people see the value in solar and other renewable energy sources, demand is likely to increase such that electric utilities will continually increment the percentage of their energy derived from renewable sources (M. Perez, personal communication, August 4, 2016). For instance, EPE's current and future energy supply plans eliminate coal and increase the amount of solar and wind energy in their generation mix (El Paso Electric Company, n.d.-a, n.d.-b, 2016d). If solar energy continues to play an increasingly important part in EPE's generation mix, the KBH plant will benefit more from solar energy just through its grid energy consumption.

The key mystery lies in how EPE's policies for distributed generation systems will change to accommodate municipal utilities, businesses, and homeowners who wish to install solar energy systems on their premises (L. Perea, personal communication, September 2, 2016). Although EPE is eagerly selling power from its new solar facilities to enthusiastic customers, it

still wishes to impose a monthly fee for residential and small commercial customers with solar distributed generation systems (El Paso Electric Company, 2017c; Kolenc, 2017a, 2017b). It is unclear how this fee structure would affect utility customers like the KBH plant (El Paso Electric Company, 2017). But, distributed generation systems for customers such as the KBH plant could be a net benefit for EPE. According to Art Ruiz, when EPE's demand is excessively high, it warns large customers like the KBH plant to activate emergency power supplies (personal communication, August 2, 2016). When events like these occur, a solar-powered microgrid could not only reduce the strain on the grid but also help EPE meet its demand through any excess electricity. Consequently, it is important for EPE to consider these scenarios when formulating future policies for distributed generation systems, especially in light of the increasing electricity demands from El Paso's rapidly growing population (El Paso Electric Company, 2017; Fullerton, 2006).

Summary

The future holds many great opportunities for El Paso to become a world leader in desalination with solar energy. EPW and UTEP's initiatives already prove that El Paso is embracing the idea of utilizing various desalination methods to meet the city's water needs. EPW's past initiatives to utilize solar power for the KBH plant demonstrate the potential solar energy has to power El Paso's future desalination operations. EPE's energy procurement policies further attests to the viability of solar energy to not only supply desalination operations but also electricity supplies in general. But, more research is necessary to address the policy and technological obstacles that stand in the way of incorporating solar energy into El Paso's

desalination operations. The next section describes other concepts that future research should address in order to increase the viability of a solar-powered microgrid at the KBH plant.

Chapter 6 Conclusions and Further Research

HOMER Model Results

The HOMER model's results suggest that solar energy is a promising resource with which to power the KBH plant in the future. Improved solar technology and further price declines will only increase the strong potential for solar energy's usage not only in the KBH plant but also in desalination plants around the world. Given that HOMER's results state that the best electricity supply configuration for the KBH plant includes electricity from the grid, future research should explore the best policies for EPE and customers who wish to generate solar energy with distributed generation systems. This research could also further investigate the hourly rates the KBH plant pays for grid electricity. Additionally, future studies could use HOMER to ascertain how a solar-powered microgrid at the KBH plant would reduce greenhouse gas emissions associated with grid electricity production from non-renewable energy resources.

KBH Plant's Future Electricity Load Profile

As El Paso's population grows, desalination will only play an even more important part in securing freshwater supplies for the city. EPW officials have plans to expand the KBH plant's water production levels so that it can meet these new demands. Furthermore, Craig Pedersen, the Senior Vice President at EWM, stated that his company's plant would require two treatment trains at the KBH plant to run full time in order to supply EWM's facility with sufficient brine (personal communication, July 27, 2017). These signs point to substantial growth in the KBH plant's electricity consumption patterns, which could increase the economic viability of a solar-

powered microgrid. Future studies could utilize HOMER to incorporate this load growth and determine how it changes the prospects for a solar-powered microgrid at the plant.

Solar Power for the EWM Plant

Subsequent research could also use HOMER to assess the feasibility of building a solar-powered microgrid to supply electricity to the EWM plant. According to Mr. Petersen, the EWM plant will not use electricity from EPE's grid but rather will obtain all of its electricity from a 6.5 MW natural gas generator (personal communication, July 27, 2017). Given the uncertainty regarding future natural gas prices and the rapidly declining cost of solar technology, solar power could be a plausible solution to offset the EWM plant's electricity costs and improve its carbon footprint. Moreover, a future solar-powered microgrid could meet both the KBH and EWM plant's electricity needs, which could in turn make the prices from '100 MW utility' scale more feasible. Such a project would require at least five years of energy consumption data from the EWM plant in order to gauge its average electricity usage across different levels of production and ascertain an appropriate load profile for the HOMER model. Fortunately, five years provides ample time for developers to improve solar technology and reduce its costs, which could further expand the viability of solar power for these plants.

International Technological Collaboration on Desalination

El Paso's location next to Juarez combined with the fact that the two cities share the Hueco Bolson aquifer opens opportunities for the water utilities from both cities to work together on expanding desalination with renewable energy on both sides of the border while collaborating

on water sustainability initiatives. The cities' uncertain climactic future combined with their growing populations increases the need for these two cities to work together. All of Juarez's water supplies currently come from the Hueco Bolson; there is no agreement between the cities regarding pumping from the aquifer (S. Reinert, personal communication, September 12, 2016). Both EPW and Juarez's water utility, JMAS, are looking for outside water sources to reduce withdrawals from the Hueco Bolson (S. Reinert, personal communication, September 12, 2016). Future studies should determine how expanding water desalination with renewable energy in El Paso and Juarez could mutually benefit both cities' water supplies. This will provide ample opportunity for scholars and policymakers from the United States and Mexico to set an example for the world on how international cooperation can secure a vital source that all of humanity requires to live.

Appendix

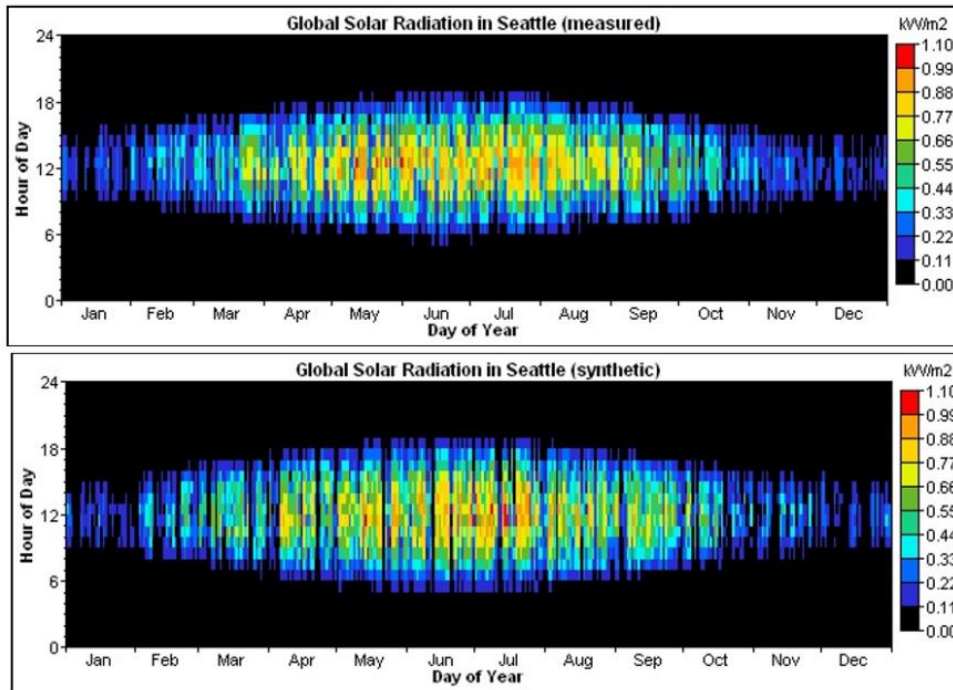


Figure A – Comparison of measured average hourly solar radiation across a year for Seattle compared with the Graham Algorithm's modeled hourly solar radiation across a year (Graham & Hollands, 1990; HOMER Energy, 2016g, 2016h).

References

Chapter 1

- Adaramola, M. S., Paul, S. S., & Oyewola, O. M. (2014). Assessment of decentralized hybrid PV solar-diesel power system for applications in Northern part of Nigeria. *Energy for Sustainable Development*, 19, 72–82. <http://doi.org/10.1016/j.esd.2013.12.007>
- Al-Karaghoul, A., Renne, D., & Kazmerski, L. L. (2009). Solar and wind opportunities for water desalination in the Arab regions. *Renewable and Sustainable Energy Reviews*, 13, 2397–2407. <http://doi.org/10.1016/j.rser.2008.05.007>
- Ardani, K., Shaughnessy, E. O. ', Fu, R., McClurg, C., Huneycutt, J., & Margolis, R. (2017). *Installed Cost Benchmarks and Deployment Barriers for Residential Solar Photovoltaics with Energy Storage: Q1 2016*. Golden. Retrieved from <http://www.nrel.gov/docs/fy17osti/67474.pdf>
- Blakeslee, A. M. (1997). Activity, Context, Interaction, and Authority. *Journal of Business and Technical Communication*, 11(2), 125–169. <http://doi.org/10.1177/1050651997011002001>
- Bredehoeft, J., Ford, J., Harden, B., Mace, R., & Rumbaugh, J. I. (2004). *REVIEW AND INTERPRETATION OF THE HUECO BOLSON GROUNDWATER MODEL Prepared For EL PASO WATER UTILITIES*. El Paso. Retrieved from http://www.epwu.org/water/hueco_bolson/ReviewTeamReport.pdf
- El-Sayed, Y. M. (2007). The rising potential of competitive solar desalination. *Desalination*, 216, 314–324. <http://doi.org/10.1016/j.desal.2007.01.009>
- Elimelech, M., & Phillip, W. (2011). The Future of Seawater Desalination: Energy, Technology, and the Environment. *Science*, 333(712), 1–7. Retrieved from https://www.researchgate.net/profile/Menachem_Elimelech/publication/51547620_The_Future_of_Seawater_Desalination_Energy_Technology_and_the_Environment/links/02e7e51e88c0a7f890000000/The-Future-of-Seawater-Desalination-Energy-Technology-and-the-Environment
- EPW. (2014). *El Paso Water Utilities 2014 Water Conservation Plan As per Rule 363 . 15 Required Water Conservation Plan Texas Water Development Board*.
- EPW. (2015). El Paso Water Utilities - Public Service Board | El Paso's Water Resources. Retrieved November 22, 2015, from http://www.epwu.org/water/water_resources.html
- EPW. (2016). El Paso Water Utilities - Public Service Board | Desalination Plant. Retrieved January 25, 2017, from http://www.epwu.org/water/desal_info.html
- Fiorenza, G., Sharma, V. K., & Braccio, G. (2003). Techno-economic evaluation of a solar powered water desalination plant. *Energy Conversion and Management*, 44(14), 2217–2240. [http://doi.org/10.1016/S0196-8904\(02\)00247-9](http://doi.org/10.1016/S0196-8904(02)00247-9)
- Fu, R., Chung, D., Lowder, T., Feldman, D., Ardani, K., & Margolis, R. (2016). U.S. Solar Photovoltaic System Cost Benchmark: Q1 2016, NREL (National Renewable Energy Laboratory).
- Fullerton, T. M. (2006). Water transfers in El Paso County, Texas. *Water Policy*, 8(3), 255–268. <http://doi.org/10.2166/wp.2006.031>
- Gold, G. M., & Webber, M. E. (2015). The Energy-Water Nexus: An Analysis and Comparison of Various Configurations Integrating Desalination with Renewable Power. *Resources*, 2,

- 227–276. <http://doi.org/10.3390/resources4020227>
- Henryson, M., & Svensson, M. (2004). *Renewable Power for the Swedish Antarctic Station Wasa Swedish Polar Research Secretariat Polarforskningssekretariatet*. Royal Institute of Technology - Sweden.
- Heywood, C. E., & Yager, R. M. (2003). *Simulated Ground-Water Flow in the Hueco Bolson, an Alluvial-Basin Aquifer System near El Paso, Texas*. *Water-Resources Investigations Report 02-4108*. Albuquerque.
- HOMER Energy. (2014). HOMER Pro - Microgrid Software for Designing Optimized Hybrid Microgrids. Retrieved July 19, 2017, from http://homerenergy.com/HOMER_pro.html
- Hutchison, W. (2006). Groundwater management in El Paso, Texas. Retrieved from http://books.google.com/books?hl=en&lr=&id=FP8V-yNRTdkC&oi=fnd&pg=PR3&dq=Groundwater+Management+in+El+Paso+,+Texas&ots=4pYLH7PoS5&sig=PBx0G9N1M7k2d7Avou4wwYPD_00
- Karagiannis, I. C., & Soldatos, P. G. (2008). Water desalination cost literature: review and assessment. *Desalination*, 223(1–3), 448–456. <http://doi.org/10.1016/j.desal.2007.02.071>
- Karimi, L., Abkar, L., Aghajani, M., & Ghassemi, A. (2015). Technical feasibility comparison of off-grid PV-EDR and PV-RO desalination systems via their energy consumption. <http://doi.org/10.1016/j.seppur.2015.07.023>
- Lilienthal, P., & Lambert, T. (2004). HOMER: The Micropower Optimization Model. National Renewable Energy Laboratory (NREL) Innovation for Our Energy Future (Fact Sheet). Golden: National Renewable Energy Laboratory.
- Ma, T., Yang, H., Lu, L., & Peng, J. (2015). Pumped storage-based standalone photovoltaic power generation system: Modeling and techno-economic optimization. *Applied Energy*, 137, 649–659. <https://doi.org/10.1016/j.apenergy.2014.06.005>
- Pingel, S., Zemen, Y., Frank, O., Geipel, T., & Berghold, J. (2009). *Mechanical Stability of Solar Cells Within Solar Panels*. Berlin. Retrieved from https://www.researchgate.net/profile/Sebastian_Pingel/publication/266091257_Mechanical_Stability_of_Solar_Cells_within_Solar_Panels/links/546de0720cf26e95bc3d0af6.pdf
- Rodriguez, C., & Amaratunga, G. A. J. (2008). Long-Lifetime Power Inverter for Photovoltaic AC Modules. *IEEE Transactions on Industrial Electronics*, 55(7), 2593–2601. <https://doi.org/10.1109/TIE.2008.922401>
- Shahzad, M. W., Burhan, M., Ang, L., & Ng, K. C. (2017). Energy-water-environment nexus underpinning future desalination sustainability. *Desalination*, 413, 52–64. <http://doi.org/10.1016/j.desal.2017.03.009>
- Shatat, M., Worall, M., & Riffat, S. (2013). Opportunities for solar water desalination worldwide: Review. *Sustainable Cities and Society*, 9, 67–80. <http://doi.org/10.1016/j.scs.2013.03.004>
- Sheng, Z. (2013). Impacts of groundwater pumping and climate variability on groundwater availability in the Rio Grande Basin. *Rio Grande Basin. Ecosphere*, 4(1). <http://doi.org/10.1890/ES12-00270.1>
- Turner, D. W. (2010). The Qualitative Report Qualitative Interview Design: A Practical Guide for Novice Investigators Qualitative Interview Design: A Practical Guide for Novice Investigators. *The Qualitative Report*, 15(3), 754–760. Retrieved from <http://nsuworks.nova.edu/tqr>

- TWDB. (2012). Chapter 4 Climate of Texas. *Water For Texas 2012 State Water Plan*. Austin. Retrieved from <https://www.mendeley.com/viewer/?fileId=0ec0c4ff-06ba-832f-0042-1a4fa3e46231&documentId=0abfb413-0a9d-3fa4-8c83-87957a3263c7>
- US Department of Commerce, NOAA, N. (n.d.). El Paso Extreme Weather Records. Retrieved July 20, 2017, from https://www.weather.gov/epz/el Paso_extreme_weather
- Wiser, R., Millstein, D., Mai, T., Macknick, J., Carpenter, A., Cohen, S., ... Heath, G. (2016). *On the Path to SunShot: The Environmental and Public Health Benefits of Achieving High Penetrations of Solar Energy in the United States*. Golden. Retrieved from <https://emp.lbl.gov/sites/default/files/65628.pdf>

Chapter 2

- Abbott, C. (1997). The International City Hypothesis: An Approach to the Recent History of U.S. Cities. *Journal of Urban History*, 24, 28–52. <http://doi.org/10.1177/009614429702400102>
- Al-Karaghoul, A., Renne, D., & Kazmerski, L. L. (2009). Solar and wind opportunities for water desalination in the Arab regions. *Renewable and Sustainable Energy Reviews*, 13, 2397–2407. <http://doi.org/10.1016/j.rser.2008.05.007>
- Anthes, R. A., Corell, R. W., Holland, G., Hurrell, J. W., Maccracken, M. C., & Trenberth, K. E. (2006). Hurricanes and Global Warming — Potential Linkages and Consequences. *American Meteorological Society*, 623–628. <http://doi.org/10.1175/BAMS-87-5-617>
- Ardani, K., Shaughnessy, E. O. ', Fu, R., McClurg, C., Huneycutt, J., & Margolis, R. (2017). *Installed Cost Benchmarks and Deployment Barriers for Residential Solar Photovoltaics with Energy Storage: Q1 2016*. Golden. Retrieved from <http://www.nrel.gov/docs/fy17osti/67474.pdf>
- Ashworth, J., Herrera, J., & Albright, J. (2016). *Far West Texas Water Plan*. Austin. Retrieved from https://www.twdb.texas.gov/waterplanning/rwp/plans/2016/E/Region_E_2016_RWP.pdf
- Austin Energy. (2015, December 3). Customer Assistance Programs. Retrieved December 4, 2015, from http://austinenergy.com/wps/portal/ae/residential/your-bill/customer-assistance-programs/customer-assistance-programs!/ut/p/a1/jZBNb4MwDIZ_Sw8cwW5QV7QbzSrK-sFhGqW5TCkKAQkSIKRF2q8f0y7b1C_fLD-vLT_AoACm-LmR3DVa8fa7Z08fSCKyokjSZE4ijBO6WM_y3XSKOAKH30C2zF4wzbM8
- Baker, L. A., Brazel, A. T., & Westerhoff, P. (2004). Environmental consequences of rapid urbanization in warm, arid lands: case study of Phoenix, Arizona (USA). *The Sustainable City III*. Retrieved from <https://www.witpress.com/Secure/elibrary/papers/SC04/SC04016FU.pdf>
- Bing Images. (n.d.). North Arrow. Retrieved July 25, 2017, from <https://www.bing.com/images/search?view=detailV2&ccid=NX1Bymic&id=CAB58DE93EC5F0E4AB5D0076DCBB5B657034D01E&thid=OIP.NX1BymicMfJAnv0QDx1YPADUES&q=north+arrow&simid=608020826455802226&selectedIndex=1&ajaxhist=0>
- Borderplex Alliance (2012). Population | The Borderplex Alliance | Regional Economic Development. Retrieved November 27, 2015, from <http://www.borderplexalliance.org/regional-data/el-paso/overview/population>

- Bredehoeft, J., Ford, J., Harden, B., Mace, R., & Rumbaugh, J. I. (2004). *REVIEW AND INTERPRETATION OF THE HUECO BOLSON GROUNDWATER MODEL Prepared For EL PASO WATER UTILITIES*. El Paso. Retrieved from http://www.epwu.org/water/hueco_bolson/ReviewTeamReport.pdf
- Cane, M. A. (2005). The evolution of El Niño, past and future. <http://doi.org/10.1016/j.epsl.2004.12.003>
- Connall, D. D. (1982). A History of the Arizona Groundwater Management Act. *Ariz. St. L.J.*, 211(313).
- Cook, E. R., Woodhouse, C. A., Eakin, C. M., Meko, D. M., & Stahle, D. W. (2004). Long-Term Aridity Changes in the Western United States. *Science*, 306, 1015–1018. Retrieved from <http://science.sciencemag.org/content/sci/306/5698/1015.full.pdf>
- Corral-Verdugo, V., Bechtel, R. B., & Fraijo-Sing, B. (2003). Environmental beliefs and water conservation: An empirical study. *Journal of Environmental Psychology*, 23(3), 247–257. [http://doi.org/10.1016/S0272-4944\(02\)00086-5](http://doi.org/10.1016/S0272-4944(02)00086-5)
- Daly, C., Halbleib, M., Smith, J. I., Gibson, W. P., Doggett, M. K., Taylor, G. H., ... Pasteris, P. P. (2008). Physiographically sensitive mapping of climatological temperature and precipitation across the conterminous United States. *INTERNATIONAL JOURNAL OF CLIMATOLOGY Int. J. Climatol.* <http://doi.org/10.1002/joc.1688>
- Daly, C., Neilson, R. P., & Phillips, D. L. (1994). A Statistical-Topographic Model for Mapping Climatological Precipitation over Mountainous Terrain. *Journal of Applied Meteorology*, 33, 140–158. Retrieved from <http://andrewsforest.oregonstate.edu/pubs/pdf/pub4955.pdf>
- Daly, C., Redmond, K., Gibson, M., Doggett, J., Taylor, G., Pasteris, P., & Johnson, G. (2005). Opportunities for improvements in the quality control of climate observations. In *15th AMS Conference on Applied Climatology*. Savannah: American Meteorological Association. Retrieved from http://www.prism.oregonstate.edu/documents/pubs/2005appclim_QCopportunities_daly.pdf
- Daly, C., Taylor, G., & Gibson, W. (n.d.). The Prism Approach to Mapping Precipitation and Temperature. Retrieved from <http://citeseerx.ist.psu.edu/viewdoc/download?doi=10.1.1.730.5725&rep=rep1&type=pdf>
- Dettinger, M. (2011). Climate Change, Atmospheric Rivers, and Floods in California – A Multimodel Analysis of Storm Frequency and Magnitude Changes 1. *Journal of the American Water Resources Association (JAWRA)*, 47(3), 514–523. <http://doi.org/10.1111/j.1752-1688.2011.00546.x>
- Easterling, D. R., Peterson, T. C., & Karl, T. R. (1996). *On the Development and Use of Homogenized Climate Datasets*. Asheville. Retrieved from <http://journals.ametsoc.org/doi/pdf/10.1175/1520-0442%281996%29009%3C1429%3AOTDAUO%3E2.0.CO%3B2>
- Eischeid, J. K., Pasteris, P. A., Diaz, H. F., Plantico, M. S., & Lott, N. J. (2000). Creating a Serially Complete, National Daily Time Series of Temperature and Precipitation for the Western United States. *Journal of Applied Meteorology*, 39, 1580–1591.
- El-Sayed, Y. M. (2007). The rising potential of competitive solar desalination. *Desalination*, 216, 314–324. <http://doi.org/10.1016/j.desal.2007.01.009>
- Ellis, A. W., Saffell, E. M., & Hawkins, T. W. (2004). A Method for Defining Monsoon Onset and Demise in the Southwestern USA. *International Journal of Climatology*, 24, 247–265.

- <http://doi.org/10.1002/joc.996>
- El Paso Electric Company. (2016). Schedule No. DG Interconnection and Parallel Operation of Distributed Generation. Retrieved June 19, 2017, from https://www.epelectric.com/files/html/Schedule_No_DG_-_Interconnection_and_Parallel_Operation_of_Distributed_Generation.pdf
- Englehart, P. J., & Douglas, A. V. (2003). Urbanization and Seasonal Temperature Trends: Observational Evidence from a Data-Sparse Part OF North America. *International Journal of Climatology*, 23, 1253–1263. <http://doi.org/10.1002/joc.935>
- Enviro Water Minerals Company. (n.d.). Projects | Enviro Water Minerals Company, Inc. Retrieved July 26, 2017, from <http://www.envirowaterminerals.com/projects.html>
- EPA. (2017). National Environmental Policy Act Review Process. Retrieved July 26, 2017, from <https://www.epa.gov/nepa/national-environmental-policy-act-review-process>
- EPW. (n.d.). El Paso Water Utilities - Public Service Board | Conservation Ordinance. Retrieved November 23, 2015, from <http://www.epwu.org/conservation/ordinance.html>
- EPW. (2014). *El Paso Water Utilities 2014 Water Conservation Plan As per Rule 363 . 15 Required Water Conservation Plan Texas Water Development Board.*
- EPW. (2015). El Paso Water Utilities - Public Service Board | El Paso's Water Resources. Retrieved November 22, 2015, from http://www.epwu.org/water/water_resources.html
- EPW. (2016). El Paso Water Utilities - Public Service Board | Desalination Plant. Retrieved January 25, 2017, from http://www.epwu.org/water/desal_info.html
- EPW. (2017). El Paso Water Utilities - Public Service Board | El Paso's Water Resources. Retrieved March 14, 2017, from http://www.epwu.org/water/water_resources.html
- ERCOT. (n.d.). About ERCOT. Retrieved July 21, 2017, from <http://www.ercot.com/about>
- Feddema, J., Oleson, K., Bonan, G., Mearns, L., Buja, L., Meehl, G., & Washington, W. (2005). The Importance of Land-Cover Change in Simulating Future Climates. *Science*, 310, 1674–1678. <http://doi.org/10.1126/science.1118160>
- Fiorenza, G., Sharma, V. K., & Braccio, G. (2003). Techno-economic evaluation of a solar powered water desalination plant. *Energy Conversion and Management*, 44(14), 2217–2240. [http://doi.org/10.1016/S0196-8904\(02\)00247-9](http://doi.org/10.1016/S0196-8904(02)00247-9)
- Fullerton, T. M. (2006). Water transfers in El Paso County, Texas. *Water Policy*, 8(3), 255–268. <http://doi.org/10.2166/wp.2006.031>
- Fye, F. K., Stahle, D. W., & Cook, E. R. (2003). Paleoclimatic Analogs to Twentieth-Century Moisture Regimes Across the United States. *American Meteorological Society*, 901–909. <http://doi.org/10.1175/BAMS-84-7-901>
- Gibson, W., Daly, C., Kittel, T., Nychka, D., Johns, C., Rosenbloom, N., ... Taylor, G. (2002). Development of a 103-Year High-Resolution Climate Data Set For The Conterminous United States. In *Proceedings of the 13th AMS Conference on Applied Climatology* (pp. 181–183). Portland: American Meteorological Society. Retrieved from http://www.prism.oregonstate.edu/documents/pubs/2002appclim_103yearDataset_gibson.pdf
- Gober, P., & Kirkwood, C. W. (2010). Vulnerability assessment of climate-induced water shortage in Phoenix. *Proceedings of the National Academy of Sciences*, 107, 21295–21299. <http://doi.org/10.1073/pnas.0911113107>
- Gober, P., Wentz, E. A., Lant, T., Tschudi, M. K., & Kirkwood, C. W. (2011). WaterSim: a

- simulation model for urban water planning in Phoenix, Arizona, USA. *Environment and Planning B: Planning and Design*, 38, 197–215. <http://doi.org/10.1068/b36075>
- Gold, G. M., & Webber, M. E. (2015). The Energy-Water Nexus: An Analysis and Comparison of Various Configurations Integrating Desalination with Renewable Power. *Resources*, 2, 227–276. <http://doi.org/10.3390/resources4020227>
- Gonzalez, H. (2013). *El Paso's Diversified Water Resources Portfolio*. El Paso. Retrieved from https://www.epa.gov/sites/production/files/2013-11/documents/presentation_to_border_2020_november_19_2013_2.pdf
- Greenlee, L. F., Lawler, D. F., Freeman, B. D., Marrot, B., & Moulin, P. (2009). Reverse osmosis desalination: Water sources, technology, and today's challenges. *Water Research*. <http://doi.org/10.1016/j.watres.2009.03.010>
- Hadjipaschalis, I., Poullikkas, A., & Efthimiou, V. (2009). Overview of current and future energy storage technologies for electric power applications. *Renewable and Sustainable Energy Reviews*, 13, 1513–1522. Retrieved from https://www.researchgate.net/profile/Dr_Andreas_Poullikkas/publication/222816062_Overview_of_current_and_future_energy_storage_technologies_for_electric_power_applications/links/0fcfd50f4236acd555000000.pdf
- Halder, B. K., Tandon, V., Chintalapalle, R. V., Roy, D., & Tarquin, A. (2015). A potential biological approach for sustainable disposal of total dissolved solid of brine in civil infrastructure. *Construction and Building Materials*, 76, 51–60. <http://doi.org/10.1016/j.conbuildmat.2014.11.044>
- Hales, J. E. (1974). Southwestern United States Summer Monsoon Source - Gulf of Mexico or Pacific Ocean? *Journal of Applied Meteorology*, 331–342. Retrieved from [http://journals.ametsoc.org/doi/pdf/10.1175/1520-0450\(1974\)013%3C0331:SUSMS%3E2.0.CO%3B2](http://journals.ametsoc.org/doi/pdf/10.1175/1520-0450(1974)013%3C0331:SUSMS%3E2.0.CO%3B2)
- Harlan, S. L., Yabiku, S. T., Larsen, L., & Brazel, A. J. (2009). Household Water Consumption in an Arid City: Affluence, Affordance, and Attitudes. *Society & Natural Resources*, 22(8), 691–709. <http://doi.org/10.1080/08941920802064679>
- Heywood, C. E., & Yager, R. M. (2003). *Simulated Ground-Water Flow in the Hueco Bolson, an Alluvial-Basin Aquifer System near El Paso, Texas*. *Water-Resources Investigations Report 02-4108*. Albuquerque.
- Hutchison, W. (2006). Groundwater management in El Paso, Texas. Retrieved from http://books.google.com/books?hl=en&lr=&id=FP8V-yNRTdkC&oi=fnd&pg=PR3&dq=Groundwater+Management+in+El+Paso+,+Texas&ots=4pY LH7PoS5&sig=PBx0G9N1M7k2d7Avou4wwYPD_00
- Jansky, M. (2004). *Fort Bliss Desalination Plant Environmental Impact Statement*. Dallas: United States Environmental Protection Agency. Retrieved from <https://cdxnodengn.epa.gov/cdx-enepa-II/public/action/eis/details?eisId=81927>
- Jenkins, R. (1991). The Political Economy of Industrialization: A Comparison of Latin American and East Asian Newly Industrializing Countries. *Development and Change*, 22(2), 197–231. <http://doi.org/10.1111/j.1467-7660.1991.tb00409.x>
- Karagiannis, I. C., & Soldatos, P. G. (2008). Water desalination cost literature: review and assessment. *Desalination*, 223(1–3), 448–456. <http://doi.org/10.1016/j.desal.2007.02.071>

- Karimi, L., Abkar, L., Aghajani, M., & Ghassemi, A. (2015). Technical feasibility comparison of off-grid PV-EDR and PV-RO desalination systems via their energy consumption. <http://doi.org/10.1016/j.seppur.2015.07.023>
- Karl, T. R., Melillo, J. M., & Peterson, T. C. (2009). *Global Climate Change Impacts in the United States*. New York: Cambridge University Press. Retrieved from <http://aquaticcommons.org/2263/1/climate-impacts-report.pdf>
- Kelly, M. E. (2002). Water Management in the Binational Texas / Mexico Río Grande / Río Bravo Basin. *Human Population and Freshwater Resources: US Cases and International Perspectives*, 115–148.
- Khawaji, A. D., Kutubkhanah, I. K., & Wie, J. M. (2008). Advances in seawater desalination technologies. *Desalination*, 221(1–3), 47–69. <http://doi.org/10.1016/j.desal.2007.01.067>
- Landsat, & Google Maps. (2017). Kay Bailey Hutchison Desalination Plant - Google Maps. El Paso: Google Maps. Retrieved from <https://www.google.com/maps/place/Kay+Bailey+Hutchison+Desalination+Plant/@31.8342663,-106.4113408,33151m/data=!3m1!1e3!4m5!3m4!1s0x86e7453c22fbf2b7:0xca5b28b143f9571c!8m2!3d31.8048712!4d-106.3270247>
- Lapeyrouse, L. M., Morera, O., Heyman, J. M. C., Amaya, M. A., Pingitore, N. E., & Balcazar, H. (2011). A Profile of US-Mexico Border Mobility Among a Stratified Random Sample of Hispanics Living in the El Paso-Juarez Area. <http://doi.org/10.1007/s10903-011-9453-x>
- Lempert, R., Popper, S., & Bankes, S. (2003). *Shaping the Next One Hundred Years: New Methods for Quantitative, Long-Term Policy Analysis*. Santa Monica. Retrieved from https://www.rand.org/content/dam/rand/pubs/monograph_reports/2007/MR1626.sum.pdf
- Liu, L., Yang, H., Hocker, J. E., Shafer, M. A., Carter, L. M., Gourley, J. J., ... Adhikari, P. (2012). Analyzing projected changes and trends of temperature and precipitation in the southern USA from 16 downscaled global climate models. *Theoretical and Applied Climatology*, 109, 345–360. <http://doi.org/10.1007/s00704-011-0567-9>
- MacDonald, G. M. (2010). Climate Change and water in Southwestern North America special feature: water, climate change, and sustainability in the southwest. *Proceedings of the National Academy of Sciences of the United States of America*, 107(50), 21256–62. <http://doi.org/10.1073/pnas.0909651107>
- Maia, L. C., Alves, A. C., & Leão, C. P. (2011). Sustainable Work Environment with Lean Production in Textile and Garment Industry. *ICIEOM- International Conference on Industrial Engineering and Operations Management*, 1–10.
- MALC. Lawsuit from Mexican American Legislative Caucus of Texas (2011). Retrieved from <http://malc.org/wp-content/uploads/2011/04/malc-v-texas.pdf>
- Meko, D., Stockton, C. W., & Boggess, W. R. (1995). THE TREE-RING RECORD OF SEVERE SUSTAINED DROUGHT1. Retrieved from <http://onlinelibrary.wiley.com/store/10.1111/j.1752-1688.1995.tb03401.x/asset/j.1752-1688.1995.tb03401.x.pdf?v=1&t=j1xslarq&s=267f5e70e197aa4d17a2277f99568e12ed59225d>
- Morris, R., Devitt, D., Crites, A., Borden, G., & Allen, L. (1997). Urbanization and Water Conservation in Las Vegas Valley Nevada, 123(3), 189–195. Retrieved from http://www.colorado.edu/geography/class_homepages/geog_4501_s11/readings/Morris.et.al

1998.pdf

- Nielsen-Gammon, J. W. (2011). The Changing Climate of Texas. In J. Schmandt, G. R. North, & J. Clarkson (Eds.), *The Impact of Global Warming on Texas* (pp. 1–33). Austin: University of Texas Press. Retrieved from <https://pdfs.semanticscholar.org/4e30/b4ba40e0b93ff5e5c5ac38f779afda21277e.pdf>
- Novosel, T., Gaparović, G., Ćosić, B., Mustafa, M., Krajačić, G., Pukšec, T., & Duić, N. (2014). Integration of Desalination and Renewables, a Demonstration of the Desalination Module in the H2RES Model: Case Study for Jordan. *Chemical Engineering Transactions*, 39, 1–6.
- Pick, J. B., Viswanathan, N., & Hettrick, J. (2001). The U.S.-Mexican borderlands region: a binational spatial analysis. *The Social Science Journal*, 38(4), 567–595. [http://doi.org/10.1016/S0362-3319\(01\)00152-5](http://doi.org/10.1016/S0362-3319(01)00152-5)
- Quiring, S. M., & Goodrich, G. B. (2008). Nature and causes of the 2002 to 2004 drought in the southwestern United States compared with the historic 1953 to 1957 drought. *Climate Research*, 36(1), 41–52. <http://doi.org/10.3354/cr00735>
- Revelle, R. R., & Waggoner, P. E. (1983). Effects of a Carbon Dioxide-Induced Climatic Change on Water Supplies in the Western United States. *Changing Climate*, 419–432. Retrieved from <https://portal.azoah.com/oedf/documents/08A-AWS001-DWR/Omnia/19830000>
- Revelle and Waggoner Effects of Climate Change on Water.pdf
- Seager, R. (2007). The Turn of the Century North American Drought: Global Context, Dynamics, and Past Analogs. *American Meteorological Society*, 20, 5527–5552. Retrieved from <http://journals.ametsoc.org/doi/pdf/10.1175/2007JCLI1529.1>
- Seager, R., Naik, N., & Vecchi, G. A. (2010). Thermodynamic and Dynamic Mechanisms for Large-Scale Changes in the Hydrological Cycle in Response to Global Warming*. *American Meteorological Society*, 23, 4651–4668. <http://doi.org/10.1175/2010JCLI3655.1>
- Seager, R., Ting, M., Held, I., Kushnir, Y., Lu, J., Vecchi, G., ... Naik, N. (2007). Model Projections of an Imminent Transition to a More Arid Climate in Southwestern North America. *Science*, 316, 1181–1184. Retrieved from <https://www.mendeley.com/viewer/?fileId=68fc386f-15c2-6337-63f5-0fcd96baf6c5&documentId=96e14b25-1245-30ea-a00b-792a0db56b37>
- Shahzad, M. W., Burhan, M., Ang, L., & Ng, K. C. (2017). Energy-Water-Environment Nexus Underpinning Future Desalination Sustainability. *Desalination*, 413, 52–64. <http://doi.org/10.1016/j.desal.2017.03.009>
- Shatat, M., Worall, M., & Riffat, S. (2013). Opportunities for Solar Water Desalination Worldwide: Review. *Sustainable Cities and Society*, 9, 67–80. <http://doi.org/10.1016/j.scs.2013.03.004>
- Sheng, Z. (2013). Impacts of groundwater pumping and climate variability on groundwater availability in the Rio Grande Basin. *Rio Grande Basin. Ecosphere*, 4(1). <http://doi.org/10.1890/ES12-00270.1>
- Shepherd, J. M. (2006). Evidence of urban-induced precipitation variability in arid climate regimes. *Journal of Arid Environments*, 67, 607–628. <http://doi.org/10.1016/j.jaridenv.2006.03.022>
- Solomon, S., Qin, D., Manning, M., Marquis, M., Averyt, K., Tignor, M., ... Chin, Z. (2007). *Climate Change 2007 The Physical Science Basis*. New York. Retrieved from <https://www.ipcc.ch/pdf/assessment-report/ar4/wg1/ar4-wg1-frontmatter.pdf>

- St. Hilaire, R., Arnold, M. A., Wilkerson, D. C., Devitt, D. A., Hurd, B. H., Lesikar, B. J., ... Zoldoske, D. F. (2008). Efficient Water Use in Residential Urban Landscapes. *HortScience*, 43(7), 2081–2092.
- St. Jacques, J.-M., Sauchyn, D. J., & Zhao, Y. (2010). Northern Rocky Mountain Streamflow Records: Global Warming Trends, Human Impacts or Natural Variability? *Geophysical Research Letters*, 37(6), n/a-n/a. <http://doi.org/10.1029/2009GL042045>
- Stahle, D. W., Cook, E. R., Cleaveland, M. D., Therrell, D. M., Meko, H. D., Grissino-Mayer, E. W., & Luckman, B. H. (2000). Tree-ring Data Document 16th Century Megadrought Over North America. *Eos*, 81(21), 121–125. <http://doi.org/10.1029/00EO00076>
- Swetnam, T. W., & Betancourt, J. L. (1998). Mesoscale Disturbance and Ecological Response to Decadal Climatic Variability in the American Southwest. *Journal of Climate*, 11, 3128–3147. Retrieved from <http://journals.ametsoc.org/doi/pdf/10.1175/1520-0442%281998%29011%3C3128%3AMDAERT%3E2.0.CO%3B2>
- Tanski, J. M. & Bath, C. R. (1995). Resolving water disputes along the US–Mexico Border. New Mexico State University Border Research Institute, Las Cruces, NM in Fullerton 2006.
- TCEQ. Brine Evaporation Pits, Chapter 218 1–7 (2008). TCEQ. Retrieved from <https://www.tceq.texas.gov/assets/public/legal/rules/rules/pdfflib/218%60.pdf>
- TCEQ. Groundwater Classification, 32TCEQ Regulatory Guidance 1526–1579 (2010). TCEQ Remediation Division. Retrieved from https://www.tceq.texas.gov/publications/rg/rg-366_trrp_08.html
- TRNCC (2002). Rights to Surface Water in Texas. GI-228, Texas Commission on Environmental Quality, Austin, TX in Fullerton 2006.
- TWDB. (2012). Chapter 4 Climate of Texas. *Water For Texas 2012 State Water Plan*. Austin. Retrieved from <https://www.mendeley.com/viewer/?fileId=0ec0c4ff-06ba-832f-0042-1a4fa3e46231&documentId=0abfb413-0a9d-3fa4-8c83-87957a3263c7>
- US Department of Commerce, NOAA, N. (n.d.). El Paso Monthly Precipitation Totals. Retrieved February 28, 2017, from https://www.weather.gov/epz/el Paso_monthly_precip
- Water-Technology. (n.d.). Perth Seawater Desalination Plant - Water Technology. Retrieved July 22, 2017, from <http://www.water-technology.net/projects/perth>
- Weiss, J., Castro, C., & Overpeck, J. (2009). Distinguishing Pronounced Droughts in the Southwestern United States: Seasonality and Effects of Warmer Temperatures. *Journal of Climate*, 5918–5932. <http://doi.org/10.1175/2009JCLI2905.1>
- White, D. E., Baker, E. T., & Sperka, R. (1997). *Hydrology of the Shallow Aquifer and Uppermost Semiconfined Aquifer Near El Paso, Texas Water-Resources Investigations Report 97-4263 In cooperation with the El Paso Water Utilities-Public Service Board*. Austin. Retrieved from <https://pubs.usgs.gov/wri/1997/4263/report.pdf>
- Younos, T. (2005). Environmental Issues Environmental Issues of Desalination. *Journal of Contemporary Water Research & Education*, (132), 11–18. <http://doi.org/10.1111/j.1936-704X.2005.mp132001003.x>

Chapter 3

- Albright, G., Edie, J., & Al-Hallaj, S. (2012). A Comparison of Lead Acid to Lithium-ion in Stationary Storage Applications. Retrieved from http://www.master-instruments.com.au/files/knowledge-centre/education-and-learning/technical-articles/lead_acid_v_s_li_ion_white_paper___allcell_technologies.pdf
- Argeseanu, A., Ritchie, E., & Leban, K. (2010). New Low Cost Structure for Dual Axis Mount Solar Tracking System Using Adaptive Solar Sensor. In *12th International Conference on Optimization of Electrical and Electronic Equipment* (pp. 1109–1114). <https://doi.org/10.1109/OPTIM.2010.5510446>
- Barley, C. D., & Winn, C. B. (1996). OPTIMAL DISPATCH STRATEGY IN REMOTE HYBRID POWER SYSTEMS. *Pergamon Solar Energy*, 58(4), 6–165. Retrieved from http://ac.els-cdn.com/S0038092X96000874/1-s2.0-S0038092X96000874-main.pdf?_tid=17fd80e4-5f4c-11e7-b91a-00000aacb360&acdnt=1499016788_cf78c19059a53c747821fb2346a26a77
- BLS. (2017). 12-month percentage change, Consumer Price Index, selected categories. Retrieved March 15, 2017, from <https://www.bls.gov/charts/consumer-price-index/consumer-price-index-by-category.htm>
- Blue Oak Energy. (n.d.). The Ideal Inverter Loading Ratio (ILR) for Commercial and Utility Solar Plants | Blue Oak Energy. Retrieved June 18, 2017, from <http://www.blueoakenergy.com/blog/inverter-loading-ratio/>
- Blume, S. W. (2011). Overview of High Voltage Protection for Telecommunications. In *High Voltage Protection for Telecommunications* (pp. 1–9). Hoboken, NJ, USA: John Wiley & Sons, Inc. <https://doi.org/10.1002/9781118127018.ch1>
- Brhimat, F., & Mekhtoub, S. (2014). *PV Cell Temperature/ PV Power Output Relationships Homer Methodology Calculation* (No. 2). Algiers. Retrieved from http://ipco-co.com/IJSET_Journal/CIER'13-IJSET/ID_244.pdf
- Cambell, M. (2008). The Drivers of the Levelized Cost of Electricity for Utility-Scale Photovoltaics. Retrieved from <http://www.sunpowercorp.com/sites/sunpower/files/media-library/white-papers/wp-levelized-cost-drivers-electricity-utility-scale-photovoltaics.pdf>
- Christensen, L. R., & Greene, W. H. (1976). Economies of Scale in U.S. Electric Power Generation Authors: Laurits R . Christensen and William H . Greene Source : *Journal of Political Economy* , Vol . 84 , No . 4 , Part 1 (Aug . , 1976), pp . 655-676 Published by : The University of Chicago, 84(4), 655–676.
- Coakley, J. A. (2003). *Reflectance and Albedo, Surface*. Corvallis. Retrieved from http://curry.eas.gatech.edu/Courses/6140/ency/Chapter9/Ency_Atmos/Reflectance_Albedo_Surface.pdf
- Consumer Price Index, 1913- | Federal Reserve Bank of Minneapolis. (n.d.). Retrieved February 19, 2017, from <https://www.minneapolisfed.org/community/teaching-aids/cpi-calculator-information/consumer-price-index-and-inflation-rates-1913>
- Diorio, N., Dobos, A., & Janzou, S. (2015). *Economic Analysis Case Studies of Battery Energy Storage with SAM*. Golden. Retrieved from <http://www.nrel.gov/docs/fy16osti/64987.pdf>
- Duffie, J. A., & Beckman, W. A. (1991). *Solar engineering of thermal processes*. Wiley. Retrieved from

- https://openlibrary.org/books/OL1867035M/Solar_engineering_of_thermal_processes
 Earickson, R., & Harlin, J. M. (1994). *Geographic measurement and quantitative analysis*. Macmillan.
- El-Shimy, M. (2012). Analysis of Levelized Cost of Energy (LCOE) and Grid Parity for Utility-Scale Photovoltaic Generation Systems. In *International Middle East Power Systems Conference* (pp. 1–8). Alexandria. Retrieved from https://www.researchgate.net/profile/Mohamed_EL-Shimy/publication/307584165_Analysis_of_Levelized_Cost_of_Energy_LCOE_and_grid_parity_for_utility-scale_photovoltaic_generation_systems/links/57cc76fb08ae89cd1e86ceec.pdf
- El Paso Electric Company. (n.d.-a). Electricity for West Texas and Southern New Mexico | El Paso Electric | Rate Tariffs. Retrieved June 22, 2017, from <https://www.epelectric.com/tx/business/rate-tariffs-2>
- El Paso Electric Company. (n.d.-b). Electricity for West Texas and Southern New Mexico | El Paso Electric | Texas. Retrieved June 21, 2017, from <https://www.epelectric.com/about-el-paso-electric/texas>
- El Paso Electric Company. (2011a). FAQs: Texas Net Metering. Retrieved March 19, 2017, from https://www.epelectric.com/files/html/Renewable/Website_Update/FAQ_Texas_Net_Metering.pdf
- El Paso Electric Company. (2011b). Non-firm Purchased Power Service From Distributed Generators, Distributed Renewable Generators, and Qualifying Facilities. Retrieved June 19, 2017, from https://www.epelectric.com/files/html/Dist._Gen._Interconnection/TX/39582_Clean_Tariff_Schedule_No._48.pdf
- El Paso Electric Company. (2016a). Backup Power Service for Qualifying Facilities. Retrieved June 19, 2017, from https://www.epelectric.com/files/html/Schedule_No_47_-_Backup_Power_Service_for_Qualifying_Facilities.pdf
- El Paso Electric Company. (2016b). Maintenance Power Service for Qualifying Facilities. Retrieved June 19, 2017, from https://www.epelectric.com/files/html/Schedule_No_46_-_Maintenance_Power_Service_For_Qualifying_Facilities.pdf
- El Paso Electric Company. (2016c). Schedule 96 - Military Base Discount Recovery Factor. Retrieved June 21, 2017, from https://www.epelectric.com/files/html/MBDRF_DocketNo.46164.pdf
- El Paso Electric Company. (2016d). Schedule No. 11 - Time of Use Municipal Pumping Service Rate. Retrieved June 21, 2017, from https://www.epelectric.com/files/html/Schedule_No_11-TOU_-_Time-of-Use_Municipal_Pumping_Service_Rate.pdf
- El Paso Electric Company. (2016e). Schedule No. DG Interconnection and Parallel Operation of Distributed Generation. Retrieved June 19, 2017, from https://www.epelectric.com/files/html/Schedule_No_DG_-_Interconnection_and_Parallel_Operation_of_Distributed_Generation.pdf
- El Paso Electric Company. (2017a). Energy Efficiency Cost Recovery Factor. Retrieved June 19, 2017, from https://www.epelectric.com/files/html/PUCT_Docket_No._45885_EECRF.pdf
- El Paso Electric Company. (2017b). Schedule No. 98 - Fixed Fuel Factor. Retrieved June 19,

- 2017, from
https://www.epelectric.com/files/html/TX_Sch_No_98_Proposed_Fixed_Fuel_Factor_-_Clean.pdf
- EPWU. (2015). El Paso Water Utilities - Public Service Board | El Paso's Water Resources. Retrieved November 22, 2015, from http://www.epwu.org/water/water_resources.html
- Faranda, R. S., Hafezi, H., Leva, S., Mussetta, M., & Ogliari, E. (2015). The optimum PV plant for a given solar DC/AC converter. *Energies*. <https://doi.org/10.3390/en8064853>
- Fedkin, M. (2015). 11.5. Efficiency of Inverters | EME 812: Utility Solar Power and Concentration. The Pennsylvania State University. Retrieved from <https://www.e-education.psu.edu/eme812/node/738>
- Feldman, D., Barbose, G., Margolis, R., Bolinger, M., Chung, D., Fu, R., ... Wiser, R. (2015). Photovoltaic System Pricing Trends: Historical, Recent, and Near-Term Projections, 2015 Edition (Presentation), Sunshot, U.S. Department of Energy (DOE). Retrieved from <http://www.nrel.gov/docs/fy15osti/64898.pdf>
- Fu, R., Chung, D., Lowder, T., Feldman, D., Ardani, K., & Margolis, R. (2016). U.S. Solar Photovoltaic System Cost Benchmark: Q1 2016, NREL (National Renewable Energy Laboratory).
- García, M. C. A., & Balenzategui, J. L. (2004). Estimation of photovoltaic module yearly temperature and performance based on Nominal Operation Cell Temperature calculations. *Renewable Energy*, 29. <https://doi.org/10.1016/j.renene.2004.03.010>
- Givler, T., & Lilienthal, P. (2005). *Using HOMER ® Software, NREL's Micropower Optimization Model, to Explore the Role of Gen-sets in Small Solar Power Systems Case Study: Sri Lanka*. Golden. Retrieved from <http://www.nrel.gov/docs/fy05osti/36774.pdf>
- Graham, V. A., & Hollands, K. G. T. (1990). A method to generate synthetic hourly solar radiation globally. *Solar Energy*, 44(6), 333–341. [https://doi.org/10.1016/0038-092X\(90\)90137-2](https://doi.org/10.1016/0038-092X(90)90137-2)
- Haque, E., Negnevitsky, M., Muttaqi, K. M., Haque, M. E., Negnevitsky, M., & Muttaqi, K. M. (2010). A novel control strategy for a variable-speed wind turbine with a permanent-magnet synchronous generator. *IEEE Transactions on Industry Applications IEEE Transactions on Industry Applications IEEE TRANSACTIONS ON INDUSTRY APPLICATIONS*, 46(1), 331–339. Retrieved from <http://ro.uow.edu.au/infopapers/3407>
- HOMER Energy. (2016a). HOMER Energy | Modeling an inverter only or rectifier o... Retrieved June 18, 2017, from <http://usersupport.homerenergy.com/customer/en/portal/articles/2188846-modeling-an-inverter-only-or-rectifier-only-with-the-conv->
- HOMER Energy. (2016b). HOMER Energy | System warnings. Retrieved July 2, 2017, from <http://usersupport.homerenergy.com/customer/en/portal/articles/2188864-system-warnings>
- HOMER Energy. (2016c). HOMER Energy | Using HOMER Optimizer™ for More Effectiv... Retrieved June 5, 2017, from <http://usersupport.homerenergy.com/customer/en/portal/articles/2513270-using-homer-optimizer™-for-more-effective-modeling>
- HOMER Energy. (2016d). HOMER Model User Manual. In 7.91. Denver.
- HOMER Energy. (2016e). HOMER Model User Manual. In 7.105. Denver.
- HOMER Energy. (2016f). HOMER Model User Manual. In 7.28. Denver.

HOMER Energy. (2016g). HOMER Model User Manual. In 5.9.1. Denver.
HOMER Energy. (2016h). HOMER Model User Manual. In 5.16. Denver.
HOMER Energy. (2016i). HOMER Model User Manual. In 26. Denver.
HOMER Energy. (2016j). HOMER Model User Manual. In 7.33. Denver.
HOMER Energy. (2016k). HOMER Model User Manual. In 5.5. Denver.
HOMER Energy. (2016l). HOMER Model User Manual. In 28. Denver.
HOMER Energy. (2016m). HOMER Model User Manual. In 33. Denver.
HOMER Energy. (2016n). HOMER Model User Manual. In 7.144. Denver.
HOMER Energy. (2016o). HOMER Model User Manual. In 5.15. Denver.
HOMER Energy. (2016p). HOMER Model User Manual. In 7.96. Denver.
HOMER Energy. (2016q). HOMER Model User Manual. In 4. Denver.
HOMER Energy. (2016r). HOMER Model User Manual. In 4.1. Denver.
HOMER Energy. (2016s). HOMER Model User Manual. In 7.125. Denver.
HOMER Energy. (2016t). HOMER Model User Manual. In 14. Denver.
HOMER Energy. (2016u). HOMER Model User Manual. In 5.8. Denver.
HOMER Energy. (2016v). HOMER Model User Manual. In 7.128. Denver.
HOMER Energy. (2016w). HOMER Model User Manual. In 7.84. Denver.
HOMER Energy. (2016x). HOMER Model User Manual. In 7.127. Denver.
HOMER Energy. (2016y). HOMER Model User Manual. In 7.123. Denver.
HOMER Energy. (2016z). HOMER Model User Manual. In 7.129. Denver.
HOMER Energy. (2016aa). HOMER Model User Manual. In 17. Denver.
HOMER Energy. (2016ab). HOMER Model User Manual. In 45. Denver.
HOMER Energy. (2016ac). HOMER Model User Manual. In 30.1. Denver.
HOMER Energy. (2016ad). HOMER Model User Manual. In 30.2. Denver.
HOMER Energy. (2016ae). HOMER Model User Manual. In 30.3. Denver.
HOMER Energy. (2016af). HOMER Model User Manual. In 30.4. Denver.
HOMER Energy. (2016ag). HOMER Model User Manual. In 30.5. Denver.
HOMER Energy. (2016ah). HOMER Model User Manual. In 7.82. Denver.
HOMER Energy. (2016ai). HOMER Model User Manual. In 7.83. Denver.
HOMER Energy. (2016aj). HOMER Model User Manual. In 30.6. Denver.
HOMER Energy. (2016ak). HOMER Model User Manual. In 7.145. Denver.
HOMER Energy. (2016al). HOMER Model User Manual. In 7.148. Denver.
HOMER Energy. (2016am). HOMER Model User Manual. In 31. Denver.
HOMER Energy. (2016an). HOMER Model User Manual. In 7.98. Denver.
HOMER Energy. (2016ao). HOMER Model User Manual. In 7.29. Denver.
HOMER Energy. (2016ap). HOMER Model User Manual. In 7.115. Denver.
HOMER Energy. (2016aq). HOMER Model User Manual. In 7.113. Denver.
HOMER Energy. (2016ar). HOMER Model User Manual. In 32. Denver.
HOMER Energy. (2016as). HOMER Model User Manual. In 34. Denver.
HOMER Energy. (2016at). HOMER Model User Manual. In 35. Denver.
HOMER Energy. (2016au). HOMER Model User Manual. In 36. Denver.
HOMER Energy. (2016av). HOMER Model User Manual. In 7.39. Denver.
HOMER Energy. (2016aw). HOMER Model User Manual. In 7.97. Denver.
HOMER Energy. (2016ax). HOMER Model User Manual. In 7.92. Denver.

- HOMER Energy. (2016ay). HOMER Model User Manual. In 7.163. Denver.
- HOMER Energy. (2016az). HOMER Model User Manual. In 7.170. Denver.
- HOMER Energy. (2016ba). HOMER Model User Manual. In 7.6. Denver.
- HOMER Energy. (2016bb). HOMER Model User Manual. In 7.31. Denver.
- HOMER Energy. (2016bc). HOMER Model User Manual. In 7.114. Denver.
- HOMER Energy. (2016bd). HOMER Model User Manual. In 7.90. Denver.
- HOMER Energy. (2016be). HOMER Model User Manual. In 7.133. Denver.
- HOMER Energy. (2016bf). HOMER Model User Manual. In 3.2.1. Denver.
- HOMER Energy. (2016bg). HOMER Model User Manual. In 38. Denver.
- HOMER Energy. (2016bh). HOMER Model User Manual. In 7.142. Denver.
- HOMER Energy. (2016bi). HOMER Model User Manual. In 3.1. Denver.
- HOMER Energy. (2016bj). HOMER Model User Manual. In 7.141. Denver.
- HOMER Energy. (2016bk). HOMER Model User Manual. In 39. Denver.
- HOMER Energy. (2016bl). HOMER Model User Manual. In 7.52. Denver.
- HOMER Energy. (2016bm). HOMER Model User Manual. In 7.134. Denver.
- HOMER Energy. (2016bn). HOMER Model User Manual. In 385. Denver.
- HOMER Energy. (2016bo). HOMER Model User Manual. In 41. Denver.
- HOMER Energy. (2016bp). HOMER Model User Manual. In 371. Denver.
- HOMER Energy. Scaled average value. (n.d.). Retrieved March 12, 2017, from <http://usersupport.homerenergy.com/customer/en/portal/articles/2188784-scaled-average-value>
- Jordan, D. C., & Kurtz, S. R. (2012). *Photovoltaic Degradation Rates -- An Analytical Review: Preprint*. Golden. Retrieved from <http://www.osti.gov/bridge>:
- Lubitz, W. D. (2010). Effect of manual tilt adjustments on incident irradiance on fixed and tracking solar panels. <https://doi.org/10.1016/j.apenergy.2010.11.008>
- Ma, T., Yang, H., Lu, L., & Peng, J. (2015). Pumped storage-based standalone photovoltaic power generation system: Modeling and techno-economic optimization. *Applied Energy*, 137, 649–659. <https://doi.org/10.1016/j.apenergy.2014.06.005>
- McGowan, J. G., & Manwell, J. F. (1988). Wind/Diesel Energy Systems: Review of Design Options and Recent Developments. *Solar Energy*, 41(6), 561–575. Retrieved from https://www.researchgate.net/profile/James_Manwell/publication/223544136_Winddiesel_energy_systems_Review_of_design_options_and_recent_developments/links/543e780f0cf2eac07e63601.pdf
- Muller, M. (2010). NREL Test & Evaluation Measuring and Modeling Nominal Operating Cell Temperature (NOCT). Retrieved from <http://www.nrel.gov/docs/fy10osti/49505.pdf>
- National Institute of Standards and Technology. (2013). 1.3.6.2. Related Distributions. In J. Filliben, C. Croarkin, & P. Tobias (Eds.), *Engineering Statistics Handbook*. US Department of Commerce. Retrieved from <http://www.itl.nist.gov/div898/handbook/eda/section3/eda362.htm>
- NREL. (n.d.). Glossary of Solar Radiation Resource Terms. Retrieved March 18, 2017, from http://rredc.nrel.gov/solar/glossary/gloss_d.html
- NREL. (2016). NREL: Energy Analysis - Energy Technology Cost and Performance Data. Retrieved March 19, 2017, from http://www.nrel.gov/analysis/tech_lcoe_re_cost_est.html
- Park, K. E., Kang, G. H., Kim, H. I., Yu, G. J., & Kim, J. T. (2009). Analysis of thermal and

- electrical performance of semi-transparent photovoltaic (PV) module. *EGY*, 35, 2681–2687.
<https://doi.org/10.1016/j.energy.2009.07.019>
- Pingel, S., Zemen, Y., Frank, O., Geipel, T., & Berghold, J. (2009). *Mechanical Stability of Solar Cells Within Solar Panels*. Berlin. Retrieved from
https://www.researchgate.net/profile/Sebastian_Pingel/publication/266091257_Mechanical_Stability_of_Solar_Cells_within_Solar_Panels/links/546de0720cf26e95bc3d0af6.pdf
- Poullikkas, A. (2013). A comparative assessment of net metering and feed in tariff schemes for residential PV systems. *Sustainable Energy Technologies and Assessments*, 3, 1–8.
 Retrieved from
https://www.researchgate.net/profile/Dr_Andreas_Poullikkas/publication/257745865_A_comparative_assessment_of_net_metering_and_feed_in_tariff_schemes_for_residential_PV_systems/links/00b7d5269efaf9438e000000.pdf
- PUCT. (n.d.). About the Public Utility Commission of Texas - Mission & History.
 Retrieved June 21, 2017, from <http://www.puc.texas.gov/agency/about/mission.aspx>
- PUCT. General Provisions of Customer Service and Protection Rules, Pub. L. No. 25, Substantive Rules Applicable to Electric Service Providers 1 (2017). Public Utility Commission of Texas. Retrieved from
<http://www.puc.texas.gov/agency/rulesnlaws/subrules/electric/ch25complete.pdf>
- Rodriguez, C., & Amaratunga, G. A. J. (2008). Long-Lifetime Power Inverter for Photovoltaic AC Modules. *IEEE Transactions on Industrial Electronics*, 55(7), 2593–2601.
<https://doi.org/10.1109/TIE.2008.922401>
- Roy, A., Kedare, S. B., & Bandyopadhyay, S. (2010). Optimum sizing of wind-battery systems incorporating resource uncertainty. *Applied Energy*, 87, 2712–2727.
<https://doi.org/10.1016/j.apenergy.2010.03.027>
- Simpson, J. R., & Mcpherson, E. G. (1998). SIMULATION OF TREE SHADE IMPACTS ON RESIDENTIAL ENERGY USE FOR SPACE CONDITIONING IN SACRAMENTO. *Atmospheric Environment*, 32(1), 69–74.
- Solomon, A. A., Faïman, D., & Meron, G. (2010). An energy-based evaluation of the matching possibilities of very large photovoltaic plants to the electricity grid: Israel as a case study. *Energy Policy*, 38, 5457–5468. Retrieved from
https://www.researchgate.net/profile/Solomon_Asfaw3/publication/227415180_An_energy-based_evaluation_of_the_matching_possibilities_of_very_large_photovoltaic_plants_to_the_electricity_grid_Israel_as_a_case_study/links/57d7ab0e08ae601b39ac35b6.pdf
- Stackhouse, P. W., Chandler, W. S., Zhang, T., Westberg, D., Barnett, A. J., & Hoell, J. M. (2016). Surface meteorology and Solar Energy (SSE) Release 6.0 Methodology Version 3.2.0.
- Su, W., Yuan, Z., & Chow, M. (2010). Microgrid planning and operation: Solar energy and wind energy. In *Power and Energy Society General Meeting* (pp. 1–7). Providence: IEEE.
 Retrieved from
http://s3.amazonaws.com/academia.edu.documents/30528640/pes2010_microgrid_planning_and_operation_solar_energy_and_wind_energy.pdf?AWSAccessKeyId=AKIAIWOWYYGZ2Y53UL3A&Expires=1496452865&Signature=hmD4AeOdvgnLm%2BaGs9oFoZ09Fs0%3D&response-content-dispositio
- US Department of Commerce, NOAA, N. (n.d.). El Paso Monthly Precipitation Totals. Retrieved

February 28, 2017, from https://www.weather.gov/epz/el Paso_monthly_precip
US Department of Commerce, NOAA, N. W. S. (n.d.). Climate Data for El Paso. Retrieved June 19, 2017, from <https://www.weather.gov/epz/climatedataforel Paso>
Vignola, F., Mavromatakis, F., & Krumsick, J. (2008). *PERFORMANCE OF PV INVERTERS*. Eugene. Retrieved from <http://solardat.uoregon.edu/download/Papers/PerformanceofPVInverters.pdf>
Vogel, R. (ASCE), & Fennessey, N. (ASCE). (1994). FLOW-DURATION CURVES. h NEW INTERPRETATION AND CONFIDENCE INTERVALS. *Journal of Water Resources Planning Management*, 120(4), 485–504. Retrieved from [http://ascelibrary.org/doi/pdf/10.1061/\(ASCE\)0733-9496\(1994\)120:4\(485\)](http://ascelibrary.org/doi/pdf/10.1061/(ASCE)0733-9496(1994)120:4(485))

Chapter 4 References

Feldman, D., Barbose, G., Margolis, R., Bolinger, M., Chung, D., Fu, R., ... Wiser, R. (2015). Photovoltaic System Pricing Trends: Historical, Recent, and Near-Term Projections, 2015 Edition (Presentation), Sunshot, U.S. Department of Energy (DOE). Retrieved from <http://www.nrel.gov/docs/fy15osti/64898.pdf>
Hadjipaschalis, I., Poullikkas, A., & Efthimiou, V. (2009). Overview of current and future energy storage technologies for electric power applications. *Renewable and Sustainable Energy Reviews*, 13, 1513–1522. Retrieved from https://www.researchgate.net/profile/Dr_Andreas_Poullikkas/publication/222816062_Overview_of_current_and_future_energy_storage_technologies_for_electric_power_applications/links/0fcfd50f4236acd555000000.pdf
Helwa, N. H., Baghat, A. B. G., & El-Shafee, A. M. R. (2000). Maximum Collectable Solar Energy by Different Solar Tracking Systems. *Energy Sources*, 22(1), 23–34. <https://doi.org/10.1080/00908310050014180>
Lubitz, W. D. (2010). Effect of manual tilt adjustments on incident irradiance on fixed and tracking solar panels. <https://doi.org/10.1016/j.apenergy.2010.11.008>
US Department of Commerce, NOAA, N. W. S. (n.d.). Climate Data for El Paso. Retrieved June 19, 2017, from <https://www.weather.gov/epz/climatedataforel Paso>

Chapter 5 References

Ayodele, R., & Ogunjuyigbe, S. (2014). Mathematical Methods and Software Tools for Designing an Economic Analysis of Hybrid Energy System. *International Journal of Renewable Energy*, 9(1), 57–68.
Bredehoeft, J., Ford, J., Harden, B., Mace, R., & Rumbaugh, J. I. (2004). *REVIEW AND INTERPRETATION OF THE HUECO BOLSON GROUNDWATER MODEL Prepared For EL PASO WATER UTILITIES*. El Paso. Retrieved from http://www.epwu.org/water/hueco_bolson/ReviewTeamReport.pdf
Duffie, J. A., & Beckman, W. A. (1991). *Solar engineering of thermal processes*. Wiley. Retrieved from https://openlibrary.org/books/OL1867035M/Solar_engineering_of_thermal_processes
El Paso Electric Company. (n.d.-a). Purchased Power Agreement Projects. Retrieved July 24,

- 2017, from <https://www.epelectric.com/tx/business/purchased-power-agreement-projects>
- El Paso Electric Company. (n.d.-b). Solar Power Systems at El Paso Electric's Power Plants. Retrieved July 24, 2017, from <https://www.epelectric.com/tx/business/solar-power-systems-at-el-paso-electrics-power-plants>
- El Paso Electric Company. (2011). Non-firm Purchased Power Service From Distributed Generators, Distributed Renewable Generators, and Qualifying Facilities. Retrieved June 19, 2017, from https://www.epelectric.com/files/html/Dist._Gen._Interconnection/TX/39582_Clean_Tariff_Schedule_No._48.pdf
- El Paso Electric Company. (2016a). Backup Power Service for Qualifying Facilities. Retrieved June 19, 2017, from https://www.epelectric.com/files/html/Schedule_No_47_-_Backup_Power_Service_for_Qualifying_Facilities.pdf
- El Paso Electric Company. (2016b). Maintenance Power Service for Qualifying Facilities. Retrieved June 19, 2017, from https://www.epelectric.com/files/html/Schedule_No_46_-_Maintenance_Power_Service_For_Qualifying_Facilities.pdf
- El Paso Electric Company. (2016c). Schedule No. DG Interconnection and Parallel Operation of Distributed Generation. Retrieved June 19, 2017, from https://www.epelectric.com/files/html/Schedule_No_DG_-_Interconnection_and_Parallel_Operation_of_Distributed_Generation.pdf
- El Paso Electric Company. (2016d, August 2). EPE Becomes the First Regional Utility to Go Coal-Free. *EPE Newsletter*. El Paso. Retrieved from <https://www.epelectric.com/about-el-paso-electric/article/epe-becomes-the-first-regional-utility-to-go-coal-free>
- El Paso Electric Company. (2017a). Schedule No. 98 - Fixed Fuel Factor. Retrieved June 19, 2017, from https://www.epelectric.com/files/html/TX_Sch_No_98_Proposed_Fixed_Fuel_Factor_-_Clean.pdf
- El Paso Electric Company. (2017b). Energy Efficiency Cost Recovery Factor. Retrieved June 19, 2017, from https://www.epelectric.com/files/html/PUCT_Docket_No._45885_EECRF.pdf
- El Paso Electric Company. (2017c, February 13). El Paso Electric Files 2017 Texas Rate Case. *EPE Newsletter*. El Paso. Retrieved from <https://www.epelectric.com/about-el-paso-electric/article/el-paso-electric-files-2017-texas-rate-case>
- Fullerton, T. M. (2006). Water transfers in El Paso County, Texas. *Water Policy*, 8(3), 255–268. <http://doi.org/10.2166/wp.2006.031>
- Heywood, C. E., & Yager, R. M. (2003). *Simulated Ground-Water Flow in the Hueco Bolson, an Alluvial-Basin Aquifer System near El Paso , Texas*. *Water-Resources Investigations Report 02-4108*. Albuquerque.
- HOMER Energy. (2014). HOMER Pro - Microgrid Software for Designing Optimized Hybrid Microgrids. Retrieved July 19, 2017, from http://homerenergy.com/HOMER_pro.html
- Klise, G. T., & Stein, J. S. (2009). Models Used to Assess the Performance of Photovoltaic Systems. *SANDIA REPORT*, 1–53.
- Kolenc, V. (2017a, March 21). El Paso Electric sells solar-power subscriptions. *El Paso Times*, p. 1. El Paso. Retrieved from <http://www.elpasotimes.com/story/news/local/el-paso/2017/03/21/el-paso-electric-offers-solar-power-energy-alternative/99429374/>
- Kolenc, V. (2017b, April 7). 1,000 El Paso Electric customers join solar plan. *El Paso Times*, p.

1. El Paso. Retrieved from <http://www.elpasotimes.com/story/news/local/el-paso/2017/04/07/el-paso-electric-solar-energy-rates/100170884/>
- Liu, B. Y. H., & Jordan, R. C. (1963). *A Rational Procedure for Predicting The Long-Term Average Performance of Flat-Plate Solar-Energy Collectors With Design Data for the U. S., Its Outlying Possessions and Canada**. Minneapolis. Retrieved from <http://citeseerx.ist.psu.edu/viewdoc/download?doi=10.1.1.470.5866&rep=rep1&type=pdf>
- Natural Resources Canada. (n.d.). RETScreen | Natural Resources Canada. Retrieved July 23, 2017, from <http://www.nrcan.gc.ca/energy/software-tools/7465>
- New Mexico Public Regulation Commission. (n.d.). Utility - Renewable Energy. Retrieved July 24, 2017, from <http://www.nmprc.state.nm.us/utilities/renewable-energy.html>
- Okedu, K. E., & Uzunwangho, R. (2014). Optimization of Renewable Energy Efficiency using HOMER, 4(2).
- Pöchacker, M., Khatib, T., & Elmenreich, W. (2014). *The Microgrid Simulation Tool RAPSIm: Description and Case Study*. Klagenfurt. Retrieved from https://mobile.aau.at/publications/poehacker-2014-The_Microgrid_Simulation_Tool_RAPSIm.pdf
- SourceForge. (n.d.). RAPSIm - Microgrid Simulator download | SourceForge.net. Retrieved July 23, 2017, from <https://sourceforge.net/projects/rapsim/>
- UMass-Amherst. (n.d.). Hybrid2 | Wind Energy Center. Retrieved July 23, 2017, from <http://www.umass.edu/windenergy/research/topics/tools/software/hybrid2>
- US Department of Energy, & North Carolina State University. (n.d.). Database of State Incentives for Renewables and Efficiency. Retrieved July 24, 2017, from <http://programs.dsireusa.org/system/program?state=TX>
- US Department of the Interior. (1982). Payments in Lieu of Taxes | U.S. Department of the Interior. Retrieved July 24, 2017, from <https://www.doi.gov/pilt>
- Walton, J., & Ohlmacher, G. (2000). *Surface and Ground Water Interactions: El Paso – Juarez Region*. El Paso. Retrieved from http://windowoutdoors.com/Research/SCERP_Surface_and_Groundwater_Interaction_Rio_Grande/SCERP0997/SCERPMonographWWWVersion.pdf